


Multi-Tier Fuel-Cycle Approach to Nuclear Waste Management

Los Alamos National Laboratory, Argonne National Laboratory
Oak Ridge National Laboratory, Pacific Northwest National Laboratory
Brookhaven National Laboratory, Lawrence Livermore National Laboratory
Idaho National Engineering and Environmental Laboratory, Idaho Accelerator Center
University of Nevada, University of Michigan, University of California, University of Texas
Burns & Roe, Enterprises, Inc., General Atomics, Westinghouse Savannah River Company

Blank Page

AAA Technical Quarterly Report
April - June 2002
LA-UR-02-5515

Approval



Date 8/30/02

Michael Cappiello
LANL AAA Program Manager
Advanced Accelerator Applications

Blank Page

Table of Contents

| | |
|---|-------------|
| Major Contributors..... | viii |
| Acronyms and Symbols..... | ix |
| I. INTRODUCTION..... | 1 |
| II. HIGHLIGHTS..... | 3 |
| III. TECHNOLOGY DEVELOPMENT | 7 |
| 1. FUELS DEVELOPMENT..... | 7 |
| Scope..... | 7 |
| Highlights..... | 7 |
| Fabrication Development..... | 9 |
| Metal Fuel | 9 |
| Nitride Fuel..... | 12 |
| Dispersion Fuels..... | 32 |
| TRISO Fuel | 34 |
| Fuels Irradiation Testing | 37 |
| ATW-1 Irradiation Test | 37 |
| ATR Fast Neutron Flux Booster..... | 40 |
| FUTURIX Irradiation Test in Phénix | 42 |
| Fuel Performance..... | 42 |
| Assessment of Radiation Tolerance of ZrN and the Metal Matrix NiAl | 42 |
| Modeling and Fuel Properties..... | 47 |
| Atomistic and Continuum Scale Modeling..... | 47 |
| 2. SEPARATIONS TECHNOLOGY | 52 |
| Scope..... | 52 |
| Highlights..... | 52 |
| Oxide Fuel Processing—Electrolytic Oxide Reduction (PYROX) Process..... | 53 |
| Electro-Refining Process Development - U/TRU Electrolysis Technology Development..... | 57 |
| UREX Process Development..... | 59 |
| LWR Spent Fuel Treatment | 59 |
| Sodium Iodide Production from Molten Salts | 63 |
| SANEX Process Studies | 65 |
| Dissolution of Dresden Reactor Fuel..... | 65 |
| Modified Direct Denitration (MDD) Demonstration | 67 |
| Evaluation of Alternate Complexants/Reductants | 67 |
| Radiation Chemistry of AHA in the UREX Process | 69 |
| Alternative Fuel Treatment Process Development..... | 70 |
| TRISO Spent Fuel Reprocessing | 70 |
| 3. TRANSMUTATION SCIENCE..... | 71 |
| 3.1 Integration and Analytical Support..... | 71 |
| Scope..... | 71 |
| Highlights..... | 72 |

| | |
|--|------------|
| Third International Workshop on Utilization and Reliability of High Power Proton Accelerators..... | 72 |
| MYRRHA Review Meeting..... | 73 |
| 3.2 Materials | 74 |
| Scope..... | 74 |
| Highlights..... | 75 |
| PNNL Activities..... | 75 |
| ANL Activities | 75 |
| LANL Hot-Cell Work..... | 76 |
| Materials Handbook | 76 |
| Meetings/Conferences/Workshops | 77 |
| 3.3 Lead-Bismuth Eutectic Technology | 77 |
| Scope..... | 77 |
| Highlights..... | 78 |
| LBE Technology Development..... | 79 |
| DELTA Loop Operations..... | 81 |
| 3.4 LANSCE Irradiation Experiments | 83 |
| Scope..... | 84 |
| Highlights..... | 85 |
| Neutron Yield and Spectrum Tests | 85 |
| Helium and Hydrogen Production Tests | 87 |
| Corrosion Studies..... | 88 |
| 3.5 High-Energy Physics..... | 91 |
| Scope..... | 91 |
| Highlights..... | 92 |
| MCNPX Code Development..... | 93 |
| Nuclear Data and CEM2k Code Development | 94 |
| LA150 Actinide Cross Section Evaluations for ²³⁹ Pu and ²³⁸ U..... | 97 |
| 3.6 Reactor Physics | 97 |
| Scope..... | 97 |
| Highlights..... | 98 |
| MUSE Benchmark..... | 99 |
| MUSE Experimental Activity..... | 99 |
| PROFIL Experiment..... | 100 |
| Safety Analysis..... | 100 |
| Uncertainty Assessment | 101 |
| Method Development..... | 102 |
| TREAT-Coupling Experiments | 102 |
| 3.7 International Support | 103 |
| Scope..... | 104 |
| Highlights | 104 |
| Current Status of MEGAPIE | 104 |
| MEGAPIE Neutronics Work..... | 107 |
| 3.8 LANL-Sponsored Directed-Research University Programs | 108 |
| Scope..... | 108 |
| Highlights..... | 110 |

| | |
|---|------------|
| University of California – Berkeley..... | 111 |
| University of Michigan | 113 |
| 4. SYSTEMS TECHNOLOGIES | 115 |
| Scope | 115 |
| Highlights | 116 |
| Accelerator-Driven Test Facility (ADTF) | 117 |
| ADS Reference Design | 117 |
| Functional Requirements | 117 |
| Sodium-Cooled Engineering Design | 119 |
| Target Assembly..... | 121 |
| Alternative Target Designs..... | 122 |
| Multiplier Primary System Thermo-Hydraulics | 124 |
| Preliminary Results for SCM Target/Blanket..... | 124 |
| Micro Accelerator-Driven System (ADS) Proof-of-Principle (POP)..... | 125 |
| Coupling Experiments | 125 |
| Transmutation Technology Development Plan | 128 |
| Fuels and Materials Experiments | 128 |
| Advanced Cavity Development..... | 130 |
| 5. PROJECT INTEGRATION | 131 |
| 5.1 Systems Studies..... | 131 |
| Scope | 131 |
| Highlights | 132 |
| Approach and Direction..... | 132 |
| Sample (Interim) Results from NFCSim Simulation Model | 134 |
| Neutronics Support..... | 136 |
| 5.2 University Programs..... | 137 |
| Scope | 137 |
| Highlights | 138 |
| Technical Progress..... | 139 |
| Idaho State University | 139 |
| Accelerator-Produced Neutrons for Reactor/Accelerator Coupling Experiments..... | 140 |
| References | 142 |

Major Contributors

| | |
|-------------------------|---|
| Fuels Development: | D. Crawford (ANL) K. Chidester (LANL) M. Meyer (ANL) S. Hayes (ANL) R. Margevicius (LANL) K. McClellan (LANL) |
| Separations Technology: | J. Laidler (ANL) |
| Transmutation Science: | K. Pasamehmetoglu (LANL) E. Pitcher (LANL) L. Waters (LANL) M. James (LANL) M. Chadwick (LANL) N. Li (LANL) V. Tcharnotskaia (LANL) S. Wender (LANL) S. Maloy (LANL) B. Haight (LANL) G. Morgan (LANL) S. Lillard (LANL) R. Klann (ANL) G. Palmiotti (ANL) |
| Systems Technologies: | M. Cappiello (LANL) S. McConnell (LANL) K. Pasamehmetoglu (LANL) J. Roglans (ANL) R. Guffee (LANL) H. Cohen (BREI/GA) J. Herceg (ANL) W. Chaves (LANL) G. Willcutt (LANL) J. Elson (LANL) H. Ludewig (BNL) M. Todosow (BNL) |
| Project Integration: | L. Guillebaud (LANL) W. Davidson (LANL) R. Krakowski (LANL) D. Beller (LANL) A. Hechanova (UNLV) J. Lee (Univ Michigan) E. Greenspan (UC Berkeley) W. Charlton (UT Austin) |

Acronyms and Symbols

| | |
|------------------|---|
| AAA | Advanced Accelerator Applications |
| AC | Accelerating cavities |
| ADS | Accelerator-Driven System |
| ADTF | Accelerator-Driven Test Facility |
| ADMAB | Accelerator-Driven Minor Actinide Burner |
| AES | Advanced Energy Systems (formerly Northrup-Grumman Corp.) |
| AET | Ability Engineering Technology |
| AFM | Atomic Force Microscopy |
| Ah | Ampere-Hour |
| AHA | Acetohydroxamic acid |
| Am | Americium |
| AMUSE | Argonne Model for Universal Solvent Extraction, the generic TRUEX model expanded to include UREX and PUREX processing |
| ANL | Argonne National Laboratory (Chicago) |
| ANL-W | Argonne National Laboratory-West (Idaho Falls) |
| ANRC | Amarillo National Research Center |
| ANS | American Nuclear Society |
| ANSYS | structural analysis modeling code |
| appm | atomic parts per million |
| APT | Accelerator Production of Tritium |
| ASME | American Society of Mechanical Engineers |
| ATR | Advanced Test Reactor (INEEL) |
| ATW | Accelerator Transmutation of Waste |
| Ba | Barium |
| BCM | Beam-Current Monitor |
| BCP | Baseline Change Proposal |
| BCP | Buffered Chemical Polishing |
| Be | Beryllium |
| Beta (β) | Ratio to the speed of light |
| Bi | Bismuth |
| BISTRO | Two-Dimensional Discrete Ordinates Code |
| BNFL | British Nuclear Fuels, Ltd |
| BNL | Brookhaven National Laboratory |
| BOF | Balance of Facility |
| BOL | Beginning of Life |
| BOP | Balance of Plant |
| BOR-60 | Sodium-Cooled Fast Reactor (Dmitrovgrad, Russia) |
| BPM | Beam-Position Monitor |
| BSE | backscattered electron (images) |
| CCDTL | Coupled-Cavity Drift-Tube Linac |
| CCL | Coupled-Cavity Linac |
| Ce | Cerium |
| CEA | Commissariat à l'Energie Atomique (France) |
| CEM | Cascade Exciton Model code (Model-based Monte-Carlo particle transport code) |
| CERCA | Compagnie Pour L'Etude Et La Realisation De Combustibles Atomiques |
| cercer | Ceramic-Ceramic |
| cermet | Ceramic-Metal |
| CFD | Computational Fluid Dynamics |
| CINDER90 | Computer Code |
| CLWR | Commercial Light-Water Reactor |
| Cm | Curium |
| CMPO | Neutral Extractant |

| | |
|-----------|--|
| CMR | Chemistry and Metallurgy Research (facility at LANL) |
| CONCERT | COMbined Neutron Center for European Research and Technology |
| Cs | Cesium |
| Cu | Copper |
| CVD | Chemical Vapor Deposition |
| cw | Continuous Wave (100% duty factor) |
| DACS | Data Acquisition and Control System |
| DAS | Data Acquisition System |
| DBTT | Ductile-To-Brittle Transition Temperature |
| DCR | Design Change Request |
| DDN | Design Data Need |
| DIAMEX | Aqueous Solvent Extraction Process for TRU Recovery |
| DOE | Department of Energy |
| dpa | Displacements per Atom |
| EBR | Experimental Breeder Reactor |
| ED&D | Engineering Development and Demonstration |
| EDS | Energy Dispersive Spectrometry |
| EPFD | Effective Full-Power Day |
| EFTTRA-T4 | Radiation Test Sponsored by the European Union |
| EIS | Electrochemical Impedance Spectroscopy |
| EIS | Environmental Impact Statement |
| ENDF | Evaluated Nuclear Data File – Evaluations that can be used in MCNPX for more accurate predictions of fission, criticality, transport, and radiation damage |
| EOI | End of Irradiation |
| EOL | End of Life |
| EPICS | Experimental Physics and Industrial Control System |
| ERANOS | Computer modeling code |
| ERC | External Review Committee |
| ES&H | Environmental, Safety, and Health |
| ESS | European Spallation Source |
| ESSAB | Energy System Acquisition Advisory Board (DOE) |
| Eu | Europium |
| FDD | Facility Design Description |
| Fe | Iron |
| FFTF | Fast Flux Test Facility |
| FMF | Fuel Manufacturing Facility |
| FODO | Focus-Drift-Defocus-Drift |
| FPY | Full-Power Year |
| FWHM | Full Width Half Maximum |
| FZJ | Forschungs Zentrum Jülich (German Laboratory) |
| FZK | Forschungs Zentrum Karlsruhe (German Laboratory) |
| g/L | Grams per Liter |
| GA | General Atomics Inc. |
| GNASH | Nuclear Reaction Code |
| GSI | Gesellschaft für Schwerionenforschung (Darmstadt, Germany) |
| GT-MHR | Gas Turbine Modular Helium Reactor |
| H | Hydrogen |
| HAN | Hydroxylamine |
| HCP | Hazard Control Plan |
| He | Helium |
| HEBT | High-Energy Beam Transport |
| HEU | Highly enriched uranium |
| Hf | Hafnium |
| HFIR | High Flux Isotope Reactor (ORNL) |
| HFR | High Flux Reactor (Petten, Netherlands) |
| Hg | Mercury |

| | |
|----------|--|
| HIP | Hot Isostatic Process (for bonding materials) |
| HM | Heavy metal |
| HPRF | High-Power Radio Frequency |
| HS/WS | Halo-Scraper/Wire-Scanner (diagnostic device) |
| HX | Heat exchanger |
| I&C | Instrumentation and Control |
| IAC | Idaho Accelerator Center |
| IAEA | International Atomic Energy Association (Vienna, Austria) |
| ICP-MS | Inductively Coupled Plasma-Mass Spectrometry |
| ICS | Integrated Control System |
| IFMIF | International Fusion Materials Irradiation Facility |
| IFR | Integral Fast Reactor |
| IHX | Intermediate Heat Exchanger |
| IMS | Information Management System |
| INEEL | Idaho National Engineering and Environmental Laboratory |
| IPBT | In-Pile Beam Tube |
| IPPE | Institute of Physics and Power Engineering, Obninsk, Russia. |
| ISABEL | Physics Modeling Code |
| ISTC | International Science and Technology Centre (Moscow) |
| ITER | International Thermonuclear Experimental Reactor |
| ITU | Institute for Transuranium Elements (Karlsruhe, Germany) |
| JAERI | Japan Atomic Energy Research Institute |
| JCNNM | Johnson Controls Northern New Mexico |
| JLAB | Jefferson Laboratory (VA) |
| K | Potassium |
| KAERI | Korean Atomic Energy Research Institute |
| KEK | National Laboratory for High-Energy Physics (Tsukuba, Japan) |
| keV | Kiloelectron Volt |
| LA150n | Los Alamos generated nuclear data library, extending up to 150 MeV |
| LAHET | Los Alamos High-Energy Transport |
| LANL | Los Alamos National Laboratory |
| LANSCE | Los Alamos Neutron Science Center |
| LBE | Lead-bismuth eutectic |
| LBHM | Low- β Hot Model |
| L/d | Length-to-diameter ratio |
| L/hr | Liter per hour |
| LEBT | Low-Energy Beam Transport |
| LEDA | Low-Energy Demonstration Accelerator |
| LINAC | A computer code based on PARMILA that has been modified to include CCDTL and SCRF elliptical cavities as options |
| LLFP | Long-lived fission product |
| LLNL | Lawrence Livermore National Laboratory |
| LLRF | Low-level radio frequency |
| LME | Liquid-metal embrittlement |
| LMR | Liquid-metal reactor |
| LWR | Light-water reactor |
| <u>M</u> | Molar |
| MA | Minor actinide |
| mb | Millibarn |
| MCA | Multi-criteria analysis |
| mCi | Millicurie |
| MCNP | Monte Carlo N-Particle Transport Code |
| MCNPX | Merged code—Los Alamos High-Energy Transport (LAHET) and Monte Carlo N-Particle Codes (MCNP) |
| MCWO | MCNP Coupling With ORIGEN2 burnup calculation code |
| MDD | Modified Direct Denitration |

| | |
|----------|--|
| MEGAPIE | Megawatt Pilot Experiment |
| MFM | Magnetic Flow Meter |
| MIT | Massachusetts Institute of Technology |
| mL | Milliliter |
| Mo | Molybdenum |
| MOX | Mixed oxide fuel |
| mR | Millirad (a measure of radiation) |
| MT | Metric Ton |
| MTL | Materials Test Loop |
| MUSE | CEA-Cadarache Zero-Power Subcritical Experiments |
| MW | Megawatt |
| MWD/T | Megawatt Days per Ton (standard unit for burnup) |
| MWth | Megawatt thermal |
| N | Nickel or nitride |
| Np | Neptunium |
| n/p | Neutrons per proton |
| NDA | Nondestructive analyses |
| NEA | Nuclear Energy Agency (Paris) |
| NEPA | National Environmental Protection Agency |
| NERAC | Nuclear Energy Research Advisory Committee |
| NERI | Nuclear Energy Research Initiative |
| NFC | Nuclear Fuel Cycle |
| NFF | Nonfertile Fuel |
| O | Oxygen or Oxide |
| O&M | Operations and Maintenance |
| OECD | Organization for Economic Cooperation and Development (Paris) |
| ORIGEN | A computer code system for calculating the buildup, decay, and processing of radioactive materials |
| ORNL | Oak Ridge National Laboratory |
| P&ID | Piping and Instrumentation Diagram |
| P&T | Partitioning and transmutation |
| PACS | Personnel Access Control System |
| PARMTEQM | RFQ simulation code |
| Pb | Lead |
| PCM | Pulse Control Modulation |
| Pd | Paladium |
| PFD | Process Flow Diagram |
| PHA | Preliminary Hazards Assessment |
| PHENIX | Fast Reactor in France |
| PIE | Post-irradiation examination |
| PNNL | Pacific Northwest National Laboratory |
| POP | Proof of Performance, Proof of Principle |
| PRAD | Proton Radiography |
| PRISM | Power Reactor Innovative Small Module |
| PSAR | Preliminary Safety Analysis Report |
| PSS | Personnel Safety System |
| PSI | Paul Scherrer Institute (Switzerland) |
| Pu | Plutonium |
| PUREX | Plutonium-Uranium Extraction |
| PWR | Pressurized Water Reactor |
| PYRO | Pyrochemical process |
| Q | Quality factor |
| QA | Quality Assurance |
| QAC | Quick ATW Costing |
| R | Rad (a measure of radiation) |
| RAMI | Reliability, Availability, Maintainability, and Inspectability |

| | |
|-----------|--|
| RBS | Rutherford Backscattering Spectrometry |
| RERTR | Reduced Enrichment for Research and Test Reactors program |
| RF | Radio Frequency |
| RFQ | Radio-Frequency Quadrupole |
| RCCS | Resonance-Control Cooling System |
| RIA | Rare Isotope Accelerator |
| RIAR | Russian Institute of Atomic Reactors |
| rms | root mean square |
| RRR | Residual Resistance Ratio |
| RSICC | Radiation Safety Information Computational Center |
| RTD | Surface Temperature Detector |
| RTH | Royal Institute of Technology (Stockholm, Sweden) |
| Ru | Ruthenium |
| SAA | Systems Approaches Analysis |
| SANEX | Aqueous Solvent Extraction Process for Am and Cm Recovery |
| SAR | Safety Analysis Report |
| SC | Superconducting |
| SCM | Subcritical Multiplier |
| SCRF | Superconducting RF |
| SDD | System Design Description |
| SEM | Scanning Electron Microscopy |
| SFT | Stacking-Fault Tetrahedral |
| SHR | shutdown heat-removal |
| SINQ | Spallation Neutron Source at Paul Scherrer Institute (Switzerland) |
| SNF | Spent Nuclear Fuel |
| SNL | Sandia National Laboratory |
| SRS | Savannah River Site |
| SRTC | Savannah River Technology Center |
| Star-CD | Computational fluid dynamics code |
| STAYSL | A computer code to analyze results of activation foil measurements |
| STAYSL2 | A computer code to analyze results of activation foil measurements in both a proton and neutron flux |
| STP | Standard Temperature and Pressure |
| STIP | Spallation Target Irradiation Program (at PSI) |
| T/p | Tritons (nucleii of tritium atoms) per Proton |
| T/B | Target / Blanket |
| Ta | Tantalum |
| TBP | Tri- <i>n</i> -butyl Phosphate or Tributylphosphate |
| Tc | Technitium |
| TEM | Transmission Electron Microscopy |
| TESLA | International Collaboration on a TeV Superconducting Linear Accelerator |
| TGA | Thermal Gravimetric Analysis |
| TJNAF | Thomas Jefferson National Accelerator Facility |
| TMT | Target and Materials Test Station |
| TRAC | Transient Reactor Analysis Code |
| TRACE 3-D | Interactive computer code that calculates the envelopes of a bunched beam through a user-defined transport system |
| TREACS | TReat Experiment for ACcelerator-driven Systems |
| TREAT | Transient Reactor Test Facility |
| TRISO | Tri-isotropic, referring to a multi-layered fuel-particle coating consisting of pyrolytic carbon and silicon carbide |
| TRADE | <u>TR</u> IGA <u>A</u> ccelerator <u>D</u> riven <u>E</u> xperiment |
| TRIGA | Small Reactor Type |
| TRISPAL | Refers to the French APT Program |
| TRL | Technical Readiness Level |
| TRU | Transuranics (americium, curium, neptunium, and plutonium) |

| | |
|---------|--|
| TRUEX | Aqueous solvent extraction process for TRU recovery |
| U | Uranium |
| UFP | University Fellowship Program |
| UNLV | University of Nevada Las Vegas |
| UPP | University Participation Program |
| UREX | Uranium Extraction (an aqueous partitioning process) |
| URA | University Research Alliance |
| URP | University Research Program |
| USQD | Unreviewed Safety Question Determination |
| V | Vanadium |
| VPS | Vapor Plasma Spray |
| VARIANT | Three-Dimensional Nodal Transport Code |
| W | Tungsten |
| WBS | Work Breakdown Structure |
| WNR | Weapons Neutron Research (facility at LANL) |
| WPPT | Working Party on Partitioning and Transmutation |
| WSRC | Westinghouse Savannah River Company |
| Xe | Xenon |
| XRD | X-ray Diffraction |
| Y | Yttrium |
| ZPPR | Zero Power Physics Reactor |
| Zr | Zirconium |

Advanced Accelerator Applications

Quarterly Report

January – March 2002

I. INTRODUCTION

The Advanced Accelerator Applications (AAA) Program, a Department of Energy (DOE) program commissioned by Congress in FY2000, is a national effort consisting of DOE laboratories (Los Alamos, Argonne, Savannah River, Livermore, and Oak Ridge), industry (Burns and Roe Engineering Inc, General Atomics) and universities (UC-Berkeley, Texas, Michigan, Nevada). The primary mission of the AAA Program is to develop the technology base for the transmutation of nuclear waste and to demonstrate its practicality and value for long-term waste management.

The AAA Program was constituted by combining two programs: the Accelerator Production of Tritium (APT) Program and the Accelerator Transmutation of Waste (ATW) Program. The APT Program was established in 1995 with a commercial light-water reactor (CLWR) program as part of a dual-path strategy for development of a new tritium-production technology for the nation. From 1995 through 2001, DOE-Defense Programs invested in the design and development of an accelerator to produce tritium, including a full-scale prototype of the front end of the accelerator. In December 1998, the DOE chose the CLWR as the primary technology for tritium production, leading to the closeout of APT at the end of FY01. The ATW Program, which was investigating the feasibility of accelerator-driven systems to transmute long-lived toxic components of spent nuclear fuel, benefited from the technology development of APT.

The goal of the AAA Program is to evaluate the effectiveness of transmutation of spent nuclear fuel against the following criteria:

- (1) Reduce the long-term radiological impact of waste;
- (2) Enable development of a simpler, cheaper repository;
- (3) Reduce proliferation risk; and
- (4) Improve long-term prospects for nuclear power.

Improving the long-term prospects for nuclear power means not only demonstrating through proof-of-performance the practicality of the transmutation of nuclear waste and its meaningful impact on nuclear materials, waste management, and economics, but also defining and executing activities designed to support the country's nuclear science and engineering infrastructure.

For the short term, the AAA Program is focusing its efforts on the following:

- (1) Evaluating the most effective systems for transmutation of spent nuclear fuel;
- (2) Developing separations technologies to partition long-lived radioactive waste from reusable nuclear material;
- (3) Developing and testing potential transmutation fuels;

- (4) Developing a spallation target to provide an effective environment for transmutation;
- (5) Establishing and supporting a national university program to re-energize development and training in nuclear-related fields; and
- (6) Collaborating in international research efforts with nations involved in evaluating nuclear waste management.

Through these efforts, the AAA Program is defining the key experiments, analyses, and facilities needed to demonstrate the technical viability of partitioning and transmutation of long-lived nuclear wastes.

Additionally, a key future objective of AAA is the construction of an accelerator-driven test facility (ADTF). The goal of the facility would be to demonstrate the transmutation of nuclear waste and to function as a national nuclear science and engineering user facility.

The AAA Program will soon transition into what is being called the “Advanced Fuel Cycle” or AFC Program, with similar goals, but with more emphasis and focus on the development of fuels and separations technologies.

II. HIGHLIGHTS

Fuels Development

- Metal fuel slug fabrication was completed in June. All specimens planned for irradiation in the Advanced Test Reactor (ATR) in Experiment ATW-1 have been fabricated. Final reports on the chemical and isotopic analyses of some of the fuel specimens were issued.
- Pristine and ion-irradiated ZrN samples were implanted with He and shipped to the Institute for Transuranium Elements (ITU) in Karlsruhe, Germany for He release studies.
- Scanning Electron Microscopy (SEM) examination of two Pu-12Am-40Zr samples showed the as-cast materials to have a uniform microstructure and a limited amount of fine pore formation.
- Initial power calculations were completed for the proposed metallic, nitride and oxide fuel pins in the FUTURIX fast-spectrum fuel experiment in the Phénix reactor. Results for the metallic and nitride fuels appear excellent, with adequate margins to melting.
- Modeling efforts on lanthanide and transition nitrides have revealed that the nitrogen-to-metal ratio is an important factor in overall structural stability.
- Several batches of U-N were synthesized via direct metathesis of U(III) iodide with lithium nitride to investigate the feasibility of direct forming of actinide nitride. The results vary but show promise if properly controlled.
- Actinide nitride material was successfully synthesized from Pu, Np, and Am oxide powders. Sintering tests were completed with blends of ZrN and PuN materials. Several of the samples reached the desired density of >80%TD after sintering.
- TRISO particles containing a non-radioactive surrogate kernel (ZrO₂) were coated in a configuration and manner approximating the proposed deep burn driver fuel.

- Approximately 4 kg of Dresden reactor fuel has been dissolved in a hot cell at SRS in preparation for the UREX hot demonstration.
- Experiments with the electrolytic oxide reduction (PYROX) process have shown a marked improvement in UO₂ reduction rate and efficiency with decreasing fuel-particle size. The reduction of lanthanide fission product oxides is a challenging problem, but initial experimental results are encouraging.
- Valuable data related to the complexation constants for acetohydroxamic acid (AHA) with plutonium and minor actinides were obtained from foreign sources and used to update the AMUSE code.

Transmutation Science

- Under the auspices of the DOE AAA Program, LANL hosted a successful and productive 3-day workshop in May, the *Third International Workshop on Utilization and Reliability of High Power Proton Accelerators*, held in Santa Fe, New Mexico.
- LANL Materials Team co-sponsored the *Fifth International Workshop on Spallation Materials Technology* held May 20-24 in Charleston, SC. The team members presented a number of papers at this workshop.
- The safety basis for the unmanned operations of the DELTA loop was completed, reviewed, and approved.
- The first fully-parallel version of the MCNPX code was produced and tested on a LINUX cluster at LANL.
- Results relative to the PROFIL-1 analyzed with JEF2.2 data are in good agreement with the corresponding results coming from previous studies performed at CEA.
- The ISTC target (LBE target) fabricated by the Institute of Physics and Power Engineering (IPPE) in Obninsk, Russia, was delivered to the US, arrived at UNLV in May, and was carefully unloaded.

Systems Technologies

- A final draft of the Transmutation Technology Development Plan (TTDP) was issued for review. The section on coupling experiments, including TREACS and TRADE, was completed and incorporated in the draft TTDP.

Systems Studies

- The *NFCSim* simulation model is successfully simulating past history of nuclear power plant deployment and spent nuclear fuel (SNF) generation in the US.
- The *FCOPT* optimization code is successfully optimizing a broad subset of nuclear fuel cycle (NFC) technologies on the basis of cost and proliferation risk.

University Programs

- The University Research Alliance (URA) finalized selection of AAA Fellowships for 2002 and notified recipients. Through this new group of fellows, the AAA Project has engaged seven new universities: Purdue, Georgia Tech, University of Florida, University of Illinois at Chicago, North Carolina State, University of New Mexico, and University of Tennessee Knoxville.
- Two AAA Fellows received their Master's Degrees in Nuclear Engineering in May.
- The University Projects Leader has been highly instrumental in the formation of a University Consortium (~12 universities) for Transmutation Research to be led by UNLV and managed by the University Research Alliance. This proposed consortium is part of the Energy Appropriations bill currently under consideration by Congress.

- UC-Berkeley generated 5 refereed papers from AAA funded work.
- Proliferation Resistance Assessment methodology with complete time-dependence was completed at UT-Austin and applied to four long-term nuclear fuel systems.
- The UNLV AAA University Participation Program (UPP) now supports a total of 25 graduate students with assistantships.

Blank Page

III. TECHNOLOGY DEVELOPMENT

1. FUELS DEVELOPMENT

Scope

AAA fuels development activities are directed toward the development and qualification of fuels for safe transmutation of actinides at maximal rates. The objective of the effort is to provide one or more transmutation fuel forms at Technical Readiness Level (TRL) 6 at the time that transmutation technology overall is to begin integral demonstration. Thus far, requirements for such fuels include nonfertile compositions in forms suitable for fast-spectrum transmuters and a homogenous fuel cycle (i.e., all minor actinides would be maintained in the same fuel and processing stream). However, the AAA transmutation program is considering additional transmuter architectures, the use of which would imply different requirements for fuels; therefore, the fuel development program is evolving as the nature of and approach for the overall transmutation mission evolves.

The specific R&D activities include development of techniques to fabricate transmutation fuels from LWR fuel-derived actinide feed and from actinide feed recycled from transmuters. As-fabricated samples are chemically and microstructurally characterized to evaluate the success of fabrication processes and to better understand the nature of the fuel materials. Evaluation of proposed fuel forms (nitride, oxide, metal, carbide, dispersion, etc.) requires irradiation testing, so near-term irradiation tests are being planned and will be performed through the course of this program. Finally, the understanding of in-service fuel behavior is best demonstrated through the development and validation of fuel behavior models that are eventually incorporated into fuel performance codes. Such models are being developed, concurrent with an effort to develop thermal models that allow calculation of fuel and cladding temperatures in service and during testing.

Highlights

- Metal fuel slug fabrication was completed in June. All specimens planned for insertion in ATW-1 metal alloy capsules ATW-1B and ATW-1D have been fabricated, including three Pu-12Am-40Zr casts, five Pu-10Np-10Am-40Zr casts, and six Pu-40Zr casts. Final reports on the chemical and isotopic analyses of the Pu-60Zr and Pu-10Np-40Zr fuel specimens were issued.
- Milling of nitride powders has been shown to have a significant impact on sinterability and quantitative results for ZrN are presented.
- A lattice parameter mismatch study using YN as a PuN surrogate paralleled the anomalous sintering behavior of mixed PuN/ZrN powders.
- Pristine and ion-irradiated ZrN samples were implanted with He and shipped to the Institute for Transuranium Elements (ITU) in Karlsruhe, Germany for He release studies.

- In preparation for ion damage studies of NiAl, high-quality stoichiometric (Ni/Al ratio=1) single-crystal samples were prepared and successfully characterized using Rutherford Backscattering/ion channeling (RBS/C). This will enable a quantitative ion damage accumulation study in the future.
- Microstructures of two Pu-40 wt% Zr-10 wt% Np specimens were analyzed using scanning electron microscope (SEM) with energy-dispersive and wavelength-dispersive spectrometers (EDS/WDS) and x-ray diffraction (XRD). SEM and XRD confirm the presence of a δ -(Pu,Np) face-centered cubic phase and a (potentially oxygen stabilized) (Pu,Np)Zr₂-like hexagonal phase.
- SEM examination of two Pu-12Am-40Zr samples showed the as-cast materials to have a uniform microstructure and a limited amount of fine pore formation. XRD shows only the presence of a δ -(Pu)-type face-centered cubic phase.
- Quartz reactor vessels, a top loading vessel for gaseous and liquid precursors and a side loading vessel for solid precursors, were ordered from Powdermet Corporation with anticipated delivery in July 2002 for trials on dispersion fuel particle coating.
- Detailed pretest analysis of the ATW-1A, -1B, -1C and -1D irradiation tests continued and included an effort to evaluate the radial power profiles inside the fuel rodlets. The radial power profiles of Pu-12Am-40Zr and Pu-40Zr were calculated at beginning-of-life and after 110 days of irradiation using the MCWO methodology—a coupled MCNP/ORIGEN code.
- Initial power calculations were completed for the proposed metallic, nitride and oxide fuel pins in the FUTURIX fast-spectrum fuel experiment in the Phénix reactor. The peak estimated linear power for the inert-matrix oxide fuel compositions proposed by the CEA, namely 40 vol% (Pu_{0.5},Am_{0.5})O₂ fuel particles dispersed in an MgO matrix, are too high; resulting calculated centerline fuel temperatures are near melting. However, results for the metallic and nitride fuels appear excellent, with adequate margins to melting.
- Activities to obtain thermo-physical property correlations for nitride fuel resulted in recommended materials property correlations for heat capacity, density and thermal expansion, and thermal conductivity.
- An initial assessment of the mechanical properties of ZrN was conducted on available material. Trends in mechanical properties were observed, verifying that the proposed test methods and geometries are compatible with available sample geometries.
- Modeling efforts on lanthanide and transition nitrides have revealed that the nitrogen-to-metal ratio is an important factor in overall structural stability.
- The partial pressure of nitrogen in the Pu-N system was modeled as well as a preliminary assessment of the U-N phase diagram in preparation for assessment of the phase diagram.
- Several batches of U-N were synthesized via direct metathesis of U(III) iodide with lithium nitride to investigate the feasibility of direct forming of actinide nitride. The results have varied but show promise if properly controlled.

- Actinide nitride material was successfully synthesized from Pu, Np, and Am oxide powders. Sintering tests were completed with blends of ZrN and PuN materials. Several of the samples reached the desired density of >80%TD after sintering.
- TRISO particles containing a non-radioactive surrogate kernel (ZrO_2) were coated in a configuration and manner approximating the proposed Deep Burn driver fuel.

Fabrication Development

Metal Fuel

Metal fuel slug fabrication was completed in June. All specimens planned for insertion in metal-alloy fuel-test capsules ATW-1B and ATW-1D have been fabricated. A cold demonstration of the ATW-1 fuel pin fabrication process was completed in the Engineering Development laboratory. Eight jackets were prepared, loaded with sodium, fuel slugs, and pellet stacks of size and density prototypic of metal and nitride fuel. Top-end plugs were welded in place using established procedures. Fuel slugs and pellets were settled into sodium and bonded. Radiographic inspection was conducted to verify sodium height, slug position, and weld quality. This demonstration established that the individual processes selected and designed for fuel pin fabrication work as planned when integrated.

Fuel specimens are currently being characterized by x-ray diffraction, scanning electron microscopy (SEM) with energy and wavelength dispersive spectroscopy, wet chemical, and isotopic analysis. Some of the ongoing analysis of Pu-10Np-40Zr is presented here.

Microstructures of two Pu-40wt% Zr-10wt% Np specimens from two fuel pins were analyzed using SEM with energy-dispersive and wavelength-dispersive spectrometers (EDS/WDS). Figures 1 and 2 show SEM images of the microstructure of the samples. Uniform microstructures are observed moving from the center of the samples toward the outer edge.

Higher magnification micrographs of the microstructures for both samples show that the alloy microstructures contain single-phase and two-phase regions (see Fig. 3). The two-phase regions contain discrete precipitates. Precipitates larger in size than those in the two-phase regions were also observed to occur randomly throughout the alloy microstructures. X-ray maps produced for Np, Pu, Zr, and O (see Fig. 4) indicate that Np, Pu, and Zr are present in all the alloy phases. The brighter-contrast, single-phase areas are enriched in Pu and Np (see Fig. 3). The darker-contrast, two-phase regions are enriched in Zr. The precipitate phases are enriched in O. At the outer periphery of the alloy samples is a 50–100- μm -wide band that exhibits different phase morphologies (see Fig. 5). It appears that this change in alloy microstructure is due to the penetration of oxygen and/or other impurities into the fuel pin, probably from the quartz molds.

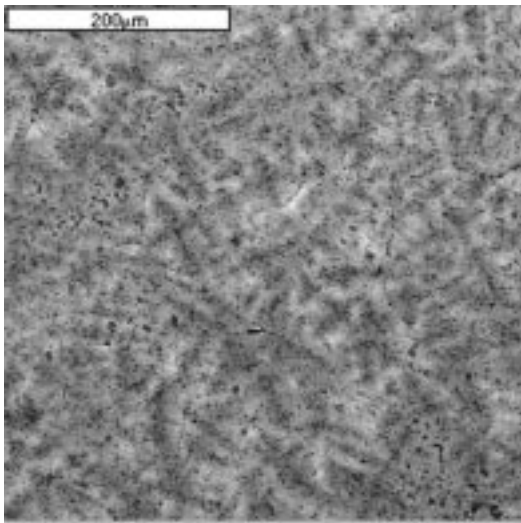


Fig. 1. SEM micrograph of the microstructure observed in sample MB008.

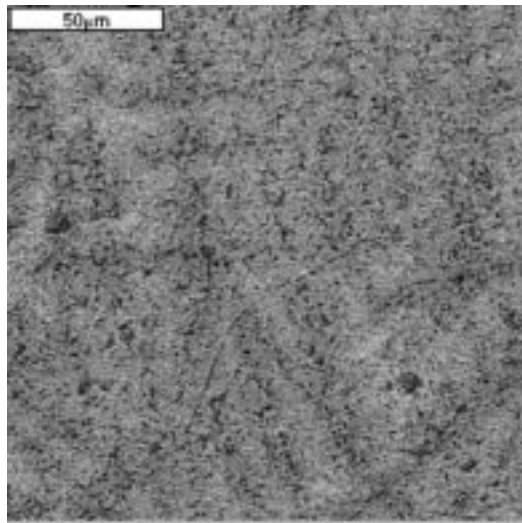


Fig. 2. SEM micrograph of the microstructure observed in sample MB010.

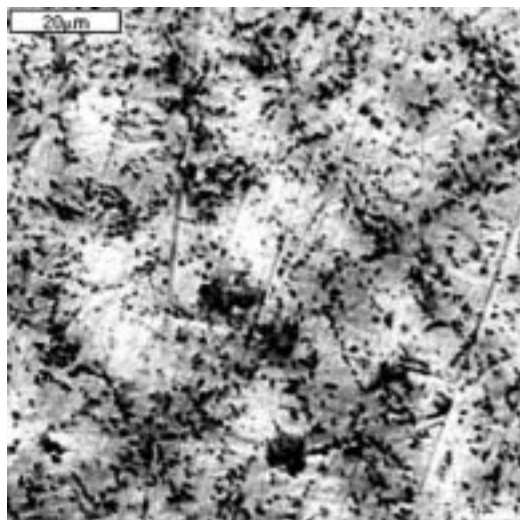


Fig. 3. SEM micrograph showing bright-contrasted regions that are primarily single-phase and darker-contrasted regions that are two-phase.

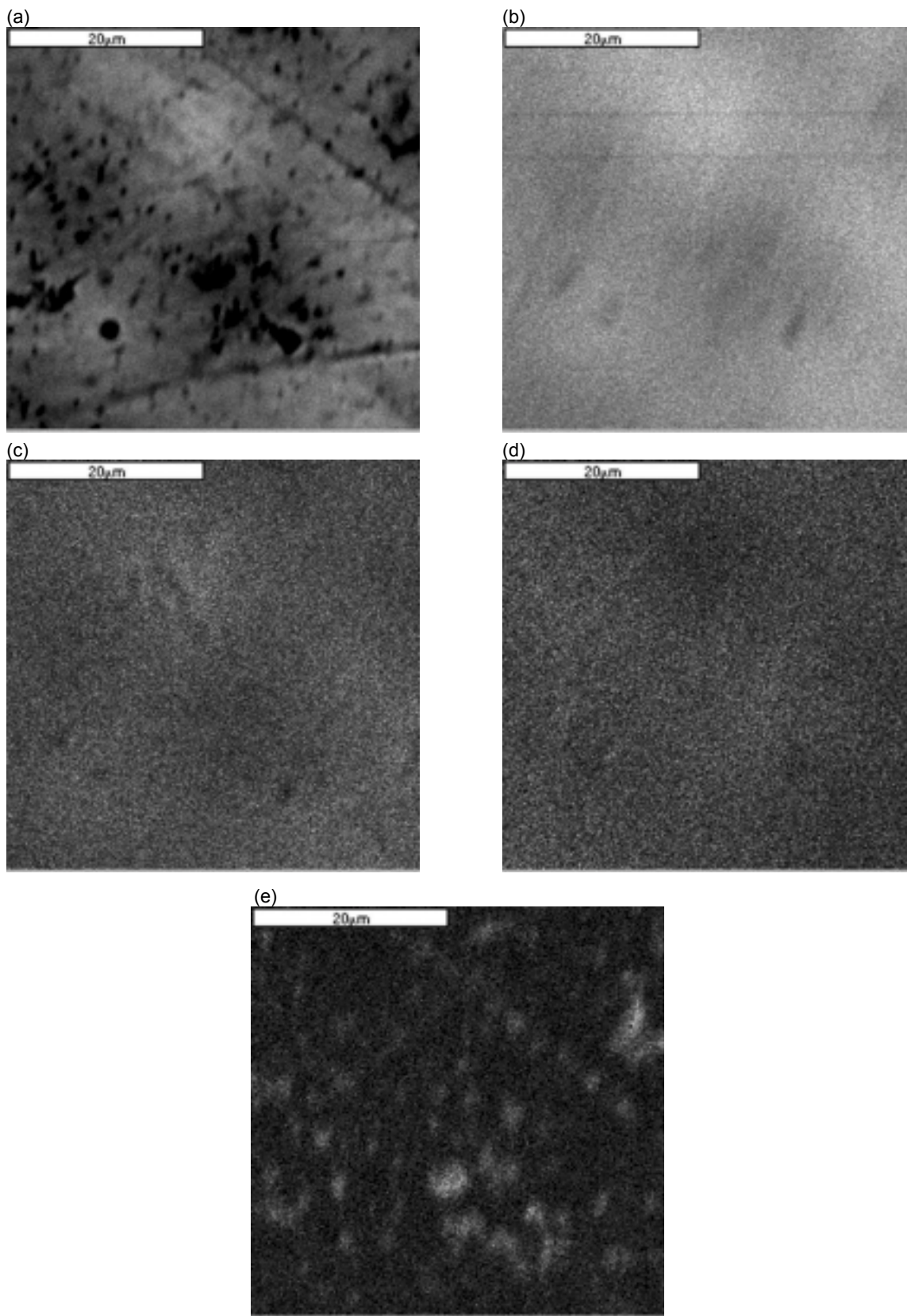


Fig. 4. (a) A backscattered electron image of sample MB008 along with X-ray maps for (b) Pu, (c) Np, (d) Zr, and (e) O.

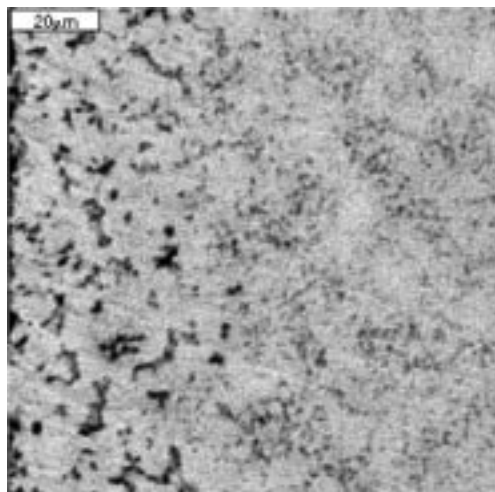


Fig. 5. SEM micrograph of sample MB010 showing a region of the alloy microstructure near the sample periphery with different phase morphologies. The edge of the sample (previously in contact with the quartz mold) is shown at left.

Nitride Fuel

ZrN Matrix Processing Tests

ZrN pellets can typically be cold pressed to a green density of <75% and additional densification can be achieved with sintering above ~1650°C for –325 mesh powders. However, for the desired final density of 85% for the ATW-1 irradiation fuel pellets, it is necessary to mill the starting nitride powders to reduce the particle size, i.e., increase the driving force for sintering by increasing the surface area of the powder. This milling study examined the relation between particle size and distribution to pellet sintering.

ZrN powder (–200/+325 mesh) was milled for various times with and without –325 mesh Pd powder added as a sintering aid. All powder handling and preparation was carried out in a glovebox with a nitrogen atmosphere ($P_{O_2} \sim 1\text{--}3$ ppm). The Pd content for the ZrN/Pd pellets was fixed at 0.3 vol%. 0.2 wt% of polyethylene glycol (PEG) and zinc stearate (ZnST) were added as particle binder and lubricant, respectively. Powders were milled in a SPEX mill with stainless steel milling media (jar and ball). Milling times of 0, 15, 30, and 45 minutes were used for two milling methods: (1) all material milled together (co-mill), or (2) all starting material except Pd milled together then blended with Pd (mill/blend). Pellets were pressed at 500 MPa with an L/D of ~0.75 and fired in a Mo tube furnace under flowing UHP Ar at 1400°C for 20 hrs.

All starting powders were characterized using SEM and particle-size analysis for the morphology and particle-size distribution of the as-received and milled powders. After sintering, dimensional analysis was performed on the pellets and geometric densities were calculated (Fig. 6).

The graph shows that milling provides a higher sintered density; a ~15% increase in density is observed from the as-received ZrN relative to the ZrN milled for 45 minutes. The density seems to plateau above ~15 minutes of milling time using the SPEX mill.

SEM images of the ZrN powders are shown in Fig. 7. Powder agglomeration can be seen in the 30- and 45-minute milled samples accompanying a significant reduction

particle size. Particle size distributions of the as-received and 45-minute milled powders are shown in Fig. 8. The flowability of large diameter agglomerates along with the increased driving force of the small diameter individual particles enables the significant increase in sinterability of ZrN beyond the as-receive materials.

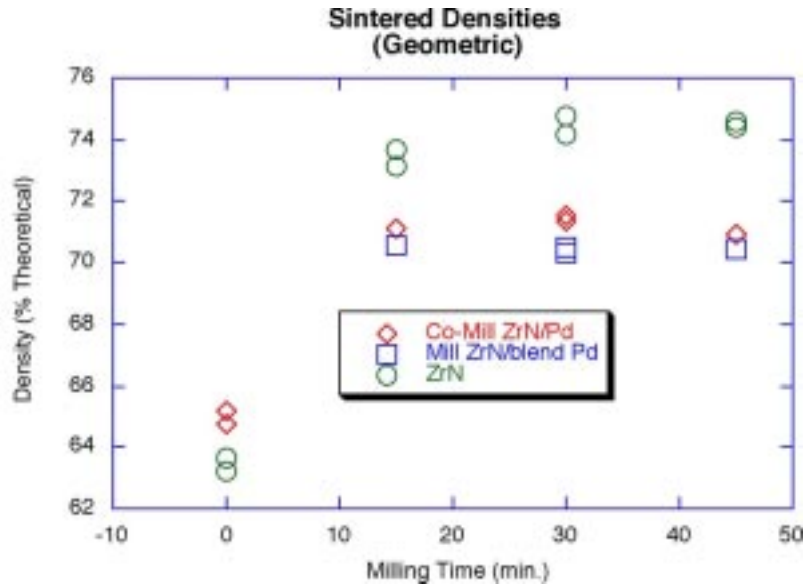


Fig. 6. Geometric densities of ZrN pellets sintered at 1400°C as a function of milling time.

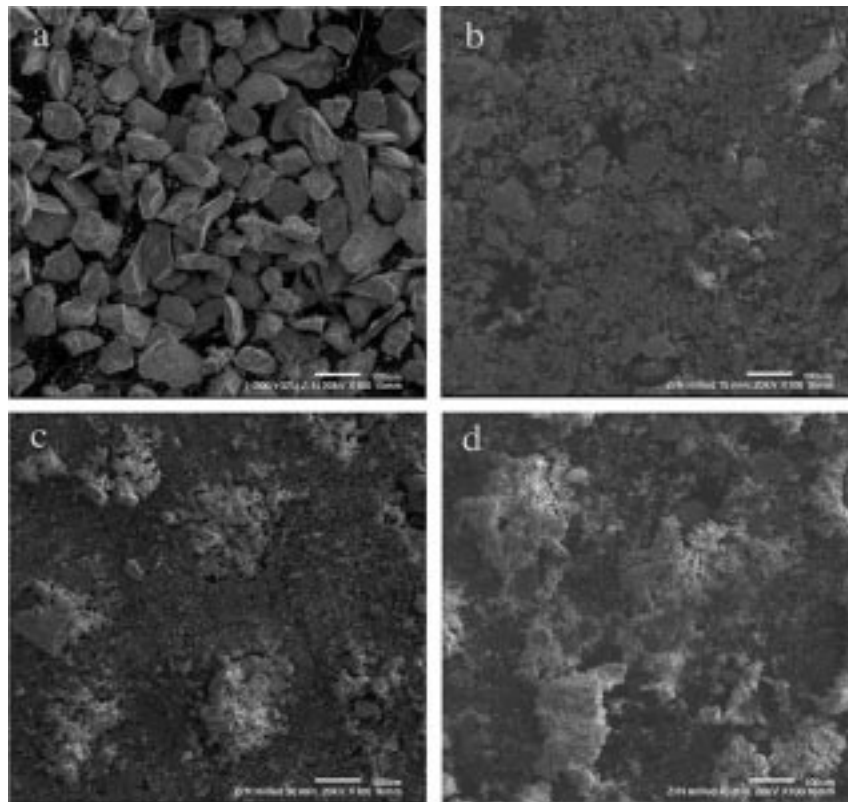


Fig. 7. SEM images of ZrN powder a) as-received –200/+325 mesh, (b) milled 15 min, (c) milled 30 min, and (d) milled 45 min.

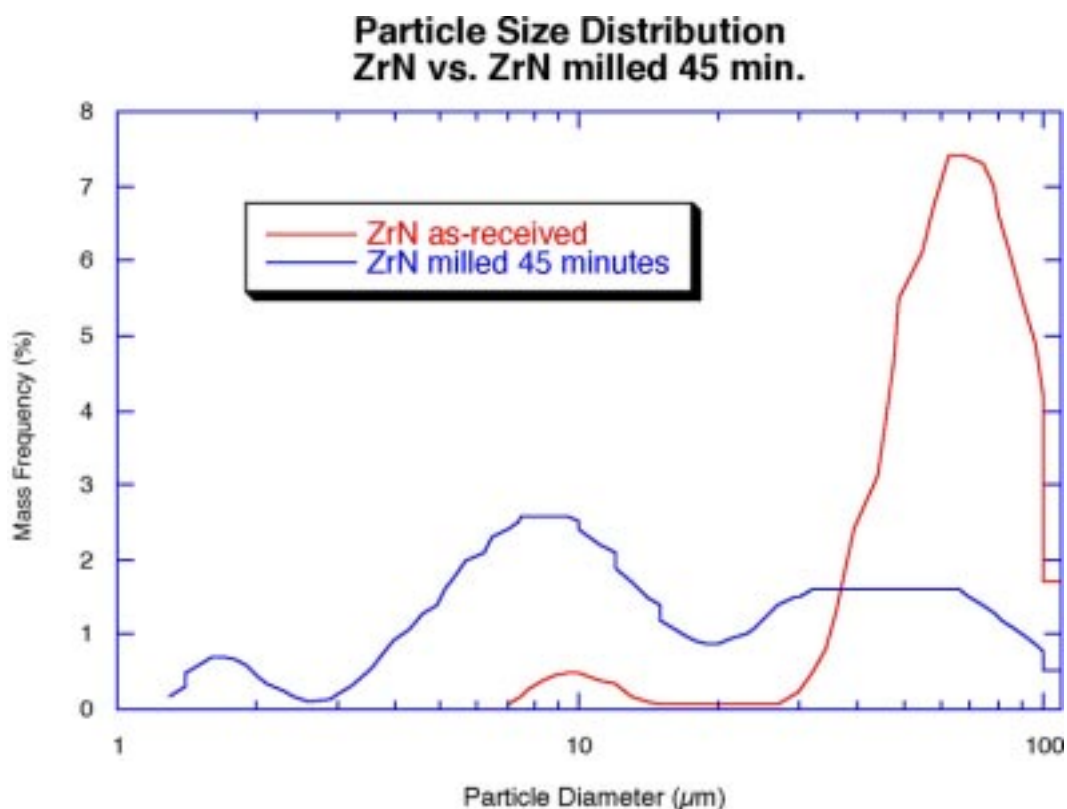


Fig. 8. Particle size distribution plot of as-received -200/+325 mesh ZrN and the same powder milled for 45 minutes.

Lattice Parameter Mismatch (LPM) Study

During the processing of PuN/ZrN fuel pellets, it was observed that the blends of the two nitride powders showed behavior different than that expected from experience on just ZrN and PuN. A surrogate study was initiated to examine the role of reactions between different mononitrides and to establish a methodology for studying the specific reactions in the (TRU)N/ZrN fuels materials. YN was chosen as a surrogate for PuN in this study because of their similar LPM values with ZrN (ZrN/PuN LPM= 6.5%, ZrN/YN LPM= 6.0%). TiN/YN is also examined for comparison since the TiN/YN LPM = 13.2%.

YN, TiN, ZrN, YN/TiN, YN/ZrN - YN/ZrN and YN/TiN powders were studied with the powder mixtures being at a ratio of 50 atomic%. All powders were SPEX milled for 45 min in stainless steel milling media. No sintering aid, binder or particle lubricant was added. Pellets were pressed at 300MPa and sintered in a Mo tube furnace at 1400°C for 10 hours under UHP Ar. After sintering was complete, pellets were ground into powder with a mortar and pestle, re-milled, re-pressed and sintered under the same parameters. Pellets were sintered/reacted a total of four times to promote any reaction between the constituent mononitride powders.

Figure 9 is a plot of the green vs. sintered density values for each pellet composition after the first reaction stage. The negligible densification of the YN/ZrN should be noted relative to the ~5% increase in percent theoretical density for the other materials.

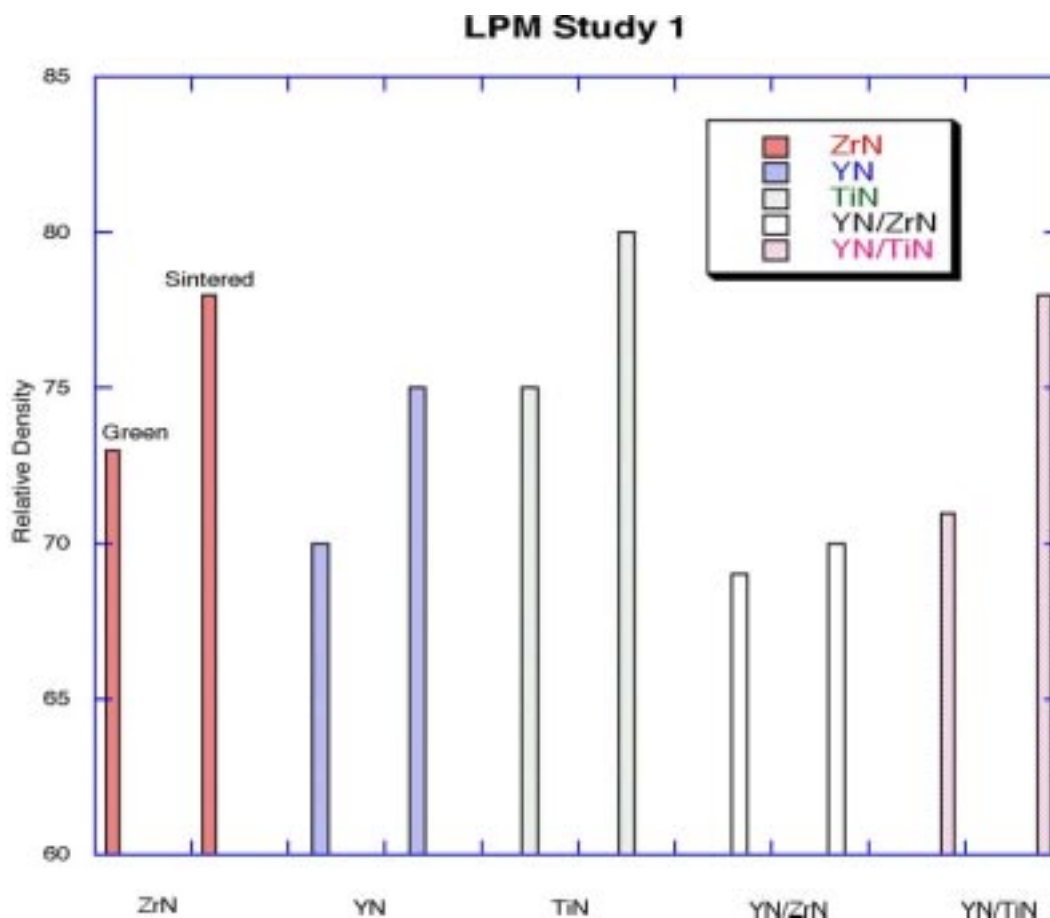


Fig. 9. Geometric density measurements the green state versus sintered state for ZrN, YN, TiN, YN/ZrN, and YN/TiN pellets.

After the final reaction stage, pellets were examined using XRD (in air). The results are shown in Fig. 10 for the YN/TiN and YN/ZrN materials.

No indication of a reaction is observed in the YN/TiN system while there is evidence of reaction in the YN/ZrN (new peaks next to the constituent mononitride peaks). This result is consistent with what has been observed in the PuN/ZrN system and this approach will be developed to establish a method for characterizing reactions in the (TRU)N/ZrN systems.

Thermophysical Properties of Nitride Fuels

Activities to obtain thermophysical property correlations for nitride fuel continued. Recommended materials property correlations developed during the reporting period included heat capacity, thermal expansion and density, and thermal conductivity. The following are a brief summary of the results.

Heat capacity

The heat capacity correlation for ZrN is:

$$C_p = 45.86 + 6.82 \times 10^{-3} T - \frac{5.54 \times 10^5}{T^2}$$

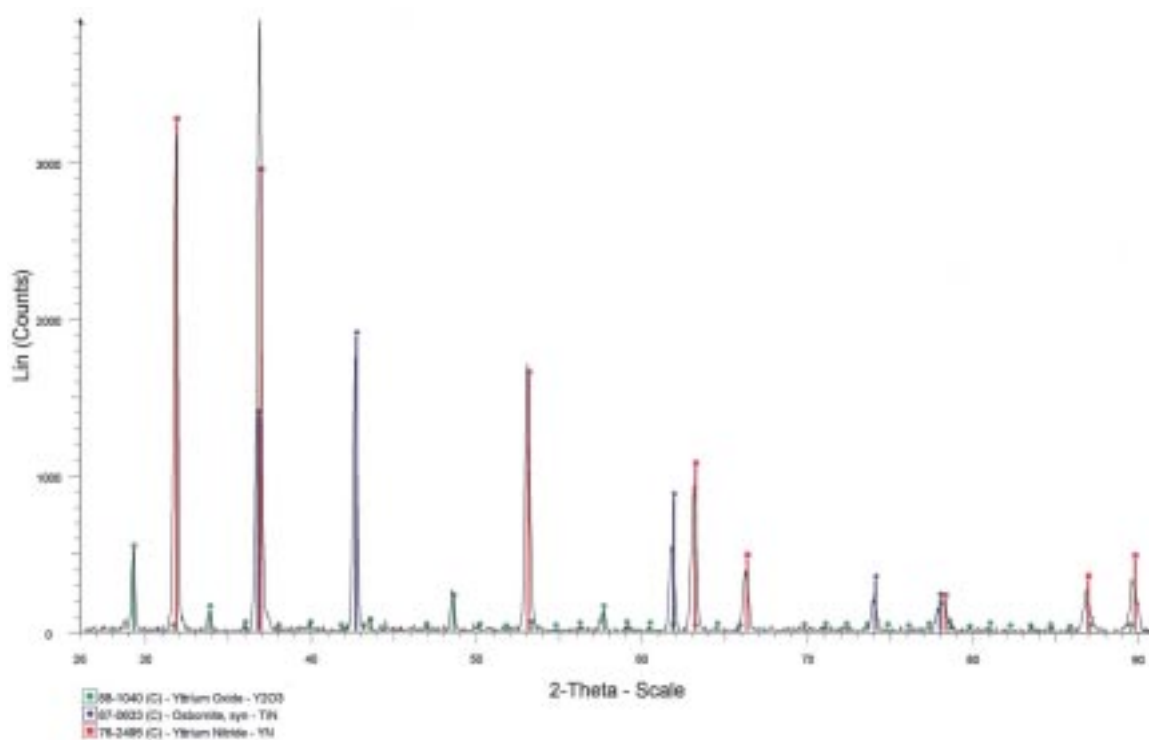


Fig. 10a. XRD pattern for the YN/TiN pellet.

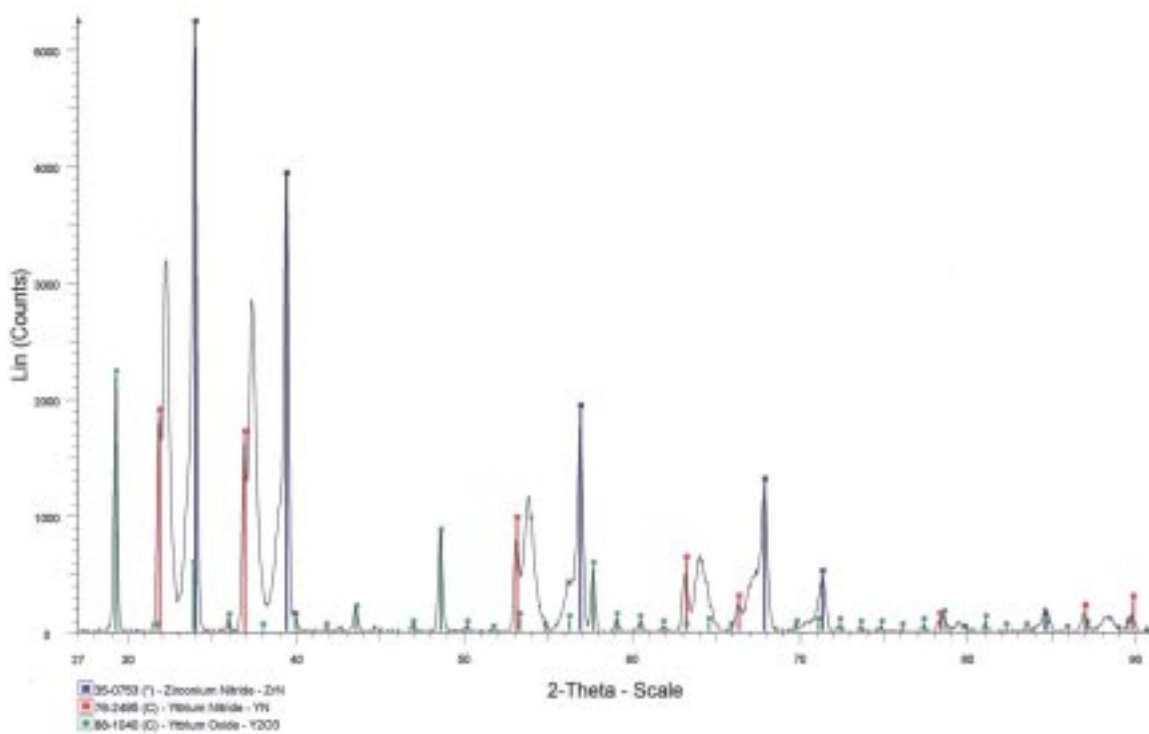


Fig. 10b. XRD pattern for the YN/ZrN pellet.

Here, C_p is in J/K-mole and T in K. The correlation for PuN is:

$$C_p = 44.89 + 1.548 \times 10^{-2} T$$

The heat capacity data of ZrN and PuN solid solutions have not been reported. Therefore, the heat capacity of (Pu,Zr)N is estimated by using the Neumann-Kopp rule,

$$C_p = a_{ZrN} C_{p,ZrN} + a_{PuN} C_{p,PuN}$$

where a is the molar fraction of PuN and ZrN in the solid solution. As an example, the heat capacity of (Pu_{0.2}Zr_{0.8})N is compared in Fig. 11 with those of ZrN and PuN. No heat capacity data are available for TRU nitrides. The correlation for (Pu,Zr)N is therefore recommended for (TRU,Zr)N.

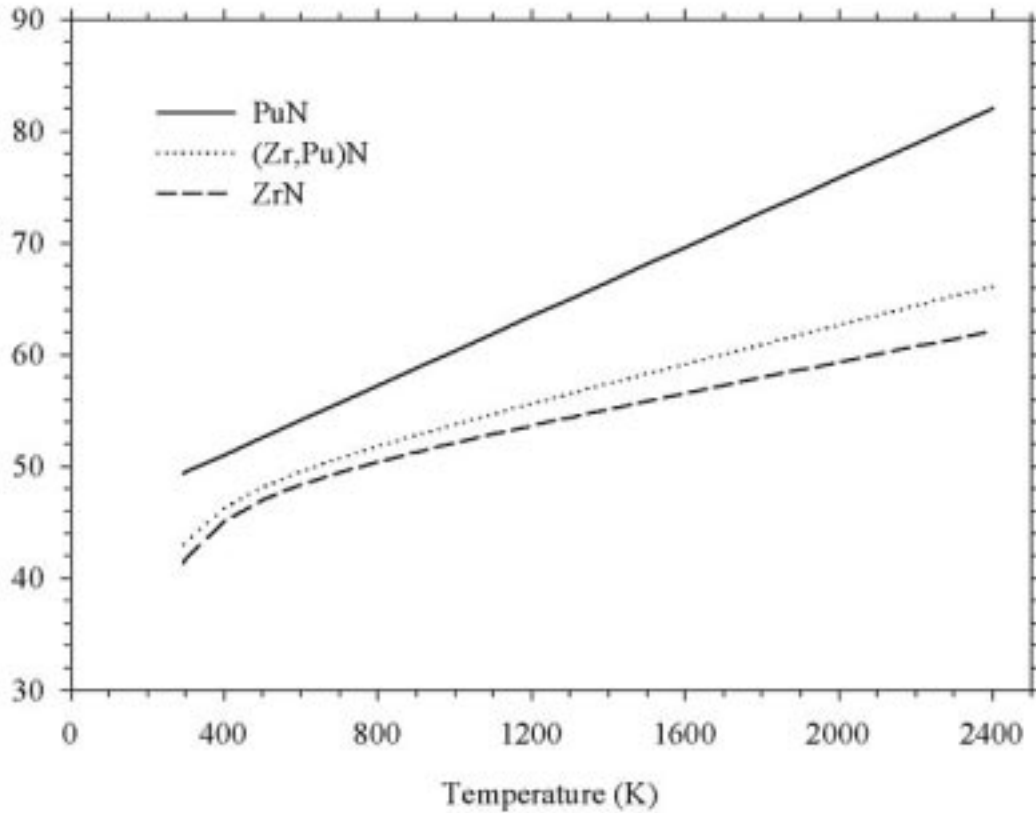


Fig. 11. Comparison of the heat capacity of PuN, ZrN, and (Zr,Pu)N.

Thermal Expansion and Density

The correlation for thermal linear expansion of ZrN is given by:

$$\Delta L / L_o = -0.182 + 5.816 \times 10^{-4} T + 1.333 \times 10^{-7} T^2 - 7.822 \times 10^{-12} T^3$$

where $\Delta L / L_o$ is in % and T in K. The instantaneous linear thermal expansion coefficient is obtained by best fit of the literature data:

$$\alpha_l = 6.572 + 1.825 \times 10^{-3} T - 1.203 \times 10^{-5} / T^2$$

where α_l is in 10^{-6} K^{-1} .

The density of ZrN at room temperature has been reported several places. For the present handbook, 7.22 g/cm^3 is recommended. The density change as a function of temperature can be obtained by using the following relation,

$$\rho = \frac{\rho_o}{1 + \Delta L / L_o} + \frac{1 - (1 + \Delta L / L_o)^3}{(1 + \Delta L / L_o)^3} \rho_o$$

The thermal expansion and density of ZrN are tabulated in Table 1.

Table 1. Thermal Expansion Coefficient and Density of ZrN.

| T (K) | $\Delta L / L_o (\times 10^{-2})^a$ | $\alpha_l (\times 10^{-6} \text{ K}^{-1})^b$ | $\rho (\text{g.cm}^{-3})^c$ |
|-------|-------------------------------------|--|-----------------------------|
| 293 | 0.000 | 5.705 ^b | 7.220 |
| 300 | 0.004 | 5.783 | 7.219 |
| 400 | 0.071 ^a | 6.550 | 7.205 |
| 500 | 0.141 | 7.003 | 7.190 |
| 600 | 0.213 | 7.333 | 7.174 |
| 700 | 0.288 | 7.604 | 7.158 |
| 800 | 0.365 | 7.844 | 7.142 |
| 1000 | 0.525 | 8.277 | 7.107 |
| 1200 | 0.694 | 8.678 | 7.072 |
| 1400 | 0.872 | 9.066 | 7.034 |
| 1600 | 1.058 | 9.445 | 6.996 |
| 1800 | 1.251 | 9.820 | 6.956 |
| 2000 | 1.452 | 10.192 | 6.914 |
| 2200 | 1.659 | 10.562 | 6.872 |
| 2400 | 1.874 | 10.931 | 6.829 |

a: For example, this value should read as $\Delta L / L_o = 0.071 \times 10^{-2}$ at $T = 400 \text{ K}$.

b: Instantaneous coefficient of linear expansion. This value reads as $\alpha_l = 5.705 \times 10^{-6} \text{ K}^{-1}$ at 293 K .

c: Calculated based on $\rho_o = 7.22 \text{ g/cm}^3$ (at $T_o = 293 \text{ K}$).

The linear thermal expansion of PuN (in %) is:

$$\Delta L / L_o = -0.342 + 1.154 \times 10^{-3} T + 5.561 \times 10^{-8} T^2 - 1.205 \times 10^{-11} T^3$$

The coefficient of linear thermal expansion is:

$$\alpha_l = 8.861 + 2.324 \times 10^{-3} T$$

The room temperature density of PuN is 14.235 g/cm^3 . The temperature-dependent density change is given in Table 2.

Table 2. Thermal Expansion Coefficient and Density of PuN

| T (K) | $\Delta L/L_0$ ($\times 10^{-2}$) | α_l ($\times 10^{-6}$ K ⁻¹) b | ρ (g.cm ⁻³) |
|-------|-------------------------------------|---|------------------------------|
| 293 | 0.000 | 9.542 | 14.235 |
| 300 | 0.009 | 9.558 | 14.231 |
| 400 | 0.128 | 9.791 | 14.181 |
| 500 | 0.247 | 10.023 | 14.130 |
| 600 | 0.368 | 10.255 | 14.079 |
| 700 | 0.489 | 10.488 | 14.028 |
| 800 | 0.611 | 10.720 | 13.977 |
| 900 | 0.733 | 10.953 | 13.927 |
| 1000 | 0.856 | 11.185 | 13.876 |
| 1100 | 0.979 | 11.417 | 13.825 |
| 1200 | 1.102 | 11.650 | 13.775 |
| 1300 | 1.226 | 11.882 | 13.724 |
| 1400 | 1.350 | 12.115 | 13.674 |
| 1600 | 1.597 | 12.579 | 13.574 |
| 1800 | 1.845 | 13.044 | 13.475 |
| 2000 | 2.092 | 13.509 | 13.378 |
| 2200 | 2.338 | 13.974 | 13.282 |
| 2400 | 2.581 | 14.439 | 13.187 |

There is no data for thermal expansion of (Pu,Zr)N in the literature. The simple law of mixtures is recommended, i.e., the thermal expansion and the coefficient of linear thermal expansion are estimated as follows:

$$(\Delta L / L_0)_{(Pu,Zr)N} = v_{PuN} (\Delta L / L_0)_{PuN} + v_{ZrN} (\Delta L / L_0)_{ZrN}$$

$$\alpha_{(Pu,Zr)N} = v_{PuN} \alpha_{PuN} + v_{ZrN} \alpha_{ZrN}$$

where v is the volume fraction.

The density of (Pu,Zr)N solid solution is also approximated by the rule of mixtures.

$$\rho_{(Pu,Zr)N} = v_{PuN} \rho_{PuN} + v_{ZrN} \rho_{ZrN}$$

where ρ is the density of the nitride solid solution.

The thermal expansion, the coefficient of linear thermal expansion and the density of (Pu_{0.2}Zr_{0.8})N as calculated are tabulated in Table 3. Figure 12 shows a comparison between the coefficient of linear thermal expansion of PuN, ZrN and (Pu_{0.2}Zr_{0.8})N. Since there is no data in the literature, the methods used for (Pu,Zr)N are also suggested for (TRU,Zr)N.

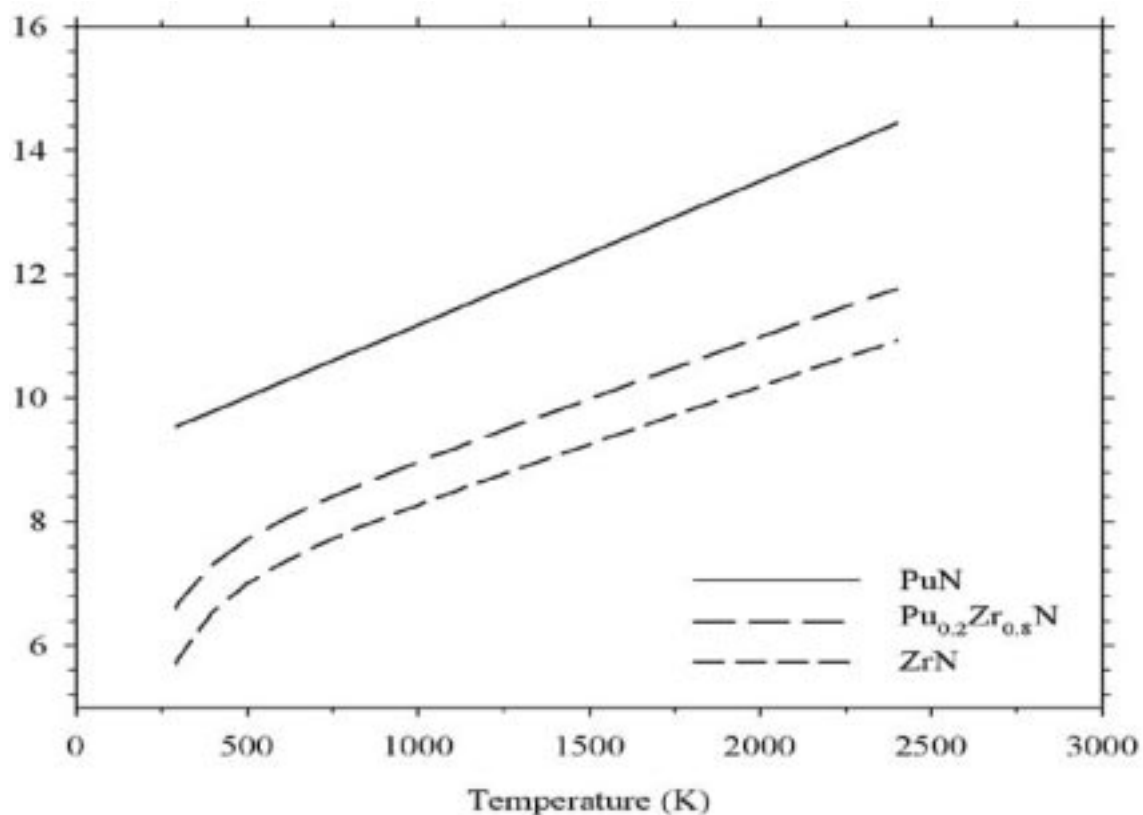


Fig. 12. Comparison of the linear thermal expansion coefficients of ZrN, PuN, and (Pu_{0.2}Zr_{0.8})N.

Table 3. Thermal Expansion, Linear Thermal Expansion Coefficient and Density of (Pu_{0.2}Zr_{0.8})N

| T (K) | ΔL/L ₀ (× 10 ⁻²) | α _l (× 10 ⁻⁶ K ⁻¹) | ρ (g.cm ⁻³) |
|-------|--|---|-------------------------|
| 293 | 0.000 | 6.610 | 8.874 |
| 300 | 0.005 | 6.673 | 8.872 |
| 400 | 0.085 | 7.315 | 8.851 |
| 500 | 0.166 | 7.717 | 8.830 |
| 600 | 0.250 | 8.024 | 8.808 |
| 700 | 0.335 | 8.287 | 8.785 |
| 800 | 0.423 | 8.526 | 8.762 |
| 900 | 0.512 | 8.751 | 8.739 |
| 1000 | 0.604 | 8.968 | 8.715 |
| 1100 | 0.697 | 9.178 | 8.691 |
| 1200 | 0.791 | 9.386 | 8.667 |
| 1400 | 0.986 | 9.792 | 8.617 |
| 1600 | 1.187 | 10.193 | 8.566 |
| 1800 | 1.393 | 10.590 | 8.513 |
| 2000 | 1.605 | 10.985 | 8.460 |
| 2200 | 1.822 | 11.379 | 8.406 |
| 2400 | 2.043 | 11.771 | 8.352 |

Thermal Conductivity

The thermal conductivity of (Pu,Zr)N is not available in the literature, and a method to estimate it is needed. The following correlation is recommended.

$$k_{(Pu,Zr)N} = (1 - \sqrt{1 - x_{ZrN}}) k_{ZrN} + \sqrt{1 - x_{ZrN}} \{x_{ZrN} k_m + (1 - x_{ZrN}) k_{PuN}\}$$

where

$$k_{ZrN} = 1.423 + 2.402 \times 10^{-2} T - 6.404 \times 10^{-6} T^2,$$

$$k_{PuN} = 6.906 + 7.653 \times 10^{-3} T - 2.011 \times 10^{-6} T^2,$$

$$k_m = -8.432 + 14.438 x_{ZrN} + 0.014 T - 1.957 \times 10^{-6} T^2 - 1.549 \times 10^{-3} x_{ZrN} T,$$

and x_{ZrN} is the molar fraction of ZrN in (Pu,Zr)N.

The predicted result by the model is compared with ZrN and PuN data from the literature and plotted in Fig. 13. At lower temperatures, the solid solution thermal conductivity is lower than that of PuN due to the increased impurity effect at low temperatures.

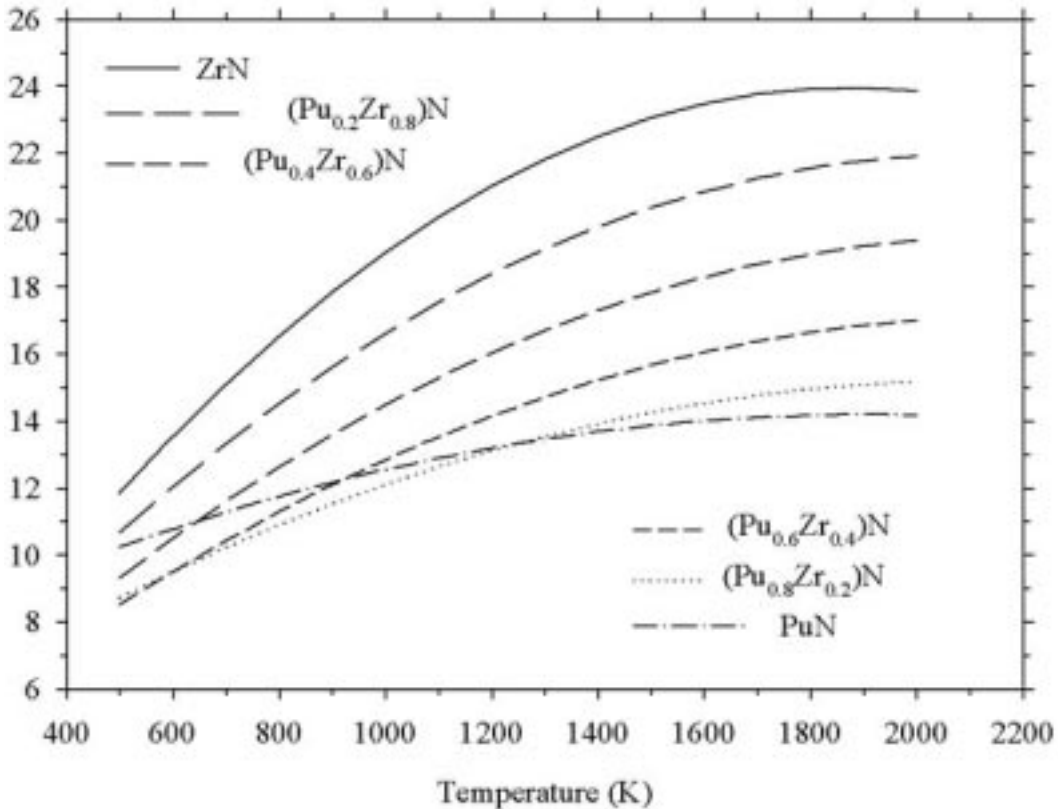


Fig. 13. Thermal conductivity of ZrN, PuN, and (Pu,Zr)N solid solution.

The Maxwell-Eucken equation is suggested for porosity correction:

$$k_p = \frac{1-P}{1+P} k_{TD}$$

where k_p is the thermal conductivity of a matrix including porosity P , k_{TD} the thermal conductivity of the matrix with 100% theoretical density, and P porosity fraction.

Synthesis and Characterization

The primary goal of this portion of AAA fuels development involves understanding the interactions of dysprosium in a zirconium-nitride matrix. Studies carried out by JAERI indicate that the volatility of Dy closely matches that of Am. The initial objective was to determine phase formation in the Dy/ZrN system. Experiments were carried out using a variety of starting materials. One set of experiments examined the reaction between ZrN powder and Dy metal while a separate set of experiments looked at the reaction of pre-alloyed Zr-Dy with nitrogen. In addition to the (Zr,Dy)N experiments, reactions were carried out to synthesize non-stoichiometric dysprosium nitride. Little is known about the dysprosium nitrogen system and no complete phase diagram has been published. Knowing the crystal structures of non-stoichiometric DyN is important in relation to radiation effects studies.

The different materials and corresponding synthesis methods were as follows:

- Dysprosium Nitride (DyN) - Dysprosium metal (-40 mesh) was reacted with nitrogen gas at 1200°C for 24 hours. This reaction was carried out in an alumina boat lined with Zr metal foil to protect against unwanted oxidation.
- Dysprosium/Zirconium Nitride (Dy/ZrN) Pellets - Pellets were prepared via two different routes. One set of pellets was prepared using Dy metal (-40 mesh) and pre-made ZrN powder (-300 mesh). Another set of pellets was prepared using Dy metal (-40 mesh) and Zr metal powder (-300 mesh). In the latter set of pellets, the ZrN matrix was formed during the sintering process. Powders were blended together using a SPEX mill and green compacts were sintered in a tube furnace in alumina boats lined with Zr metal foil. The sintering conditions were 1400°C for 24 hours.
- Zr-Dy Alloys - Zr metal powder and Dy metal powder were mixed together in various atomic ratios in a nitrogen-filled glovebox. The mixtures were then cold-pressed into pellets under 300 MPa of pressure. The Zr-Dy pellets were arc-melted under an Ar atmosphere. In some experiments, the pellets were annealed at 800°C for 12 hours.
- Non-Stoichiometric Dysprosium Nitride (DyN_{1-x}) - Dy metal powder was mixed with pre-made DyN powder in a nitrogen-filled glovebox. The mixtures were then cold-pressed into pellets under 300 MPa of pressure. The pellets were loaded into an alumina boat lined with Zr foil and placed in a flow through furnace under Ar gas. The pellets were heated to 1400°C for 24 hours.

The primary method of structural phase characterization was powder X-ray diffraction using a Bruker D8 powder diffractometer. Reactivity and thermophysical properties were investigated using differential scanning calorimetry (DSC), TA instruments, and thermogravimetric analysis (TGA) on a Shimadzu TGA-50H. Microstructure of Zr-Dy alloys was examined using scanning electron microscopy (SEM).

(Zr,Dy)N Studies

Reactions carried out with various ratios of Dy metal or DyN and ZrN powder did not yield any new line compounds when reacted together at 1400°C for 24 hours. The main method of characterization for these experiments was powder X-ray diffraction. The powder patterns from these reactions all showed two distinct phases, ZrN and DyN. In some cases, zirconia and dysprosia were present as well. Unreacted Dy metal was not found in any of the reactions. In some reactions, however, another set of diffraction lines was found that most likely corresponds to the presence of a (Zr,Dy)N solid solution. The powder diffraction pattern in Fig. 14 is from a reaction of Dy metal with two equivalents of Zr metal. The mixture was then pressed into a pellet and heated under N₂ gas at 1400°C for 24 hours. Lattice parameter calculations using the program "Unit Cell" determined a lattice constant of 4.781 Å for the solid solution. When compared with the lattice parameters for DyN and ZrN, this solid solution is a positive deviation based on Vegard's Law. Another experiment involved the reaction of Dy metal with two equivalents of ZrN. The powder pattern from this reaction contains evidence of a similar (Zr,Dy)N solid solution to the one found in the reaction of the two metals. A plot of the lattice parameters for the two solid solutions is shown in Fig. 15.

One set of experiments was carried out where Zr and Dy were alloyed together using arc-melting prior to reaction with N₂ gas at 1400°C for 24 hours. No new compounds or solid solutions were formed in these reactions. Two powder patterns are shown in Fig. 16. The pattern corresponding to experiment "Arc_2" is from a 64/36 at% mixture of Zr/Dy that was not reacted with N₂ gas. The second pattern corresponds to experiment "Arc_5" which contained the same ratio of Zr/Dy but was then reacted with N₂ gas after arc-melting. Based on the powder patterns taken during these studies, it appears that only ZrN and DyN compound formed from the pre-alloyed mixtures. No evidence of a solid solution was found.

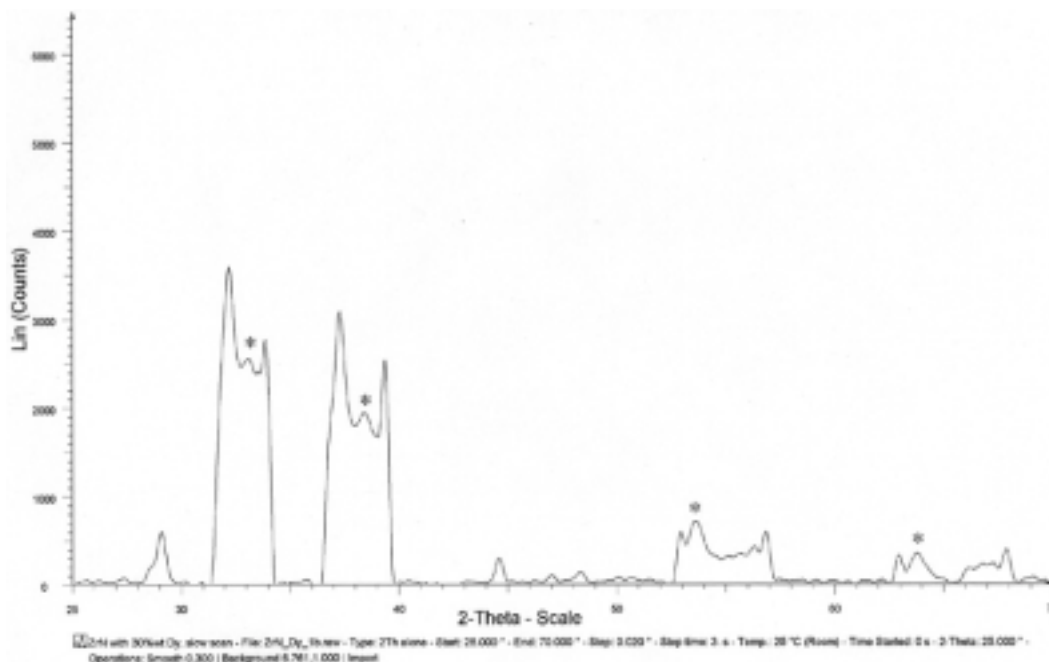


Fig. 14. Powder X-ray diffraction pattern of Dy + 2 Zr heated to 1400 °C for 24 hours. The starred lines belong to the proposed (Zr,Dy)N solid solution.

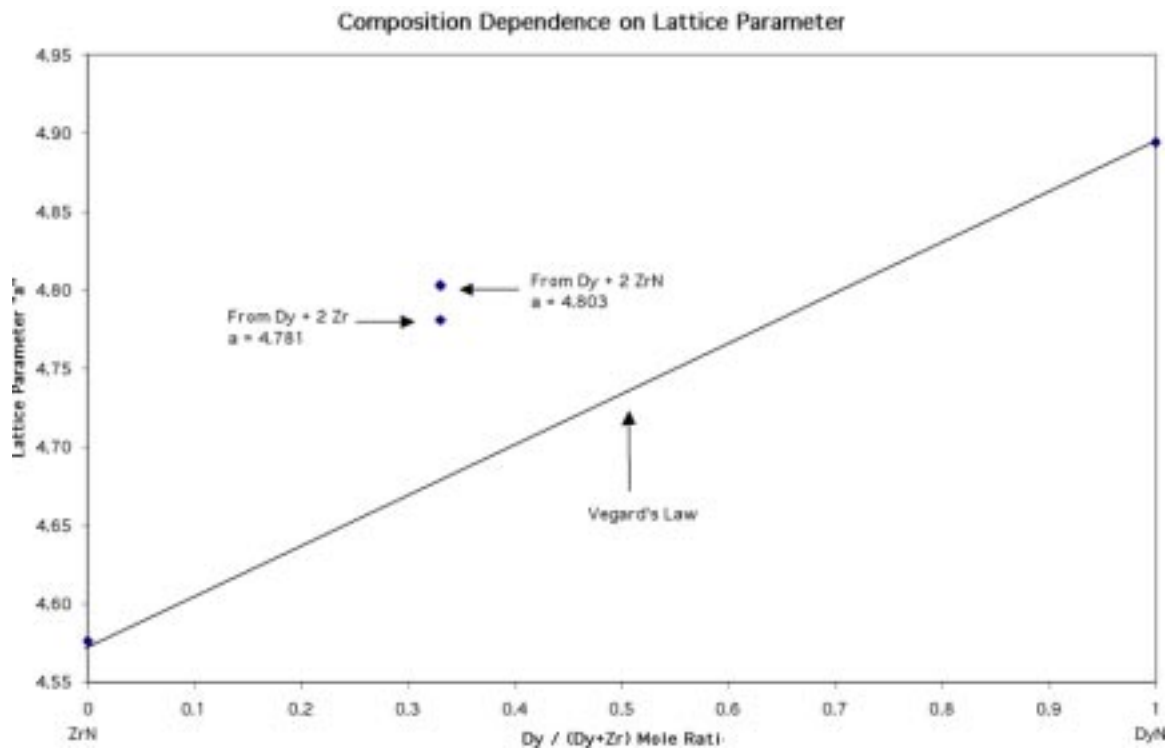


Fig. 15. Composition dependence of lattice parameters in the (Zr,Dy)N system.

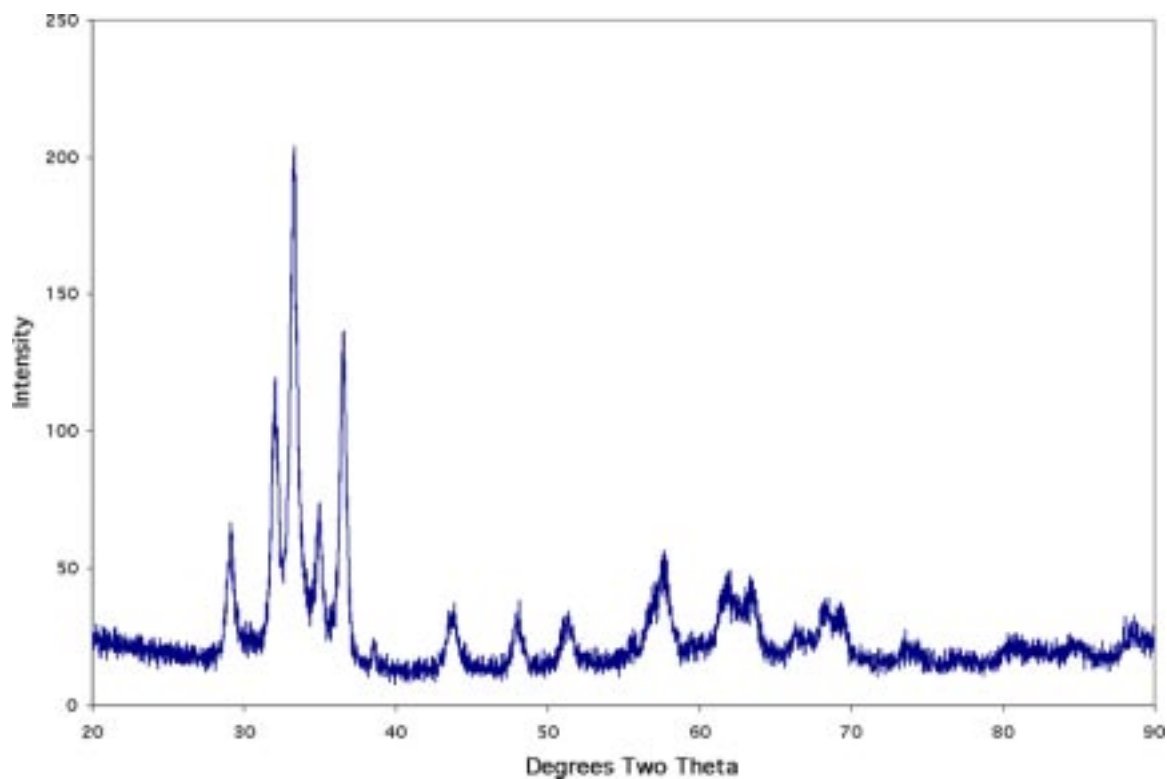


Fig. 16a. Powder diffraction pattern of a 64/36 at% Zr/Dy arc-melted button. All of the diffraction lines correspond to either Zr metal or Dy metal.

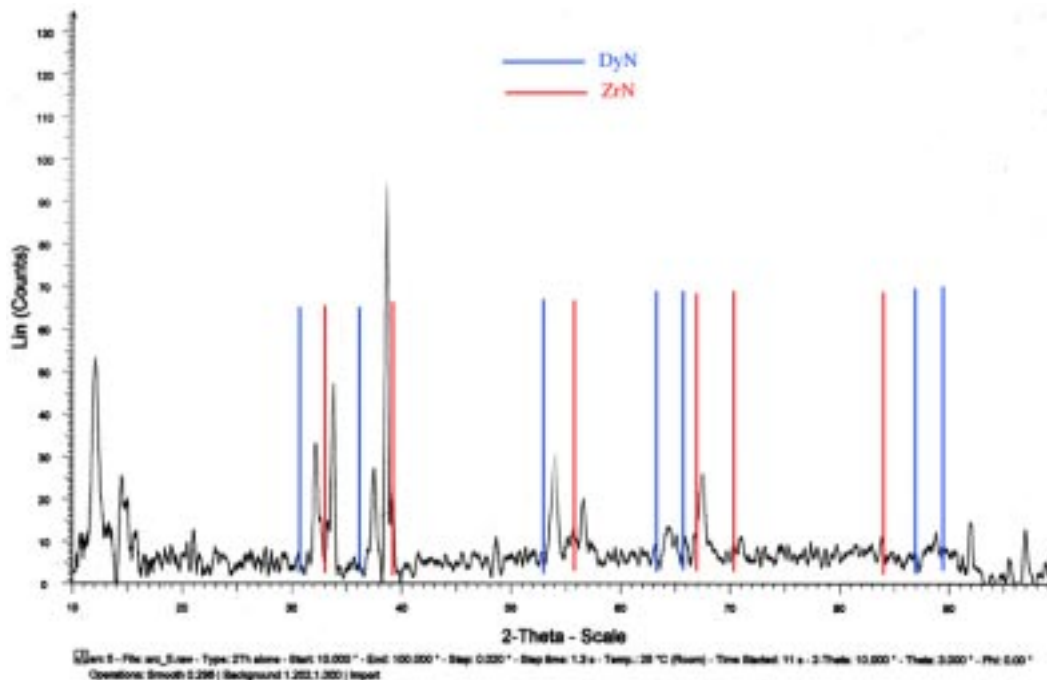


Fig. 16b. Powder diffraction pattern of a nitrided 64/36 at% Zr/Dy arc-melted button. Evidence of unreacted metal is not present.

Thermo-Mechanical Characterization

Preliminary Survey of Mechanical Properties in Sintered ZrN Pellets

A preliminary survey of mechanical properties was carried out in samples taken out of low-density sintered ZrN pellets ($\rho \sim 70\text{--}75\%$) with different amounts of Pd added as a sintering aid. These samples were archived samples from the early stages of ZrN processing and had low densities and significant levels of cracking from an unoptimized pressing procedure.

ZrN pellets (12 mm dia., ~ 3 mm thick) with different Pd contents, 0, 0.3, 1 and 5 wt%, were sintered at LANL and tested at ASU. Samples for metallographic characterization and microhardness testing were cut from these pellets using Wire Electro-Discharge Machining (WEDM). These samples were first polished with SiC paper (600, 800 and 1200 grit) and then finished with 1 μm diamond paste. Samples for fracture toughness were also cut using WEDM in the form of micro-beams. Notches with lengths of approximately one half of the height were also made using WEDM. The surfaces of these beams were polished with SiC paper up to 1200 grit.

Hardness testing was performed in standard microhardness testing apparatus using a Vickers indenter with a load of 500 g. Five indents were made per sample to obtain average values of the hardness. Fracture toughness testing was performed using a screw-driven loading stage under displacement control. The load resulting in fracture was measured using a 100-lb load cell.

Microstructural characterization, measurement of indents for hardness determination, and fractography were performed using Scanning Electron Microscopy (SEM) in a

JEOL JSM-840 equipped with an X-ray detector for Energy Dispersion Spectroscopy (EDS).

Hardness - Relatively low hardness values as compared to other ceramics and nitrides were observed ($\sim 320 \text{ Kg/mm}^2$ for low Pd contents). The presence of porosity is the most likely explanation for the low hardness. Images of individual indents and their relation to the microstructure are shown in Fig. 17. Note the porosity is much smaller than the indents for all compositions between 0–1 wt% Pd. This suggests that the values measured correspond to the “effective” hardness of a composite made of the matrix material and the porosity itself. The collapse of the pores and the propagation of micro-cracks resulting from them can certainly result in lower hardness in these materials.

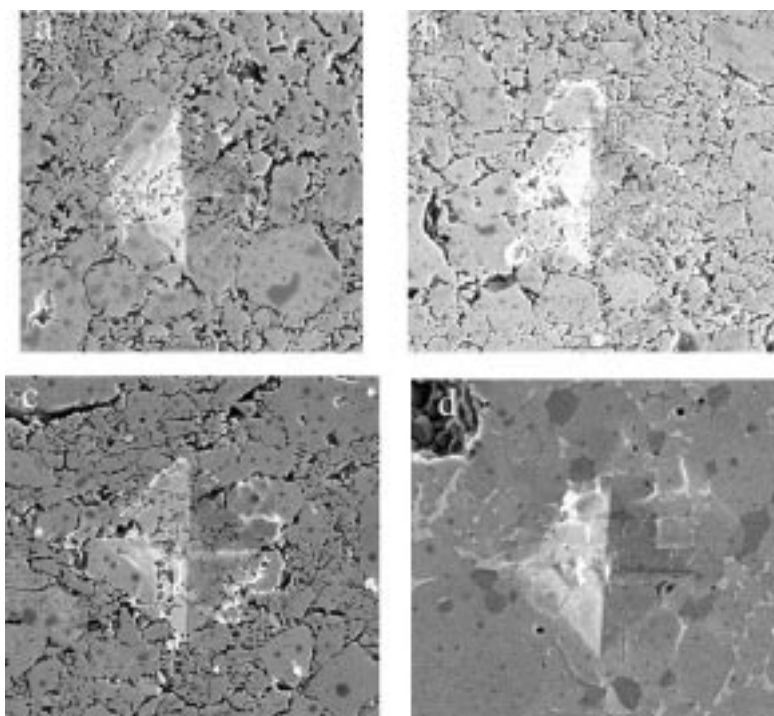


Fig. 17. SEM images of individual indents for samples with different Pd contents. (a) 0%, (b) 0.3%, (c) 1% and (d) 5%. The micron bar in (a), (b) and (c) is $20 \mu\text{m}$, and $10 \mu\text{m}$ for (d).

The situation changes rather dramatically for the material with 5 wt% Pd, as shown in Fig. 17d. Note that the micron bar on that figure represents half of the length of the bar in the other images; therefore, the indent is much smaller than in the other samples for the same applied load. The distribution of porosity is quite different in this sample, since two differentiated length scales can be observed. There is a “local” porosity, represented by round holes to the upper right and lower left of the indent, and a “macro” porosity, an example of which is the large hole at the upper left corner of Fig. 17d. The local porosity is not as uniformly distributed as it was in the other specimens. In addition, there are large spaces in between the “macro” pores. Therefore, the hardness measured in this sample is likely to reflect the actual value for the matrix material rather than to show an “effective” hardness affected by the presence of porosity. A lower magnification picture of the microstructure in the sample with 5 wt% Pd is shown in Fig. 18.

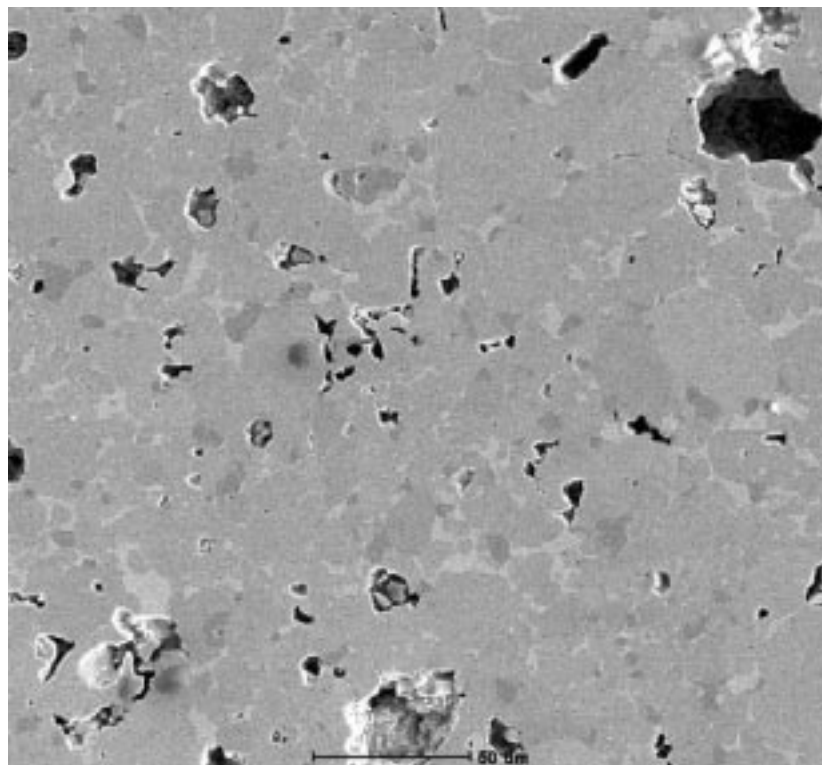


Fig. 18. Porosity distribution in a sample with 5 wt% Pd.

The presence of the two length scales of pores can be seen more clearly in Fig. 18. Large pores are located far apart and small pores are seen scattered throughout the matrix. Large regions seemingly free of porosity can be seen in between. Indents were made on these regions in order to measure the actual properties of the matrix.

The micrograph shown in Fig. 18 also suggests that a second phase might be present in this material. Hence, backscattered electron (BSE) images were collected using SEM to identify the presence of second phases due to the addition of Pd. In this sense, no second phase was detected in the sample with 0 wt% Pd and only a few small scattered particles were found in the specimen with 0.3 wt% Pd, as shown in Fig. 17.

Fracture toughness and Fractography - Fracture toughness was measured using the three-point bending method as per ASTM E-399, using miniature samples due to the small amount of material available. Tests for 0 and 5 wt% Pd were carried out to observe the variation for the two extremes in the microstructure. More samples need to be fabricated to perform more tests to gather statistics of the variation of the toughness within a population of samples; nevertheless, the preliminary results obtained suggest that the addition of Pd can have a measurable effect on the toughness of the material. The results of the experiments indicate that pure ZrN has a toughness of $\sim 2 \text{ MPa}\cdot\text{m}^{1/2}$, whereas the sample with 5% Pd showed a toughness of about $3 \text{ MPa}\cdot\text{m}^{1/2}$. The difference in the microstructure observed between these two samples could have produced a change in the fracture mechanisms. Therefore, the fracture surfaces were examined using SEM in order to elucidate what mechanisms were at work during cracking. An image showing the fracture surface of the specimen with 0% Pd is shown in Fig. 19.

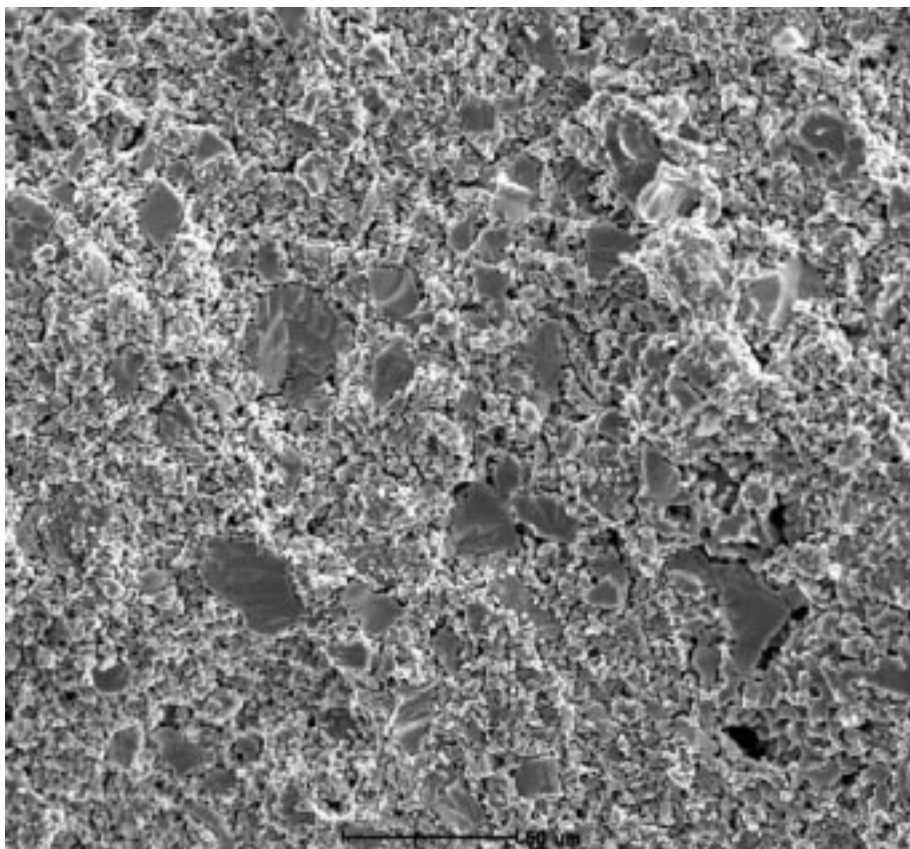


Fig. 19. Fracture surface of a sample with 0% Pd. The micron bar is 50 μm long.

A distinctive feature in the fracture surface shown in Fig. 19 is the presence of two components: a matrix with a high density of porosity and a number of particles embedded in it. The appearance of the matrix in between the particles, along with the micro-cracks that can be seen in it, suggest that fracture in this part of the microstructure occurred due to linkage of pre-existing pores and micro-cracks as the main crack propagated. The large particles, on the other hand, show an appearance typical of brittle fracture. In particular, the ridges that can be observed in some of them indicate that cleavage was operating in this case. The crack was quite flat at the macroscopic level, but it is obviously rough at the micro level. This may explain the value of fracture toughness obtained— $2 \text{ MPa}\cdot\text{m}^{1/2}$; and although obviously low, it is somewhat higher than what was initially expected, particularly for the large amount of porosity present in the material. However, the crack deflections at the micro level, along with the fracture strength of the particles present in the crack path, must have produced enough resistance to fracture to reach the level of toughness measured. Note that some monolithic ceramics and intermetallics can have similar levels of toughness.

The fracture surface of the sample with 5% Pd is quite different and is shown in Fig. 20. Note that the fractions of porous matrix and monolithic particles are now almost opposite to those observed in the sample with 0% Pd. The presence of large pores can also be seen. However, it is clear from the picture that most of the cracking occurs along the particles themselves. Flat facets with and without ridges can be seen, suggesting brittle fracture due to cleavage and intergranular decohesion, respectively. The roughness of the fracture plane is also higher than in the previous

case. All these factors combined can explain the increased toughness of the material. In addition, the presence of a higher fraction of second phase, as found during the microstructural characterization, can lead to larger values of toughness, due to the additional crack deflections when the crack propagates from one phase to another. Nevertheless, the second phase could also contribute to reduce the toughness if it were weaker than the matrix. In that case, the fracture surface could show a higher fraction of second phase than the matrix. A BSE image of the fracture surface taken to elucidate this is shown in Fig. 21.

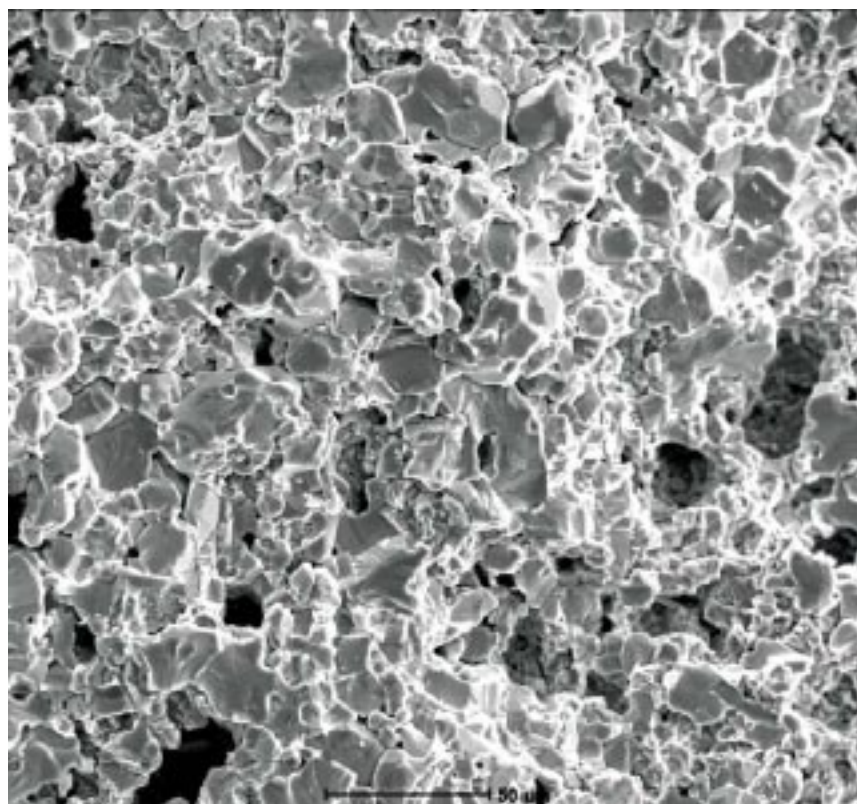


Fig. 20. Fracture surface of a sample with 5% Pd. The micron bar is 50 μm long.

The bright particles in Fig. 19 are made of the Pd-rich phase. The area fraction of these particles does not seem to be qualitatively higher than their fraction in the matrix. In fact, it seems to be qualitatively lower, suggesting that cracks may deflect to avoid the second phase. More studies are necessary to test this hypothesis. The image in Fig. 21 shows quite clearly the ridges typical of cleavage and the flat facets that can usually be seen during intergranular fracture. This variety of fracture mechanisms can lead to toughening as observed in other ceramics, e.g., crack deflections due to differences in moduli and fracture strength between particles and grains can increase fracture resistance.

In summary, the preliminary assessment of the mechanical properties of sintered ZrN pellets leads to the conclusion that the mechanical properties of the ZrN-based fuels may be significantly influenced by both the microstructure/porosity and by any sintering aid additions. Future work on ZrN materials using more optimized processing parameters will be conducted to more fully examine the basic mechanical properties that can be expected for the AAA nitride fuels.

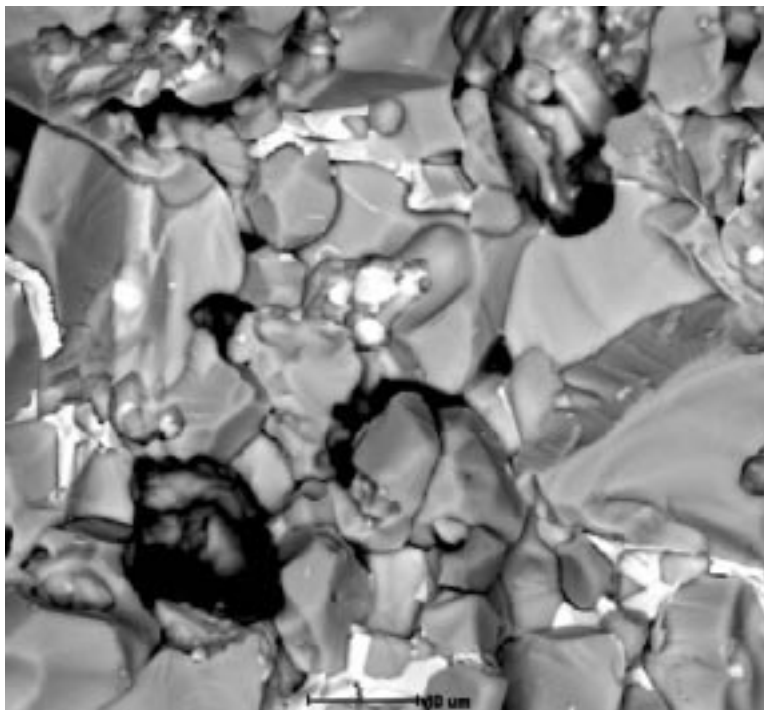


Fig. 21. BSE image of the fracture surface of a sample with 5% Pd. The micron bar is 10 μm long.

Nitride Synthesis (Alternate Methods) – We plan to develop and demonstrate, on a 1-20g scale, fabrication of actinide nitride powders for potential use as TRU fuel kernels. The process will be demonstrated with Pu and U feed materials. Characterization and limited modification of physical properties will be done on potential dispersion fuel matrix material.

Literature surveys and discussions with staff at UCLA indicated that direct metathesis of the trivalent actinide (as a halide) with lithium nitride would be acceptable for small-to-moderate-scale synthesis of the desired nitrides. It has the added benefit of being a potential route to other nitride compounds for coatings and/or matrix materials. Other alternative methods considered involved the use of liquefied ammonia and strong alkali metal reducing agents. These were determined to be of questionable utility in a nuclear facility.

Several batches of UN have been synthesized via direct metathesis of U(III) iodide with lithium nitride. The solution-based reaction goes as expected, although the kinetics are poor at room temperature. The final amorphous powder converts to well-crystallized material at 800°C. Solid-state metathesis (SSM) is more erratic, producing either nicely crystallized UN or a total mess with small changes in reaction conditions. However, the purity and crystallinity of the UI_3 starting material for the SSM reactions has been an issue, so the inconsistent results may arise from variability in the reactants. In both cases, solution and solid-state, the UN product is intermixed with small amounts of other uncharacterized compounds. Methods to either purify the UN or reduce the unwanted side-products are being investigated. However, since Pu is much less likely than U to form sesquinitrides and mixed iodide-nitride species, corresponding metathesis reactions with Pu may not require such extensive clean-up. Thus, the work will transition to the Pu systems as soon as possible.

Work authorization documents to cover these reactions at the CMR building have been completed. However, the glovebox refurbishment has been delayed due to the requirement that the fan to be installed meet ISO 9000 engineering specifications. Meanwhile, facilities in the Alpha Wing of LANL TA-48 are being used to conduct experiments on depleted U. We anticipate conducting Pu reactions at TA-55.

Actinide Nitride Pellet Fabrication - Actinide nitride powders were synthesized by carbothermic reduction (Table 4). The various nitride powders were synthesized using slightly different conditions, but all three lost approximately the weight as predicted, although the NpN weight loss was slightly higher than the predicted amount. It is unclear whether impurities in the starting oxide powder boiled off, or whether Np itself boiled off. After the Np conversion, the inside of the furnace had a larger amount of residue than the runs with the other actinides. X-ray diffraction remains to be done to confirm the presence of nitride.

Table 4. Actinide Nitride Synthesis

| Actinide nitride type | Oxide-to-nitride conversion | Measured weight loss (%) | Predicted weight loss (%) | X-ray diffraction complete? | Measured/literature lattice parameter (Å) |
|-----------------------|-----------------------------|--------------------------|---------------------------|-----------------------------|---|
| PuN | Yes | 17.59 | 17.95 | Yes | 4.901/4.905 |
| NpN | Yes | 20.50 | 17.50 | TBD | NA |
| AmN | Yes | 17.76 | 17.95 | TBD | NA |

The burning of minor actinides may require that they be diluted into some type of matrix. For irradiation tests being scheduled for 2003 at ATR, ZrN has been chosen as the matrix or diluent. The actinide (viz., Pu, Np, and Am) nitride powders will be mixed in different ratios; the content of the actinides in the pellets is always 64 wt%. The ZrN content is 36 wt%. Figure 22 shows the sintering development. Various grinding methods were employed: powders were milled in a SPEX mill either once, twice, or three time (1X, 2X, 3X SPEX) with intermediate sinterings at 1500°C; or ground in a mortar and pestle four times (4X M&P) with intermediate sinterings at 1400°C. Palladium (Pd) as a sintering aid was either added at 0.3 vol% or not; and pure ZrN (ZrN), pure PuN (PuN) and the mixed 64 wt% PuN 36 wt% ZrN powders were sintered (unlabeled samples are 64 wt% PuN 36 wt% ZrN) at temperature from 1400°C–1750°C. The cold-pressed densities for all the materials ranged from about 69%-71%. Interestingly, SPEX-milling the mixed PuN-ZrN powders one time leads to a decreased sintered density (~60% at 1400°C and 1500°C). This decrease in sintered density suggests the reaction of PuN with ZrN that decreases the density. The sequence of milling, sintering, then milling a second time (2X SPEX) shows increased density (going from ~70% cold-pressed density to about 75-85% at temperatures of 1400°C–1675°C). The additional milling of the twice-milled, twice-sintered material did not improve the density (3X SPEX compared to the 2X SPEX). The addition of Pd improved the sintered density for pure ZrN, decreased it for pure PuN, and it remained unchanged for the PuN-ZrN mixture. Milling with the mortar and pestle four times (4X M&P) was very similar to once SPEX-milling, suggesting the comparatively benign milling in a mortar and pestle did not produce this reaction.

While these are initial results, synthesis and fabrication routes are being developed to produce high-density actinide/zirconium nitride pellets. Figure 23 shows PuN-ZrN pellets that have densities and diameters that meet the initial specifications.

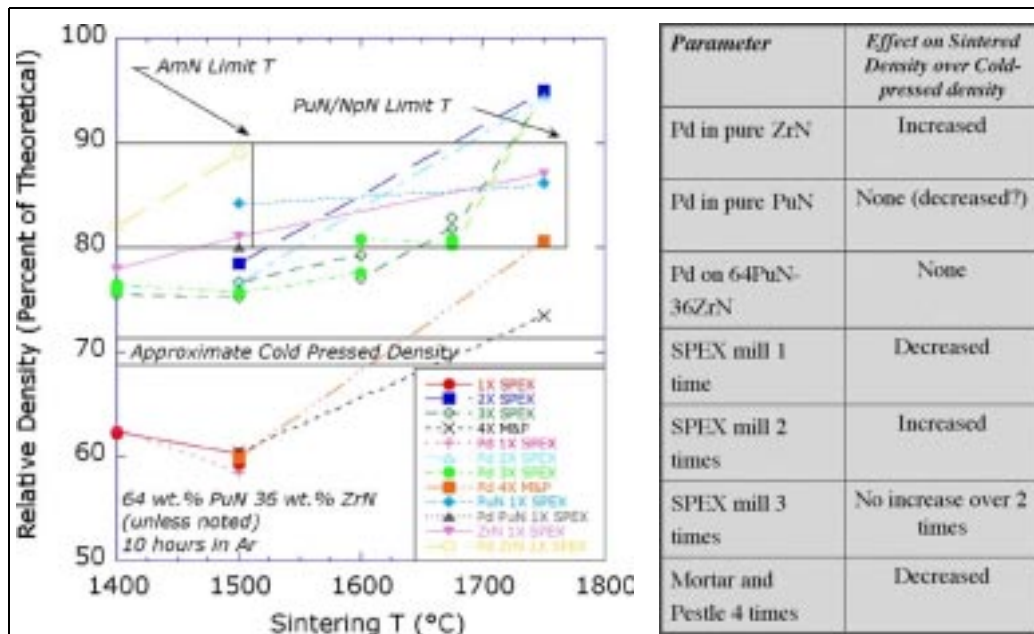


Fig. 22. Sintering conditions for 64 wt% PuN and 36 wt% ZrN.

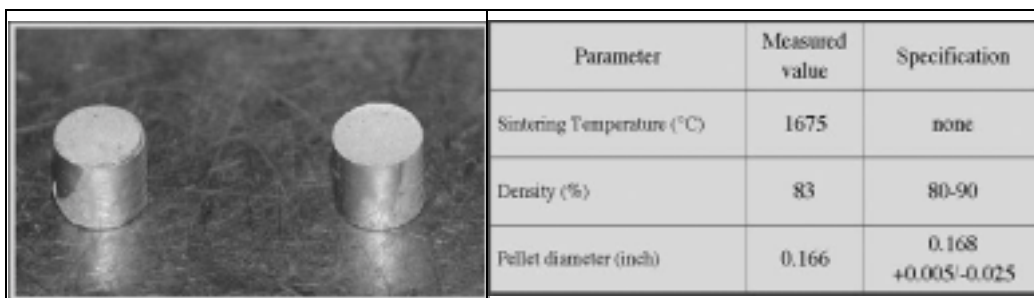


Fig. 23. PuN-ZrN pellets.

Dispersion Fuels

A zirconium matrix cermet (Ceramic-Metal) is one of several potential forms being fabricated for the ATW-1 test series. The fuel particles will be oxide and nitride compounds. The objective in this effort is to develop methods for (1) coating the TRU oxide and nitride particles and (2) the fabrication of experimental cermet fuel pins containing the coated-fuel particles. The coating selected in this task must ensure thermal contact between the TRU microspheres, the matrix, and the fuel rod surface while chemically isolating the fuel granules from the zirconium matrix (filler).

Progress was made in three areas during this reporting period. First, a specialty materials company (Powdermet, Inc.) was identified as having fluidized-bed CVD equipment available that is capable of coating niobium and other refractory metals onto particles as small as 10 μm in diameter. We sent a small batch of 100- μm -dia. yttria-stabilized zirconia (YTZ) microspheres for a coating demonstration before purchase. The YTZ spheres were easily "fluidized" in the Powdermet apparatus. The quartz reactor vessels, a top loading vessel for gaseous and liquid precursors and a side-loading vessel for solid precursors, were ordered from Powdermet with anticipated delivery in July 2002. The remaining components for the CVD process

assembly are being assembled such that we can begin to establish the best and safest precursor among inorganic and organo-metallic choices. The interesting aspect of the side loading CVD reactor design is that sublimation of the solid precursor will occur within the reactor vessel, eliminating the need for a sublimator.

Second, an “oxygen-stabilized” Zr-metal-matrix option is being evaluated as an alternative to microsphere coating. Analysis of our starting zirconium metal powder indicates that it is already slightly oxidized with 0.35 wt% oxygen (~2 atom %) measured by Leco oxygen analysis. The first set of Zr metal-oxide (Zr-ZrO_2) mixtures have been pressed into pellets and fired in a controlled-atmosphere furnace to evaluate the requisite processing variables to generate oxygen-stabilized α -Zr. The pellets exhibited a low cohesive strength. Powder from each pellet was retained for X-ray Diffraction (XRD) and metallographic analysis. Microstructural analysis of the Zr powder indicates oxidation has occurred, but metallic characteristics of the powder appear to be maintained.

Third, progress was made in the area of fabrication. Stainless steel tubes were prepared for consolidation on our ARI Draw Bench. Three (3) basic fuel surrogate mixtures were prepared by mixing microspheres in a Zr-metal matrix: (1) 45- μm WC-Co microspheres, (2) 100- μm -dia. yttria-stabilized zirconia (YSZ) microspheres, and (3) 200- μm -dia. YSZ microspheres. The sample tubes were drawn a maximum of four (4) times with inter-draw anneals in air at 800°C. Metallographic cross sections of the samples were prepared to document dispersion of the oxide fuel surrogate within the matrix (Figs. 24-26).

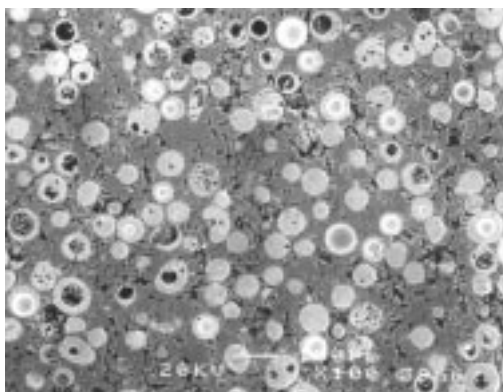


Fig. 24. 45 μm WC-Co dispersed in a zirconium metal matrix.

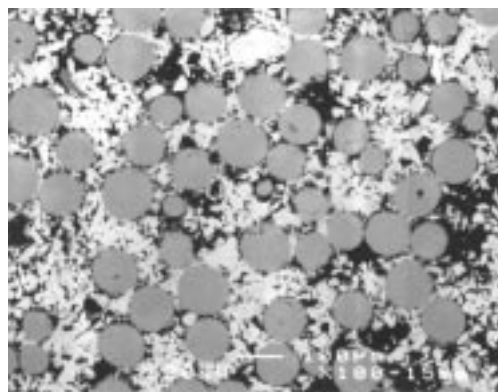


Fig. 25. 100 μm YSZ dispersed in a zirconium metal matrix.

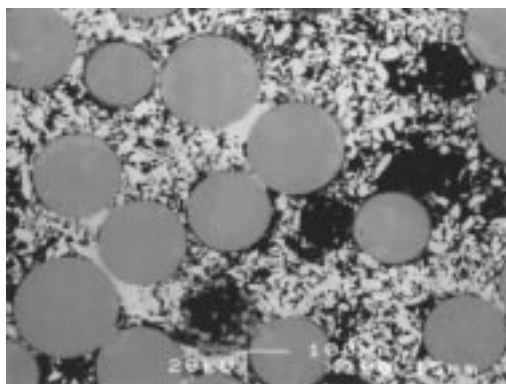


Fig. 26. 200 μm YSZ dispersed in a zirconium metal matrix.

TRISO Fuel

Primary efforts were focused on coating non-radioactive surrogate particles. Commercial sources of hafnia and zirconia microparticles that can serve as kernels were identified and procured. The hafnia particle is the best nonradioactive simulant to mimic the density of an actinide oxide kernel, while the zirconia chemistry is useful because it exhibits low neutron activation, and is proposed as an inert diluent in some applications. Both are excellent refractory materials suitable for TRISO development work. The commercial zirconia was used in the early coating trials.

Dense zirconia microspheres with diameters of 200, 300, 500, and 1000 μm were purchased from Tosoh Ceramics and are being used in the early coating trials. As noted, the chemistry of zirconia is similar to that of the actual kernel materials, as is the thermal expansion. The density of hafnia is greater than for zirconia and is more closely matched to that of the actual fuel materials. Both oxide ceramics have benefits and thus are being used in the experiments to explore and optimize deposition parameters and inspection and classification techniques.

Existing laboratory equipment was modified for making surrogate TRISO particles. New inlet cones and gas-injection assemblies were fabricated for the coating furnace. A series of coating runs were made to establish suitable coating conditions for making surrogate TRISO that would approximate transmutation fuels. Candidate coating conditions were based upon recommendations from General Atomics, literature sources, and a review of ORNL laboratory notebooks from previous coating developments with these exact coaters. A stepwise investigation of each coating layer was necessary. The results of the final coating trial with all 4 layers of the TRISO particle is shown in Fig. 27 as a metallographic section of the particle.

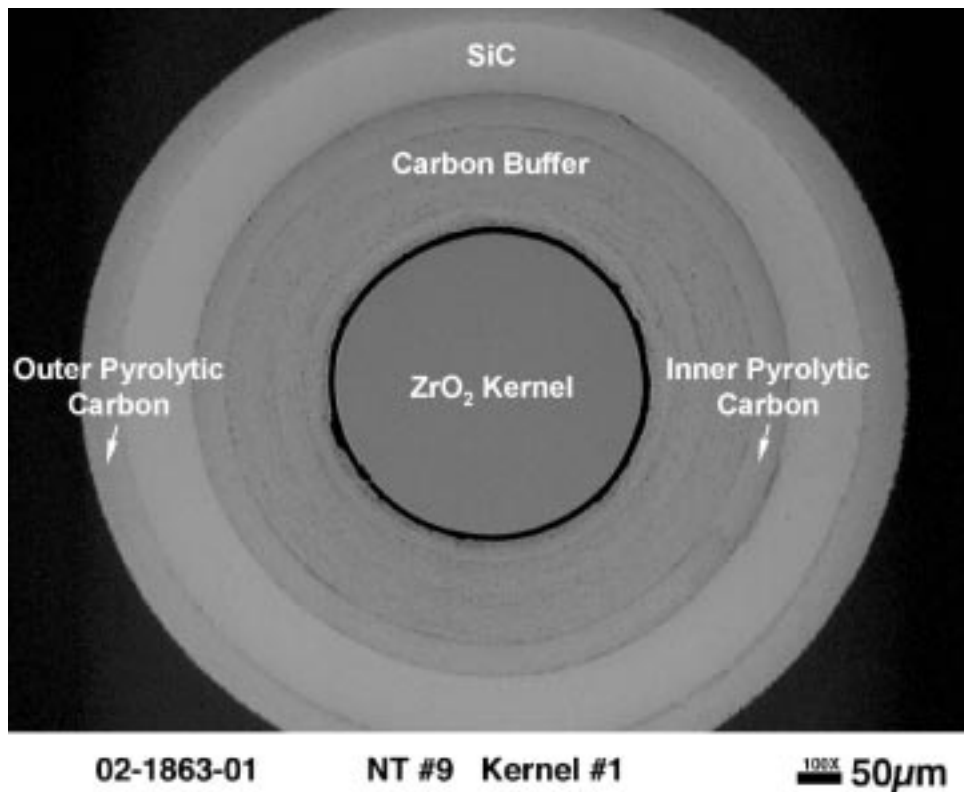


Fig. 27. Micrograph of surrogate TRISO from NT-9 trial.

This micrograph shows many features that are representative of what will be desired in transmutation fuel: a large buffer layer (~100 mm thick) to accept fission product gases, inner and outer dense pyrolytic carbon layers (~ 40 mm each), and a silicon carbide ceramic layer. The thicknesses of the various layers have not been fully optimized, thus are not representative of the preliminary fuel designs. The SiC thickness shown is thicker than anticipated in the preliminary driver and transmutation fuel designs. A laboratory apparatus is being assembled to measure each coating density. Work is continuing on establishing the optimum coating conditions, and a full report will be issued at the end of the fiscal year.

Work continued on establishing kernel-making and coating labs for uranium-bearing coated particles. These should be complete and in operation in the next quarter.

TRISO Fuel Design

A thermo-chemical evaluation of the proposed driver and transmutation TRISO fuels was undertaken. The focus of this evaluation was primarily to assess volatility issues, oxygen management during burnup, and fundamental compatibility issues. Results are generated in the form of monographic Ellingham diagrams for the systems Pu-O-C, and Am-O-C. Preliminary results show that oxide fuels appear to present no particular volatility difficulties. Carbide-containing fuels appear acceptable for Pu, but marginal for Am from the standpoint of volatility. This assessment is being refined and reviewed, and should be issued next quarter. The equilibria arising from SiC and ZrC will also be included in order to assess coating interactions and the possible use of ZrC getters for oxygen management.

We are looking at an alternate design for the transmutation particle (Pu/Np/Am/Cm oxide) with a kernel produced by the ORNL resin-loading process. The kernel will have a low density so its diameter may be larger than the 200 μm initially used for a dense kernel. Kernels with a density of 5 grams/cm^3 and the same metal content as the 200- μm dense kernel require an acceptably low particle packing fraction in the compacts.

A number of design calculations have been performed to better understand the design of the driver particle. These calculations have been performed using the General Atomic PISA code. The changes in coating stresses in particles with a range of IPyC coating thicknesses and a range of SiC coating stresses have been calculated. The calculated stresses in the coating layers were not consistent with coating behavior observed during particle irradiations at fluences greater than about $5 \times 10^{25} \text{ n/m}^2$. It has been concluded that the major discrepancy is in the representation of the irradiation-induced creep in the pyrocarbon layers. The creep coefficient representation appears to be too small and its dependence on coating temperature too strong. We are re-analyzing the pyrocarbon creep coefficient data to determine if other representations of the creep can be obtained if attention is restricted to very isotropic pyrocarbons. The following conclusions have been made based on the particle calculations done to date:

- Coating performance strongly dependent on PyC performance
- PyC performance is a weak function of internal pressure (burnup)
- PyC performance is a strong function of fast neutron fluence
- PyC performance is a strong function of crystallite orientation, irradiation induced creep coefficient, and Poisson's ratio for irradiation-induced creep

- If either the IPyC or OPyC stays intact, the forces caused by pyrocarbon shrinkage are sufficient to overcome internal pressure forces and keep the SiC in compression (SiC does not fail)

TRISO Fuel Development Plan

Work continued on a comprehensive Fuel Development Plan for TRISO-based transmutation. This plan uses the programmatic 5-year Plan as a starting basis. The various development phases defined by the AAA Program have been included in this plan. This plan is in the final phases of review and revision, and should be issued the end of July. Drafts of all sections of the Fuel Development Plan are complete and have been reviewed by program participants. A meeting was held at General Atomics in late June where most of the comments on the drafts were resolved. Authors are now incorporating the comment resolutions into the drafts. The Design Data Needs and the bases for the Fuel Development Plan were also revised based on comments by reviewers.

Pu-Np Kernels Facility

Activities to make ~150 g of resin-loaded kernels containing Pu-Np-Am continued. The basic flowsheet for this operation is contained in Fig. 28. The dissolution of plutonium oxide using the Catalyzed Electrolytic Plutonium Oxide Dissolution (CEPOD) equipment was successfully demonstrated by dissolving 18 grams of the plutonium to be used in the resin-loading process. This dissolution work supports both the CERMET (dispersion) fuels activity and establishing early operations of the Pu/Np kernel line. Our efforts now focus on establishing the anion exchange purification and solution-adjustment equipment needed for both the resin-loading operations and the kernels line. A longer-term activity involves establishing the glovebox for making the plutonium kernels by internal gelation. The focus of this work has been on some of the specialized equipment needs, simplifying the process equipment for glovebox operations, and preparing a conceptual design for the procurement of a glovebox for this process equipment.

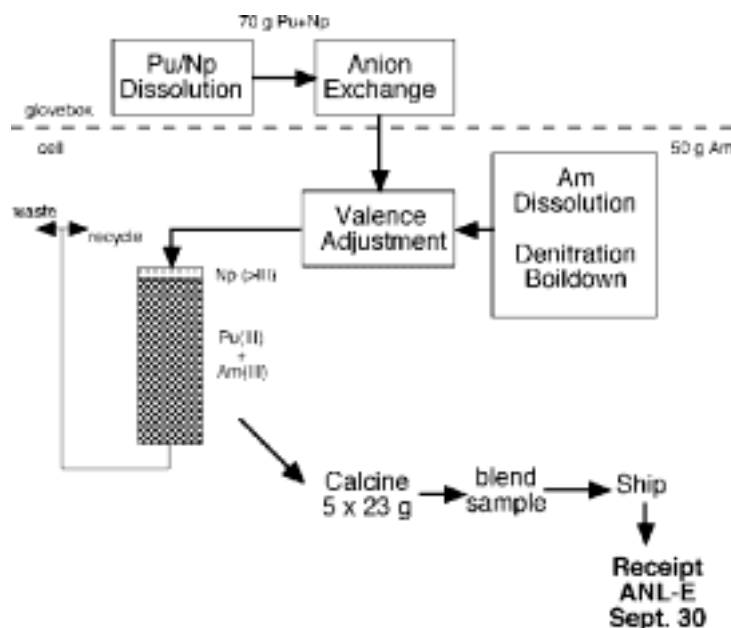


Fig. 28. Resin-loading operations flowsheet.

Support for Coated Particle Separations Operations

We have supported coated-particle separations operations by providing coated-particle information obtained in earlier coated-particle fuel-recycle programs performed at GA for the DOE. This includes both methods for removing compacts from fuel elements and cracking coatings to access the kernels, and dissolving the kernels.

Fuels Irradiation Testing

ATW-1 Irradiation Test

The ATR operating schedule was changed. Irradiation of ATW-1B & ATW-1D will now begin in November 2002.

Detailed pre-test analysis of the ATW-1A, -1B, -1C and -1D irradiation tests continued during this quarter and included an effort to evaluate the radial power profiles inside the fuel rodlets. The ability to accurately predict fuel power is essential in the fuel capsule design for the ATW-1 test series in the ATR. Detailed fission power and temperature profiles are needed to assess the thermal performance. Most of the fission heat generated in the transmutation metal fuel (Pu-12Am-40Zr, rodlet 4) and (Pu-40Zr, rodlet 3) capsules will be transferred radially to the coolant. Therefore, the prediction of the radial fission power profiles over the metal fuel slug at the beginning of life (BOL) and at the end of each effective full power day (EFPD) interval are important for metal fuel performance analysis and capsule design for testing in ATR.

Continuous-energy Monte Carlo is an accurate method to analyze neutron self-shielding effects in fuel burnup calculations. Within each desired region, MCNP-calculated fluxes and reaction rates for neutrons in the energy range from 0–20 MeV are normalized to one group flux and burnup-dependent one-group cross sections (BDOGXS), which are then input to ORIGEN2 isotope buildup and depletion calculations. Following the ORIGEN2 calculations, the calculated isotopic concentrations in each cell are transferred back to the MCNP model for the next static calculation. Throughout the fuel depletion process, UNIX shell scripts handle the data conversion between the two codes. MCNP can calculate the burnup-dependent cross sections that rigorously account for spatial and spectral self-shielding effects. The MCNP Coupling With ORIGEN2 burnup calculation code, MCWO, can analyze the rim effect in the transmutation metal fuel pins. The validated MCWO can compute neutronics characteristics and fuel burnup.

A model of the transmutation fuel test assembly has been developed and incorporated into the MCNP model of the ATR. There are 6 fuel rodlet test sections axially, with the center section at the core mid-plane. Each fuel column is assumed to be 0.158-inches in diameter and 1.5-inches in length. Each fuel pin was subdivided into 36 equal-volume mini-cells for a detailed radial power profile analysis. To reduce the statistical tally uncertainty in the mini-cell, a spherical boundary neutron source was used in the MCNP calculations.

The MCWO-calculated relative fission power profiles of a Pu-12Am-40Zr metal fuel slug (rodlet 4) at beginning-of-life (BOL) is shown in Fig. 29 and at 110 EFPDs (the end of Phase-1 irradiation) with depleted Al-B₄C shroud is shown in Fig. 30. The peak radial local-to-average ratio (LTAR) of the Pu-12Am-40Zr rodlet 4 at BOL is

1.80. The peak LTAR of the Pu-12Am-40Zr rodlet 4 increases to 1.91 at the end of Phase-1 irradiation.

The MCWO-calculated relative fission axial power profiles of a Pu-40Zr metal fuel slug (rodlet 3) at beginning-of-life (BOL) and 110 EFPDs with depleted Al-B₄C shroud are shown in Figs. 31 and 32 respectively. The peak LTAR of the Pu-40Zr rodlet 4 at BOL is 1.79. The peak LTAR of the Pu-40Zr rodlet 4 increases to 2.02 at the end of Phase-1 irradiation.

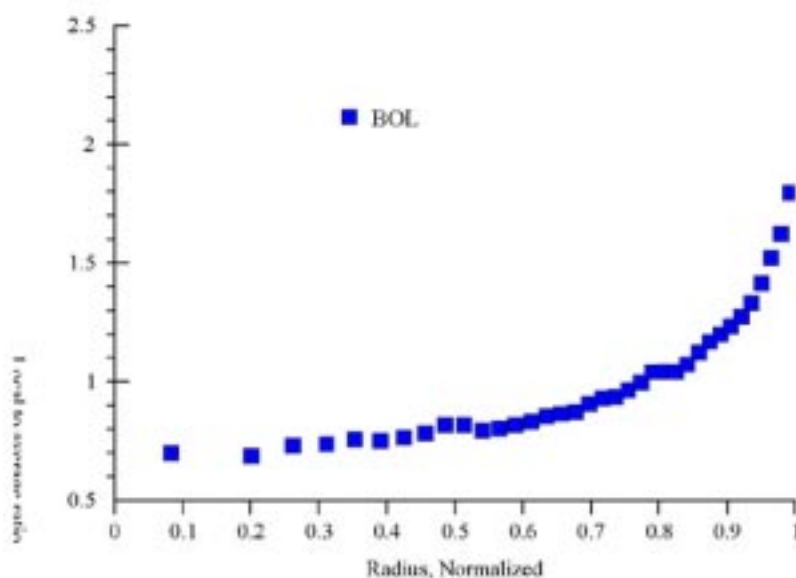


Fig. 29. Relative radial fission power profile for the transmutation metal fuel (Pu-12Am-40Zr) pin at East flux trap position at the beginning of irradiation.

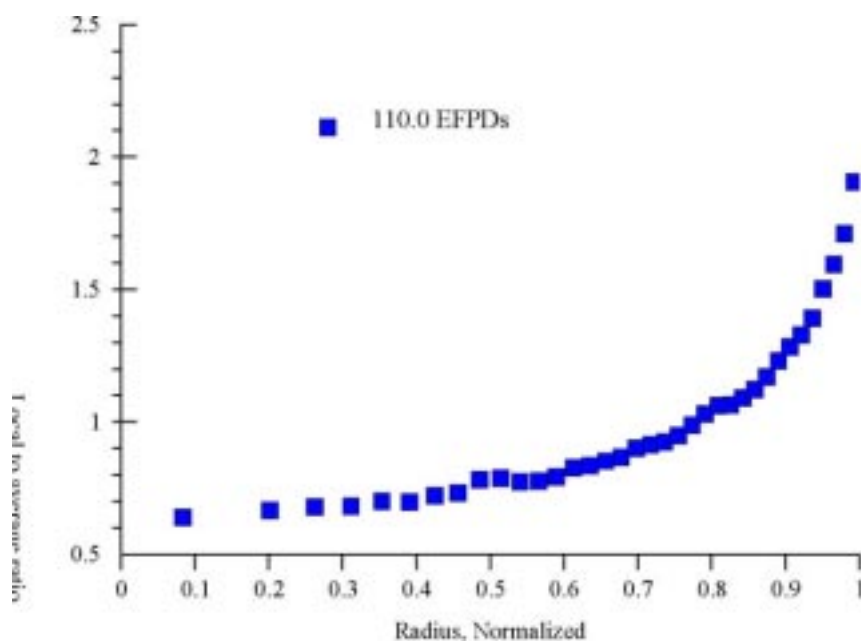


Fig. 30. Relative radial fission power profile for the transmutation metal fuel (Pu-12Am-40Zr) pin at East flux trap position at 110 EFPDs of irradiation.

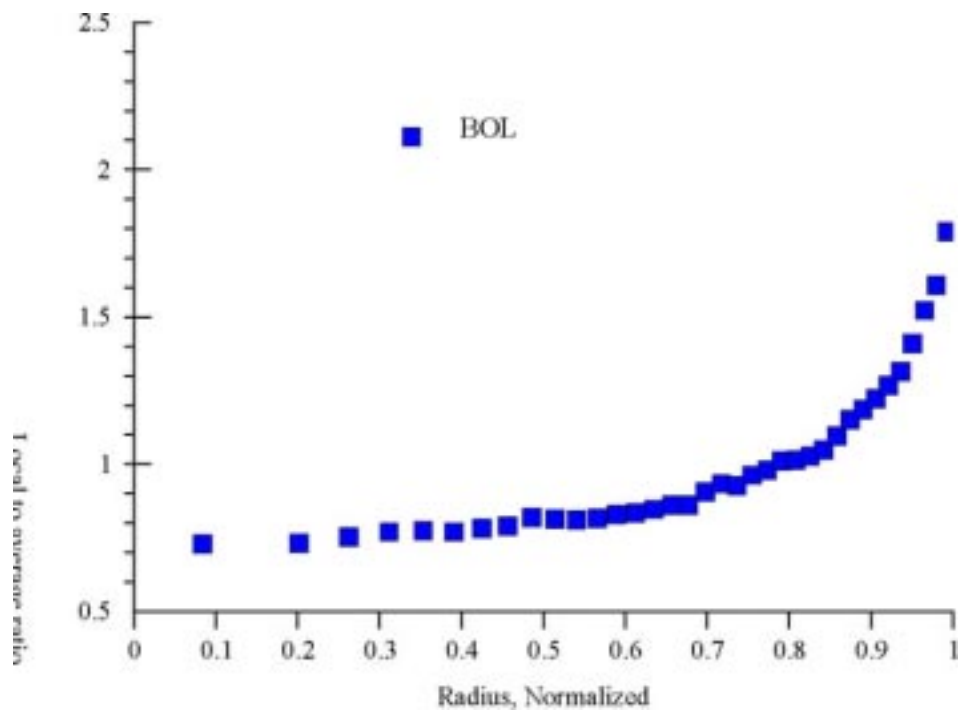


Fig. 31. Relative radial fission power profile for the transmutation metal fuel (Pu-40Zr) pin at East flux trap position at the beginning of irradiation.

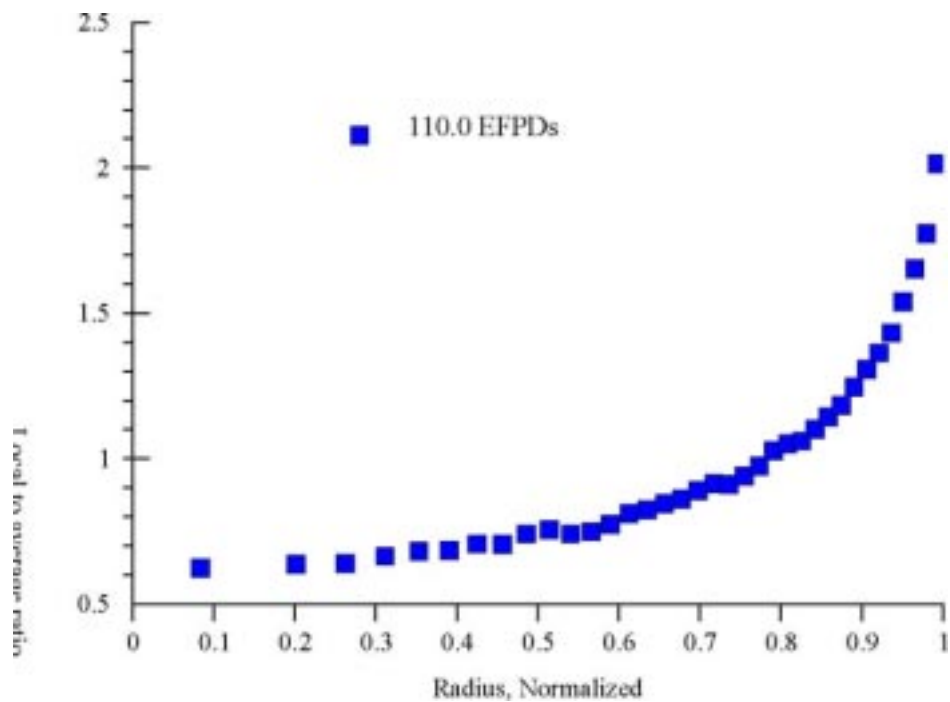


Fig. 32. Relative radial fission power profile for the transmutation metal fuel (Pu-40Zr) pin at East flux trap position at 110 EFPDs of irradiation.

ATR Fast Neutron Flux Booster

A vitally important component of implementing nuclear waste transmutation technology will be development of actinide transmutation fuel forms for second-tier application. Initial scoping fast-spectrum fuel irradiation tests can be conducted in existing U.S. thermal spectrum test reactors, although development beyond the scoping stage will require the availability of a hard spectrum irradiation environment, which is no longer available in this country. Recognizing these needs, scoping calculations have been performed to investigate the viability of an enhanced fast-neutron-flux facility within the Advanced Test Reactor. The flux booster would be designed as a local facility contained within an ATR flux trap. Initial calculations show the possibility of achieving a significant hardening of the ATR neutron spectrum.

Objectives for the Fast Neutron Flux Booster (FNFB) are listed here.

- Hardening of the neutron flux spectrum to achieve a fast neutron flux ($E > 0.1$ MeV) to thermal neutron flux ($E < 0.625$ eV) F/T ratio of at least 6.
- Effective test volume should be ~ 1150 cc (OD=4.0 cm, length=91.5 cm).
- Peak fast neutron flux should be $0.7\text{--}1.0 \times 10^{15}$ n/cm²-sec, and the test volume average fast neutron flux should be $0.5\text{--}0.8 \times 10^{15}$ n/cm²-sec.
- FNFB Test-facility should achieve 20–25 dpa/year in SS specimens.
- The installation of the FNFB should comply with ATR operation constraints and safety regulations.
- The FNFB enhancement fuel lifetime should be about 280 EFPDs.

The ATR core consists of a serpentine and rotationally symmetric fuel assembly about the z-axis of the core center. A passive absorber-type filter, Al-B₄C is currently used for the ATW-1 irradiation test in the actinide-fuel capsule design for the East flux trap position in ATR, to depress the linear heat generation rate (LHGR) in the experimental fuels and to harden the neutron spectrum.

A validated depletion tool is used to analyze the test, which applies the Monte-Carlo code, MCNP, coupled with an isotope depletion code, ORIGEN-2; this is the MCWO methodology. MCWO can provide accurate reactor parameters, such as neutron flux spectrum, isotopic concentrations and compositions, and fission power vs burnup. At the beginning of irradiation, the peak LHGR (Linear Heat Generation Rate) of the metal fuel capsule (Pu-12Am-40Zr) with and without the absorber filter was 890 w/cm and 198 w/cm, respectively, which represents a factor of 4.5 in reduction of LHGR. The Al-B₄C cans also effectively harden the neutron spectrum as shown in Fig. 33. The fast/thermal flux ratio increases from 1.02 to 30.1. However, the peak fast neutron flux of the fuel capsule with and without the absorber filter showed little or no increase in fast neutron flux ($\sim 3.02 \times 10^{14}$ n/cm²-sec) as expected.

The absorber-type Al-B₄C filter can effectively reduce the LHGR by hardening the neutron flux spectrum to meet the design requirement as discussed above. However, to effectively demonstrate transmutation of the LLMA, the AFCL/AAA program will require a higher fast neutron flux in the range of $0.7\text{--}1.0 \times 10^{15}$ n/cm²-sec. An active fuel-type filter was chosen for the purpose of performing scoping calculations to determine the potential to achieve the hardened neutron spectrum required to provide a realistic environment for transmuter fuel testing. The filter used for scoping

calculations was composed of UO_2 (^{235}U 20 wt%) and modeled in the South flux trap position of the ATR. At the beginning of irradiation, the fast neutron flux ($E > 0.1$ MeV) in the fuel capsule, with and without the active fuel-type filter, was 3.0×10^{14} and 8.3×10^{14} n/cm²-sec, respectively, which shows a factor of 2.77 enhancement in fast neutron flux. The active filter effectively hardens the neutron spectrum and provides an environment more suitable for fuels testing, as shown by comparison to a typical Advanced Liquid Metal-cooled Reactor (ALMR) fast neutron flux spectrum as shown in Fig. 33. The fast/thermal flux ratio is about 35. These scoping calculations show that by insertion of an active fuel filter into an ATR flux trap position, a neutron spectrum suitable for irradiation testing of fast-spectrum fuels can be obtained.

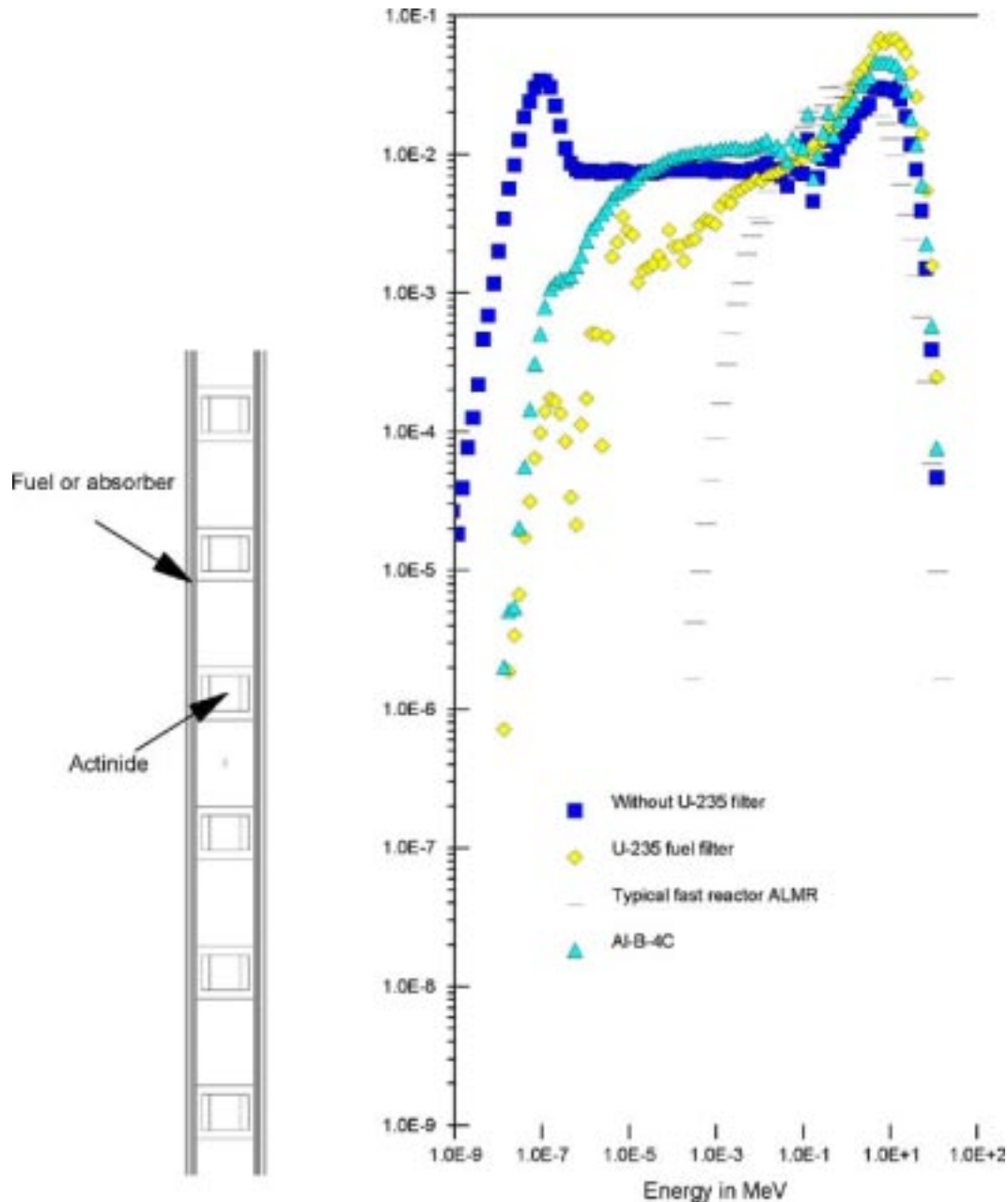


Fig. 33. Comparison of neutron spectrum without filter, with absorber-type Al-B₄C filter, and with active fuel-type ^{235}U (20 wt%) filter to a typical ALMR fast reactor

FUTURIX Irradiation Test in Phénix

Initial power calculations have been completed for the proposed metallic, nitride and oxide fuel pins. The fuel compositions proposed and the designated fuel fabricator is shown in Table 5; the composition and design single dispersion fuel pin has not yet been defined. The results of the preliminary calculations are shown in Table 6.

Table 5. Preliminary Fuel Test Matrix for FUTURIX Experiment in Phénix

| Fabricator | Fuel Compositions |
|------------|---|
| ANL | Pu-27.5Am-5Np-40Zr and Pu-44Am-5Np-40Zr |
| LANL | (Pu _{0.18} ,Am _{0.72} ,Np _{0.10})N-28ZrN and (Pu _{0.45} ,Am _{0.45} ,Np _{0.10})N-28ZrN |
| CEA | (Pu _{0.5} ,Am _{0.5})O ₂ -60MgO |
| ITU | Dispersion and (U,Pu,Am)O ₂ |

Table 6. Preliminary Performance Calculations for FUTURIX Exp. in Phénix

| Fuel Composition | HM Burnup (at%) | Am Burnup (at%) | LHGR (W/cm) | Max. Temp. (°C) |
|--|-----------------|-----------------|-------------|-----------------|
| (Pu _{0.5} ,Am _{0.5})O ₂ -60MgO | 11.6 | 22.7 | 277 | 2261 |
| (U,Pu,Am)O ₂ | 5.5 | 22.7 | 325 | 2239 |
| Pu-27.5Am-5Np-40Zr | 11.3 | 22.7 | 330 | 854 |
| Pu-44Am-5Np-40Zr | 7.1 | 22.8 | 220 | 717 |
| (Pu _{0.18} ,Am _{0.72} ,Np _{0.10})N-28ZrN | 7.1 | 22.8 | 227 | 791 |
| (Pu _{0.45} ,Am _{0.45} ,Np _{0.10})N-28ZrN | 11.2 | 22.7 | 328 | 881 |

The peak estimated linear power for the inert-matrix oxide fuel compositions proposed by the CEA, namely 40 vol% (Pu_{0.5},Am_{0.5})O₂ fuel particles dispersed in an MgO matrix, are too high; resulting calculated centerline fuel temperatures are near melting. Either the fuel particle loading must be decreased, or the experiment position within the Phénix core must be changed, or the Pu isotopics must be degraded. Results for the metallic and nitride fuels appear excellent.

Fuel Performance

Assessment of Radiation Tolerance of ZrN and the Metal Matrix NiAl

Zirconium Nitride (ZrN)

For irradiation damage studies of zirconium nitride (ZrN), we require highly dense samples with surfaces polished to produce very low surface roughness. To achieve this goal, we produced a hot isostatically pressed (HIPed) pellet of ZrN. The pellet was HIPed in a sealed tantalum container at T=1850°C and P=200 MPa. This HIPing procedure resulted in a 1x3-inch pellet with a density near 99% theoretical density.

Figure 34a shows an optical micrograph obtained from a polished surface of one of the ZrN samples used for irradiation experiments. Grains range from ~10 to 50 µm in diameter. The dark spots visible in the micrograph in Fig. 34a are voids. These voids occur both within the interior of grains, as well as at boundaries and triple junctions. Fig. 34b shows an X-ray diffraction (XRD) pattern obtained from a typical polished

ZrN sample. These XRD results demonstrate that the phase purity of the HIPed ZrN pellet is exceptional. It should be noted, however, that a grain boundary phase of unknown structure and composition at some interfaces between grains was detected.

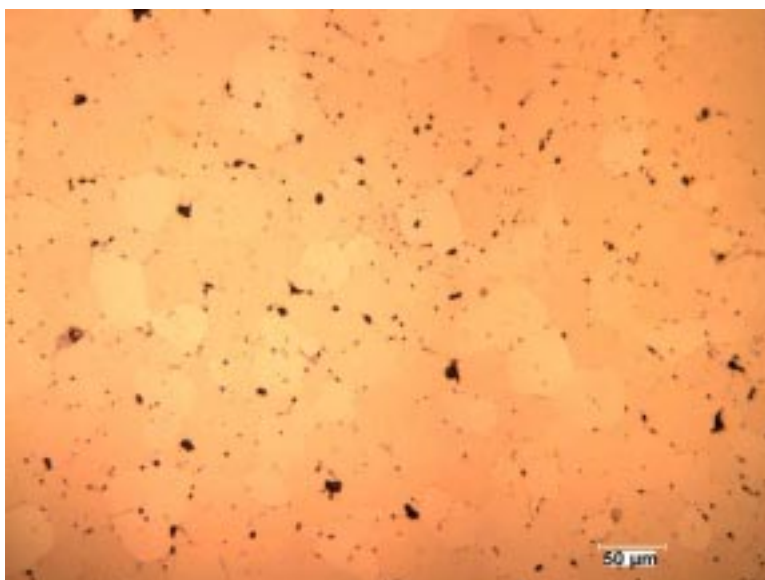


Fig. 34a. Optical micrograph showing the microstructure of the HIPed ZrN pellet.

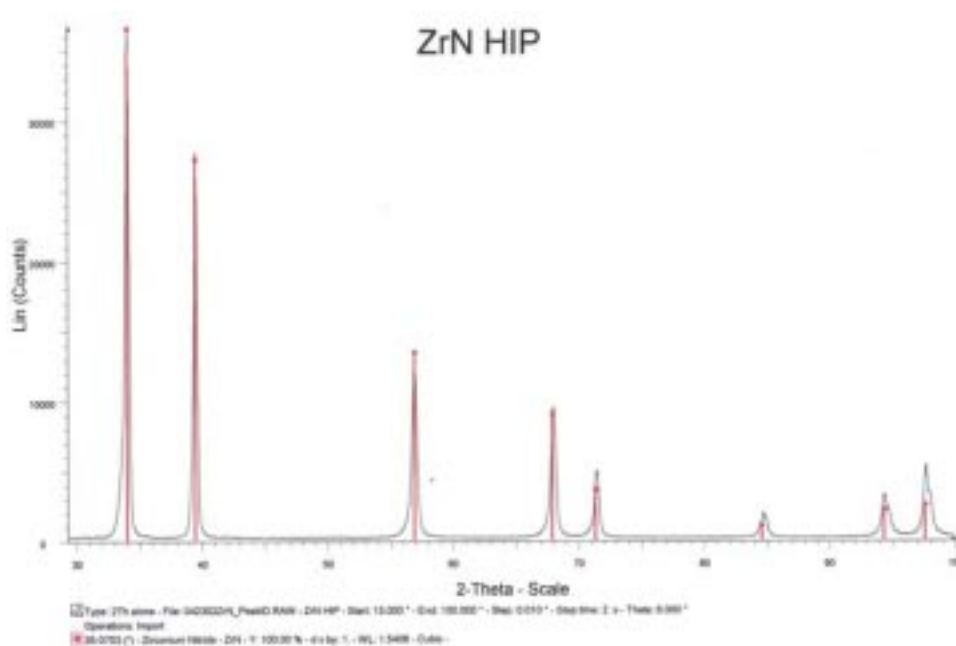


Fig. 34b. X-ray diffraction pattern obtained from a polished section of the HIPed ZrN pellet. Red lines indicate the scattering positions for reflections corresponding to the cubic phase of ZrN (Cu K_{α} radiation).

ZrN samples were irradiated with Xe ions and then implanted with He ions in preparation for He release experiments. The purpose of the Xe ion irradiation was to produce a pre-existing radiation damage state in the ZrN, in order to assess the effect

of radiation damage on He mobility and release. Three sets of samples were implanted with He:

- pristine ZrN with no pre-existing damage;
- ZrN irradiated with a low dose of Xe to produce a peak damage state of ~3.5 dpa (displacements per atom); and
- ZrN irradiated with a high dose of Xe to produce a peak damage state of ~35 dpa.

Figure 35 shows a schematic diagram of the geometry for the Xe and He ion irradiations.

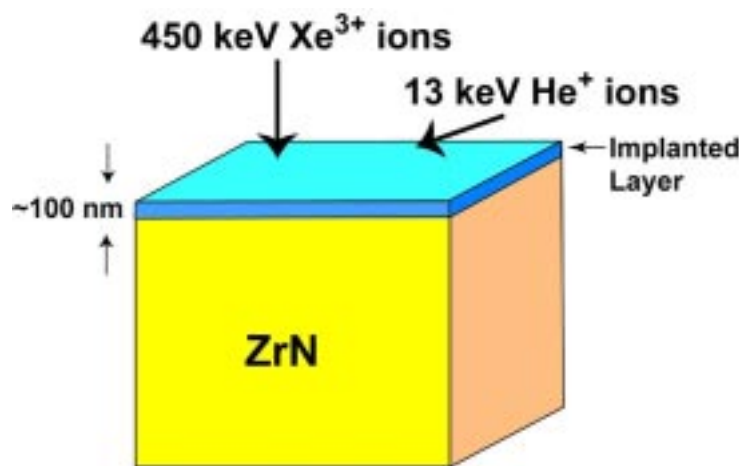


Fig. 35. Schematic diagram of the ZrN sample geometry for Xe and He ion irradiations.

Xe Ion Irradiations - 450 keV Xe^{3+} ions were used for the Xe ion irradiations. Ions were directed at normal incidence relative to the sample surface. This produces a peak in the ZrN displacement damage at a depth of ~500 Å beneath the sample surface (according to Monte Carlo simulations of ion stopping in ZrN). The peak displacement damage under these conditions is ~3.5 dpa per 10^{15} Xe/cm^2 unit of fluence (again based on Monte Carlo simulations). Irradiations were carried out under cryogenic conditions (substrates were maintained at $T \sim 77\text{K}$). Fluences used were $1 \cdot 10^{15}$ and $1 \cdot 10^{16}$ Xe/cm^2 .

He Ion Implantations - 13 keV He^+ ions were used for the He ion implantations. Ions were directed at 60° away from normal incidence (30° with respect to the sample surface) in order to place the peak of the He implantation profile in coincidence with the peak in the Xe ion-induced displacement damage profile (i.e., at a sample depth of ~500 Å). Monte Carlo simulations indicate that approximately 30% of the implanted He is lost to backscattering events under these implantation conditions. All implantations were carried out at cryogenic temperature ($T \sim 77\text{K}$) to a fluence of $1 \cdot 10^{15}$ He/cm^2 .

Figure 36 shows the ion damage profile induced by the Xe ion implantation vs depth beneath the sample surface (based on Monte Carlo computer simulations). Also shown in Fig. 36 is the He ion implantation profile (also based on Monte Carlo). Experimental parameters such as ion energy and beam orientation were adjusted to

produce the almost optimum overlap of the He ion concentration and Xe ion damage profiles shown.

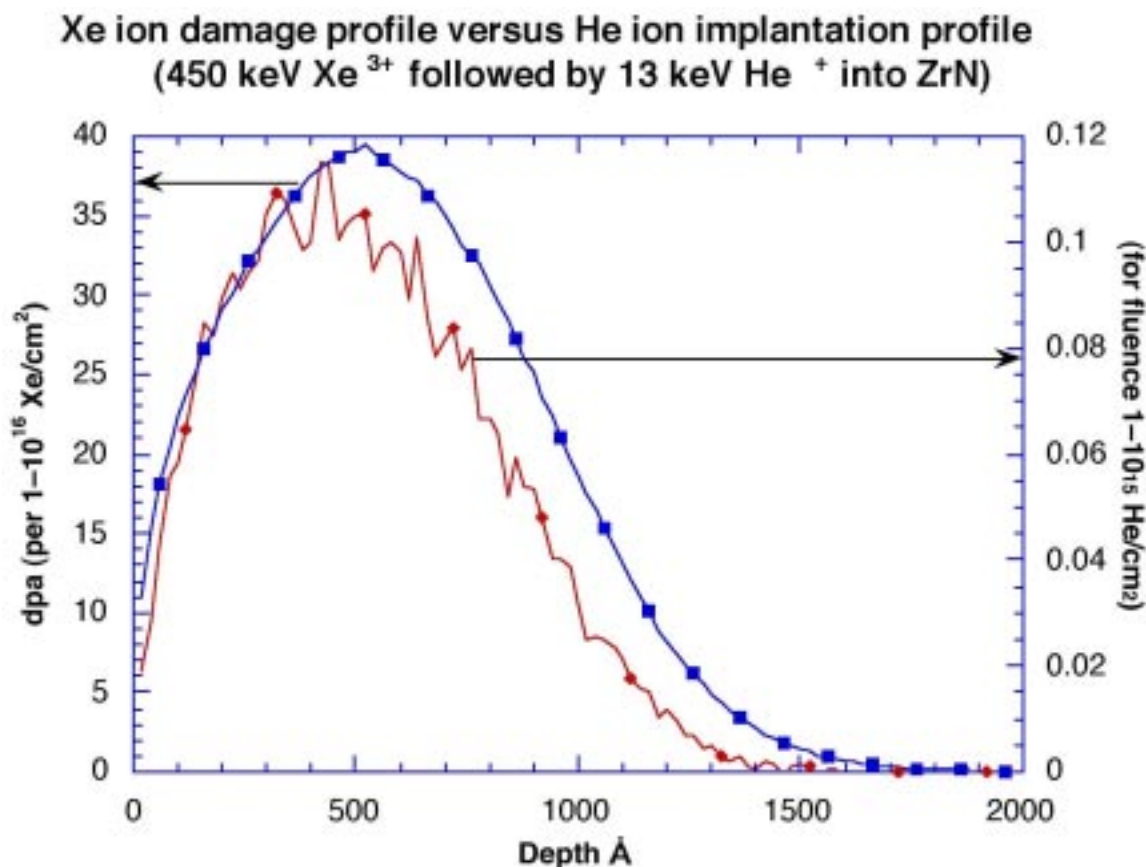


Fig. 36. Blue Curve: Calculated ion damage profile induced by Xe-ion implantation vs depth beneath the sample surface (based on Monte Carlo computer simulations) for an ion fluence of $1 \cdot 10^{16}$ Xe/cm². Red Curve: Calculated He ion implantation concentration profile (also based on Monte Carlo). For the lower fluence irradiation used in the study, $1 \cdot 10^{15}$ Xe/cm², the values on the left-hand ordinate should be divided by 10.

Figure 37 shows an optical photograph of the ZrN surfaces before and after ion irradiation. Clearly, the implantation of Xe causes a discoloration of the ZrN.

The ion irradiated ZrN samples described above were shipped to the Institute for Transuranium Elements (ITU) in Karlsruhe, Germany for He release analyses. Samples will be heated in a Knudsen cell apparatus and evolution of He with time and temperature will be monitored with a residual gas analyzer. The measurements to be performed at ITU will determine the effect of pre-existing radiation damage on He trapping and He mobility in ZrN.

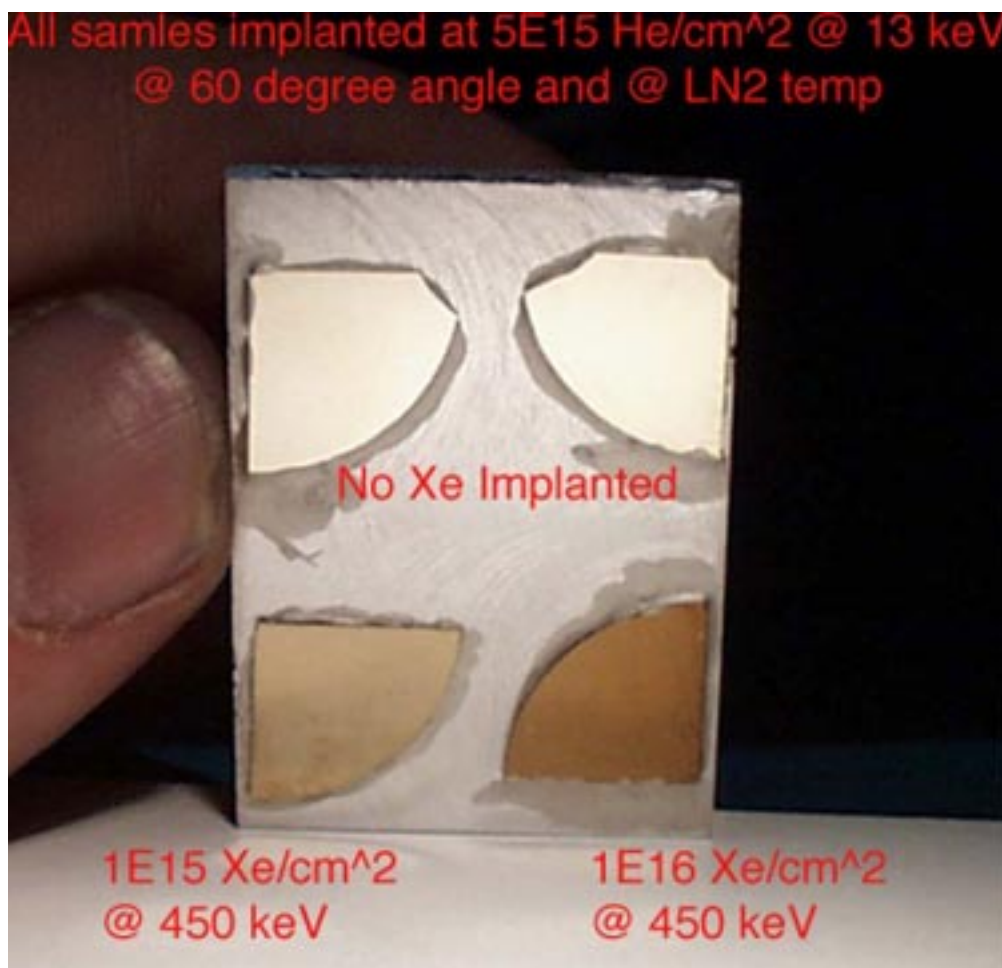


Fig. 37. Photograph showing optical changes in the surface color of polished ZrN following Xe and He ion implantations to the fluences labeled.

Metal Matrix NiAl

NiAl is a candidate matrix for AAA dispersion fuel because of a number of attractive features such as its high thermal conductivity. The large single-phase field for NiAl suggests that it also can accommodate significant disorder, which may hint at good radiation tolerance. A study was initiated to investigate radiation damage effects in single crystal NiAl using ion implantation followed by ion beam channeling analysis to assess the rate of radiation damage accumulation in NiAl.

Samples were prepared for heavy ion damage experiments on single crystal NiAl. Crystal quality was assessed using Rutherford backscattering/ion channeling (RBS/C) analytical procedures. Figure 38 shows an RBS/C spectrum obtained from a NiAl single crystal oriented along a $\langle 110 \rangle$ crystallographic direction. Also shown in Fig. 38 is an RBS spectrum obtained in a “random” sample orientation. Crystal perfection can be qualitatively determined by measuring the ratio of the backscattered He ion yield in the channel orientation vs the yield in a random orientation. This ratio, referred to as χ_{min} , was found to be approximately 5%. This represents very high crystalline quality compared to single crystals of other compounds examined by this same procedure.

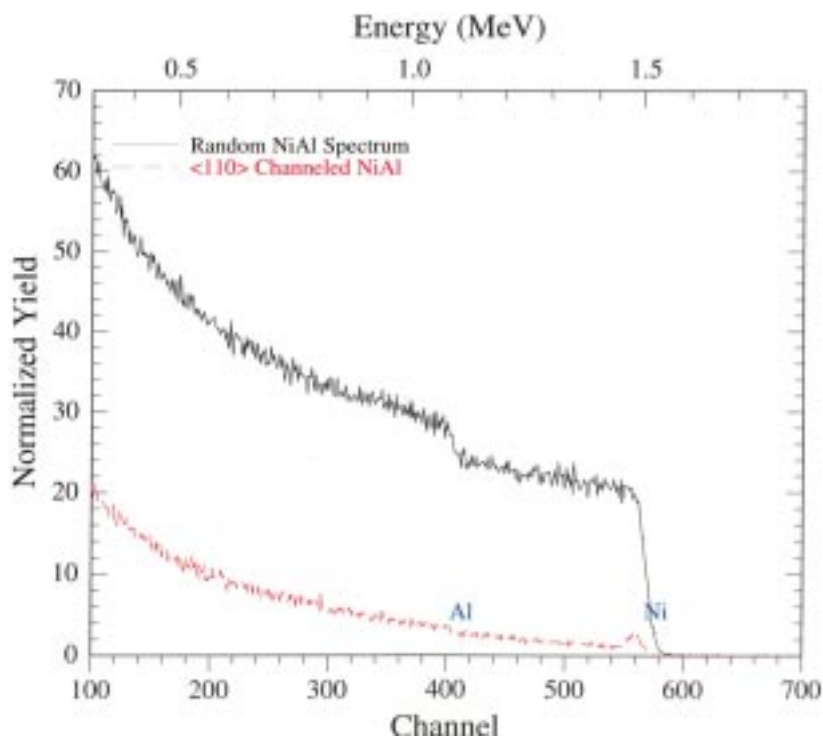


Fig. 38. Red curve: RBS/C spectrum obtained from a NiAl single crystal in a $\langle 110 \rangle$ crystallographic orientation. Black curve: RBS spectrum obtained from the same NiAl single crystal in a “random” sample orientation.

Modeling and Fuel Properties

Atomistic and Continuum Scale Modeling

Continuum Scale Modeling of Nuclear Fuels

Thermodynamic data for the U-N and Pu-N systems have been collected from the literature and from the available commercial databases and other sources. The modeling process consisted of analyzing the data using an uncertainty evaluation procedure based on Bayesian statistics.

The U-N system is being used to tune up the phase stability modeling process in the Pu-N system. There is much more information about the U-N system, and the phase diagram is qualitatively similar with the Pu-N phase diagram, mainly in the Pu-PuN region. A preliminary assessment of the U-N phase diagram is presented in Fig. 39. The non-stoichiometry of the UN_{1-x} compound was much lower than previously reported. [3]

Work on the Pu-N phase diagram concentrated on modeling the free energy of the solution phases. The number of interaction parameters in the excess Gibbs free energy as well as the polynomial form of the temperature dependency have been retrieved from the U-N model. To determine the actual values of the interaction parameters, the thermodynamic calculation of partial pressure of nitrogen over the PuN_{1-x} compound and over the liquid-UN two-phase region was necessary. The results of the calculations are shown in Fig. 40.

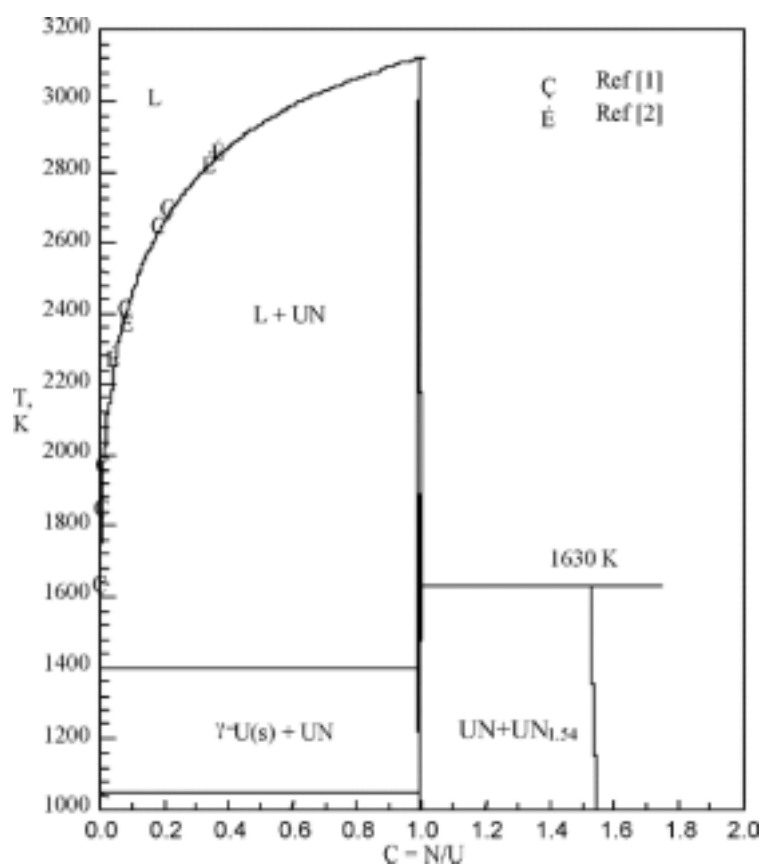
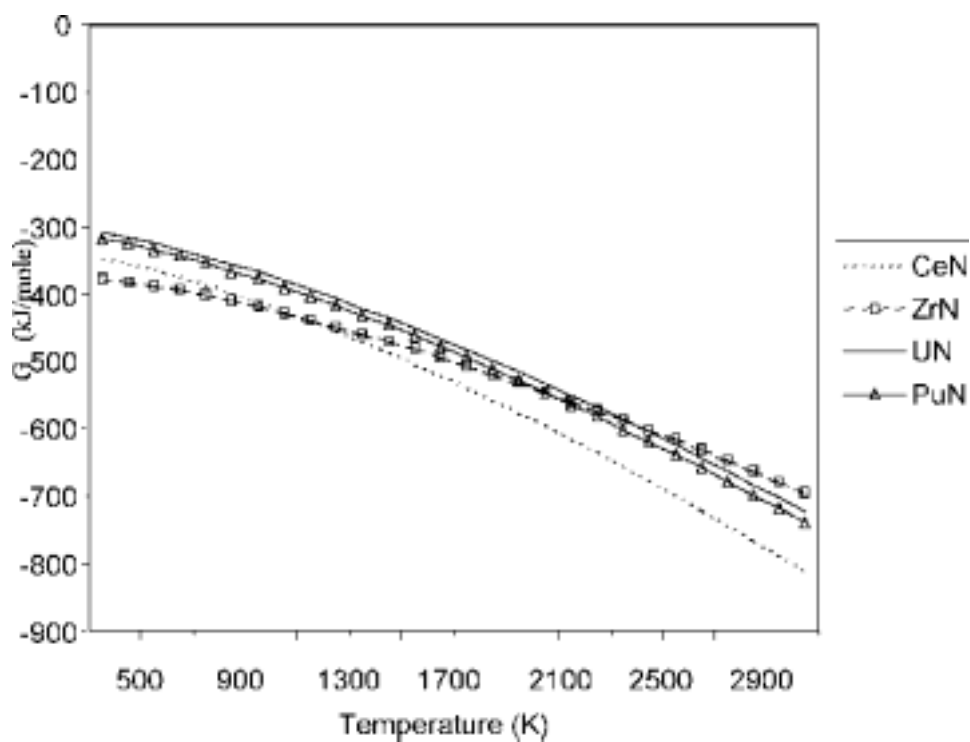


Fig. 39. Preliminary assessment of the U-N phase diagram.

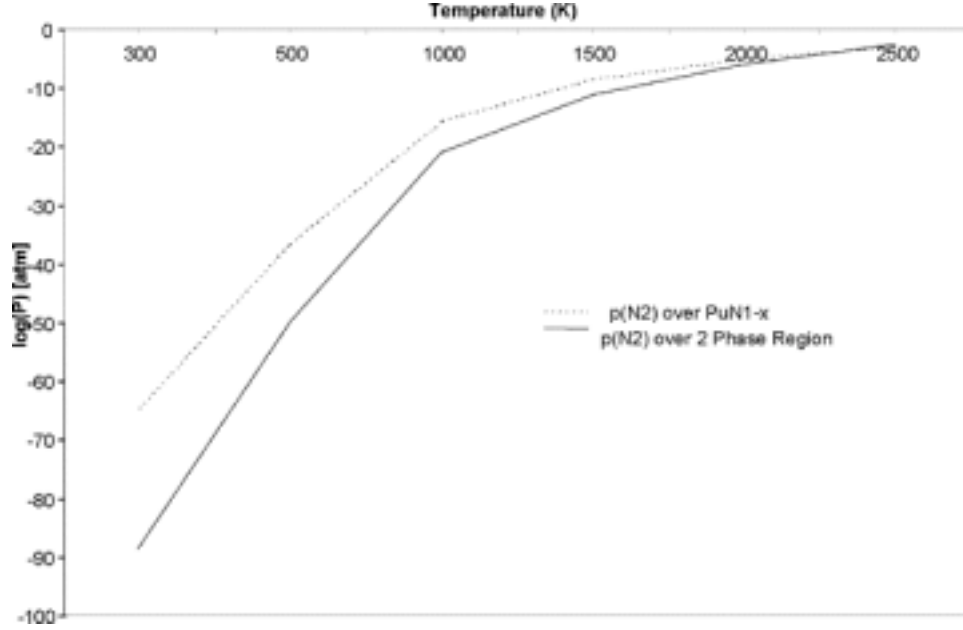


Fig. 40. Calculations of the partial pressure of nitrogen over PuN_{1-x} and over the liquid-solid solution region of the Pu-N phase diagram.

Atomistic Simulation

Simulations based on the Born model [4] of ionic solids have been used to study a range of nitride materials of interest to fuel development. Both long-range columbic and short-range atomic interactions are included in the model. The energy, E_{ij} , for the interaction between two ions, i and j , takes the form,

$$E_{ij} = \frac{q_i q_j}{4\pi\epsilon_0 r_{ij}} + E_{sr}$$

where q is the charge on the ion, r_{ij} is the ion separation and E_{sr} is the short-range contribution to the energy. Ion coordinates are relaxed until a minimum lattice energy (E_L) is found. Physical properties are calculated from the 1st and 2nd differential of the lattice energy. The Mott-Littleton approximation [5] is used to calculate point defect energies. Further details can be found in reference [6]. This methodology is implemented in the GULP [7] simulation code, which has been used throughout.

There are several forms for E_{sr} . Here we use the Buckingham potential, which has the form,

$$E_{sr} = A_{ij} \exp\left(\frac{r_{ij}}{\rho_{ij}}\right) - \frac{C_{ij}}{r_{ij}^6}$$

where A_{ij} , ρ_{ij} and C_{ij} are variable parameters. These parameters can either be derived empirically, by fitting to observable data, or non-empirically, by fitting the potential to calculated electron density overlap between pairs of ions.

Trivalent actinide, lanthanide, and transition metals form nitrides with the rocksalt structure (space group $Fm\bar{3}m$), thus the aim is to develop potentials that reproduce these structures. The simulation can be used to predict various physical properties. Such potential parameters are critical and several established relationships are used to ensure that potentials are valid. One such relationship is seen between A_{ij} and cation radii. This is used as a guide since lattice parameter also scales with cation radii. However, with reference to Fig. 41, which shows a plot of the experimental lattice parameter of various rocksalt structure nitrides vs. ionic radii [8], actinide nitride lattice parameters do not scale with established ionic radii.

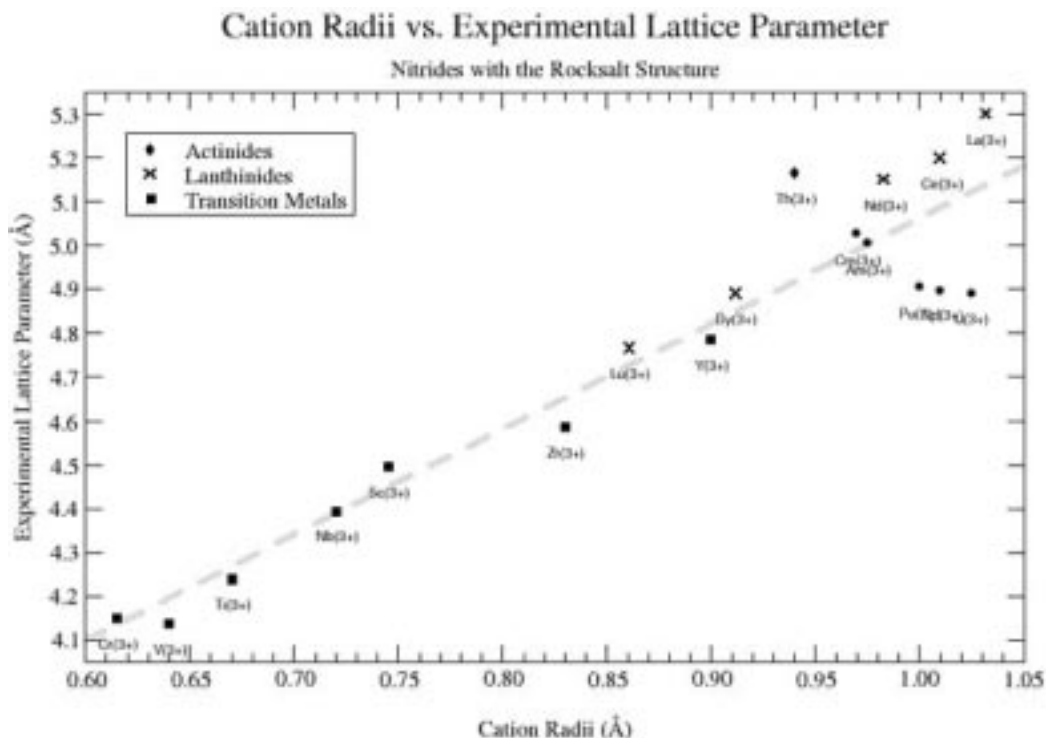


Fig. 41. Plot of the experimental lattice parameter of various rocksalt structure nitrides vs. ionic radii. Note that the actinide nitride lattice parameters deviate significantly from the established trend for ionic radii.

This anomaly, and the lack of other experimental data, makes it difficult to fit empirical potentials. Thus, non-empirical potentials have been derived using the electron gas code of Harding and Harker [9].

Electron gas potentials successfully reproduce the lattice parameters for the materials of interest. All these materials are predicted to have positive phonon frequencies and so form stable lattices. Some predicted properties for these materials are presented here.

The reliability of our potential parameters can be assessed by how closely the simulation reproduces the lattice parameter (see Table 7). The bulk elastic tensor has been predicted and is given in Table 8 with predicted bulk modulus. Intrinsic defect energies are important to any atomic process and calculated intrinsic defect energies, and associated disorder reaction energies, per defect, are given in Table 9.

Table 7. Experimental [7-10] and Calculated Lattice Parameter for Several Nitride Compounds

| | expt.(Å) | calc. (Å) |
|-----|----------|-----------|
| CmN | 5.0027 | 5.0034 |
| AmN | 5.005 | 4.987 |
| DyN | 4.89 | 4.83 |
| ZrN | 4.585 | 4.619 |

Table 8. Calculated Elastic Tensor and Bulk Modulus for Several Nitride Compounds

| | $C_{11}(\text{GPa})$ | $C_{12}(\text{GPa})$ | $C_{44}(\text{GPa})$ | Bulk Modulus (GPa) |
|-----|----------------------|----------------------|----------------------|--------------------|
| CmN | 430 | 207 | 207 | 281 |
| AmN | 407 | 211 | 211 | 277 |
| DyN | 495 | 243 | 243 | 327 |
| ZrN | 474 | 308 | 308 | 363 |

Table 9. Intrinsic Defect and Disorder Reaction Energies (eV) for Several Nitride Compounds

| | V_N^\bullet | V_M' | N_i^\bullet | M_i' | E_L | Schottky | Anion Frenkel | Cation Frenkel |
|-----|---------------|--------|---------------|--------|-------|----------|---------------|----------------|
| CmN | 50.8 | 45.9 | -22.5 | -20.8 | -79.0 | 8.81 | 14.15 | 12.59 |
| AmN | 50.2 | 45.4 | -19.7 | -21.6 | -79.1 | 8.32 | 15.25 | 11.91 |
| DyN | -21.8 | 48.0 | -20.5 | 52.7 | -82.1 | 9.28 | 16.14 | 13.10 |
| ZrN | -26.3 | 47.9 | -7.8 | 52.7 | -85.3 | 7.62 | 25.60 | 22.44 |

Defect energies show that all of these materials are dominated by Schottky disorder; however, the formation energies are high, indicating that at the stoichiometric composition very few intrinsic defects will exist at equilibrium. Previous work [14] indicated that materials with high intrinsic defect energies are more likely to undergo amorphization under irradiation. As such, these simple nitride materials should not respond well under irradiation. However, all the results presented so far have been for stoichiometric materials. TiN, for example, is reported to exhibit significant nitrogen deficient non-stoichiometry [15]. Non-stoichiometry may well provide sufficient mechanisms for the accommodation and subsequent annealing of irradiation damage. Accordingly, non-stoichiometry will be investigated in detail over the next quarter.

Quantum-mechanical-based simulations using the CASTEP [16] code have also been initiated. Results for TiN are highly encouraging with the experimental lattice parameter being reproduced well: $a=4.39\text{\AA}$ compared to the experimental value of 4.238\AA [17]. Over the next quarter, considerably more effort will be expended on quantum mechanical simulations of all nitride materials of interest including actinides.

2. SEPARATIONS TECHNOLOGY

Scope

The separations technology activity consists of three tasks addressing the various stages in the process of partitioning irradiated fuels for subsequent fissioning of transuranic elements and transmutation of long-lived fission products. The tasks are as follows:

Light-Water Reactor Spent Fuel Treatment

This task involves the development and demonstration of efficient and economic means for the separation of uranium, transuranic elements, specific long-lived fission products, and other fission products from LWR spent fuel. An aqueous partitioning process (UREX) is envisioned for the initial treatment of LWR fuel, involving the extraction of U for disposal as a low-level waste. A pyrochemical process (PYRO-A) will follow to separate the transuranic elements from fission products. Pyrochemical processes for the direct treatment of LWR spent fuels are also being developed for possible future use.

Transmutation Fuel Treatment

Fertile or nonfertile fuel that has been irradiated in the transmuter to fission transuranic elements must be processed to recover and recycle the unburned transuranics and to extract newly generated, long-lived fission products for transmutation. This task accomplishes the development and demonstration of the means for processing that blanket fuel. A pyrochemical process (PYRO-B) is planned for the separation of unburned transuranics and long-lived fission products. Such processes are favored because the reagents are stable under high-radiation fields, and because the processes are normally operated at elevated temperatures with the use of molten salts and can thus accommodate high levels of decay heating. In certain cases, aqueous separations processes may prove appropriate, and methods are being developed that will enable the optimum combination of aqueous and non-aqueous processes.

Waste Form Production

One of the overarching criteria for AAA separations technology development is the minimization of high-level waste generation. Design of the hybrid LWR fuel-treatment process has been oriented toward the elimination of liquid high-level waste streams, and the pyrochemical processes are similarly being designed to minimize high-level waste volumes. This task involves the development and qualification of durable high-level waste forms to accommodate the two principal waste streams (salt and metal) that emanate from the separations process as well as the waste form for the disposal of the pure U extracted from the spent LWR fuel.

Highlights

- A total of 3.98 kg of Dresden reactor fuel with a burnup of ~24,000 MWd/t was dissolved in the hot cell at the Savannah River Technology Center (SRTC) in preparation for the UREX hot demonstration.
- Experiments with the electrolytic oxide reduction (PYROX) process have shown a marked improvement in UO_2 reduction rate and efficiency with

decreasing fuel-particle size. The reduction of lanthanide fission product oxides is found to be a challenging problem, but initial experimental results are encouraging.

- Valuable data related to the complexation constants for acetohydroxamic acid (AHA) with plutonium and minor actinides have been obtained from foreign sources and have been used to update the AMUSE code.
- Experiments directed toward the trapping of fission product iodine as NaI are progressing. Trapping efficiencies of 20%–93% have been obtained to date.

Oxide Fuel Processing—Electrolytic Oxide Reduction (PYROX) Process

Experiments were initiated to study the feed particle-size effects on the electrolytic reduction rate. Four particle size ranges (0.045–0.6, 0.6–1.2, 1.2–2.8, and 2.8–4.0 mm) were selected for this study using UO_2 as the feed material. As part of this study, we developed a new cathode design and cell-operating procedure. Three UO_2 electrolytic reduction experiments were completed during this quarter. The results of these experiments are summarized in Table 10. The first experiment, EWR-35, was performed with the largest feed particle size under consideration. The cell in EWR-35 was operated under similar conditions as those for the two lower particle size fractions, reported previously. Yet, the conversion was only 75% in EWR-35 while the conversions were $\geq 95\%$ for the two lower particle size fractions. The results suggest that particle size has a significant effect on the conversion extent and rate in the 2.8–4.0-mm particle-size range. In the last two experiments, EWR-36 and EWR-37, listed in Table 10, the cells were continuously operated for 21 and 18 hours, respectively. In contrast, all the earlier experiments were performed over two days with the cell operating for about 5–7 hours a day. The purpose of these continuous operations is to obtain a more precise measure of the total reduction time. In the interrupted measurements, some chemical reduction occurs overnight when the cell is under open-circuit conditions, due to the presence of residual lithium metal. Although the duration of this open-circuit chemical reduction has been estimated, it causes some uncertainty in the calculated reduction time. The continuous operations were successful and yielded results that were consistent with earlier measurements. The results in Table 10 show that for the two particle-size ranges tested, the conversions were 94% and 89%. These experiments will be continued to refine the reduction time estimates for the four particle-size fractions.

Table 10. UO_2 Conversion in Reduction Experiments

| Experiment No. | Mass of UO_2 (g), Particle Size Range (mm) | Termination Point (F/mol.) | Conversion, wt% (water-washed product) |
|-----------------------|---|-----------------------------------|---|
| EWR-35 | 17.5 g, 2.8 – 4.0 mm | 9.6 | 75 |
| EWR-36 | 16.7 g, 1.2 – 2.8 mm | 10.0 | 94 |
| EWR-37 | 15.1 g, 0.6 – 1.2 mm | 6.4 | 89 |

Two electrolytic reduction experiments with rare earth oxides were conducted as summarized in Table 11. Both the experiments were performed in an MgO cell

container with no dissolved Li_2O in the electrolyte at the start of the experiment. Cell voltage, electrode potentials, current, oxygen- and chlorine-evolution rates were measured and recorded with an automated data-acquisition system. The total charge passed and Faraday per mole (F/mol.) of rare-earth (RE) oxide was calculated from the recorded data (e.g., 6 F/mol. is the theoretical charge required for complete reduction of any given mass of Nd_2O_3 at 100% efficiency).

Table 11. Summary of Electrolytic Reduction Experiments

| Cell No. | LRNd-10 | LRNd-11 |
|---|-------------------------|--|
| Anode | Graphite rod | Graphite rod |
| Reference Electrode | None | None |
| Cathode Lead | Ta wire pan | Ta wire pan |
| RE-Oxide(s) in Cathode | Nd_2O_3 | $\text{Nd}_2\text{O}_3 + \text{La}_2\text{O}_3 + \text{CeO}_2 + \text{Ce}_{0.5}\text{Nd}_{0.5}\text{O}_{1.75}$ |
| Mass of RE-oxide(s) in Cathode Compartment, g | 1.00 | 0.90 |
| Electrolyte | LiCl | LiCl |
| Temperature, °C | 650 | 700 |
| Number of hours of cell operation | 28 | 41 |
| Termination Point, F/mol. | 14.2 | 37.8 |

The first experiment, LRNd-10, was performed with a single-phase material, Nd_2O_3 . The second experiment, LRNd-11, was performed with a multi-phase mixture of rare-earth oxides. The feed material for this experiment was prepared by grinding a 3:2:1 molar ratio (rare-earth metals basis) of Nd_2O_3 , CeO_2 , and La_2O_3 , cold pressing and sintering at 1200°C for 6 hours. The resulting pellet was analyzed by x-ray diffraction (XRD). The XRD results showed the presence of four phases: Nd_2O_3 , CeO_2 , La_2O_3 , and $\text{Ce}_{0.5}\text{Nd}_{0.5}\text{O}_{1.75}$. The last phase is a mixed oxide compound, with a stoichiometry corresponding to 2 moles of CeO_2 and 1 mole of Nd_2O_3 , formed during the high-temperature annealing treatment. The objective of experiment LRNd-11 was to evaluate the effect of chemical interactions between feed oxides and product metals on the electrolytic reduction product.

Three distinct features were observed in the LRNd-10 cell after cool down. There was a clear salt layer, a gray layer adjacent to the cathode, and a dark gray cathode layer with metal-like deposits on the cathode lead, the tantalum wire pan. These layers were separated and submitted for analysis. The results are shown in Table 12. The clear salt layer contained no Nd metal or Nd compounds. The clear salt contained very low concentrations of Li_2O , a maximum of 0.08 wt%, at the end of the run. About 9% of the Nd species present in the gray layer was Nd metal. This metal may be present as a fine dispersion in the gray layer. The major Nd compound in the gray layer was identified as Nd_2O_3 by x-ray diffraction (XRD). Some lithium metal was also observed in the gray layer. Finally, the cathode analysis showed evidence of significant quantities of Nd metal. About 23% of the Nd species in the cathode was identified as metal. The metallic yield in this experiment is quite significant considering the severe thermodynamic (low Li_2O concentrations in the cell) and kinetic (oxide diffusion through a solid bed) constraints of the system. This is the most promising result obtained so far with rare-earth oxides. A similar experiment will be performed soon in an attempt to increase the process yield. The entire cell, at the

end of this experiment, will be chemically analyzed to obtain a more precise mass balance analysis of the cathode product.

The chemical analysis of LRNd-11 is complete. However, identification of the phases in the cathode product and the mass balance analysis are not yet complete. These results will be presented in a later report.

Table 12. Summary of Analytical Results

| Samples from Cell, LRNd-10 | Nd metal | Nd Compounds [*] | Li metal | LiCl ^{**} |
|--|----------|---------------------------|----------|--------------------|
| Clear Salt | None | None | None | 8.97 g |
| Gray Layer | 21.3 mg | 217.6 mg | 8.5 mg | 0.99 g |
| Dark Gray Cathode Layer ^{***} | 37.6 mg | 127.0 mg | 30.7 mg | 0.35 g |
| Total | 58.9 mg | 344.6 mg | 39.2 mg | 10.31 g |

^{*} Nd compounds include Nd₂O₃ and perhaps other unidentified Nd-compounds. Numbers are reported on Nd-basis.

^{**} The maximum Li₂O concentration of the LiCl electrolyte at the end of the experiment was determined to be 0.08 wt%

^{***} About half the cathode was analyzed in two independent measurements. Numbers are reported for the half cathode based on the two analyses.

The pyrochemical process to treat spent LWR fuel (PYRO-A) involves the direct electrochemical reduction of oxides in a molten LiCl electrolyte at 650°C. In this process, the oxide fuel is reduced to metal at the cathode while oxygen, and possibly chlorine, are evolved at the anode. The anode environment is very oxidizing and the challenges to the anode material are significant. Platinum has been used in the lab-scale development of the process, but it has practical limitations in large-scale cell designs because it will react with chlorine and the cost is prohibitive as a consumable anode. Development of advanced anode materials for the direct electrochemical reduction process is being pursued. Of two possible solutions to consider, viz., non-consumable inert anodes and consumable graphite anodes, we have selected the first option as having the best chance of success without introducing detrimental impurities into the process.

The materials examined during this reporting period included commercial tin oxide (SnO₂) electrode material (Stannex), ruthenium oxide (RuO₂), and further tests with gold metal. The exposed area of all materials was roughly 1 cm² and all tests were conducted at about 650°C. The electrolyte was LiCl containing 1 wt% Li₂O. As previously reported, the behavior of the SnO₂ changed during the course of the earlier experiments. In the presently reported work, the test sample was annealed at 650°C until its electrical conductivity reached a steady-state high value. Repeated cyclic voltammetry scans were successfully conducted on that sample. The cause of the change in conductivity is unclear and will be investigated if this material survives further testing. One of a number of cyclic voltammetry results (with repeated scans) for SrO₂ is shown in Fig. 42. Note that the potential of the Ni/NiO reference electrode is 1.6-1.7 V relative to lithium metal.

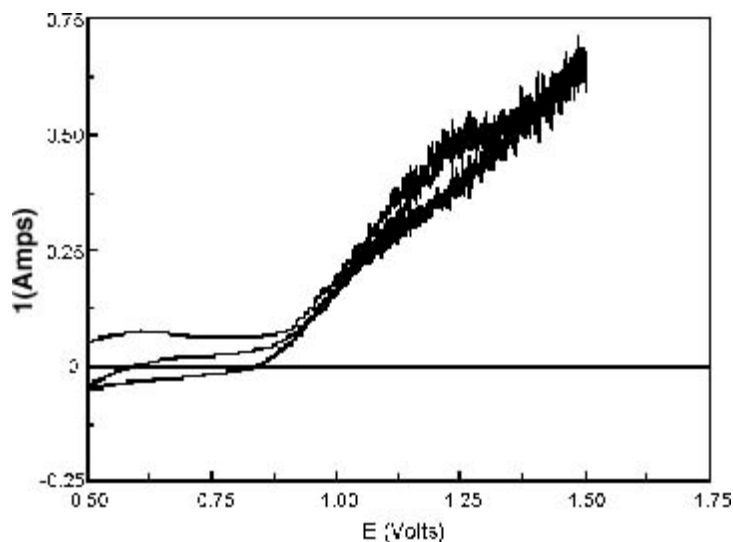


Fig. 42. Cyclic voltammetry curves for SnO_2 at 10mv/sec vs. Ni/NiO reference electrode.

The general features of these curves are similar to those observed for the results shown in the last report. There is a rapid increase in current corresponding to oxygen evolution, a leveling off, and a slight turn up in the curve that we are tentatively assigning to the onset of chlorine evolution. At the conclusion of these tests, the sample was retrieved from the cell. It appeared to be intact and in reasonable condition. Thermodynamic calculations indicate that this material should not perform well under these conditions. The actual performance of the samples appears to contradict those calculations.

Typical cyclic voltammetry results for RuO_2 are shown in Fig. 43. The general features of the curves are similar to those obtained with SnO_2 and the other oxides although there are some differences. Because only one sample of each oxide was tested, it is too soon to speculate on the causes of the differences observed.

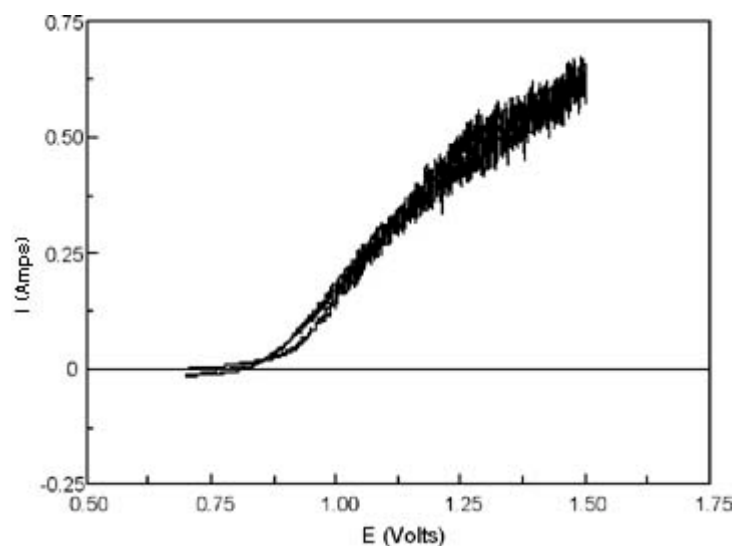


Fig. 43. Cyclic voltammetry curves for RuO_2 at 10mv/sec vs. Ni/NiO reference electrode.

A new test using a gold disk was conducted with a modified cell setup, and results are shown in Fig. 44. These results parallel the earlier results using gold wire in a previous cell design. The currents are much higher than obtained with the ceramics but there is a clearly defined peak signaling diffusion control leading to a second increase in current evidently resulting from chlorine evolution. The absence of such a peak in the oxide experiments indicates significantly slower kinetics at the electrode surface.

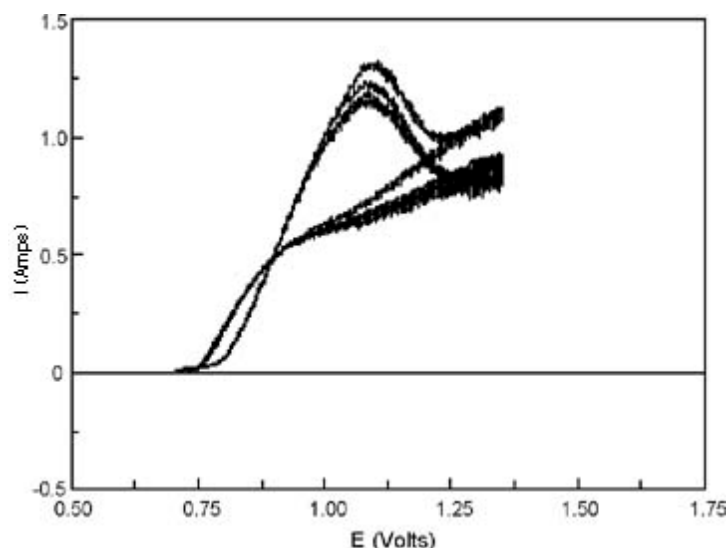


Fig. 44. Cyclic voltammetry, Au, at 5mv/sec vs. Ni/NiO reference electrode

Electro-Refining Process Development - U/TRU Electrolysis Technology Development

In most spent fuel pyroprocessing schemes, the transuranic elements build up in the electro-refiner electrolyte as metal chlorides. The simplest method to recover the transuranics (TRU) from the electrolyte is via chemical or electrochemical reduction of the metal chlorides. Electrochemical reduction has two advantages over chemical reduction. The first advantage is that the site of the reduction is localized to the cathode surface forming a cathode deposit that can be removed easily from the process equipment. The second advantage of electrochemical reduction is that the use of electrons as the reducing agent does not add to the waste volume.

Although the cathode reaction in the electrochemical reduction approach is straightforward, viz., electro-deposition of the transuranics on a solid cathode surface, the choices of the corresponding anode reaction are more varied and complex. Anode reactions under consideration include the oxidation of chloride ions to chlorine gas, oxidation of a sacrificial alloy, and oxidation of metallic uranium or reduced LWR feed material. Oxidation of chloride ions to chlorine gas is at present our reference anode reaction and we are investigating non-consumable anode materials for the chlorine anode as well as technology to capture the evolved chlorine gas. However, another approach under investigation for the treatment of spent LWR fuel is to oxidize reduced feed material at the anode.

This approach does not evolve chlorine gas, and it supplies the majority of the UCl_3 oxidant required in the flowsheet. A uranium oxidation anode reaction, however, requires isolating the anode reaction products (actinide chlorides) from the cathode. A non-conducting porous barrier can be used to isolate the anode salt (anolyte) from the cathode salt (catholyte). To evaluate this approach, a small-scale cell is being modified to accommodate a porous barrier to separate the catholyte from the anolyte. In designing the porous barrier, some calculations were made to determine the effect of porosity and thickness of the barrier on its ability to isolate the two regions of the cell. As operation of the cell progresses, a concentration gradient will develop across the porous barrier. As the concentration gradient becomes steeper, the flux of actinide cations will increase. The equation for the flux of actinide cations (as a current) across the porous barrier as a function of porosity, diffusion coefficient, barrier thickness, and anolyte and catholyte concentration is given by Eqn. (1),

$$i = nFA_b \epsilon^{3/2} D_o (c_a - c_c) / L \quad (1)$$

where n is the number of equivalents per mole ($n=3$ for most actinides), F is Faraday's constant (96485 coulombs/equivalent), ϵ is the porosity of the barrier, L is the thickness of the porous barrier, D_o is the diffusion coefficient of the actinide cation, c_a and c_c are the concentrations of the actinide chlorides in the anolyte and catholyte, respectively. At the cathode, the current due to electro-deposition of U and TRU at the cathode surface will be limited by diffusion of these species to the cathode surface. As their concentration in the catholyte decreases, the current will decrease. Eventually the rate of deposition will equal the rate of "leakage" of U and TRU into the catholyte, and a steady-state condition is then achieved. The concentration of U and TRU cannot be decreased further than this steady state concentration. Equation (2) describes the diffusion-limited current at the cathode surface.

$$i = nFA_c D_o c_c / \delta \quad (2)$$

In the above equation, A_c is the cathode area, δ is the thickness of the Nernst diffusion layer at the cathode surface ($\sim 10^{-2}$ cm) and n , F , and c_c all have the same meaning as in Eqn. (1). At the steady state condition Eqn. (1) equals Eqn. (2) and can be solved for c_c as is shown in Eqn. (3).

$$c_c = \frac{A_b \epsilon^{3/2} c_a}{\left[A_b \epsilon^{3/2} + \frac{LA_c}{\delta} \right]} \quad (3)$$

Inserting "reasonable" values for the parameters results in greater than 90% combined recovery of the actinides from the catholyte. Equation (3) is being used to size the test cell components (including the porous barrier) and will be used to evaluate the experimental results. The first test will involve only UCl_3 (~ 7 wt%) in a molten LiCl-KCl electrolyte. Once a drawdown of the UCl_3 concentration in the catholyte has been demonstrated, the test will be repeated using UCl_3 and PuCl_3 in the electrolyte.

UREX Process Development

LWR Spent Fuel Treatment

AMUSE Code Development

Work continued on developing the AMUSE user interface using the Visual Basic for Applications (VBA) macro language. Programming efforts centered on writing input verification routines. These routines will ensure that information entered by the user is within program constraints. Any input errors that are encountered are documented in a log file that can be printed to assist the user in correcting errors. AMUSE version 2.1 was fully operational for testing at the end of this quarter.

CEA – DOE Cooperation

A letter report was prepared to address questions from CEA regarding information required by CEA to model the ANL UREX demonstration. The letter report addressed (1) complexation of Np(IV), U(VI), Pu(IV) with AHA, kinetics effects and the importance of using dibutylphosphoric acid; (2) operating parameters for the UREX demonstration; (3) concentration/temperature profiles obtained during the UREX demonstration; and (4) estimated volumes of the contactors mixing and settling zones obtained during the UREX demonstration. Other information pertinent to the run was also included. The letter report was sent to the DOE team members who meet with CEA in June 2002. This report is a milestone for the DOE/CEA cooperation.

Properties of Acetohydroxamic Acid

Complexation of actinides by AHA is the key to the UREX process. In developing the AMUSE code for UREX processing, some of the AHA complexation constants were measured at ANL {Np(IV) and U(VI)}, some were taken from the literature {Fe(III) and lanthanides}, and one was estimated based on analogous chemical behavior {Pu(IV)}. The results of the simulated-feed UREX demonstration in September 2001 showed that precise values for AHA-actinide complexation constants are required to successfully predict UREX process flowsheets. Part of our efforts to improve AMUSE predictions is to gather improved complexation constants to use in AMUSE. Data have become available from two sources:

- Serguei Sinkov, Radiochemical Processing Laboratory, PNNL, who measured these and many more complexation constants in his laboratory, and
- Peter Rance, BNFL.

A comparison of complexation constants in AMUSE and these two sources is shown in Table 13. The $\log \beta_n$ values shown in Table 13 are defined by the general equation:



where M is a metal with positive charge m , Y is the anionic (deprotonated) form of AHA, and $MY_n^{(m-y)}$ is the complex with n AHA anions bound to the cation. For the extraction and scrub sections of a UREX process, where the nitric acid concentrations are above 0.1 M , the only significant AHA complexation is that for Pu(IV) and Np(IV).

Table 13. Log β_n Values for Complexation of Actinides and Fission Products by AHA

| Cation | Source | Conditions | $\log\beta_1$ | $\log\beta_2$ | $\log\beta_3$ | $\log\beta_4$ |
|----------------------|-------------------------|------------|-------------------|---------------|---------------|---------------|
| H^+ | AMUSE 1.10 | | 9.35 | | | |
| | Sinkov | a | 9.018 | | | |
| | Rance | | 9.49 | | | |
| U(VI) | AMUSE 1.10 | | 7.59 | | | |
| | Sinkov | b | 7.94 | 14.11 | | |
| | Rance | | 7.93 | 14.07 | | |
| Np(IV) | AMUSE 1.10 | | 12.52 | | | |
| | Sinkov | b | 12.83 | 22.96 | 30.06 | |
| | Rance | | 12.83 | 22.96 | 31.00 | 36.17 |
| Pu(IV) | AMUSE 1.10 | | 10.3 ^c | | | |
| | AMUSE 1.03 ^e | | 13.0 | | | |
| | Sinkov | a | 13.9 | 24.1 | 32.2 | |
| | Rance | | 13.9 | 24.1 | 32.7 | 38.8 |
| Pu(III) ^d | AMUSE 1.10 | | 5.67 | 10.2 | 13.2 | |
| | Rance | | 5.77 | 11.66 | 14.84 | |
| Eu(III) | AMUSE 1.10 | | 5.67 | 10.2 | 13.2 | |
| | Rance | | 6.19 | 11.97 | 15.85 | 17.32 |
| Am(III) | AMUSE 1.10 | | 5.67 | 10.2 | 13.2 | |
| | Rance | | 5.85 | 11.17 | 15.48 | 16.59 |
| Np(V) | AMUSE 1.10 | | none | | | |
| | Rance | | 4.83 | 8.11 | | |

a 2.0 M ionic strength was set using 1.6 M $NaClO_4$ and 0.4 M with a combination of HNO_3 and $NaNO_3$.

b 2.0 M ionic strength was set using 2.0 M $NaClO_4$.

c The AHA complexation value for Pu(IV) in AMUSE 1.10 was set based on reaction with $Pu(NO_3)_2^{2+}$ and the fit to the results of the September-2001 UREX countercurrent demonstration. This was the best fit to the results

d AMUSE treats the complexation of Pu(III), Am(III), and the lanthanides using average value for all.

e This was the version used to predict the behavior of Pu(IV) for designing the demonstration flowsheet for September 2001. It was estimated based on literature complexation constants for Np(IV) and Fe(III).

As can be seen by the results presented in Table 13, the Pu(IV)-AHA β_1 value used for AMUSE 1.05 was lower than the values provided by Sinkov and Rance. Use of this β_1 constant in AMUSE predicted that Pu would be at a concentration in the UREX solvent leaving the scrub section 5–6 orders of magnitude lower than was found experimentally. The value that best fit the experimental data from the UREX demonstration in AMUSE 1.10 is lower by a factor of 1/500. One way to explain this result, along with Pu(IV) distribution-ratio data from SRTC and Rance, is that one or more of the Pu(IV)-AHA- NO_3 complexes is extractable by the UREX solvent. A similar case was seen years ago for the TRUEX solvent, where fluoride complexation of Zr(IV) lowered the distribution of Zr significantly, but not to the extent predicted by the fluoride complexation constants and $ZrO(NO_3)_2$ being the only extractable Zr species. The experimental data were fit well by assuming a small but significant distribution ratio for ZrF_4 . We will use this same approach to fit all Pu(IV) distribution-ratio data in nitrate/AHA/hydrogen-ion media. The extractable species will have a neutral charge with a total of 4 nitrate and/or AHA anions bound to it. The new algorithm for Pu(IV) distribution will be included in AMUSE version 2.0, which will be out this summer.

Preliminary Evaluation of Solvent-Extraction and/or Ion-Exchange Processes for Meeting AAA Program Multi-Tier Systems Recovery and Purification Goals

A letter report that evaluates aqueous processing options for the multi-tier scenario was completed. The summary section of that report is copied below. Several potential processes are described and evaluated for their suitability in a multi-tier aqueous-based approach to processing dissolved spent nuclear fuel. The evaluation is focused on solvent extraction and ion exchange technologies that have been demonstrated in varying degrees. The goals of the program are to separate U, Tc, and the transuranic (TRU) elements from the fission products that are to be vitrified for disposal as high-level waste (HLW). Uranium will be disposed as a Class-C low-level waste (LLW); Tc and TRU will be formed into targets for transmutation in a thermal flux.

A number of processes were examined. The focus was on liquid-liquid solvent extraction processes because of their relatively high state of development and their suitability for high throughput processing. Ion exchange processes were also examined. PUREX and UREX were evaluated as options for recovery of U; UREX is also an option for Tc recovery. Solvent-extraction options examined for TRU recovery included TRUEX, DIAMEX, and TRPO, as well as some based on tributyl phosphate (TBP) extraction. Processes for trivalent actinide separation from lanthanides were also examined.

PUREX processes have been developed over many years, and have been refined to a significant degree. In the first cycle, U and Pu are co-extracted from dissolved spent fuel solutions by TBP in a diluent, selectively stripped, and purified in additional extraction/strip cycles. Neptunium can be extracted or driven into the raffinate by adjusting its oxidation state. Trivalent actinides and fission products remain predominantly in the raffinate, although a significant Tc fraction will co-extract with the U and Pu.

In the UREX process, the PUREX process is modified by the addition of AHA to complex and reduce Pu and Np so that they do not extract along with the U. Also, a low nitric acid concentration promotes efficient extraction of Tc with the U. Selective stripping produces separate U and Tc streams that meet AAA targets.

TRUEX, DIAMEX, and TRPO are processes that extract all of the TRU elements simultaneously (the lanthanide fission products also extract); selective oxidation/reduction and stripping can then be used to separate tetra- and hexavalent ions formed by Pu and Np from the trivalent ions such as Am and the lanthanides. Processes based on TBP can be used to selectively extract the tetra- and hexavalent species of Pu and Np. Extraction chromatography and ion exchange processes can also achieve the desired separations.

The CMPO extractant used in the TRUEX process will extract all of the actinides and lanthanides with good selectivity over most fission products (except for the lanthanides). The trivalent actinides and lanthanides can be separated from TRU elements in higher valences by a dilute acid strip. This process has been widely studied and is relatively mature. The DIAMEX process accomplishes the same separations with a diamide extractant. TRU elements are less strongly extracted at moderate acidities, therefore nitric acid or nitrate salt addition would be required if DIAMEX were used in tandem with UREX. The TRPO process uses a mixture of tri-alkyl phosphine oxides to extract the TRU and lanthanide elements at low acid concentrations. Selective co-stripping of the trivalent actinides and lanthanides

requires a high acid concentration, a drawback for this process because subsequent processes to separate this trivalent ions product stream into lanthanides and actinides require low acidities.

An alternative approach to simultaneous extraction of the TRU elements is selective extraction of tetravalent or hexavalent Pu and Np by TBP, followed by extraction of the trivalent actinides (and lanthanides) by TRUEX, DIAMEX, or TRPO. With choice of appropriate oxidation, reduction, or complexing agents, a number of processing options are possible for TRU recovery by TBP extraction. While such a multi-process approach may be more complicated than a simultaneous extraction approach, it is thought to be more certain of success. The TBP extraction options for recovery of Pu and/or Np might potentially be implemented in an expanded UREX process flowsheet, simplifying the overall system.

The separation of the trivalent actinides Am and Cm from the lanthanides is difficult because of the similarity of chemical properties. Several methods make use of the greater stability of aqueous soluble complexes of trivalent actinides with organic complexants such as DTPA. In the "direct" TALSPEAK process, the lanthanides are selectively extracted away from the actinides, which remain in the aqueous phase as complexes. In the "reverse" TALSPEAK process, both the lanthanides and actinides are extracted, and the actinides are selectively stripped away from the lanthanides into the complexant solution. Several extraction systems under development utilize the "reverse" TALSPEAK approach; among these are the so-called DIDPA, SETFICS, and PALADIN processes. Selective complexation has also been employed in cation exchange chromatography (CEC). Similar to reverse TALSPEAK, co-adsorption is followed by selective elution with complexant solutions. The large volume of liquid waste generated limits the utility of the CEC process.

Newer processes being developed for the separation of trivalent actinides and lanthanides employ solvents that selectively extract the actinides away from the lanthanides, without using complexants to keep the lanthanides in the aqueous phase. Such processes are being called SANEX processes (described below).

UREX is best suited for simultaneously achieving two objectives of the AAA program: >99.9% of the U in a stream suitable for disposal as LLW, and recovery of >95% of Tc in a stream that can be converted to transmutation targets. Many potential process combinations following UREX can meet the programmatic TRU element recovery and purification objectives. A processing system that will likely meet AAA program goals with minimal development employs (1) TBP extraction to recover Pu, Np, and residual U from UREX raffinate, (2) TRUEX to recover the trivalent actinides (lanthanides are also recovered), and (3) a SANEX process to purify the trivalent actinides. Other approaches are more speculative but lead to simpler-appearing systems. A very simple process system could include recovery of Np and Pu by TBP extraction in an expanded UREX process with recovery and purification of trivalent actinides directly from the expanded UREX raffinate by a SANEX process.

It is felt that development work should center on defining optimal redox reagents for Pu and Np recovery in various processes, development of a SANEX-type process for separation of trivalent actinides from lanthanides, and continued development of process modeling tools.

Sodium Iodide Production from Molten Salts

The purpose of this work is to demonstrate and develop a method for scrubbing iodine-containing gases (e.g., I_2 , HI, or CH_3I) from fuel processing off-gas streams via reaction and dissolution in molten salts. Specifically, the iodine-containing gas stream is bubbled through molten NaOH where it reacts and enters the molten salt as iodide. The phase diagram of the NaOH/NaI system indicates that at sufficiently high iodine concentration, NaI will precipitate as a relatively pure solid phase as the melt is cooled. A pure NaI precipitate has advantages for the point of view of later processing (e.g., accelerator transmutation). The task to be performed is to demonstrate experimentally the efficacy of iodine trapping by molten NaOH and to demonstrate the NaI precipitation suggested by analyses of the phase diagram. Thermodynamic analysis of baseline gas processing scenarios will also be carried out. Since other gases that could react with NaOH may also be present in off-gases from fuel processing (e.g. CO_2 , NO_x , H_2O), their interaction with the molten salt system will also be evaluated.

Experimental Work

The iodine content of solids and solutions was formerly calculated from simple acid/base titration of salt samples dissolved in water. Any mass contributed by presence of water, CO_2 , or other impurities was, using that method, interpreted as iodide. To obtain a more direct measure of iodine content, we established the capability to do iodide analyses using an ion-selective electrode (ISE). The primary experimental effort was directed at the capture of iodine from I_2 vapor in molten NaOH. The experimental setup is summarized in Fig. 45. Two gas sources are used, one being a helium purge and the other being a 4% H_2 /96% Ar mixture. The H_2 /Ar stream is used to entrain I_2 at its ambient temperature vapor pressure. The H_2 acts as a reducing agent to directly or indirectly convert I_2 to iodide, the form it takes in the molten salt.

The H_2/I_2 /Ar stream is directed by a two-way valve to either a bypass solution or to the molten NaOH. The molten NaOH is contained in a covered glassy-carbon crucible, in turn contained in a nickel sheath. Gas enters the molten NaOH via a graphite sparge tube. Unreacted gas escapes the heated stainless steel container via an aqueous NaOH solution (intended to capture any iodine that escapes or passes the molten salt). After an experiment, the molten salt is cooled and frozen. To determine the iodine content, it is dissolved in water for analysis. This solution, the pre-oven and post-oven aqueous NaOH solutions, and several component rinse solutions, are analyzed for iodide using the ISE method. Several experiments have been done on the I_2 / NaOH system. In addition to blank runs and shakedown experiments, four trapping runs at different conditions were done. Iodine was found in varying quantities in all hardware downstream of its source. This plumbing hold-up raises the possibility of iodine transport into or past the oven during periods when the I_2 source is off-stream. We define capture efficiency as the proportion of iodine found in the (frozen) NaOH, on the crucible, on its lid and on the sparge tube, as compared to that quantity plus iodine found on hardware downstream from the molten salt and in the post-oven aqueous NaOH solution. A summary of key experimental parameters and results is presented in Table 14.

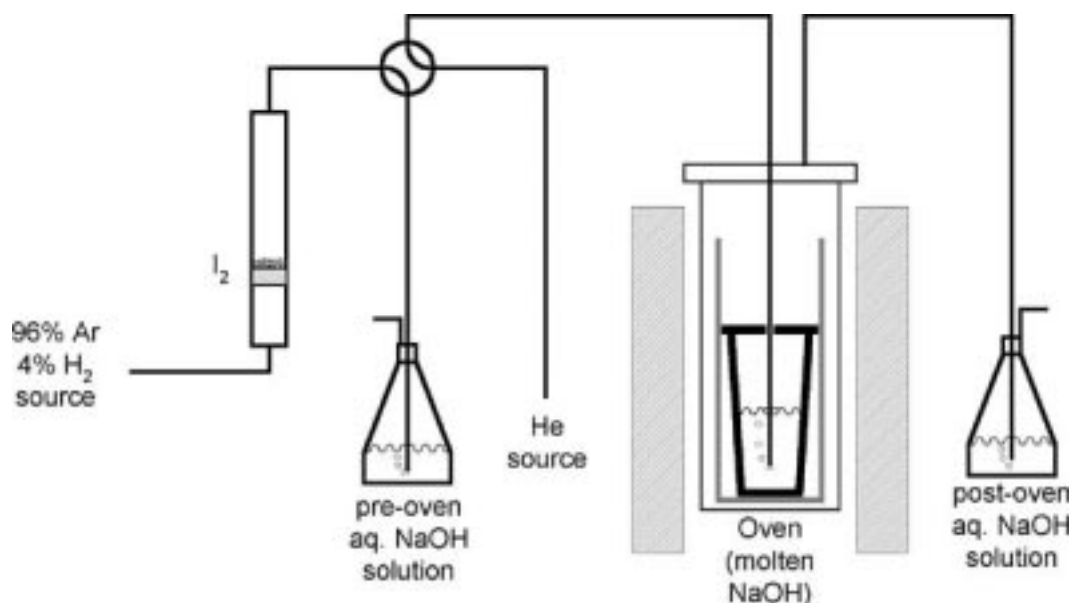


Fig. 45. Simplified experimental schematic.

Table 14. Iodine Trapping in NaOH – Experimental Results

| Experiment | T (°C) | Sparge tube depth (mm) | Capture Efficiency |
|------------|--------|------------------------|--------------------|
| Na-OH-I-05 | 370 | 15 | 22 % |
| Na-OH-I-06 | 390 | 90 | 29 % |
| Na-OH-I-08 | 505 | 90 | 93 % |
| Na-OH-I-07 | 606 | 90 | 72 % |

From results to date, it appears that higher temperatures improve trapping efficiency. At least some of the improvement in capture efficiency, however, is likely due to improving experimental technique as the runs progressed (minimizing cross contamination from previous experiments and from pre- and post-run heat-up and cool down periods; separating iodine transport during the period when the salt is at operating temperature from possible transport before and after that period). This is probably the reason that experiment Na-OH-I-08 (at 505°C) showed a higher apparent capture efficiency than did experiment Na-OH-I-07 (at 606°C, but run previous to experiment Na-OH-I-08).

In experiment Na-OH-I-08, the graphite sparge tube was retracted from the molten salt before it cooled. Separate analyses were made for iodide in the salt block proper and from material on the sparge tube. In this case, the majority of the iodide found was on the sparge tube. This can be understood when one notes that the run temperature was below the melting point of NaI. In a thoroughly mixed system, this NaI would (per the NaOH-NaI phase diagram) go into solution. The continuous gas flow through the sparge tube, however, would make the interior and tip of the sparge tube an iodide-rich region and prevent mixing with the NaOH solution. In the other three runs, the sparge tube was left submerged in the molten salt as it cooled and froze. Analysis of trapped iodine therefore yielded a combined result for material in

the salt proper vs on (or in) the sparge tube. A further observation regarding the graphite sparge tube is that, after thorough rinsing with distilled water, the graphite tube, drying in the air, exuded deposits of NaOH and NaI. A moderate fraction of the captured NaI apparently penetrated into the interior of the graphite (as determined by analyses of later rinses). The glassy carbon crucible proper did not appear to exhibit this phenomenon. Near-term upcoming experimental efforts will be directed at completion of the I₂ trapping series, and then will switch to the trapping of iodine from other gaseous species (CH₃I and HI).

SANEX Process Studies

The actinide/fission product feed sample from the processing of irradiated target material containing Am, Cm, and their associated fission products was transferred from the hot cells to the glovebox facilities for use in the testing of the SANEX reagents. A stock feed solution was prepared and dilution samples were submitted for analysis to determine the level of radioactivity needed for good counting statistics for both Am and Eu. The bis(chlorophenyl)-dithiophosphinic acid extractant was prepared from the reagent synthesized by the Chemical Sciences Division at ORNL and the diphenyl-dithiophosphinic acid extractant was prepared from a commercially obtained reagent. Both extractants were prepared at 0.5 M concentrations with 0.25 M trioctylphosphine oxide added as a synergist in a diethylbenzene diluent. A series of extraction tests were conducted at nitric acid concentrations of 0.2, 0.4, 0.7, and 1.0 M for the bis(chlorophenyl)-dithiophosphinic acid extractant and 0.2, 0.35 and 0.5 M for the diphenyl-dithiophosphinic acid extractant. Each sample was equilibrated for contact times of 4, 10, and 60 minutes each with aqueous and organic samples obtained at the end of each contact time. Analysis of the data from these experiments is in progress; however, the preliminary results show separation factors in the mid-twenties for the chlorophenyl extractant and the mid-teens for the phenyl extractant. Additional sampling, checks for precipitation, and final aqueous phase acid concentration determinations are planned or are in progress. Additional extraction tests are being planned for these reagents. The CSD personnel are investigating the preparation of the SANEX-III extractant, a bis-triazinylpyridine reagent, which will be included in future Ac/Ln separation testing.

Dissolution of Dresden Reactor Fuel

The hot demonstration of the UREX process will be done with solution prepared by dissolution of irradiated fuel from the Dresden BWR. The Dresden fuel has been in storage at Savannah River Technology Center (SRTC) since 1979. SRTC records show 3.98 kg of U, 28.54 g of Pu, and a burnup of 23,480 MWD/MT with a discharge date of September 1, 1975. ORNL has similar material irradiated to 28,000 MWD/MT that was analyzed for radionuclide content and shows 4.07 kg U, 30 g Pu, 2.5 g Am plus Cm, 163 Ci Sr⁹⁰, and 169 Ci Cs¹³⁷. The fuel was dissolved in a 6-liter glass dissolver vessel (see Fig. 46). The dissolver was equipped with a removable stainless steel basket for fuel charging and cladding containment, and a condenser to prevent evaporation of the solution during heating.

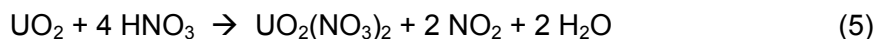


Fig. 46. Dissolution of Dresden fuel

The fuel, shown in Fig. 47, was zircalloy clad (note that some of the UO_2 has been converted to powder and coats the cladding). The material was dissolved in 3 batches starting with 4 M HNO_3 with added increments of 10 M HNO_3 to maintain reaction rate. The dissolution reaction is shown in Eqn. 5. Typically, dissolution initiated as soon as fuel was charged to the 4 M HNO_3 heel in the dissolver as evidenced by the color of NO_2 gas in the dissolver. After the initial reaction subsided, the dissolver was heated to 90°C during the remainder of the dissolution.



Fig. 47. Dresden fuel prior to dissolution.



Each batch required about 14 hours of dissolution time spread over two days. The cladding from the previous dissolution was leached with fresh 4 M acid prior to the start of the next dissolution batch. Figure 48 shows a batch of leached cladding pieces. Note the presence of undissolved black solids in the pan with the clean cladding. Interior and exterior of cladding pieces appear to be clean on visual inspection (see Fig. 49). After removal of the clean hulls from the basket, the next batch of fuel was placed in the basket and charged to the dissolver to start the next dissolution. Total weight of material put into the dissolver was 4.6 kg with 0.7 kg of cladding removed after dissolution.



Fig. 48. Leached cladding from Dresden fuel.

Several end pieces of fuel rods were found after dissolution. At completion, we have 7.3 liters of solution with a density of 1.73 g/mL and acid concentration of 1.45 M. The uranium concentration was calculated to be >450 g/L based on the density and acid concentration. Solution, cladding, and undissolved solids were sampled and submitted for actinide and fission product analyses. No analytical results are available yet.



Fig. 49. Leaching cladding piece.

Modified Direct Denitration (MDD) Demonstration

The review of the conceptual design for the glovebox-scale modified direct denitration (MDD) was completed, and a vendor bid was received. A review of the vendor design and modification was conducted and a purchase order was issued to the vendor for the MDD furnace unit. Delivery of the unit is expected in mid-July. The vendor supplied a design drawing of the unit to be fabricated and the design of the center tube for the liquid feed and off-gas capture has been completed. This center tube will be fabricated in-house since some modifications may be necessary for "fitting" with the furnace tube. Several ancillary equipment items have been obtained for use with the MDD unit including a feed pump and off-gas scrubber.

A neodymium nitrate solution was prepared for batch testing of the MDD process to determine the appropriate NH_4 /metal ratios for the furnace operations. In a simplified batch test, a solution containing an NH_4 /Nd ratio of 2 was heated in a muffle furnace at 150°C to remove excess liquid. The temperature was then ramped to 350°C forming a crystalline matrix that was converted to a powdered oxide at 500°C . A corresponding sample containing no NH_4NO_3 was run in parallel. The crystalline matrix at 350°C was not observed in this solution and the final oxide product appeared to be glassy in appearance when compared to the solution containing the NH_4NO_3 . These batch tests will continue while the furnace unit is being assembled and prepared for larger scale testing.

Evaluation of Alternate Complexants/Reductants

The UREX process is being developed to recover U and Tc from commercial LWR spent fuel. The UREX process uses tributylphosphate as the extractant and is designed to recover a pure uranium stream while sending all other actinides to the waste raffinate with the fission products. The actinides, especially Np and Pu, are kept in the aqueous stream by a combination reductant/complexant, acetohydroxamic acid (AHA). AHA is toxic to embryos (teratogenic), so a literature search was performed to identify less hazardous alternatives to AHA for use in the UREX flowsheet. Table 15 shows a list of reductants identified during the literature search which reduce either Np(VI) to Np(V) or Pu(IV) to Pu(III) rapidly enough for use in a centrifugal contactor.

In order for the flowsheet to reject both Np and Pu, they must either be adjusted to inextractable Np(V) and Pu(III) or the extractable valences (Np(VI), Np(IV) and Pu(IV)) must be complexed strongly enough to lower the distribution to the organic phase. Although AHA and its analog formohydroxamic acid (FHA) are unique among reductants and complexants in that they reduce Np(VI) instantaneously and complex Np(IV) and Pu(IV), a number of possible reductants and complexants were identified which might be used instead of AHA. Of the 13 reductants identified as having reaction rates rapid enough for use in centrifugal contactors, only two, H_2O_2 and N,N-ethyl(hydroxyethyl) hydroxylamine, reduce both Np(VI) and Pu(IV) rapidly. The remaining reductants for Np(VI) require a separate complexant for Pu(IV) and possibly Pu(VI).

Many ligands were identified as potential complexants for Pu and Np for use with Np(VI) reductants (see Table 16).

Table 15. Reductants for Neptunium and Plutonium

| Reagent | Rate^a Np(VI)--> Np(V) | Rate^a Pu(IV)--> Pu(III) |
|---|--|--|
| (CH ₃) ₂ NNH ₂ | 23.4 sec | 307 min |
| HOCH ₂ CH ₂ -NHNH ₂ | 9.1 sec | 77.7 min |
| C ₆ H ₅ -NHNH ₂ | 0.9 sec | 4.2 min |
| NH ₂ OH | 9.7 sec | 5 min |
| (CH ₃) ₂ NOH | 11.4 sec | 13.9 sec |
| (CH ₃ CH ₂) ₂ NOH | 2.04 min | 5.6 sec |
| (CH ₃) ₂ C-NHOH | 1.17 min | Not Reported |
| (CH ₃ CH ₂ CH ₂ CH ₂) ₂ NOH | 2.77 min | 18.1 sec |
| N,N-ethyl hydroxylamine | 8.3 sec | 0.34 sec |
| HNO ₂ | Instantaneous | No Reaction |
| H ₂ O ₂ | Instantaneous | Very rapid (mixture of (IV) & (III)) |
| Acetohydroxamic acid | Very rapid | Very slow |
| Formohydroxamic acid | 0.045 sec | Very slow |
| Ascorbic acid | Not Reported | Very Rapid with NO ₂ ⁻ scavenger |
| Isoascorbic acid | Not Reported | Very Rapid with NO ₂ ⁻ scavenger |
| Semicarbazide | Not Reported | Very rapid |
| Hydroquinone | Not Reported | Rapid |
| Tropolone | Rapid | Not Reported |
| 5-Methylsalicylic acid | 10 sec | Not Reported |

a Reaction times shown in minutes and seconds are for 99 % completion of reaction in 1 M HNO₃.

Table 16. Complexants for Neptunium and Plutonium

| Complexant | Log K or Beta, Np(IV) | Log K or Beta, Pu(IV) |
|---|-----------------------------------|-----------------------------------|
| Acetate | Not Reported | K ₁ = 5.31 |
| Lactate | Not Reported | K ₁ = 2.43 |
| Oxalate | K ₁ = 8.68 | K ₁ = 8.74 |
| Tartrate | Not Reported | β ₆ = 31.2 |
| Citrate | Not Reported | K ₁ = 15.34 |
| N-2-hydroxyethyl-iminodiacetate | K ₁ = 12.97 | Not Reported |
| Nitrilotriacetate (NTA) | K ₁ = 17.28 | β ₁ = 13.83 |
| EDTA | K ₁ = 24.55 | K ₁ = 24.2 |
| DTPA | K ₁ = 30.33 | K ₁ = 29.5 |
| N-(2-hydroxyethyl)-ethylenediamine N,N',N'-triacetate | K ₁ = 20.82 | Not Reported |
| Benzohydroxamic acid | K ₁ = 12.73 | K ₁ = 12.73 |
| N-benzoylphenyl-hydroxamic acid | Not Reported | K ₁ = 11.50 |
| Formohydroxamic acid | Similar to hydroxamic acids above | Similar to hydroxamic acids above |
| Acetohydroxamic acid | Similar to hydroxamic acids above | Similar to hydroxamic acids above |
| 8-Hydroxyquinoline | K ₃ = 11.4 | Not Reported |
| Malonic acid | β ₁ = 5.57 | Not Reported |
| Methylmalonic acid | β ₁ = 5.48 | Not Reported |
| Dimethylmalonic acid | β ₁ = 5.46 | Not Reported |
| 1,4-cyclohexane-dicarboxylic acid | β ₁ = 5.48 | Not Reported |
| Maleic acid | β ₁ = 4.79 | Not Reported |
| Glycolic acid | Not Reported | Not Reported |
| Pyruvic acid | Not Reported | Not Reported |
| α-picolinate | K ₁ = 6.42 | Not Reported |
| α-picolinate-N-oxide | K ₁ = 6.42 | Not Reported |
| Methylacetoacetate | Not Reported | K ₁ = 10.5 |
| Catechol | Not Reported | K ₁ = 17.72 |
| N,N-bis(2-hydroxyethyl)glycine | Not Reported | K ₁ = 13.89 |

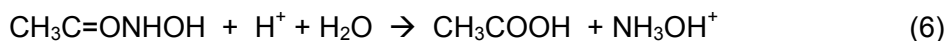
Note that the complex stability constants for both Np(IV) and Pu(IV) are not reported for many ligands. However, for those cases where both Np and Pu are reported, the values are close. Thus, it is assumed that the missing values are similar to values shown. These ligands have a wide range of complex stability constants and vary in the degree of selectivity with respect to U, which is the cation at highest concentration in solution. However, examination of the data in Tables 15 and 16 show that AHA is still the best choice for use in the UREX process because it acts as both complexant and reductant. Few of the alternative reagents can be used alone so combinations of reductants and complexant would be necessary. Work with alternative reagents is not recommended since AHA works well.

Radiation Chemistry of AHA in the UREX Process

The UREX process is being developed to process irradiated power reactor elements by dissolution in nitric acid and solvent extraction by a variation of the PUREX process. AHA (complexing agent) is added to the scrub stream to prevent the extraction of Pu(IV) and Np(VI). AHA is hydrolyzed in acid solution to acetic acid and hydroxylamine at a rate dependent on the acid concentration. The fuel to be processed is ~40 years cooled, <30,000-50,000 MWD/MT material; although only a few fission products remain, the Pu isotopes and ^{241}Am generate a radiation field estimated to be 2.6×10^2 R during processing. This study was conducted to determine the effect of this level of radiation on the stability of AHA during processing.

Solutions of AHA, HNO_3 , NaNO_3 , etc. were irradiated in a ^{60}Co source at dose rates between $9.2\text{--}8.86 \times 10^5$ R/hr. The solutions were contained in glass vials that had been heated to 500°C for 2 hours to destroy any organic material present. No further precautions were taken to avoid trace material that might cause unusual effects. Control samples were retained to allow comparison of the radiation effects, as distinct from the loss of AHA from hydrolysis.

AHA was analyzed spectro-photometrically by the absorption of the Fe(III)-AHA complex at 505-515 nm. The general procedure was to add a 25-100 μL aliquot of an AHA solution to 10 mL of 1M HNO_3 -0.1M $\text{Fe}(\text{NO}_3)_3$ and determine the absorbance immediately with an H-P diode array spectrophotometer. It was essential that the determination be made within a few minutes, since the Fe(III)-AHA complex begins to hydrolyze after 5-10 minutes. AHA hydrolyzes in acid solutions at a rate depending on the acidity as shown in the reaction (Eqn. 6):



Unirradiated control samples were analyzed to determine the effect of radiation as distinct from the loss of AHA by hydrolysis.

It was found that irradiation of AHA by ^{60}Co gammas to doses up to 1.1×10^6 R/hr decomposed a minor fraction of AHA compared to the loss by hydrolysis. The radiolysis had a weak dependence on acid concentration (see Fig. 50) and a weak dependence on total dose (see Fig. 51); a factor of five increase in dose decreased the AHA concentration by less than a factor of two. It is proposed that this effect is due to scavenging of radiation-produced species by the hydrolysis products of AHA, acetic acid and hydroxylamine. Radiation will not be a significant factor for AHA use in the UREX process.

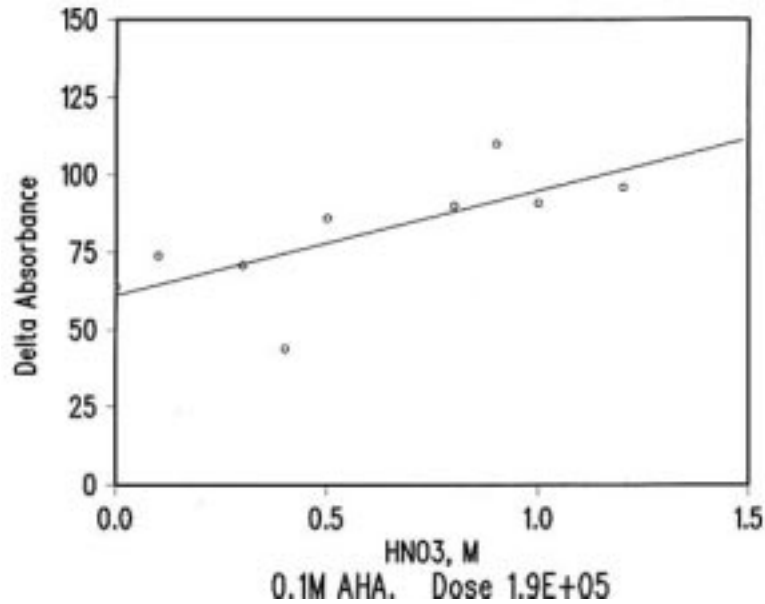


Fig. 50. Acid dependence of AHA radiolysis.

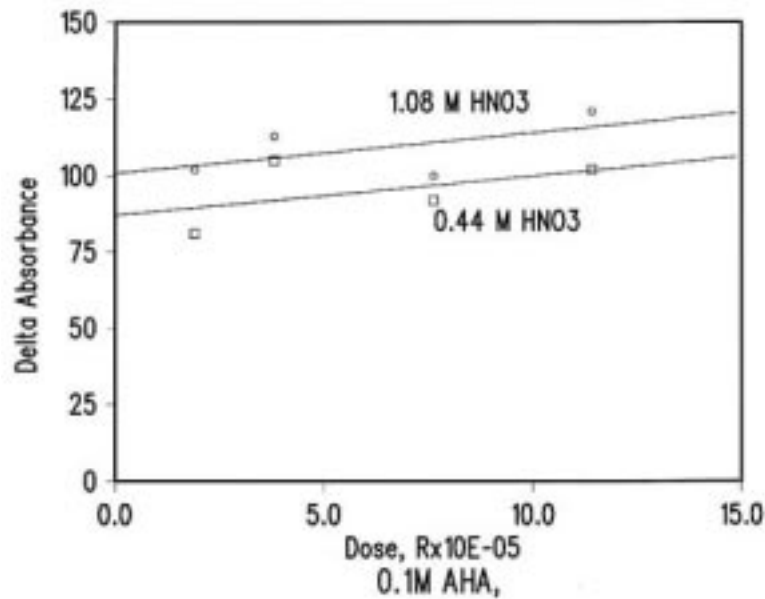


Fig. 51. Effect of radiation dose on AHA radiolysis.

Alternative Fuel Treatment Process Development

TRISO Spent Fuel Reprocessing

A visit was made to GrafTech International (formerly UCAR International) in Parma, Ohio to discuss graphite and graphite-fuel processing technologies. GrafTech presented an overview of the company's business interests and of their carbon/graphite processing technologies. ORNL personnel presented an overview of

TRISO-coated fuel characteristics and the proposed methods of separating the fuel component from the graphite and silicon carbide coatings. A tour of the technical center and the manufacturing facility was impressive. GrafTech processes graphite in a number of unit operations with well-developed equipment that is very rugged and reliable. The general consensus was that the GrafTech industrial scale processing equipment for leaching, washing, filtering, etc., could be used for the TRISO reprocessing after adapting it to a smaller scale remote operation. GrafTech is already in the nuclear grade graphite business and expressed interest in further collaboration.

As a follow-up to that meeting, a list of major development issues related to TRISO-coated fuel treatment processes was prepared to facilitate further discussion with GA. We outlined the primary processes, issues or uncertainties associated with these processes, experiments or demonstrations needed to address these uncertainties, experimental parameters to be examined, and the likely collaborators. A tentative flow sheet was prepared describing the head-end processes at the present state of development. It was agreed that the next step is to estimate the cost of laboratory-size equipment to implement a testing and development plan of the identified unit operations. The objective is to have vendor and cost information to jump-start next FY's activities. Most of the equipment can likely be tested at the prototypical scale with the exception of the dissolver. The preparation of surrogate TRISO fuel to test the dissolver at the prototypical scale is not practical; thus initially, the dissolution step will be studied at a scale of 5–10 fuel compacts per batch.

3. TRANSMUTATION SCIENCE

Transmutation science research is divided among eight major categories:

- Integration and Analytical Support
- Materials
- Lead-Bismuth Eutectic (LBE) Technology
- Irradiation Experiments
- High-Energy Physics
- Reactor Physics
- International Support
- LANL-Sponsored University Projects

The quarterly progress in each area is presented in the subsections that follow.

3.1 Integration and Analytical Support

The major objective of the integration and analytical support activities is to define and implement a consistent research plan for transmutation science.

Scope

Integration and analytical support activities include project management and integration of activities under transmutation science. The specific technical scope includes the following:

- Implement/maintain the 10-year research plan for transmutation science (experiments and supporting analyses);
- Maintain and coordinate international work packages (DOE international coordination agreements) relevant to transmutation science topics;
- Assist AAA Program management in generating other international collaboration work packages in transmutation science; and
- Participate in safety and hazard control plan (HCP) reviews for project experiments.

In general, analytical support tasks involve defining and designing the experiments, defining the test requirements and the data quality objectives, and converting the test data into technology readiness input. Defining and designing experiments involve scaling analyses, assessment of the facility limits and parametric ranges, and comparing those to the technology development needs. During this process, the specific requirements for tests as a function of a Technology Readiness Level (TRL) also are defined in terms of data quality objectives (with emphasis on accuracy requirements). Generated data must be analyzed and assessed in terms of TRL achievements and used to define design parameters or the need for supplementary and complementary tests. Specifically, tasks include:

- Integration of the Weapons Neutron Research (WNR) facility gas production test results with Blue Room neutron-yield results to map out buffering effects;
- Assessment of the data provided through international collaboration in terms of its impact on the TRL and definition of US experiments;
- Input to international test plans; and
- Completion of LBE-Na compatibility experiments begun in FY01.

Highlights

- Under the auspices of the DOE AAA Program, LANL hosted a successful and productive 3-day workshop in May, the Third International Workshop on Utilization and Reliability of High Power Proton Accelerators, held in Santa Fe, New Mexico.

Third International Workshop on Utilization and Reliability of High Power Proton Accelerators

Under the auspices of the DOE AAA Program, LANL hosted the Third International Workshop on Utilization and Reliability of High Power Proton Accelerators held May 12-17, 2002, in Santa Fe, New Mexico, with eight local organizing committee members from the LANL AAA Program.

Accelerator Utilization and Reliability Subgroup (AURS) of the Nuclear Energy Agency (NEA) Working Party on Partitioning and Transmutation (WPPT) is one of the four subgroups tasked with determining the viability of spent fuel partitioning and transmutation. The following tasks are within the scope of the AURS:

- Evaluate the potential utilization of accelerator driven spallation targets as part of the transmutation system;

- Organize one or more workshop(s) of experts on accelerator, spallation targets, and beam entrance windows in order to evaluate the potential issues related to system performance and reliability;
- Evaluate the expected performance of accelerators, spallation targets and beam entrance windows for applications associated with ADS; and
- Propose a prioritized list of issues that need to be resolved.

The workshop included 9 invited talks and 22 contributed papers covering the following topics:

- Reliability of the accelerator and impact of beam interrupts on the design and performance of the ADS.
- Spallation target design characteristics and impact on the multiplier design (Materials, radiation damage and embrittlement; enhanced corrosion; cooling issues with high-power density; and windowless design concepts)
- Safety and operational characteristics of a multiplying system driven by a spallation source.

The papers were well balanced among various topics covered by the workshop. Accelerator technology papers comprised 28% of the workshop; the spallation target technology and windowless target option comprised 36%, and the remaining papers addressed the operational and safety issues (27%) and potential test facilities (9%). In addition, there were four group discussions, viz., accelerator technology, target technology, multiplier and coupling issues, and safety issues.

The workshop was quite successful. Participation in the group discussions, which were well attended, was very energetic and resulted in a number of items that must be addressed in the overall development program. The proceedings of the workshop along with the findings of the group discussions will be published as an OECD (Organization for Economic Cooperation and Development) report.

MYRRHA Review Meeting

K. Pasamehmetoglu, a member of the International Technical Guidance Committee (ITGC) for the MYRRHA Project being developed at SCK-CEN (Belgium), chaired the first design review meeting for MYRRHA to provide recommendations on a path forward to the SCK-CEN management. The existing design of the MYRRHA project was presented, and the main challenges identified by the review committee were as follows:

- Windowless target and the interface stability require additional testing and verification. Hot spot formation and resulting excessive evaporation must also be addressed.
- Remote handling requires additional demonstration, especially fuel manipulations from under the core.
- Materials damage around the target is an issue that must be resolved through an irradiation program.
- Even though the proposed driver fuel is of known type (MOX, with previously tested enrichments), the fuel assembly needs to be

redesigned (smaller than prototypic MOX assemblies). Also, the spectrum on the fuel will be harder than what was previously tested. Thus, a fuel testing and qualification program is required.

- Finally, corrosion in LBE and corrosion control is an issue that is being worked worldwide.

The MYRRHA staff is aware of these challenges and is working on aggressive R&D tasks to address the issues. The R&D phase of the program is likely to last for another 3-4 years. The guidance committee recommended that MYRRHA should go forward with a dedicated R&D effort and continue the conceptual design, especially in areas where decisions that can impact the design optimization are not ready yet. For instance, a decision on whether to use a LINAC or a cyclotron must be made soon and then the design re-optimized based on that decision. In general, the MYRRHA schedule of 10 years to deployment is very optimistic and must be revised given the additional research that is needed.

3.2 Materials

The major objective of the materials activities is to test and quantify materials properties under proton and neutron irradiation.

Scope

The major activities in this area are continuation of the high-temperature testing of irradiated materials, irradiation test plans, collaborations with the Paul Scherrer Institute (PSI) materials program, and updating and maintaining the *Materials Handbook*. Specifically, testing in hot cells will support the AAA Program by determining the mechanical properties of structural materials at prototypic temperatures after irradiation in a proton beam. This will involve testing some materials irradiated at LANSCE at low temperatures and testing materials irradiated at PSI at high temperatures. The following are the activities in support of this mission:

- Receive and test irradiated rods from PSI;
- Order and install a high-temperature furnace for performing mechanical tests on specimens in vacuum or argon at temperatures up to 700°C;
- Perform bend tests at 300°C, 400°C, and 500°C on F82H, 9Cr-1Mo, and SS-316L;
- Perform compression tests on W at 600°C;
- Perform mechanical tests on Ta at high temperature;
- Continue high-temperature testing of 9Cr-1Mo at PNNL;
- Complete and publish new chapters of the *Materials Handbook*, including 9Cr-1Mo, W, Ta, Hg, LBE, and corrosion on various steels;
- Prepare an irradiation test plan (mostly in reactors) for cladding duct materials; and
- Review the reactor irradiation database as applicable to transmutation.

Work in the materials area has been curtailed due to budget uncertainties.

Highlights

- Two DRAFT chapters of the *Materials Handbook* were published and reviewed: Chapter 19 on 9Cr-1Mo (T91), Ferritic-Martensitic steels, and Chapter 22 on Lead-Bismuth Eutectic (LBE).
- LANL Materials Team co-sponsored the “Fifth International Workshop on Spallation Materials Technology” held May 20-24 in Charleston, SC. The team members presented a number of papers at this workshop.

PNNL Activities

Transmission Electron Microscopy (TEM) was performed on Mod 9Cr-1Mo that had been irradiated to 1.4 dpa at 35-70°C and subsequently thermally aged at 500°C for about 2 hours. Observations reveal no bubble formation. Figure 52 shows a TEM image of a thermally aged (500°C) 1.4-dpa specimen next to a 9-dpa specimen with no thermal aging.

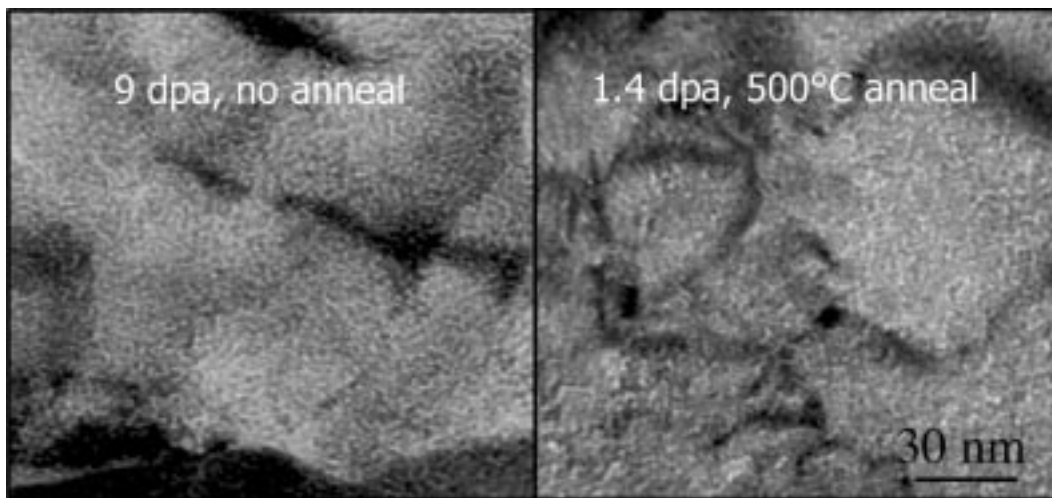


Fig. 52. TEM image showing no bubble formation after 500°C anneal of a 1.4 dpa specimen. An image of a 9 dpa specimen with no anneal is shown for comparison.

PNNL scientists reviewed the alternative design for a tensile test fixture for the tensile test system under construction at LANL. Also, another shipment of TEM specimens was returned to LANL.

We prepared manuscripts on the tensile properties of Mod 9Cr-1Mo for submission to the proceedings of two conferences. Also, a manuscript on the performance of a new shear punch fixture was submitted for publication in the ASTM's “21st Symposium on the Effects of Radiation on Materials.”

ANL Activities

A draft report, “Advanced Accelerator Applications Cladding and Duct Review,” is currently under review and will be issued in July. Based on the performance of HT-9 in the fast reactor program and the fusion energy program, the following initial conclusions and recommendations have been reached for fuel and cladding applications for ADS systems:

- 1) In the temperature range of 400°C–650°C, HT-9 has adequate swelling resistance, toughness, strength, and ductility.
- 2) At room temperature, HT-9 that has been irradiated at lower temperatures (conservatively <400°C) can become brittle and hot cell operations must ensure no excessive stress is placed on cladding and duct material. Notches or stress concentrations in the design must be avoided.
- 3) Because of the high ductile-to-brittle transition temperature (DBTT) measured in material irradiated in the High Flux Isotope Reactor (HFIR) at 400°C, which had He concentrations of 353-391 appm, He limits should be applied to HT-9 used in ADS cladding and ducts until prototypical experimental data can be obtained. Also, a minimum irradiation and minimum handling temperature for irradiated HT-9 components should be set.
- 4) Because of large amounts of hydrogen and helium generated in ADS materials relative to fast reactor conditions, a test program to determine the synergistic effects of He and H on mechanical performance and swelling should be undertaken. This test program could consist of tests in a prototypical spectrum or using ion irradiation facilities as a simulation tool. A test facility producing a prototypical spallation neutron spectrum would be ideal.
- 5) A test program needs to be continued to better understand the interaction between fuel and HT-9 cladding. Studies of barrier cladding to minimize interactions need to be undertaken. Until the mechanisms of interaction are understood, a transient limit of 725°C should be placed on the cladding inner surface.
- 6) Alloys are under development that may improve performance relative to HT-9. Programs aim to improve high temperature creep strength and low temperature toughness. For most of these alloys, insufficient performance data exists. For any new alloys tested, in addition to adequate mechanical properties and dimensional stability, coolant compatibility and fuel-cladding compatibility must be verified. A component of the ADS program should study the performance of these promising alloys systems.

TEM investigations on unirradiated HT-9 are being performed at ANL. These characterizations will be contrasted later with those of ion implanted and irradiated samples. The results of the unirradiated examinations will be reported next quarter.

LANL Hot-Cell Work

We received the specimens irradiated in the STIP-1 irradiation at the LANL hot cells. Also, the parts for the high temperature mechanical testing furnace were received from Materials Research Furnaces, although some parts had to be sent back for re-machining.

Materials Handbook

A draft of Materials Handbook Chapter 19 (T-91 [9Cr-1MoV] ferritic/martensitic steel) was completed in April and a first review completed at LANL. Comments from this review were incorporated into a second draft that has been submitted for a third party review. The chapter should be ready for final formatting early next quarter.

The first draft of Materials Handbook Chapter 22 (Pb-Bi Eutectic) was received in May from PSI. The draft received two reviews and has been returned to PSI for incorporation of review comments and some additional data and information. It should be ready for a final review and formatting next quarter.

Revisions were made to Section 7.5.2.4 (Effects of Irradiation on Yield Strength) of Chapter 7 (Tungsten) to incorporate data from compression tests on small tungsten cylinders irradiated in LANSCE. Reviews are in progress.

Corrosion sections in Chapters 2, 3, 4, and 7 (Alloy-718, SS-316L, Al-6061-T6, and Tungsten, respectively) were revised in June to incorporate results from corrosion tests conducted during 800-MeV proton irradiation at LANSCE. Reviews are in progress.

A draft Materials Handbook Chapter on the properties of HT-9 is being developed by ANL to be issued in July 2002.

Forschungszentrum Jülich (FZJ) is to provide a chapter on tantalum, but not until next fiscal year.

Meetings/Conferences/Workshops

A number of team members attended the “Fifth International Workshop on Spallation Materials Technology” held in May in Charleston, SC. Research was presented on tensile behavior of ferritic-martensitic steels irradiated in a proton and spallation neutron environment. Also, the paper, “A Comparison of Fission Neutron and Proton/Spallation Neutron Irradiation Effects on the Mechanical Behavior of Type 316 Stainless Steel” was presented. The proceedings of the conference will be published in the Journal of Nuclear Materials.

The team members also attended the 21st Symposium on the Effects of Radiation on Materials in June in Tucson, AZ. Presentations were made on high temperature testing of Mod 9Cr-1Mo and the effect of irradiation on the properties of a clad tungsten target. The proceedings of the conference will be published in an ASTM Special Technical Publication.

3.3 Lead-Bismuth Eutectic Technology

The major objective of LBE research activities is to develop a fundamental understanding of LBE performance parameters and measurement techniques when used as a nuclear coolant, with primary emphasis on spallation-target applications.

Scope

LBE Technology Development

The safe and reliable implementation of the LBE technology requires additional developments for the oxygen sensors. Development of other nonintrusive flow measurement and online corrosion measurements would significantly improve the reliable operations of an LBE target. The development will be carried out in collaboration with international partners (e.g., CEA and FZK) under DOE agreements. By collaborative testing, the objective is to achieve in 3–4 years a TRL-4 level where

a parametric (velocity, temperature, materials, thermal gradients, etc.) is developed to Pb into the spallation-target conceptual design.

The scope of this work package involves developing new sensor technologies and corrosion data analyses with the long-term objectives noted above. Some of the actual tests will be performed in the DELTA Loop (Materials Test Loop) at LANL, and testing must be closely coordinated with loop-operation work-package activities. The FY02 activities are as follows:

- Fabricate oxygen probes to be tested in the DELTA Loop;
- Develop a calibration standard in conjunction with international partners;
- Cross-calibrate oxygen sensors;
- Develop gas and solid-phase oxygen control methodology;
- Develop concepts for low-temperature oxygen probes;
- Develop ultrasonic laser velocimetry technique;
- Analyze corrosion data;
- Develop and design components for FY03 testing (with international collaboration); and
- Revise the DELTA Loop test plan according to international collaboration work packages.

DELTA Loop Operations

The DELTA Loop will be operated to validate key Russian LBE nuclear-coolant technology, to perform corrosion and thermal-hydraulic testing, and to develop diagnostics and probes for application in a high-powered spallation-target system. Again, the tests will be carried out in collaboration with international partners.

The scope of this work package involves operating, maintaining, and upgrading the DELTA Loop in accordance with the long-term objectives mentioned above. The actual test plans will be developed under the LBE technology work package, and operations must be closely coordinated with activities under that work package. The FY02 activities are as follows:

- Completing construction for operational and instrumentation testing;
- Addressing all post-start findings;
- Performing operational tests;
- Testing oxygen control techniques and procedures;
- Updating data acquisition and control (DAC) system and hazard control plans for unmanned operations;
- Installing new instruments (e.g., improved oxygen sensors and ultrasonic velocimetry) as delivered from the LBE technology team; and
- Performing 1000-hr corrosion tests (two different materials and/or two different velocities).

Highlights

- The safety basis for the unmanned operations of the DELTA loop was completed, reviewed, and approved.

LBE Technology Development

This task provides LBE technology development in several key areas to support DELTA Loop operations and development of LBE spallation targets. Important progress was made in oxygen control system and sensor calibration, corrosion modeling, and benchmarking the TRAC code with DELTA test-operation data.

An oxygen control and sensor calibration system based on a hydrogen and steam mixture was assembled and started (see Fig. 53). Preliminary testing indicated that the oxygen concentration in LBE was adjusted by hydrogen injection and the sensor responded accordingly. The gas line developed a leak and the event of air ingress was recorded, which clearly illustrated the working mechanism of the system (see Fig. 54). Improvement for increased gas/LBE interaction efficiency is underway after the leak was detected and stopped.



Fig. 53. An oxygen control and sensor calibration system based on hydrogen and steam mixture.

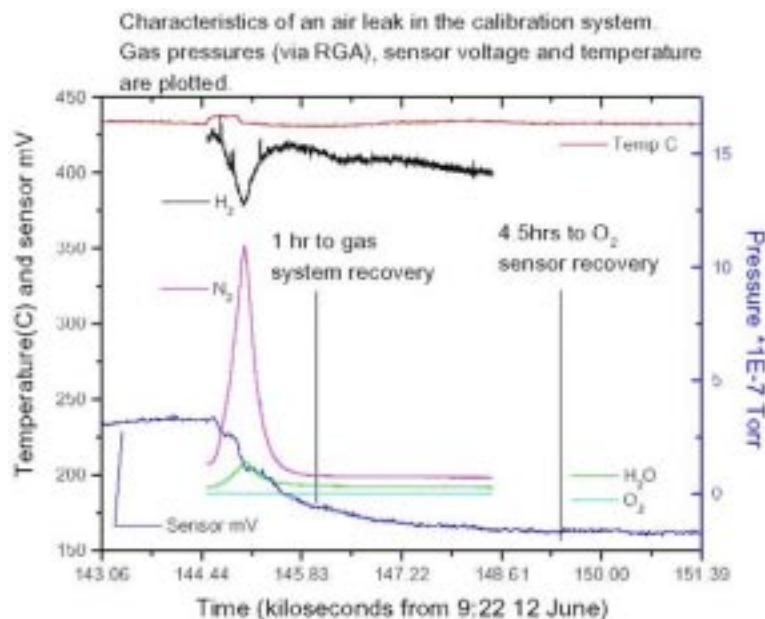


Fig. 54. RGA recorded air ingress through a gas leak into the oxygen control system.

A report on oxygen control methodology and sensor calibration strategy was issued, detailing the advantages and disadvantages of gas-phase and solid-phase oxygen control, and providing key implementation guidelines. The oxygen sensor calibration standard is established, and several alternatives for cross calibration and validation are outlined.

Significant progress has been made on the modeling of corrosion in oxygen-controlled LBE systems. The widely used corrosion-rate model based on a mass-transfer coefficient is refined by taking into account the effect of bulk corrosion-product concentration with the incorporation of the test-loop configuration. The improved model predicts corrosion rates in better agreement with the experimental results when loop dimensions are available.

The average corrosion rate in the DELTA Loop test section is mapped against the test temperature and loop temperature difference (see Fig. 55). It is found that the corrosion rate increases drastically above 550°C, and it starts to saturate after the temperature difference reaches 100°C in the 500°C– 550°C range. This result proves that the selection of the DELTA Loop test condition is near optimal.

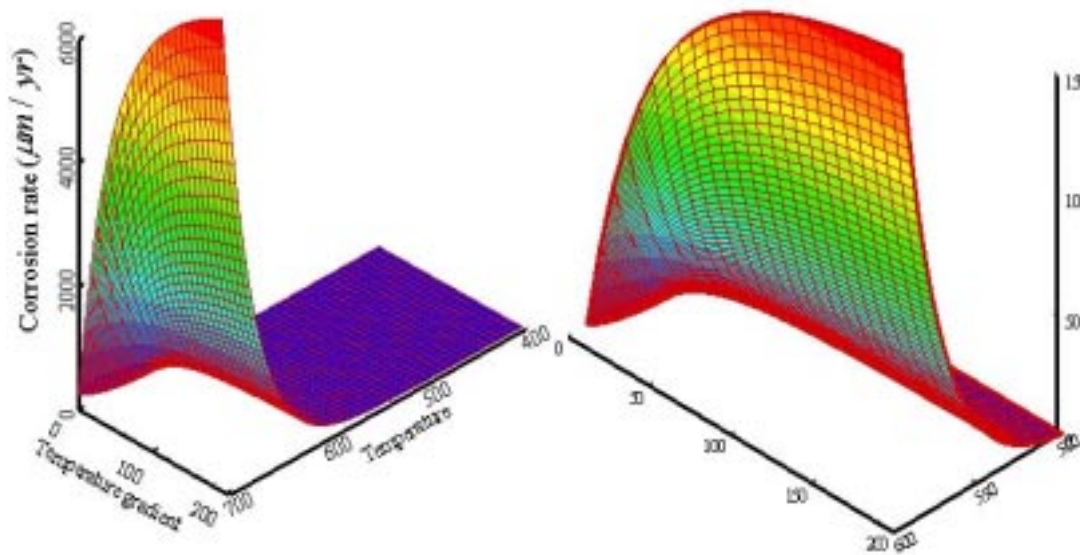
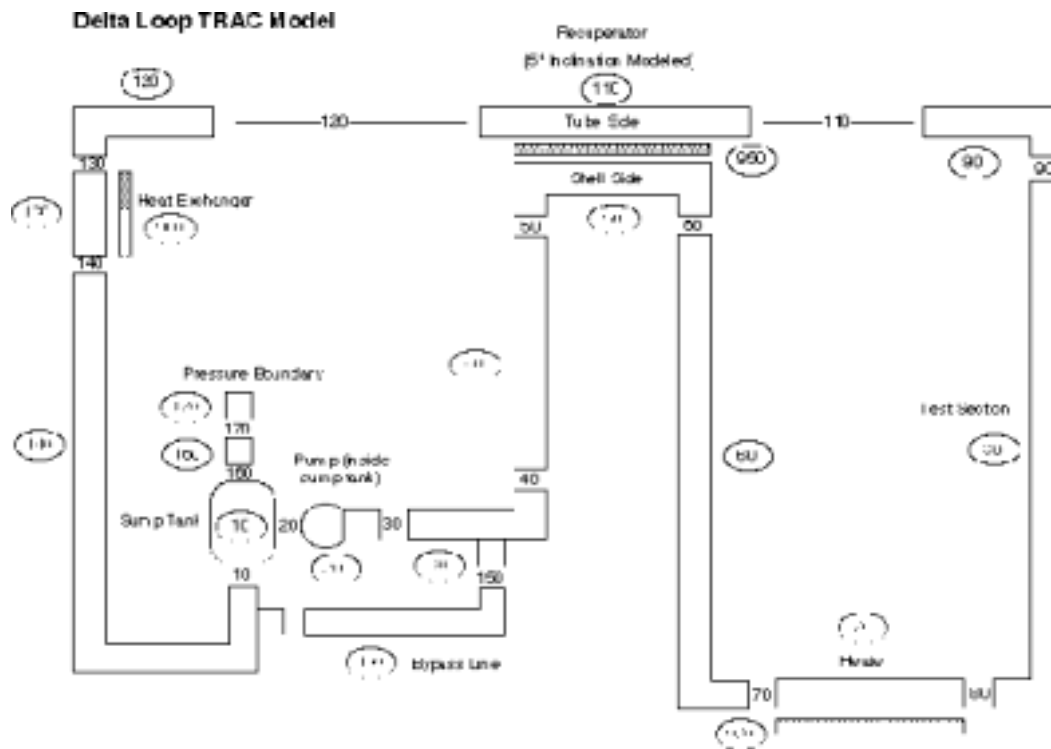


Fig. 55. Average corrosion rate in DELTA Loop test section for $v = 0.6\text{m/s}$, oxygen concentration of 10^{-6} wt\% .

A TRAC-code model for the DELTA Loop was developed with proper pipe sizes, elevation, and calculated loss coefficients (see Fig. 56). The model has been checked and calculated to steady state at several different mass flows and power settings. It will be benchmarked against the DELTA Loop test operation data. We plan to adapt TRAC to support MEGAPIE safety studies.



We continue to participate in the international and university collaborations in LBE technology development. We received 13 visits, 6 from universities and 7 international groups.

DELTA Loop Operations

For this quarter, the main tasks are to prepare for the corrosion tests in FY02. The operational tests to ensure performance and safety were conducted. Several key design features were tested successfully. Some repairs and improvements were made on components with defects uncovered during testing. It is expected that the DELTA Loop will be fully operational for the corrosion tests in the fourth quarter. We obtained management and ES&H approval for unattended operations. Key results are summarized below:

- The DELTA Loop was operated for over 70 hours at temperatures up to 400°C. It achieved steady variable flow speeds up to 35 gpm (8m³/hr), as measured by a calibrated magnetic flow meter. It was operated in isothermal regimes and with temperature gradients, with stable operation of the recuperator and heat exchanger.
- The two oxygen sensors in flowing LBE read stable signals at the expected level, and responded correctly to LBE temperature fluctuations due to trace heater regulation (see Fig. 57). The sensors received several thermal shocks on the order of 10°C during the loop fill, and were subject to several thermal cycles.

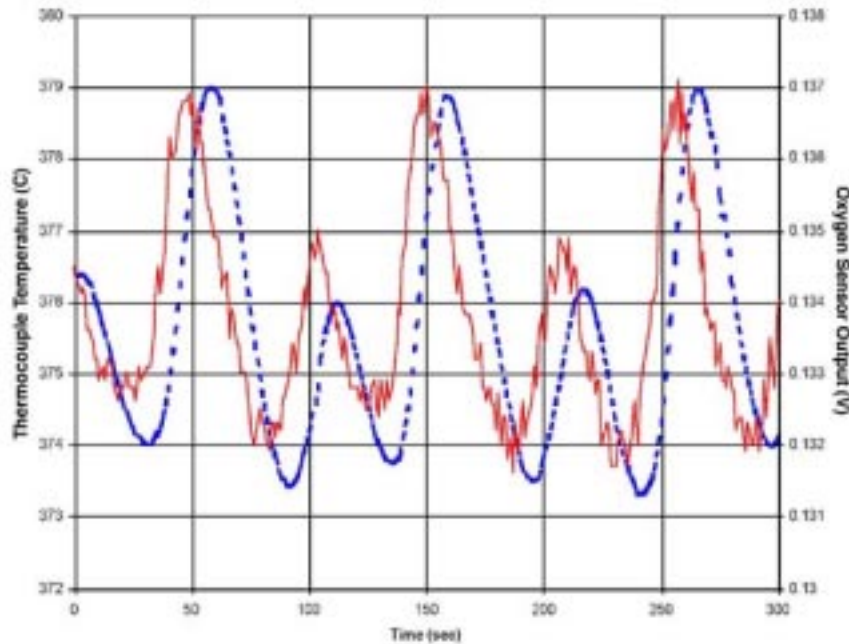


Fig. 57. Oxygen sensor readout during DELTA Loop operation.

- The freeze plug for the gas injection subsystem that performs oxygen control was upgraded after a partial blockage during the initial test. Later tests, such as forming and melting the freeze plug and maintaining constant cleaning-gas pressure, were successful.
- Unattended operations were approved and are undergoing testing. Two 48-hr unattended operations with observers were scheduled, but were interrupted due to a weld failure in an oxygen sensor. The shutdown proceeded safely with no system damage, and repairs completed.
- The data acquisition and control system including shut down controls proved reliable.
- A corrosion test plan and material selection were finalized to support programmatic needs and explore fundamental corrosion mechanisms. The programmatic (corrosion and tensile specimens) are: T-91 (MEGAPIE window candidate material), HT-9 (alternative), EP-823 (reference Russian alloy), SS-316L (base material for LBE systems), T91/316L weld (MEGAPIE design). The scientific (corrosion specimens): Ta, Si-Fe alloys (role of Si for enhanced corrosion resistance), CEA Al-316L, FZK GESA-treated 316L (surface treatment).
- The test conditions are: $T_{\max}=500^{\circ}\text{C}$, $\Delta T=100^{\circ}\text{C}$, $v=2\text{m/s}$, oxygen concentration= 10^{-6} wt%, test intervals=333, 667, & 1000 hours. The test specimens and sample holders (see Fig. 58) were designed and are undergoing fabrication.
- Plan for erosion/corrosion testing in DELTA and the needed loop extension were developed.

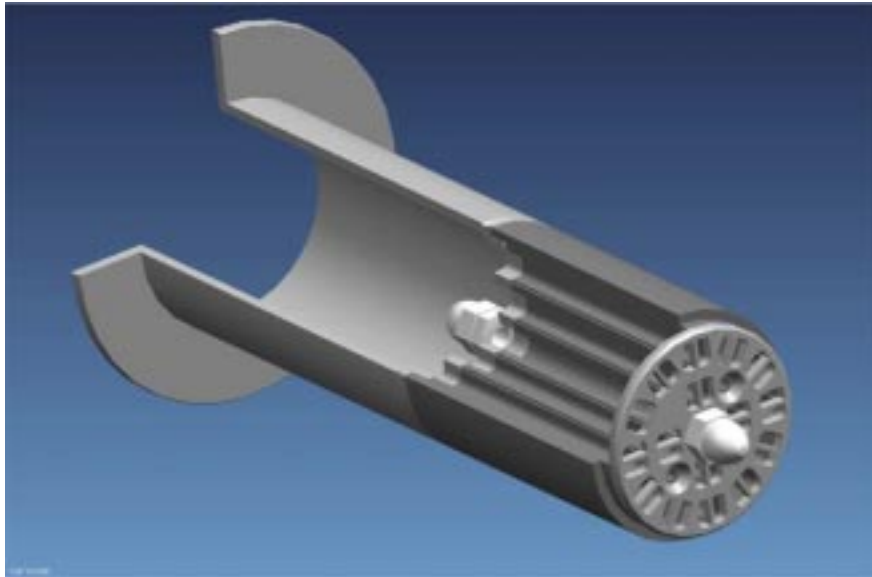
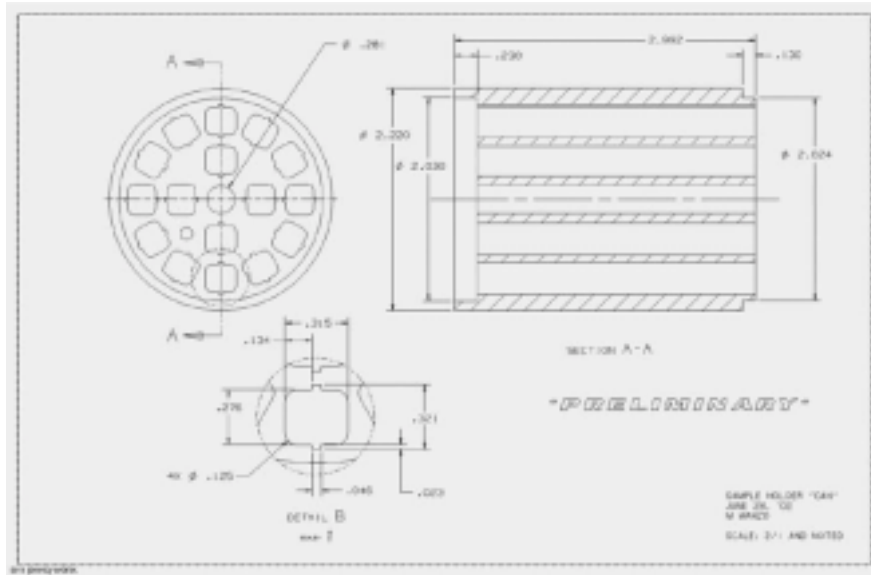


Fig. 58. DELTA Loop corrosion test sample holder design.

3.4 LANSCE Irradiation Experiments

The major objective of the LANSCE irradiation experiments is to advance the TRL for transmutation in various areas up to TRL 6 by performing small-scale proton and neutron irradiation of materials to investigate various phenomena. Specific experiments to be performed in FY02 are as follows:

- Sodium activation tests;
- Neutron yield and spectrum tests;
- Helium and hydrogen production tests; and
- Corrosion studies.

Scope

Sodium Activation Tests

If a Na-cooled spallation target is used, accurate prediction of coolant activation is important for operational and safety reasons. In the summer of FY01, we performed a series of activation tests using an 800-MeV beam. Subsequent tests at other energies were postponed because of budget reduction. The FY02 activity is limited to completing the final data report.

Neutron Yield and Spectrum Tests

Spallation neutron sources create high-energy neutrons whose energies extend up to the incident proton-energy. In the design of accelerator-driven waste transmuters, the high-energy neutrons that leak from the spallation target have three practical implications:

- They dominate the shield design because they have long attenuation lengths (18 cm in steel);
- They lead to the production of source neutrons in the fuel region, which generates a spatially dependent neutron source that influences the power density distribution in the blanket; and
- They dominate the production of helium and hydrogen atoms in the steel structural elements that reside in the multiplier region near the target, while gas production limits the lifetime of structural materials near the target.

As a means of reducing gas production in structural materials in the multiplier region, a buffer region consisting of high-atomic-mass material may be placed between the target and the multiplier. This buffer attenuates high-energy neutrons that leak from the target into the multiplier. Additionally, the configuration of the buffer and the associated beam rastering parameters are variables available to the ADTF designer for adjusting the multiplier power distribution. The objective of these experiments is to provide benchmark data for the analysis tools. The data from these tests will be combined with the gas-production test results and structural-properties test results to optimize the target and buffer design (which impacts the multiplier design). To evaluate the effectiveness of a buffer in reducing the leakage of high-energy neutrons, we propose making these measurements of high-energy neutron distributions a function of target radius.

Helium and Hydrogen Production Tests

Currently, considerable uncertainty exists in predicting the helium and hydrogen production at high energies. The objective of these experiments is to provide data to improve helium and hydrogen production cross-sections in materials near the spallation target. The data from these tests will be combined with data from spectrum tests and structural properties tests to optimize the target and buffer design (which impacts the multiplier design). Optimizing the design with large uncertainty in the design tool is not adequate and will result in a waste of time and money in the long run. Hydrogen and helium production on materials proposed for the AAA Program in the neutron-energy range up to 100 MeV will be measured. Measurements of the double differential cross-sections for proton and alpha-particle emission will provide not only data for the total hydrogen and helium production by neutrons in these materials, but also data for transport of these elements by recoil into or out of zones

of different composition in AAA designs. We will take the measurements for iron (Fe). As an integral test and to provide data quickly, an alloy of stainless steel such as SS-316 will also be studied.

Corrosion Studies

Liquid-metal corrosion is the major issue when LBE is used as a nuclear coolant or as a spallation target. If oxygen control is used to control the corrosion, it must be shown that stable oxide layers can be developed and maintained on the surfaces. This is affected by the initial conditioning of the surfaces, as well as changes in thermodynamic conditions during operations. For spallation target applications, we must also show that direct proton irradiation does not cause a drastic change in oxide layer properties adversely affecting corrosion rates. Finally, a more reliable operation is possible if a capability for online corrosion monitoring during actual operations can be developed for the loops. By collaborative testing, the objective is to achieve in 3-to-4 years a TRL 4, where a parametric is developed to lead into the spallation target conceptual design. The scope of this work involves oxide film characterization, Blue Room irradiation of oxidized surfaces, and conceptual design of corrosion probes to be used in the test loop.

Highlights

- A preliminary report publishing the results of the first quarter (Dec 01) LBE target experiments was published. Preparations for the July 02 irradiation of the 40-cm-diameter target were completed
- Preparations for the July-August irradiation for the hydrogen and helium production data on iron and chromium were completed.
- Irradiation of the oxide film in an LBE environment was postponed due to scheduling conflicts; however, laboratory work continued. Dielectric and impedance properties of a variety of oxide films formed on HT-9 and SS-316L were characterized in liquid LBE.

Neutron Yield and Spectrum Tests

Work this quarter consisted of data analysis from the Dec 01 irradiation of a 20-cm-diameter target and preparations to irradiate a 40-cm-diameter target in July 02.

For the Dec 01 irradiation, final counting of the foils was completed and all data pulled together including receipt of the full dataset from LANL Tech Area TA-48. Work continued on important refinements of the LANSCE gamma detector efficiencies that were necessary to produce precise activity estimates for the isotopes in the foils.

The time-of-flight data was analyzed and converted to a neutron spectrum. A detailed calculation in MCNPX was performed and the two results were compared. Preliminary data showed a good agreement over most of the neutron spectrum.

A preliminary report with the results of the Dec 01 experiments was published, a brief summary of which is provided here:

The experiments consisted of irradiating a solid lead-bismuth target (dia=20 cm, l=50 cm) with an 800-MeV proton beam of 20-25 nA and measuring the

neutron emission from the target by two different methods – activation foils and time-of-flight (TOF) measurements.

The foil packets consisted of several foil materials packaged together for simultaneous irradiation. The materials used for most foil packets were Bi, Nb, In, Co, Ni, Cu, Fe, Al, Au, Cd-covered Au, Rh, Ti, Zn, Lu and Tb. The materials were chosen based on the above criteria as well as to provide working experience with a few “experimental” foils such as Lu, Bi and Tb.

The irradiations and TOF measurements were conducted without incident and with minimal personnel exposure. After an initial irradiation, the foils were removed from the target and counted via gamma spectroscopy. Irradiation of the target continued with TOF measurements performed at 7.5° and 30° beam-tubes. Also, two foil packets of identical composition to the Blue Room packets were irradiated in the Target-4 facility in a known neutron spectrum to test the spectral unfolding process. Initial results from those packets show a good fit to the spectrum.

Two gamma detectors were configured at LANSCE to count the foils. Additionally, many foils were sent to the C-INC group at TA-48 and analyzed there. Initial results from the Bi foils irradiated in the Blue Room show a definite change in the hardness of the neutron spectrum over the length of the target with the spectrum decreasing in intensity but increasing in average energy as one gets further from the front face. These results are as expected, based on target modeling in MCNPX.

Preliminary results indicate that both techniques for measuring the neutron leakage provide useful and complementary information. The activation foils provide significant quantities of integral reaction data that can be used for spectral unfolding with errors representative of the uncertainties in the nuclear data. The TOF measurements provide very detailed information regarding the neutron spectra in a small solid angle (i.e. double differential data).

The goals of the initial target irradiation experiment were to: (1) provide initial experimental data for planning future irradiation campaigns, (2) provide experimental data of benchmark quality that can be used for validation of MCNPX, (3) provide experimenters with practical experience for conducting these types of measurements and data analysis activities, and (4) further develop methods and improve techniques for spectral unfolding using integral reaction data from activation foils.

Preparations for the July 02 irradiation involved fabricating a 40-cm-diameter, 50-cm-long LBE target (see Fig. 59). An aluminum stand was also fabricated to support the target in the Blue Room on a translation table that was able to shift the target location as desired. Based on experience, it was decided to use fewer foil materials but in more locations than used in the previous irradiation. Extra foil materials were ordered to create the number of packets needed, and preparations involving the cutting and weighing of materials and assembling them into packets were begun.

Two other beam-tubes at the 60° and 150° locations were made ready for use. An experimental plan was devised where the 40-cm target would be irradiated and characterized by foils and TOF, and, given time, the previous 20-cm target would be swapped into the beam to gain TOF data on it from the 2 beam tubes that had not

been previously available in December. Based on modeling, foil placement was designed to give the most effective coverage and radioactivity of the irradiated target estimated to minimize the dose to workers. Safety planning for the experiment was conducted, and protection of workers and ALARA were considered at every step.

Plans were put into place for the two university collaborators: The University of Nevada-Las Vegas (UNLV) and the University of Michigan (UM). UNLV is providing computational support with MCNPX modeling of the neutronics and CAD modeling of the experimental configurations. UM is providing assistance in neutron data and spectrum unfolding as well as long-term counting of foils. Both schools contributed summer students who arrived at LANL in mid-June for six-week appointments.



Fig. 59. 40-cm diameter, 50-cm long LBE target.

Helium and Hydrogen Production Tests

During this quarter, we improved the experimental setup in preparation for beam in the fourth quarter. Our activities included (1) improving the collimation and shielding in order to reduce backgrounds; (2) improving the light collection efficiency for the scintillator in which the charged particles stop; (3) involving three students to help in these activities and to train them in nuclear techniques; (4) preparing and presenting a progress report on this work at the Third International Workshop on the Utilisation

and Reliability of High Power Proton Accelerators, held in May in Santa Fe, New Mexico.

The collimation and shielding were significantly improved by the addition of a second shielding wall just upstream of the final shielding wall. Collimation has been improved by the fabrication and installation of new collimators with optimized dimensions before the reaction chamber, and new "clean-up" collimators in the chamber. The change in the latter is designed to reduce the charged particles produced by scattered, high-energy neutrons when they interact with the collimator. The background at the higher neutron energies should thereby be reduced.

A summer student improved the light collection efficiency for the CsI(Tl) scintillator by a factor of 3 by using a different reflector material.

We prepared and presented a paper entitled "Gas Production Cross-Section Measurements at LANSCE" at the workshop mentioned above.

Corrosion Studies

Due to WNR scheduling conflicts, we are unable to schedule beam time in July. Tentatively, we have been scheduled for WNR beam time during September. Thus, we plan to complete WNR/irradiation milestones, which were designated for the 3rd quarter in the next quarter of this FY. In areas where irradiation was not needed, considerable progress was made.

The dielectric and impedance properties of a variety of oxide films formed on HT-9 and SS-316L were characterized in liquid lead bismuth eutectic. Dielectric/impedance properties have been chosen as they reflect changes in transport characteristics that result in changes in corrosion rate. For example, substrates covered by an oxide with low specific capacitance and high impedance are generally resistant to oxidation. Thus, it may be possible to (1) use this technique to develop a real time corrosion probe for any LBE coolant system, (2) use this technique to optimize the pre-oxidation film formed in LBE loops, and (3) monitor the real-time influence of proton irradiation on oxide film properties. Earlier, we presented dielectric/impedance results from our in-beam experiments at WNR. In anticipation of additional WNR beam time in September, we have undertaken an extensive program to characterize the film properties out-of-beam. This will allow us to prepare samples for our WNR run in a more effective manner and make real-time judgments to better use our beam time. Figure 60 shows the dielectric (capacitance) and impedance of oxide films formed on HT-9 in LBE as a function of pre-oxidation time (films formed in air at 800°C). As can be seen in Fig. 60, there appears to be an optimum pre-oxidation time of approximately 48 hrs. For this pre-oxidation time, the film impedance is maximized and the capacitance is minimized. Therefore, from these results one might conclude that the pre-oxidation conditions (prior to exposure to LBE) can be adjusted to minimize corrosion rate. Currently, we are investigating these films with TEM and surface analytical techniques such as XPS to establish the mechanism of "optimization."

We are also investigating the influence of LBE operating conditions on oxide properties. For example, it is well known that oxide impedance decreases linearly with increasing temperature. An example is shown in Fig. 61. Here the impedance of an air-formed oxide film on HT-9 is measured by placing a gold foil on top of the film and measuring the impedance between the foil and the sample. As anticipated, the

impedance of the oxide decreases with increasing temperature. On returning to room temperature, the impedance of the film returns to its original state. In addition, the increasing and decreasing impedance values are in fairly close agreement. However, when this identical experiment is run using LBE instead of the gold foil, a non-linear decrease in oxide impedance with increasing temperature was observed. In addition, a hysteresis between the increasing and decreasing temperature ramps was observed (Fig. 62). That is, the impedance of the oxide does not return to its original value at the end of the experiment; exposure to the LBE has changed the native properties of the oxide. Irreversible wetting of the sample is a simple and convenient explanation for this phenomenon. This is likely an incorrect model of the system, as the sample surface was in full contact with the LBE; and further, no change in the wetting angle for LBE on this oxide was observed (Figs. 63a and 63b) with increasing temperature. We propose that this phenomenon observed in LBE is a result of absorption of LBE into the outermost monolayers of the oxide. This could occur through diffusion, as one might anticipate a temperature dependence on the diffusion coefficient as well as the kinetics associated with the transition from adsorption (wetting) to absorption. Understanding this mechanism is of importance because altering the step (through the addition of alloying materials, for example) could likely lead to materials with lower LBE corrosion rates.

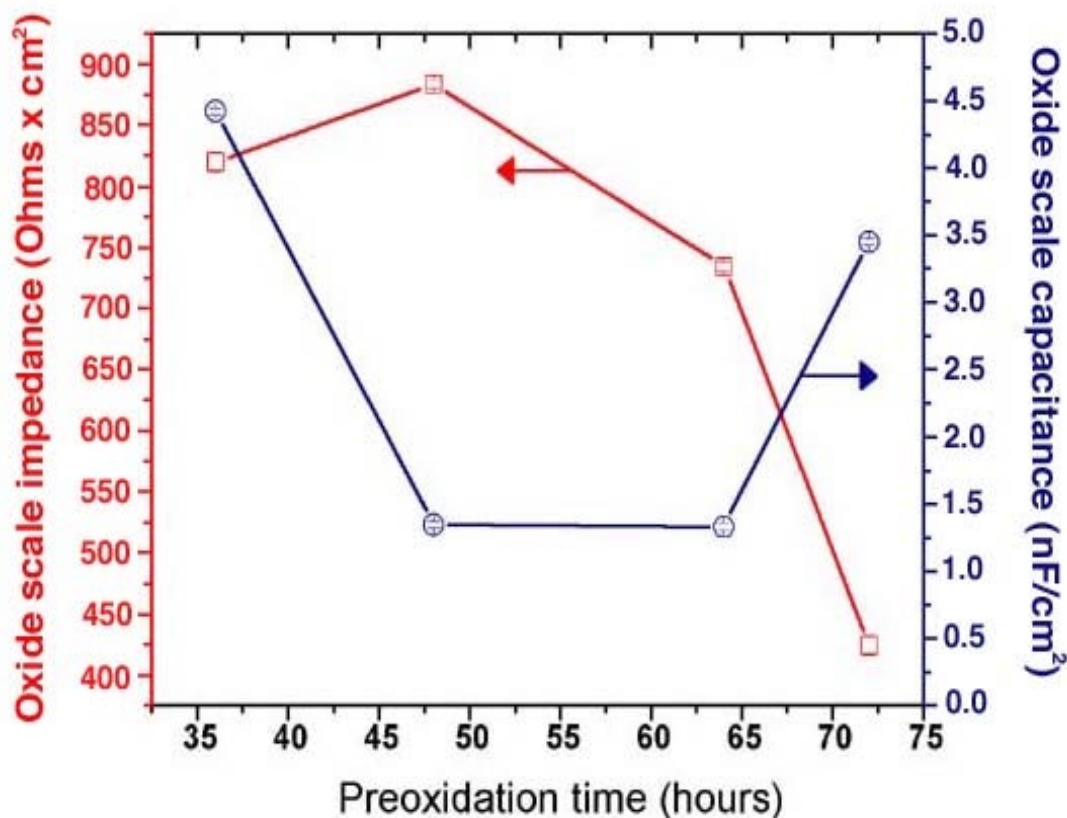


Fig. 60. Impedance and capacitance of oxides formed on HT-9 as a function of various oxidation times. All films were formed in moist air at 800°C.

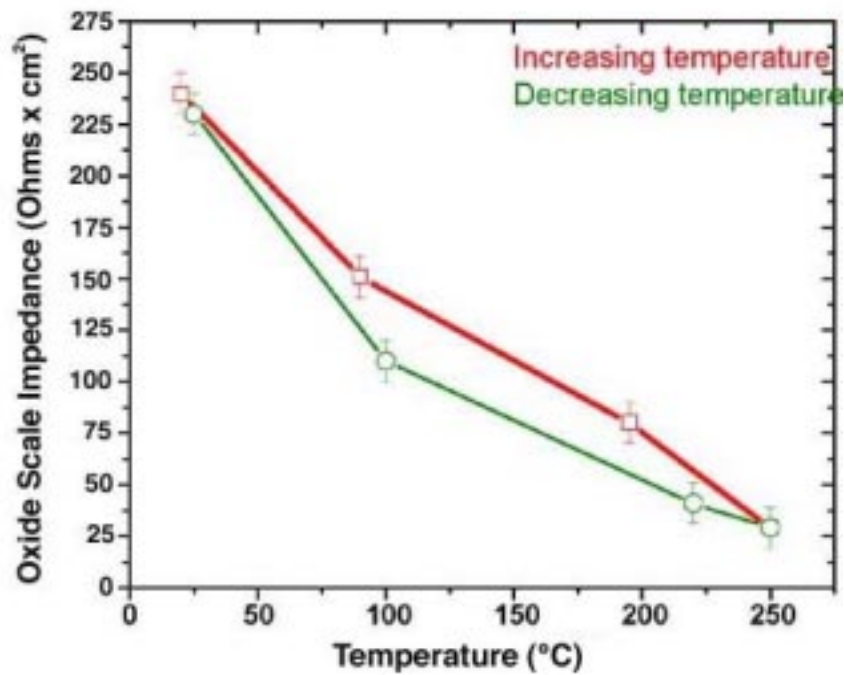


Fig. 61. Impedance of oxide film on HT-9 as a function of temperature. Values were obtained by placing a gold foil on the oxidized sample and measuring the impedance between the sample and foil in air.

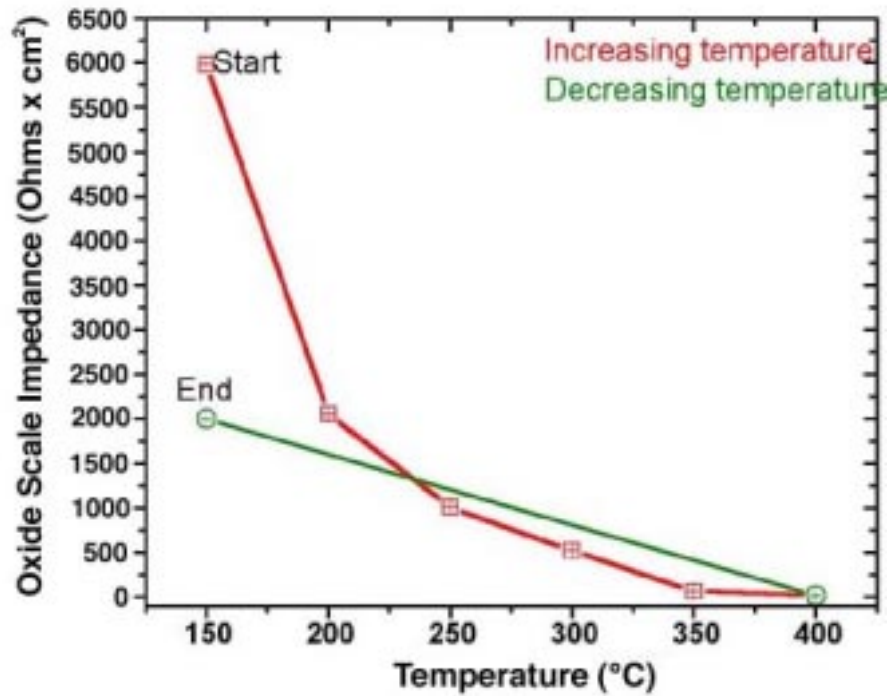


Fig. 62. Impedance of oxide film on HT-9 as a function of LBE temperature. Values were obtained by placing the oxidized sample in LBE and measuring the impedance between the oxide/LBE interface.



Fig. 63a. Wetting angle for LBE droplet on oxidized HT-9 at 210°C. Wetting angle is approximately 160°. Results were independent of the amount of oxidation prior to exposure to the LBE droplet. Similar results were obtained on other materials.

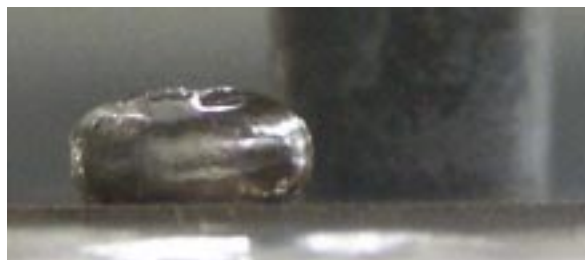


Fig. 63b. Wetting angle for LBE droplet on HT-9 at 300°C. Wetting angle is the same as in Fig. 63a at 210°C, ~160°.

3.5 High-Energy Physics

The major objective of high-energy physics activities is to improve and maintain the computer codes used in the analyses of accelerator-driven transmutation systems. As part of the improvement, the nuclear data accuracy will be reevaluated to match the desired objectives.

Scope

MCNPX Code Development

MCNPX code development consists of the following activities:

- Development of the "mix and match" capability within MCNPX, which requires production of a version of MCNPX in which evaluated data libraries with different upper-energy limits may be used within the same MCNPX run. This will allow the new LA150n data tables to be used simultaneously with the standard 20-MeV data tables for those isotopes that do not appear in LA150n. (LA150n refers to Los Alamos-generated nuclear data library, extending up to 150 MeV.)
- Incorporation of the Cugnon intranuclear cascade and Schmidt evaporation models into MCNPX, which will be carried out in collaboration with CEA-Saclay under the CEA-AAA collaboration framework. CEA will install the

models in MCNPX, with LANL oversight. LANL will perform a quality check of this work and incorporate the code changes into the official release.

- MCNPX maintenance and beta testing, which involves maintaining an approved list of beta testers for the code and fixing bugs as beta testers report them. Regular releases of MCNPX will be transmitted to the Radiation Safety Information Computational Center (RSICC) as significant improvements to the code are made.

Nuclear Data Evaluations

The nuclear data activities include production of new neutron fission and capture ENDF (Evaluated Nuclear Data File) evaluations to 150 MeV for two actinide isotopes of highest priority. This involves the following:

- Calculating fission barrier and ν -bar¹ data to 150 MeV;
- Using the results of GNASH (nuclear reaction code) to generate model-based cross-sections; and
- Using advanced statistical methods to combine discrepant experimental data in the adjustment of the GNASH-generated results to produce new evaluated cross-sections.

As part of these activities, NJOY data processing of new ENDF evaluations and generation of data files of the new ENDF evaluations using the NJOY code will be performed.

The nuclear data tasks also include improving ²⁰⁸Pb inelastic scattering ENDF cross-section and production of a new version of ENDF ²⁰⁸Pb neutron cross-section that improves the inelastic scattering in the few MeV energy regions.

Highlights

- The first fully parallel version of the MCNPX code was produced and tested on a LINUX cluster at LANL.
- A revised MCNPX User's Manual was given to RSICC for the release of MCNPX 2.3.0.
- MCNPX version 2.4.k was released to the beta test team in June.
- AAA staff collaborated with staff at ECN (The Netherlands) on high-energy nuclear models and data for ATW. The ECN staff was interested in receiving our new AAA-funded ²⁰⁸Pb ENDF evaluation to test the sensitivity of our inelastic scattering upgrade on k_{eff} (preliminary work suggests a rather large ~2.5% effect).
- Improvements of a modified version of the CEM2k code to describe fission fragment production were completed, and our CEM2k+GEM2 code can now be used with confidence to predict fission neutrons for the LA150 actinide libraries.

¹ Average number of neutrons released per fission.

MCNPX Code Development

Light ion recoil was added to the MCNPX code so that light residual nuclei are treated as fully transportable particles. A Fermi Gas treatment was also implemented for protons, which improves the accuracy of energy deposition calculations in light materials. Figure 64 shows a series of 5 energy spectra of ^3He residual nucleus recoil energies for five different neutron incident energies on ^3He (.01, 0.1, 1.0, 10.0, 100 MeV). In previous versions of the code, these light ion recoils were not transported, and their energies were deposited locally.

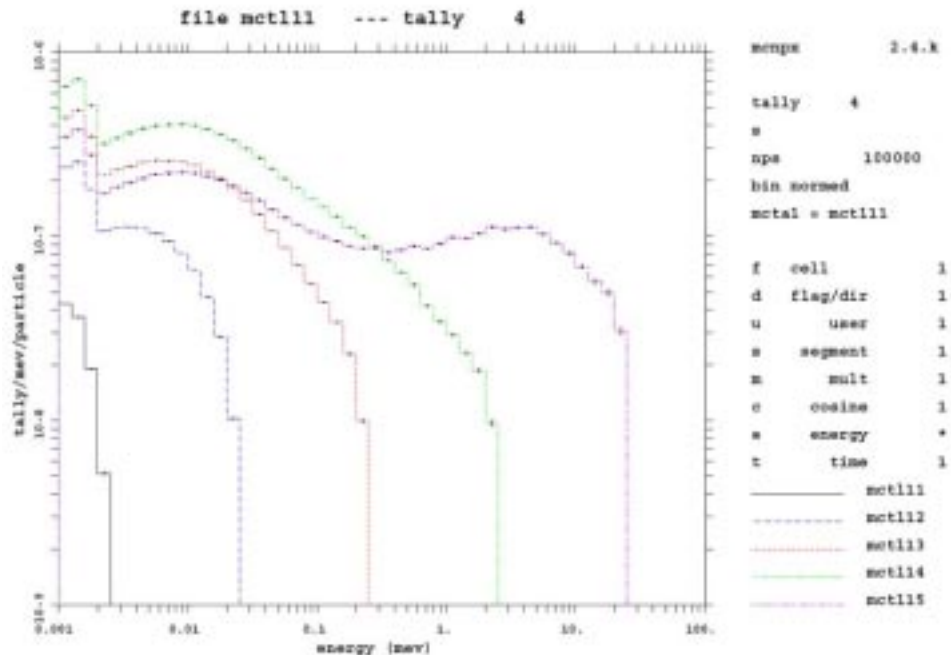


Fig. 64. Spectra of helium-3 residual recoil energy

The first fully parallel version of the code was produced and tested on a LINUX cluster at LANL. The code can do multiprocessing in both the 'tabular' and 'physics' energy regions. Also, a new source option for description of spontaneous fission from selected nuclides was added. Photonuclear reaction multipliers were added to the tally capability, so as to be consistent with the neutron and proton reaction multipliers.

The latest version of the CEM2k code was received from Oak Ridge for inclusion into MCNPX. This version also includes photonuclear physics models above the tabular region, up to ~1 GeV. The new module also runs much faster than earlier versions, due to better optimization of software coding.

In June, we also received the Cugnon INC and Schmidt evaporation models from our collaborators at Saclay. These are currently being implemented into MCNPX.

A revised User's Manual was given to RSICC for the release of MCNPX 2.3.0. This is the last version of the code based on MCNP4b. MCNPX version 2.4.k was released to the beta test team in June, including the full multiprocessing capability as well as enhancements described above (except the new CEM, Cugnon and Schmidt

models). Improvements were also made to the geometry displays so that an expanded color base is available to the user. Version 2.4.k will form the basis for the next RSICC release by the end of the fiscal year.

The team members attended the ANS Radiation Protection and Shielding meeting in Santa Fe in April, where 21 MCNPX-related papers were presented. Additionally, the team taught 20 students at a 5-day MCNPX class held in Santa Fe, NM in April, an invited MCNPX advanced class at the Paul Scherrer Institute in Switzerland in June, and 28 students at a 5-day MCNPX class at ITN, Lisbon, Portugal also in June. The Lisbon class was co-sponsored by NEA, and among others, included European "Accelerator Driven Systems" researchers from Saclay, Cadarache, and PSI.

Nuclear Data and CEM2k Code Development

We have been working on improvements of a modified version of the CEM2k code to describe fission fragment production with the subsequent evaporation of neutrons and other particles. This version of our code is a product of merging the CEM2k code with the GEM2 code by Furihata, which contains evaporation of up to 66 different particles and a fission model based on Furihata's modification of the Rutherford-Appleton fission model by Atchison from LAHET. We tested this modification of our code on fission cross sections, mass distributions and yields of fission fragments for all reactions measured recently at GSI (Gesellschaft für Schwerionenforschung in Darmstadt, Germany) and several more reactions measured earlier at other laboratories. We found that a number of modifications have to be made in the Furihata code, GEM2, to solve many technical problems we met when simulating evaporation from compound nuclei with a very high excitation energy, or when calculating evaporation of particles from light nuclei. The fission part of the Furihata code had also to be improved to be able to obtain correct fission cross-sections both for actinides and pre-actinides.

To better describe complex particle emission at the pre-equilibrium stage of reactions, we improved the calculation of the probability of several excitons to coalesce into a complex particle that can be emitted along with nucleons during the equilibration process. All these improvements allowed us to better compute both fission and spallation reactions and to obtain a better agreement with measured data in comparison with other modern codes used by the applied nuclear physics community.

An example of our fission results is compared in Fig. 65 for the yield of all measured isotopes from $p(100 \text{ MeV}) + {}^{238}\text{U}$ with experimental data from Titarenko² and with results to predictions by the NASA phenomenological model YIELDX of Sliberberg, Tsao, and Barghouty, and to the LANL phenomenological code CYF by Wahl. We see that our new CEM2k+GEM2 code describes these measurements so well that our results almost coincide with the data covering most of the data points in the Fig. 65, while both the phenomenological codes fail here. Our CEM2k+GEM2 code can now be used with confidence to predict fission neutrons for the LA150 actinide libraries.

Another example of our results, for a spallation reaction of interest to AAA, is shown in Fig. 66, where we compare the CEM2k+GEM2 predictions with the recent GSI measurement of the reaction $p(1 \text{ GeV}) + \text{Fe}56$. We also compare our calculations

² (ITEP, ISTC Report 839B-99, Moscow, 2001)

to: results obtained from the last version of the intranuclear cascade model by Cugnon coupled with the Schmidt's evaporation/fission model (INCL) incorporated recently into LAHET and MCNPX; and results from the ISABEL code, also used by both LAHET and MCNPX transport codes. Note that the INCL (Cugnon + Schmidt) code was developed and the GSI measurement was done for the HINDAS project of the European transmutation of nuclear wastes project. One can see that our new CEM2k+GEM2 code describes these data much better than the new code by Cugnon+Schmidt, and better than ISABEL. Similar results were obtained for all other reactions measured so far at GSI.

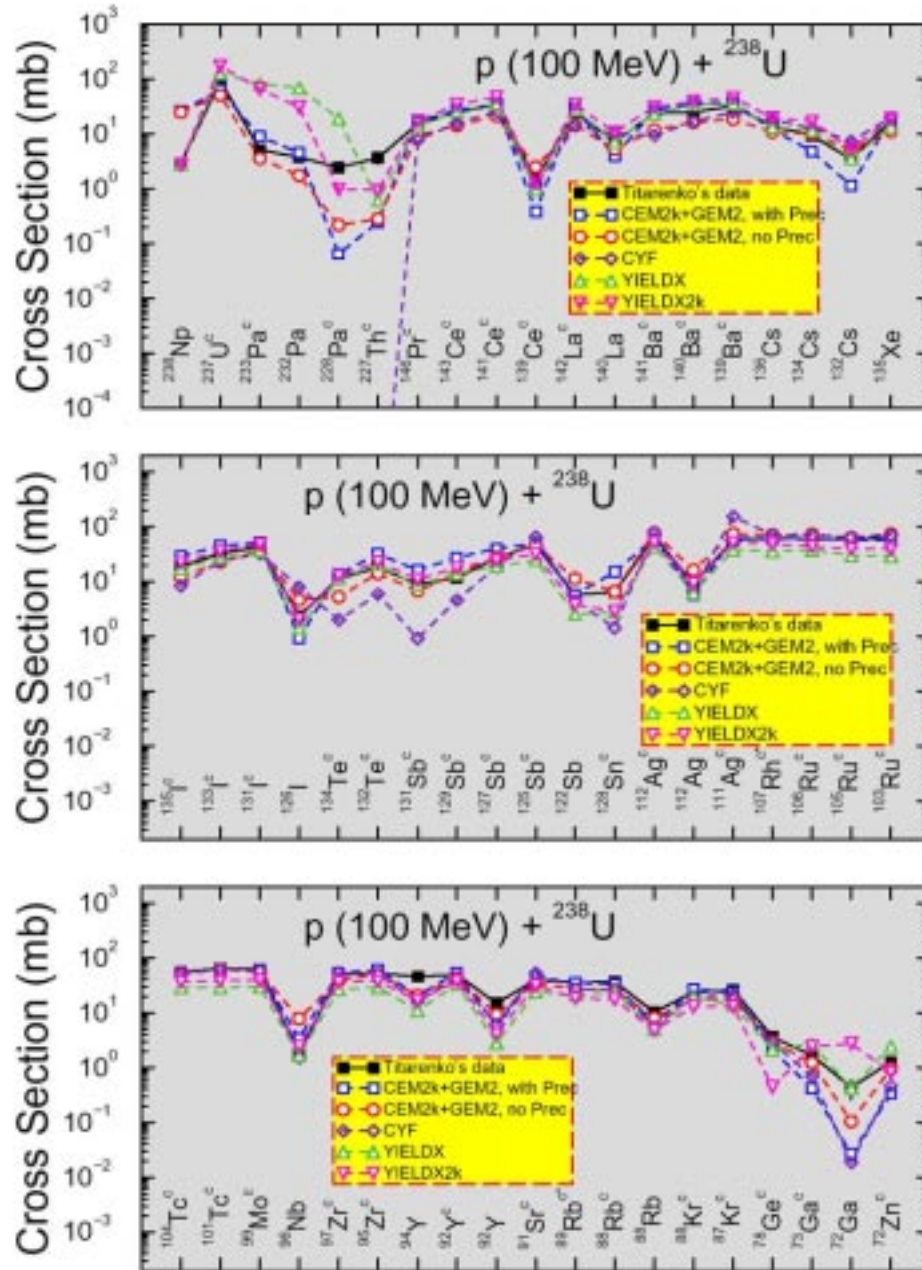


Fig. 65. Yield of all measured isotopes from $p(100 \text{ MeV}) + {}^{238}\text{U}$

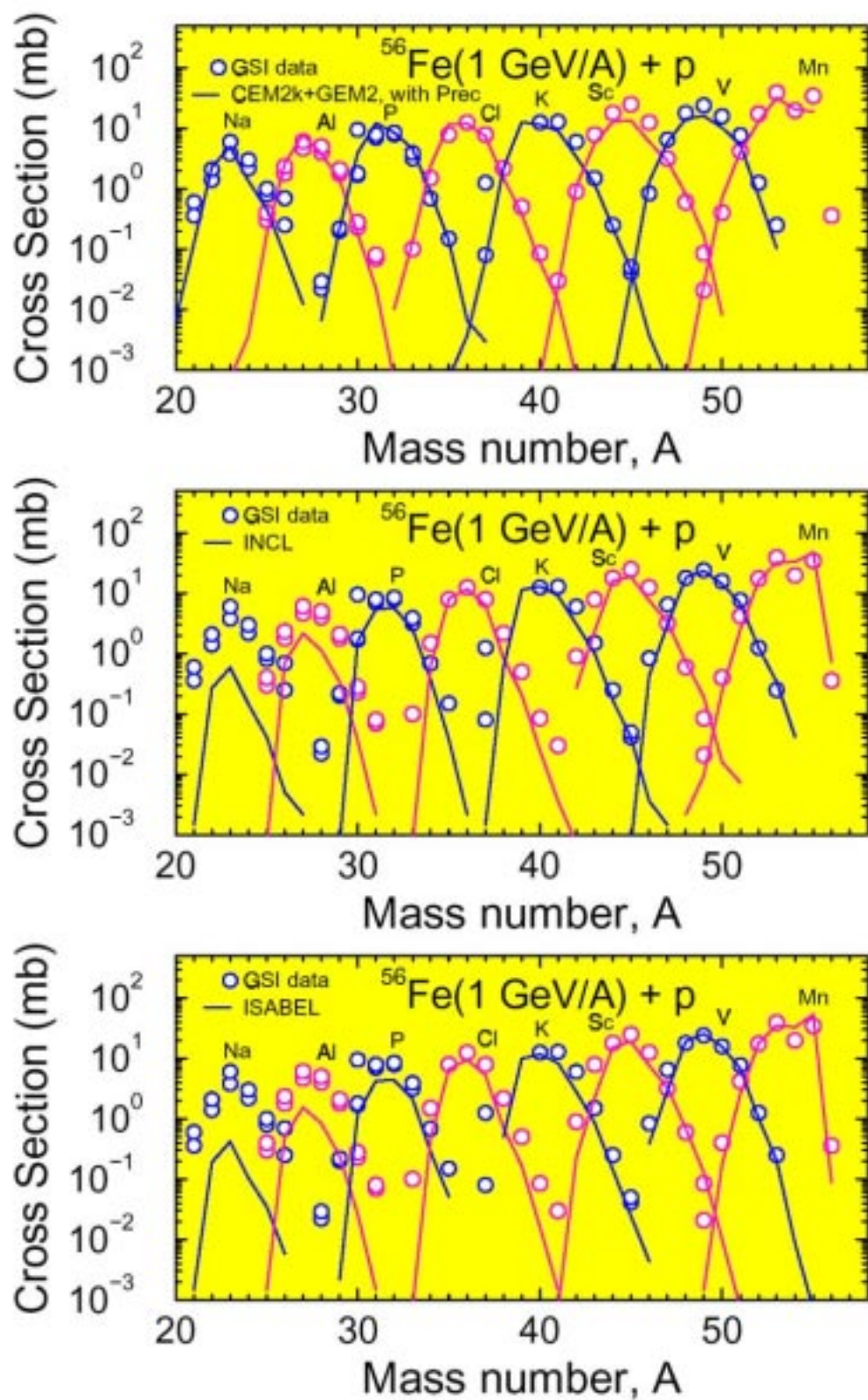


Fig. 66. Comparison of the CEM2k+GEM2 predictions with the recent GSI measurement of the reaction $p(1 \text{ GeV}) + ^{56}\text{Fe}$

During this quarter we presented our results in four invited talks at the 6th Int. Workshop on Shielding Aspects of Accelerators, Targets and Irradiation Facilities (SATIF-6), April 10-12, 2002, Stanford Linear Accelerator Center, CA, and the 12th Biennial Topical Meeting of the Radiation Protection and Shielding Division (RPSD) of the American Nuclear Society, April 14-17, 2002, Santa Fe, NM and published part of these results in LANL Reports³ and in Physics Review.

LA150 Actinide Cross Section Evaluations for ²³⁹Pu and ²³⁸U

We continued our LA150 work on $n+^{238}\text{U}$, ^{239}Pu reactions at higher energies, up to 150 MeV. The ²³⁸U nucleus is valuable to study because of the larger amount of experimental data available, compared to other actinides. The LANL total cross-section data (Abfalterer, Dietrich et al, funded by APT, and Lisowski), together with absorption and elastic scattering data, enabled us to develop a new relativistic high-energy optical potential for ²³⁸U and ²³⁹Pu. This is important for allowing us to model and evaluate (n,fission) as well as (n,xn) neutron production cross sections. Mashnik continued testing and development of his CEM code to model fission neutron production for the LA150 actinide cross-section libraries (see above).

Chadwick (LANL) attended an NEA WPEC⁴ meeting in Belgium, where the latest work on experiments and cross-section evaluations were discussed, to facilitate collaborations between the US (LANL) and European and Japanese projects. There were considerable useful discussions of work on accelerator transmutation of waste. Talou and Madland (LANL) also presented their work at this meeting. Chadwick also spent a week collaborating at ECN (The Netherlands) on high-energy nuclear models and data for ATW. ECN staff performing MCNP(X) calculations for ATW systems, were interested in receiving our new AAA-funded ²⁰⁸Pb ENDF evaluation to test the sensitivity of our inelastic scattering upgrade on k_{eff} . Their preliminary work suggests ~2.5% effect, which is considered large.

3.6 Reactor Physics

The reactor physics task involves the codes and methods used to assess the transmutation process. The objective also includes defining and designing long-term experiments needed to advance the TRL in this area.

Scope

Experiment and Safety Analysis

This task consists of analyzing physics experiments and developing a safety analysis strategy applicable to accelerator-driven system (ADS) design. Part of the physics experimental work consists of providing high-quality experimental data; and for this purpose, ANL personnel will participate in collaboration with CEA to perform the critical and subcritical experiments of the MUSE4 configuration. To validate data and methods for the neutronic design of an ADS, an analysis of the experimental results obtained in the MUSE4 program will be performed using both deterministic and stochastic codes with different data files (e.g., JEF2 and ENDF/B-VI). Additionally, the

³ LA-UR-02-0305, LA-UR-02-0608, LA-UR-02-0609, LA-UR-02-1409, LA-UR-02-2915, and in Phys. Rev. C65, 064610 (2002).

⁴ Working Party on Evaluation Cooperation

irradiation experiments PROFIL-1 and -2 will be analyzed, in which samples of actinide isotopes were irradiated in the French Phenix reactor. The objectives for safety analysis are to develop the conceptual safety design basis and criteria for ADS reactors, to develop and verify the computational safety analysis methods and computer codes necessary for safety assessment of ADS reactors, and to perform initial scoping analyses of design basis and bounding accident sequences for an ADS reactor conceptual design.

Physics Needs and Methods Development

Physics needs will be assessed by performing uncertainty evaluations and developing new capabilities for computational tools used for the neutronic analysis of ADS. Work will be performed to define physics needs and needs related to cross-section data uncertainties. In a first phase, sensitivity and uncertainty analyses will be performed for minor-actinide-dominated fuel compositions. A significant effort will be devoted to extend the present field of applicability of deterministic tools to energies >20 MeV, taking into account phenomena (e.g., gas productions) that can be affected by uncertainties in this energy range. Code and methods upgrades are needed to improve our capability to correctly calculate coupled systems with deterministic tools. The iteration strategies for equilibrium concentrations in the REBUS-3 burnup code will be modified to eliminate instabilities observed for subcritical and deep burnup conditions. Implementation of multivariate cross-section fitting capability will also be performed. Coupling with high-energy (spallation) source calculation has to be extended to the 3-D geometries (Cartesian and hexagonal) and needs to be implemented in a more flexible manner. Considerations will also be given to the possibility of developing an entirely deterministic coupled calculation (i.e., spallation and high-energy charged-particle transport treated deterministically).

Physics Experiment Planning

To simulate the physics and dynamic behavior of accelerator-driven systems and to support their design, an action will be taken to investigate the possibility of using the TREAT and ZPPR facilities located at ANL-W. The information coming from the potential experiments performed at these facilities will play a critical role in validating data, codes, and methods needed for reducing uncertainties and margins for the design of an ADS. Experiments will be planned to complement existing and future experimental programs (e.g., MUSE, TRIGA) carried out by foreign partners. The scope is to provide an experimental plan, to perform sensitivity analysis for justification of the program, and to define the objectives and feasibility of experiments.

Highlights

- The deterministic calculations of the Step 3 subcritical configurations of the MUSE benchmark using JEF2.2, ENDF/B-V and VI data and ECCO and MC²-2 cell codes were performed by ANL.
- An initial version of a utility code named FIXSOR was completed last month to couple the high-energy spallation source calculation with the deterministic codes.
- Results relative to the PROFIL-1 analyzed with JEF2.2 data are in good agreement with the corresponding results coming from previous studies performed at CEA.

MUSE Benchmark

Work continued on the MUSE benchmark. Results for the deterministic calculations have been compared against VIM, Monte Carlo calculations (see Table 17). Results indicated that a large discrepancy exist for cross section generated by MC²-2 especially for ENDF/B-VI and JEF2.2 data. Further perturbation calculations have been carried out in order to better investigate this problem. The perturbation analysis has shown that the origin of the discrepancy lies in the structural material (especially ⁵⁶Fe) cross sections for energy larger than 50 KeV. It is believed that a specific treatment of the resonance data above this energy is needed for the MC²-2 code. A specific action has been taken and results will be presented next quarter.

Table 17. Criticality Constant K_{eff}

| | Library & Codes Specifications | K_{eff} (rho [p cm]) |
|--------|--|-------------------------------|
| ERANOS | JEF2.2-ECCO-VARIANT | 1.00071 (71 pcm) |
| | JEF2.2 – MC ² -2 – VARIANT | 1.01066 (+1055 pcm) |
| | ENDF/B-V – MC ² -2 – VARIANT | 1.00718 (+713 pcm) |
| | ENDF/B-VI – MC ² -2 – VARIANT | 1.01361 (+1343 pcm) |
| VIM | JEF2.2 | 1.00436 ±0.0009 (439 ±90 pcm) |
| | ENDF/B-V | 1.0037 ±0.0010 (369 ±100 pcm) |
| | ENDF/B-VI | 1.0052 ±0.0009 (517 ±90 pcm) |

The deterministic calculations of the Step 3 subcritical configurations of the MUSE benchmark using JEF2.2, ENDF/B-V and VI data and ECCO and MC²-2 cell codes were performed and submitted as a contribution from ANL.

An iterative collapsing procedure based on conservation of reaction rates has been implemented. This procedure has allowed us (using a broad group energy structure - 33 groups) to reproduce eigenvalues and reaction rate distributions obtained with a large number of groups (800 groups) for configurations with reflector effects (spectrum transient between core and reflector zone).

MUSE Experimental Activity

In the MUSE experimental activity, the effort has been focused on dynamic experimental methods based on the reactor kinetics and neutron noise theory using time series data. A specific acquisition system has been developed to achieve this objective.

The time-series-based techniques that have been used are the inverse kinetics method, the pulsed neutron source (PNS) method, the Rossi- α method, and the Feynman- α method. In these dynamic techniques, one makes use of the fact that kinetic behavior in a reactor is related to the reactivity. However, each method is a little different in terms of sensitivity to other parameters such as background fission rate, detector efficiencies, or kinetic parameters such as the delayed neutron constants.

The PNS, Rossi- α and Feynman- α techniques have been used to infer the ratio β/Λ , a parameter that determines the time scale of kinetic behavior of a reactor system. We have found a fairly large spread (up to 20%) in our determination of this parameter as the system is perturbed by the insertion of a control rod. We have seen

two trends in the α -values (prompt neutron decay constant). As we lower the reactivity of the system, we obtain lower α -values than we would expect. Additionally, as we move from detectors in the core, to detector α s in the reactor, to finally detectors in the shield, we also see a decrease in the α -values. At the present time, we are surmising that this phenomenon is due to the slowing-down of neutrons in the reactor and shield regions, which increases the detector efficiency. This has the effect of increasing the effective generation time in these outer regions.

The time dependent measurements have just begun in the MASURCA (zero-power facility in Cadarache), and the preliminary results are encouraging. However, we need many more such measurements before we can demonstrate that we can infer the subcritical reactivity with an uncertainty on the order of 5% or less.

PROFIL Experiment

Analysis of the PROFIL experiment continued. Results relative to the PROFIL-1 analyzed with JEF2.2 data are summarized in Table 18. C/E values are in good agreement with the correspondent results coming from previous studies performed at CEA, which are also reported for comparison on Table 18.

Table 18. C/E Values for the PROFIL-1 Experiment Using JEF2.2

| Data Type (*) | C/E JEF 2.2 (CEA) | C/E JEF2.2 (ANL) |
|-------------------------------|-------------------|-------------------|
| σ_{capt} U-235 | $0.93 \pm 1.7 \%$ | $0.95 \pm 1.7 \%$ |
| σ_{capt} U-238 | $0.98 \pm 2.3 \%$ | $0.98 \pm 2.3 \%$ |
| σ_{capt} Pu-238 | $0.97 \pm 4.0 \%$ | $0.98 \pm 4.0 \%$ |
| σ_{capt} Pu-239 | $0.96 \pm 3.0 \%$ | $0.99 \pm 3.0 \%$ |
| σ_{capt} Pu-240 | $1.10 \pm 2.2 \%$ | $1.14 \pm 2.2 \%$ |
| σ_{capt} Pu-241 | $1.24 \pm 4.1 \%$ | $1.23 \pm 4.1 \%$ |

(*) All the results are average reaction rate ratios (spectral indexes) related to the ^{235}U fission rate.

Safety Analysis

The benchmark specification on *Protected Beam Overpower Transient in an Accelerator-Driven Subcritical Reactor* was completed and issued as a report. The report specifies the first in a series of benchmark problems designed to provide for comparative assessments of computational methods employed in analysis of coupled thermal, hydraulic, and neutronic transient performance of accelerator-driven, subcritical nuclear reactors. As the first in a series progressing from simple to complex, this benchmark is designed to have the minimum phenomenological and computational complexity consistent with prototypic system performance.

A paper entitled *Active and Passive Safety Control Performance in Subcritical, Accelerator-Driven Nuclear Reactors* was prepared and presented at the Third International Workshop on Utilization and Reliability of High Power Proton Accelerators, held in Santa Fe, New Mexico, in May. The paper presents the results from a computational analysis of the safety performance of subcritical ADS. Coupled kinetics and thermal-hydraulics models are used to quantify the effectiveness of traditional protection and control system designs in subcritical reactors. The analyses also quantify the role of inherent, passive reactivity feedback mechanisms in subcritical reactors. Computational results are used to develop conclusions regarding

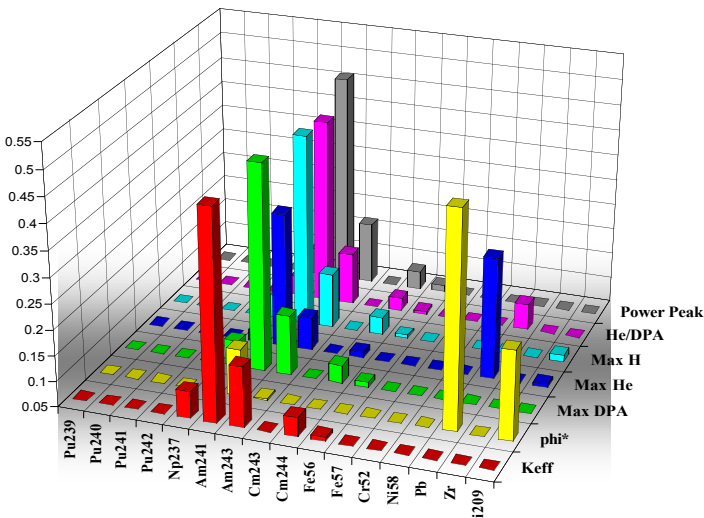
the most favorable and effective means for reactor control and protection in subcritical ADS.

Uncertainty Assessment

The uncertainty analysis related to the 150-MeV energy-effects studies was completed with the maximum helium production, the maximum DPA production, maximum helium to DPA rate ratio, and the power peak parameters. The results (absolute calculated value and associated uncertainty) are summarized in Table 19. The results have to be compared with the corresponding ones obtained with a standard 20-MeV calculation in order to evaluate how the extended energy range affects the estimations made so far for the main integral parameters characterizing an ADS. This comparison has indicated that for most parameters characterizing the dedicated core (like K_{eff} , ϕ^* , damage rate, peak-power), the effect of the appropriate inclusion of high-energy neutrons is of little impact. As expected, some effects can be observed for quantities sensitive to high-energy data like gas productions.

The corresponding uncertainty analysis indicates that the priority for new measurements and evaluations is clearly at energies below 20 MeV for selected high mass MA. This should be confirmed by an extension of the study to the case of the transmutation rate and to the production of isotopes during irradiation, which have an impact on the fuel cycle (e.g. spontaneous neutron emitters). As far as high-energy data, the priority is the (n, α) measurements for structural materials (e.g. martensitic steel components) and Pb data, but only if a critical analysis of the large existing database, would show any significant gap.

Table 19. Uncertainty Analysis Related to 150-MeV Energy-Effects Studies

| | K_{eff} | ϕ^* | Max DPA | Max He | Max H | He/DPA | Pwr Pk |
|----------------------------------|--|----------|----------|----------|----------|--------|--------|
| Absolute Calculated Value | | | | | | | |
| | 0.97280 | 1.01 | 1.89E+19 | 5.09E+18 | 3.62E+19 | 0.268 | 2.002 |
| Total Uncertainty | | | | | | | |
| | 2.88% | 2.01% | 91.1% | 36.7% | 65.4% | 63.4% | 21.2% |
| Isotope | Relative Contribution to the Total Uncertainty | | | | | | |
| Pu239 |  | | | | | | |
| Pu240 | | | | | | | |
| Pu241 | | | | | | | |
| Pu242 | | | | | | | |
| Np237 | | | | | | | |
| Am241 | | | | | | | |
| Am243 | | | | | | | |
| Cm243 | | | | | | | |
| Cm244 | | | | | | | |
| Fe56 | | | | | | | |
| Fe57 | | | | | | | |
| Cr52 | | | | | | | |
| Ni58 | | | | | | | |
| Pb | | | | | | | |
| Zr | | | | | | | |
| Bi209 | | | | | | | |

Method Development

Work continued to improve the REBUS-3 capability for subcritical source problem analyses. This quarter, new output edits pertinent to transuranic (TRU) isotope burners were added, and the discrete ordinate transport code TWODANT has been implemented as a neutronics solution option.

An initial version of a utility code named FIXSOR was completed last month to couple the high-energy spallation source calculation with the deterministic codes. This code generates a fixed source distribution dataset FIXSRC for deterministic calculations using a log file for low-energy source neutrons that is saved from a high-energy physics calculation performed with the MCNPX code. This initial version of FIXSOR is limited to mesh-wise uniform, isotropic source distributions. This month, additional verification tests were performed for this initial version of FIXSOR, and an inter-laboratory memo describing the computational options and detailed user information was completed and distributed to the internal users.

Work was started to generate the higher angular and spatial source moments for the variational nodal transport code VARIANT and the discrete ordinate transport code TWODANT. Since the higher flux moments are dependent on the specific methods of individual deterministic codes, the bases functions of VARIANT and TWODANT used in the finite series expansion of angular flux and inhomogeneous source distribution were first reviewed. Various quadrature methods were also studied to develop an accurate numerical approximation method for the angular and spatial integrals involved in higher flux moment definitions.

TREAT-Coupling Experiments

This quarter, we investigated the following issues related to the TREAT Experiment for Accelerator-Driven Systems (TREACS):

- -use of U target (simplified cylinder geometry);
- -estimation of the core k_{eff} with the presence of the target;
- -estimation of the energy deposition in the target for design of the cooling system;
- -study of the coupling core-target to validate the calibration of the target.

It was concluded that ^{238}U is a good choice for the target material. Its efficiency is increased in comparison with tungsten due to photofission neutrons. Also, we estimated that with the ^{238}U target material, the TREACS core would have enough reactivity reserve to perform dynamics behavior measurements.

The proposed core configuration for TREACS is shown in Fig. 67. The k-effective was found to be $k=1.07904 \pm 0.00298$. This corresponds to the situation with all control rods in 'up' position.

Energy deposition by electrons and gammas was estimated for the design of the cooling system.

We also investigated the possible coupling of the target with the core. The U target is placed in the center of the core; therefore, the core's neutrons and gammas might increase neutron production in the target by means of fission and photonuclear

reactions. An MCNP calculation showed that the energies of the core's gammas are not sufficiently high to induce (gamma, n) type reactions in the target. The threshold for these reactions is around 6 MeV. As to the core's neutrons, as one might expect, the ^{238}U acts as an absorber in the low energy domain since the fission cross section is very low (microbarns) and the tail of ^{238}U capture resonance extends into the thermal energy range. At higher energies ($\sim 0.1\text{--}10$ MeV), the absorption cross section is lower, and the fission (as well as downscattering) produces an opposite effect. Nevertheless, the overall effect is insignificant, and one might conclude that the core-target coupling is weak and will not rise any problems as to external neutron source calibration.

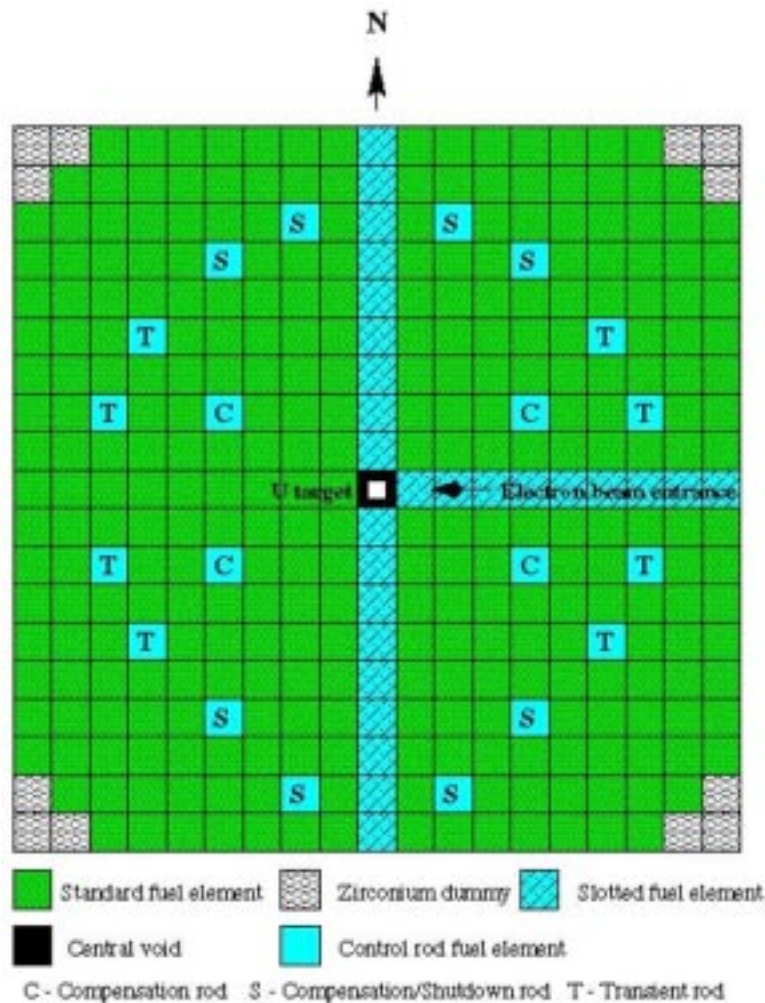


Fig. 67. The proposed core configuration for TREACS

3.7 International Support

International support and collaboration is a strong part of the research conducted under transmutation science. A major collaborator is CEA in France. However, this collaboration is defined at the basic research level, and there are no tasks specifically

conducted or funded in support of CEA's efforts. All the tasks discussed in Sections 3.1–3.6 directly or indirectly benefit this collaboration.

Some tasks are specifically funded in support of the MEGAPIE Project at Paul Scherrer Institute (PSI) in Switzerland, as well as the import of the Russian IPPE (Institute of Physics and Power Engineering) LBE target. Those tasks are discussed below.

Scope

MEGAPIE is a 1-MW LBE spallation target experiment being set up at PSI in Switzerland. DOE signed a partnership agreement on the MEGAPIE Project that includes having a US engineer participate in the MEGAPIE design and analyses on change-of-station at PSI. The objective is to provide technical support to the MEGAPIE Project and to transfer knowledge gained and related research on the project to US laboratories to advance the TRL for the US LBE target development.

The IPPE LBE target was designed and built in Russia with the initial objective of irradiating it at LANSCE (LANL). However, because of the unavailability of the irradiation facility, the target will be used as another LBE loop for basic research. Currently, the objective is to bring the target to the US, to deliver it to UNLV, and to set it up as another research loop.

Highlights

- The ISTC target (LBE target) fabricated by IPPE in Obninks, Russia was delivered to the US (with ultimate destination at UNLV).
- LANL AAA staff member (E. Pitcher) joined K. Woloshun at PSI in Switzerland for a 4-month assignment (June through September) to perform neutronics assessment in support of the MEGAPIE project.

Current Status of MEGAPIE

MEGAPIE has essentially come to the final design on the target and all external systems. Detail design reviews were held in April for the target, the electromagnetic pumps and flow meters, and all ancillary systems. The minutes of these meetings are web-posted (<ftp://megapie@ftp.psi.ch/>, password 5lmt23). The Steering Committee authorized the start of procurements at their meeting held on June 25.

Target

The target design is completed and ready for fabrication. The drawing packages are pending signed acceptance by PSI. The fabrication and assembly cost has been estimated at between 800–1200 kEuros.

The drawing package has been distributed to 11 companies for bid. Only one company has offered a quote on the package, although some of the others have bid on specific subsystems. An apparent difficulty involves fabrication of the heat exchanger; so additional vendors will be contacted. It is likely that a primary vendor will be selected while some subassemblies will be subcontracted to other companies. Initial cost estimates appear to be in an acceptable range.

A still-open issue for the target is the possibility of coating the target container both inside (for corrosion and structural protection) and outside (for leak detection). It seems unlikely that these coatings will be developed sufficiently in time to be incorporated into MEGAPIE; nevertheless, this activity may benefit future work.

Target delivery to PSI is scheduled for October 2003.

EM Pumps and EM Flow Meters

We completed fabrication of the prototype system of two pumps and flow meters, and prototype tests have begun. Although the testing phase has been delayed by one month, it is not expected to impact the delivery of the final pump assembly, scheduled for December 2002. Basic performance tests will be done, followed by specific tests to evaluate cavitation potential and other performance parameters.

Riga (Russian institution) has been slow on the delivery of documentation and drawings, but the level of detail shown in the presentation at the system review indicates that the design has been thoroughly and professionally conducted. Documentation will be produced in the coming months.

Target Window

Of all components, the target window is perhaps the greatest unknown, because of the severe environment and lack of experience with T-91 under these irradiation conditions and in the presence of lead-bismuth. A meeting of all participants in thermal modeling of the window was held (11th Megapie X4-X5 Coordination Meeting). A number of model results were presented and compared, with generally consistent results, but the number of parameters and assumptions vary, including some geometry variations, turbulence models, etc. Model results presented were for the most part the "benchmark" target, which utilizes a slanted guide tube rather than a bypass flow for hot-spot cooling.

Water flow visualization tests were conducted at FZK. Improvements in the experimental result, compared to results reported two months previously, were evident as a result of flow straighteners added at the inlet. The usefulness of the results for the design and operation of the window-cooling scheme is yet to be demonstrated. A test report has been requested. Planned cooling tests with LBE, the KILOPIE tests, have yet to be conducted (planned now for June-July, 2002). Operation of the KALLA loop at FZK for this experiment has been delayed while pressure vessel standards are being met. The optimal design of the bypass flow nozzle is as yet undecided. In short, there is progress on modeling and testing the window cooling, but definitive results are not available for design input, even as the fabrication phase approaches.

LISOR, a series of low-energy irradiation experiments on T-91 have begun. No signal was received from the tensile test machine in initial tests following a 24-hr sample immersion and about a 30-min irradiation. The source of the problem is under investigation. A signal transmission problem is the most likely error. If and when signal is restored, experiments of longer duration are planned, starting in July.

A RELAP model by Ansaldo has been made of the complete LBE/oil/water system. Preliminary results of steady-state and transient operations have been presented. The transient of the most common beam-trip event was modeled: 10 sec or less beam-off followed by a 20-sec linear ramp-up back to full beam power. Results are preliminary, but there are indications that there is a need to optimize the control

strategy to minimize the effect of beam trips on some components, particularly the secondary heat exchanger (oil-to-water). A complementary TRAC model and analysis will be conducted by LANL in the coming months. Other transients due to longer shutdowns must be modeled.

We are reconsidering the concept of allowing the LBE to freeze in the target at the end of the experiment, rather than draining to an external tank before transfer to the hot cell. This potentially reduces the risk of contamination of the facility and/or workers. However, freezing of the LBE in the target container must be accomplished without damaging the window, which would limit the usefulness of the window for PIE (post-irradiation examination). Thus, renewed investigation is underway on the issue of expansion of LBE after freezing, due to recrystallization to a second solid phase. Some tests to augment and clarify earlier results have been conducted and analysis is underway.

Because of the high difficulty in predicting window life, the MEGAPIE Advisory Committee, in a meeting in March, recommended operating under the assumption that window failure is eminent, and this failure is an acceptable end to the experiment. The MEGAPIE management has accepted this, and the Safety Analysis Report, released this quarter to the PSI internal safety review committee, reflects this position.

Safety Hull

Since target window failure is an acceptable end-of-test, from the safety point of view, the ability of the safety hull to contain the LBE under any failure scenario is critical. A spill of LBE down the beam tunnel could delay any further use of SINQ by up to 2 years. A detailed analysis of the safety hull in what is believed to be a bounding set of accident scenarios has been conducted previously, and the report is now available. A window break of an instantaneously forming hole, 1 cm in diameter, is modeled, as well as the break of the target from its flange and falling onto a target catcher. Analysis shows that the safety hull will survive these accidents.

A set of experiments was conducted to study the behavior of small LBE leaks onto the safety hull and the propensity of such leaks to flow to the low point where a signal wire is located. A report on these tests has been written but is not as yet available for release. The conclusion of these tests is that the leak detection system will be effective for any leak scenario in the vicinity of the beam window. Additional tests are planned to determine LBE-Al contact conductance and the effects of beam-degraded surface conditions.

External Systems

Considerable time and effort was spent on coming to final design and acceptance of the external, or ancillary, systems. Fabrication of these systems should be started by the end of June. External systems include the oil heat transfer loop, the cover gas system, the isolation gas system, and the fill and drain systems. Final reviews of these systems were held.

Heat Removal System and Cover Gas System

The design, analysis, and documentation for the heat removal and cover gas systems designed by Ansaldo have been essentially completed. Virtually all issues have been resolved as a result of a design review, documentation reviews and comments, and follow-up meetings. Although there remain points of discussion that will require resolution, these systems are ready for fabrication, pending approval by the Steering

Committee. One potentially serious issue that remains is the effect of thermal cycling on the chosen plate heat exchanger (oil-to-water). This does not delay start of fabrication but may impact transient operational procedures and possibly heat exchanger fabrication and materials.

Fill and Drain System

The fill and drain system, designed by ENEA, is also essentially complete and ready for fabrication. The documentation is somewhat behind, but no major issues remain. However, the issue of whether or not to drain the target at end-of life has become a topic of serious consideration, as mentioned above. ENEA has performed a system simplification study to propose a fill-only system. Cost estimates, including supporting tests, were presented in June. The goal is to come to a decision on the need for the drain system before Sept. 30.

MEGAPIE Neutronics Work

Extensive neutronics calculations have been carried out in support of the MEGAPIE project. Substantial effort went into the first neutronics benchmark report, which compared the results of several radiation transport codes used at various institutions. Calculated quantities included energy deposition in the Pb-Bi and structures, decay heat, activation, and neutron current and flux.

Energy deposition results were generally in good agreement between the various codes and groups for material directly in the proton beam path, but were poor for an aluminum wall just outside the proton beam. Residual activities in various regions calculated by the participants were in good agreement with one another, except for those obtained by PSI using MCNPX. Neutron current leaving the radial surface of the target varied by a factor of 2 for two participants (FZK and PSI), even when they used the same MCNPX code. Calculated peak thermal neutron fluxes in the heavy water moderator varied by a factor of 1.5. Calculated gas production rates in various structures varied by more than an order of magnitude between participants. This first benchmark demonstrates the need to have experience in using these fairly complex radiation-transport codes. Novice users can produce erroneous results.

Comparisons with experiment have been performed for most of the quantities calculated in this benchmark. Agreement between experiment and code predictions is generally within 20%. An effort at CEA-Saclay, is underway to identify the sources for the discrepancies in the calculated results.

A second neutronics benchmark has been undertaken that concentrates on calculating the spatial distribution of deposited power in the Pb-Bi. The participants have completed the calculations, and they are currently being compiled.

Finally, there is a report issued by Y. Foucher that provides detailed results of neutronics calculations in support of the MEGAPIE experiment. It provides detailed power density distributions in the Pb-Bi target, peak power densities in the various windows, decay heat, neutron fluxes, and estimates of atomic displacement rates for various structures.

MCNPX Model of MEGAPIE

An MCNPX model of the MEGAPIE target has been developed. The model is based on the latest drawings of the target system. A cross section through the MCNPX model is shown in Fig. 68. Many details are included in the model, including the

bypass flow tube and “target catcher” ledges. Refinement of the model is underway, including a more accurate representation of the moderator tank and beamline penetrations.

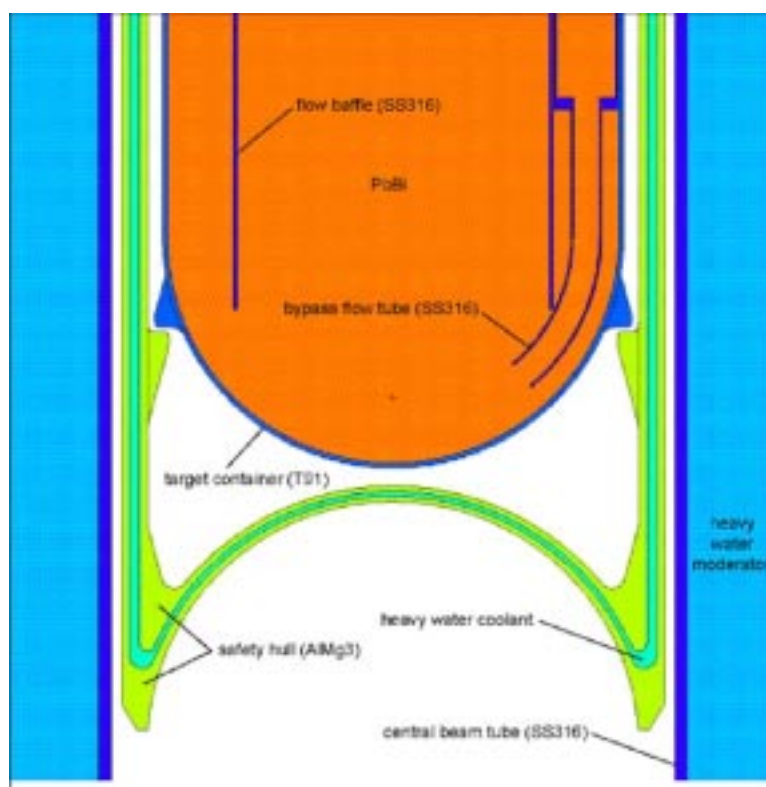


Fig. 68. MCNPX model of the MEGAPIE target.

Gas Production in the Pb-Bi

The amount of gas produced in the Pb-Bi during irradiation is an important quantity for establishing the size of a gas reservoir on the Pb-Bi loop, and determining the frequency that this reservoir must be purged. Previous calculations have provided estimates ranging from 0.24 to 2.6 npt-liters (i.e., liters at natural pressure, 1 atm, and temperature, $T=293$ K) of helium gas. A preliminary calculation was done using MCNPX, which yielded a value of 1.1 npt-liters for 6 A·h of proton charge on target. The calculation was performed using the default physics models in MCNPX, which produce a helium production cross section at high energy that is in good agreement with one measurement of 750-MeV protons on tungsten.

3.8 LANL-Sponsored Directed-Research University Programs

Scope

University support is an important part of the AAA Program. In addition to the general University programs run by the DOE-HQ, a number of universities are supported directly by the programmatic funds to provide technical assistance to the AAA

Program. The directly supported universities include University of Michigan, UC-Berkeley, UT-Austin, and North Carolina State University.

University of California – Berkeley

Provide technical support to the Systems Analyses and Transmutation science teams via specific tasks defined and coordinated through the AAA Program leads, including:

- Benchmark of the simple model for fuel cycle analysis;
- Resolve the discrepancy with ANL on actinide built-up with cycles;
- Apply fuel-cycle analysis methods to compare design alternatives;
- Compare Na vs. LBE-cooled ATW;
- ATW performance assessment using molten salt and alternative;
- ATW assessment during approach to equilibrium using molten salt; and
- Perform optimization and analyses of pebble-bed ATW.

University of Michigan

Provide technical support to the Systems Analyses and Transmutation science teams via specific tasks defined and coordinated through the AAA Program leads, including:

- Analysis of coupled accelerator core dynamics with emphasis on k_{eff} predictions and control;
- LWR-based reactor transmutation studies for equilibrium cycles;
- Assessment of LBE slowing down spectrum and the associated cross-sections;
- In collaboration with technical staff at LANL, use proton irradiation to simulate spallation neutron radiation damage in accelerator-driven systems. This work is to investigate the effect of higher gas production at significant doses (several dpa) to lay a foundation for a full-scale radiation campaign;
- Develop a detailed description of the irradiation campaign (temperatures, dose rates, doses, and He-implantation levels); and
- Conduct a single irradiation campaign (~240 hours of irradiation) on SS-T-91 at three dpa levels.

University of Texas – Austin

Provide technical support to the Systems Analyses and Transmutation Science teams via specific tasks defined and coordinated through the AAA Program leads, including:

- Participation in the helium and hydrogen production experiments in LANL/Blue Room (Summer 2002);
- Development of a test plan, and post-test analyses for spallation product benchmark experiments for targets (emphasis on LBE);
- Time-dependence incorporation on the proliferation metrics development and analysis; and
- Development of the uncertainty analysis methodology for the proliferation metrics, providing results to the Systems Analysis Team.

North Carolina State University

Calculate radiation damage (production of displacements, helium, hydrogen, and heavier transmutation products) and energy deposition in the target materials,

containment structures, and entrance windows of the target assemblies for the SINQ spallation neutron sources that are under design and development at the Paul Scherrer Institute (PSI). These targets include the Mark II and Mark III designs. In addition:

- Examine less obvious (and less well studied) mechanisms for the transfer of energy to the irradiated materials and hence the production of displacements. These mechanisms include recoil-atom damage and other interaction products.
- Analyze the effects of the calculated radiation damage on mechanical and other property changes and assess reasonable and safe lifetimes for radiation-damaged components.

Highlights

Public Interface

- The University Projects Leader visited Ohio State University, the Air Force Institute of Technology (Wright-Patterson AFB), University of Pittsburgh (Physics Dept.), Bettis Laboratory, and Westinghouse Pittsburgh to present AAA Seminars and discuss potential future projects.
- The University Projects Leader organized a pro-nuclear team of senior executives from the nuclear power industry to participate in a dinner-debate with Joanne Woodward and Paul Newman.
- The University Projects Leader has been highly instrumental in the formation of a University Consortium (~12 universities) for Transmutation Research to be led by UNLV and managed by the University Research Alliance. This proposed consortium is part of the Energy Appropriations bill currently under consideration by Congress.
- The University Projects Leader was appointed Chair of the Public Information Committee of the American Nuclear Society.

U of Michigan

- Initial modeling with the MCNPX Code of LANSCE target-irradiation experiments performed in Dec. 2001 was completed
- Alloy stocks of T-91 and HT-9 were sent out for machining of tensile bars and TEM bars for irradiation tests. ENDF/B-VI files were processed for a few nuclides to generate cross-section data for MCNP, and currently, the data is being benchmarked against existing MCNP libraries.

UC Berkeley

- UC-Berkeley generated 5 refereed papers from AAA funded work.
- Benchmarking of our ATW fuel cycle analysis code against MOCUP was completed. Results show less than a 1% difference in actinide inventories after 400 days of transmutation.
- The rate of radiation damage to the graphite structure of molten-salt transmuters was determined; the graphite lifetime is only slightly over one year.

- The first optimization of a molten-salt transmuter was completed. MS reactors appear very promising for transmuting LWR TRU.
- The development of the simplified model for fuel cycle analysis of a transmutation system was completed and incorporated into a code called WACOM.

UT-Austin

- Proliferation Resistance Assessment methodology with complete time-dependence was completed and applied to four long-term nuclear fuel systems; a report is in progress. Efforts continued on collecting expert opinions on weighting factors for this methodology.
- Work commenced on designing experiments to be performed at LANSCE for measuring spallation product yields (specifically identifying materials and deficiencies in existing data).
- LANL awarded a contract to UT-Austin for continuation of proliferation studies and experimental support.

North Carolina State University

- LANL awarded a contract to NCSU for support of the SINQ spallation neutron source at Paul Scherrer Institute (PSI).
- Radiation effects computations are ongoing to characterize the PSI SINQ targets.
- A series of LAHET calculations were conducted for 570-MeV protons on cylindrical aluminum targets of 1-cm radius and varying thicknesses. Technical results were reported under Transmutation Science.

University of California – Berkeley

Optimization of an Accelerator-Driven Molten-Salt Transmuting Reactor

Research continued on the performance of a graphite-moderated molten-salt (MS) subcritical transmuter. The MS reactor uses NaF-ZrF₄ as the coolant-fuel, with an inlet/outlet temperature of 600–700°C. The MS with actinides (Ac), where U and fission products (FPs) are completely removed, is continuously fed through the reactor at a rate of 0.8 liters/day and an Ac concentration of 12.87 mol%; the MS effluent contains a different composition and smaller Ac concentration than the feed. It is also assumed that FPs are removed from the core as soon as formed. The central question addressed is whether or not it is possible to design such a reactor to have an acceptable k_{eff} (>0.92) when at equilibrium composition, while the Ac concentration is constrained by the solubility limit of 1.56 mol% and what is the corresponding transmutation efficiency.

This quarter, we completed the optimization of the MS transmuter and investigated the neutron physics phenomena underlying the observed trends. The study and its findings have been summarized in a paper⁵ to be presented at the reactor physics

⁵ "Optimization of a Molten-Salt Transmuting Reactor," E. Rodriguez-Vietez, M. Lowenthal, E. Greenspan and J. Ahn, UC Berkeley, being prepared for presentation at the International Conference on New Frontiers of Nuclear Technology, Reactor Physics, Safety and High-Performance Computing, PHYSOR-2002, October 7-10, 2002.

topical meeting PHYSOR-2002. It concludes that from the neutronics viewpoint, MS reactors can be very efficient transmuters and deserve more consideration.

A potential drawback of the MS transmuter is the graphite lifetime. For the high power density design we have focused on—390 W/cm³ of MS—the graphite lifetime is only ~1 year. The lifetime is nearly inversely proportional to the power density. So it is possible to increase the graphite lifetime as long as one wishes by reducing the power density. The amount of TRU transmuted and the amount of fission energy generated between replacements of the graphite do not depend on power density. Economically, it is probably desirable to design the reactor to have the highest practical power density.

Future undertakings will include studying the effect of fission products; finding how long will it take to get to the equilibrium composition; studying the sensitivity to input fuel vector; and studying the feasibility of MS transmuters using ⁷LiF-BeF₂ for the MS. The optimal spectrum for this MS is likely to be softer than for NaF-ZrF₄ and the graphite lifetime longer.

A Simplified Model for Fuel Isotope Evolution in ATW Systems

The benchmarking of the simplified model and computer code we developed for simulating the evolution of the fuel isotope inventory in an ATW and its fuel cycle was completed. Very good agreement was obtained against MOCUP calculations. The model and its testing have been summarized in a paper⁶ to be presented at the Reactor Physics Topical PHYSOR-2002.

Presently, effort is focused on developing a strategy for adjusting the effective one group cross sections to the change in the inventory and composition of the actinides loaded into the core.

Neutronics Computational Benchmark

We completed the neutronic benchmarking of the MOCUP code being using for core design and analysis against the DIF3D-REBUS3 code systems in use at ANL and elsewhere. The benchmark was done for a Pu-U(Zr) fueled Pb-Bi moderated critical core. Figure 69 shows the k_{eff} comparison. Whereas very good agreement was found between UCB MOCUP and KAERI DIF3D/REBUS3 results, the ANL DIF3D/REBUS3 results are systematically ~1% lower. The difference between the KAERI and ANL results may be due to the different cross section processing procedures and codes used by the two groups.

To get accurate burnup dependent k_{eff} with MOCUP, we found it necessary to incorporate more fission products in the MCNP calculations than MCNP was set to accept – only 67 fission products in addition to 45 actinides. A modified procedure of interfacing MCNP and ORIGEN2 was developed at UCB to bypass this limitation. Figure 70 shows the effect, on k_{eff} , of the added 111 fission products.

⁶ "A Simplified Model for Fuel Isotope Evaluation in ATW Systems," M. Cheon, J. Ahn, E. Greenspan, D. Barnes and P. Chambrelé, UC Berkeley, being prepared for presentation at the International Conference on New Frontiers of Nuclear Technology, Reactor Physics, Safety and High-Performance Computing, PHYSOR-2002, October 7-10, 2002.

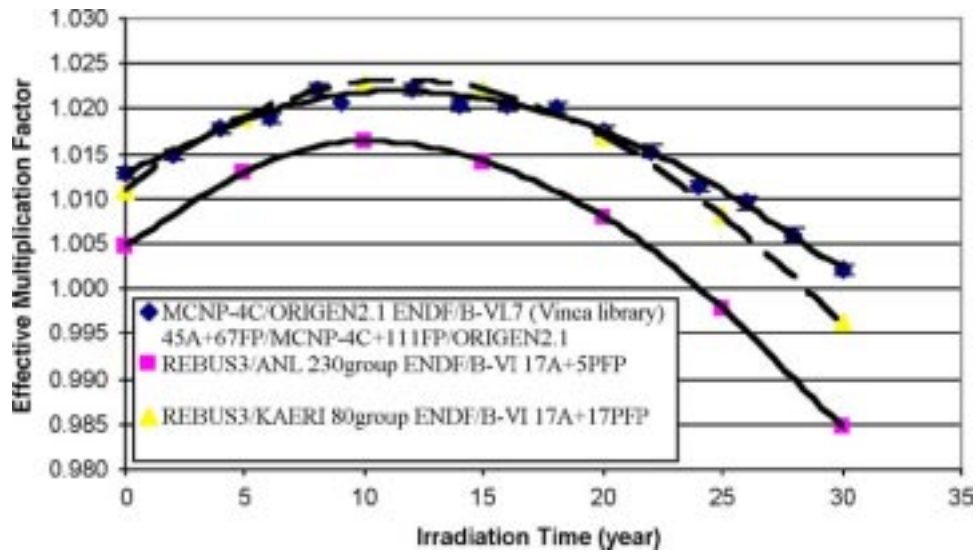


Fig. 69. k_{eff} evolution in critical Pb-Bi cooled core benchmark obtained with different code systems using ENDF-B/VI based cross sections

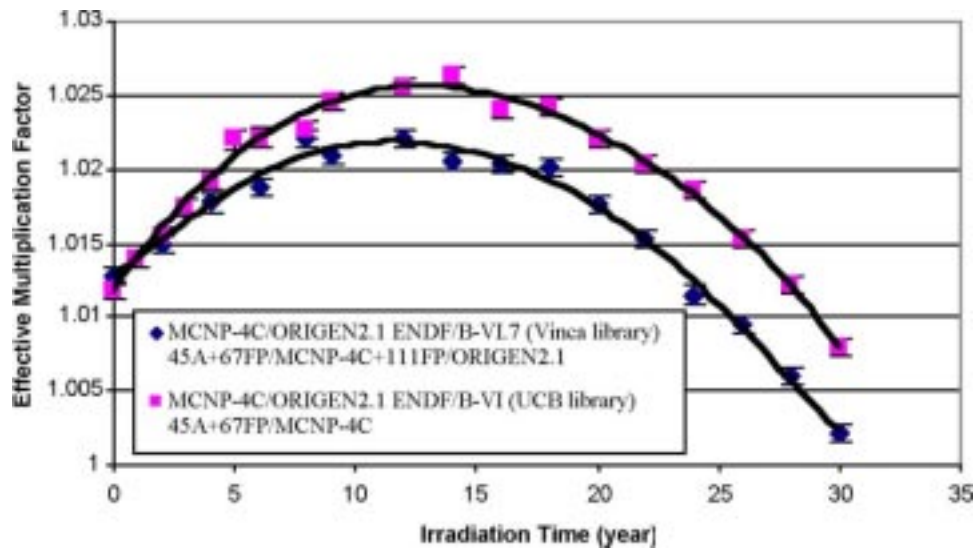


Fig. 70. Effect of number of fission products on MOCUP calculated k_{eff} evolution in the critical Pb-Bi cooled core benchmark

University of Michigan

Reactivity Measurement & Control Studies

A space-time method was developed to measure reactivity in source-driven systems. The method limits to the Sjöstrand area-ratio method in the absence of spatial effects. The method requires a computed shape function and computed estimate of the prompt neutron lifetime, but the predicted reactivity is insensitive to detector placement and shape function accuracy. The method was tested using computations.

Reactor Transmutation Studies

A comparison of LWR-based transmutation schemes is underway. Equilibrium cycles have been generated for homogeneous and heterogeneous loadings similar to the French CORAIL concept using assembly-level calculations. The heterogeneous results compare well with CORAIL results. Both loadings and recycle strategies result in zero net Pu change at equilibrium. The heterogeneous loading leads to a somewhat lower Pu inventory than the homogeneous loading (about 4/5 of the inventory of the homogeneous loading). Equilibrium is established in about 40 recycles; a robust automated strategy to compute the equilibrium is needed.

| Recycle 40 (quasi-equilibrium) | | | | |
|-------------------------------------|---------------|-------|-------------|-------|
| Fuel Content | Heterogeneous | | Homogeneous | |
| ²³⁵ U (wt%) ^a | 4.00 | | 3.97 | |
| Pu (wt%) ^b | 12.42 | | 15.00 | |
| Fissile Pu (wt%) | 39.70 | | 40.97 | |
| Element | BOC | Δ | BOC | Δ |
| U | 519.0 | -26.6 | 515.0 | -26.8 |
| Np | 0.0 | 0.3 | 0.0 | 0.3 |
| Pu | 16.1 | 0.0 | 20.0 | 0.0 |
| Am | 0.0 | 1.2 | 0.0 | 1.5 |
| Cm | 0.0 | 0.4 | 0.0 | 0.3 |
| Total TRU | 16.1 | 1.9 | 20.0 | 2.1 |
| Total HM | 535.1 | -24.7 | 535.1 | -24.7 |

Pb and Pb-Bi Spectrum Studies

A study has been undertaken of 14-MeV neutrons slowing down in Pb and Pb-Bi moderators, and the ability of the MC**2 fast reactor spectrum code to model these neutron spectra. The insights should be useful in understanding and modeling systems driven by 14-MeV neutron sources (as surrogates for spallation sources). The spectrum due to 14-MeV neutrons slowing down in Pb shows deep flux depression between 11.6–14.0 MeV. Non-elastic effects produce this depression by removing 14-MeV neutrons to below 11.6 MeV (the first excited state of ²⁰⁸Pb). A similar depression occurs for 14-MeV neutrons in Bi and Pb-Bi. The MC**2 code successfully recovered the essential features of this depression, but the spectrum computed by MC**2 deviates from that computed by MCNP at lower energy because of (n,2n) cross section. The difference is in part due to ENDF/V vs. ENDF/VI cross section evaluations, but other effects are at work and need to be understood. MC**2 cannot currently compute spectra in Pb-Bi because of a lack of Bi data for the code.

Materials Irradiation Experiments

Alloy HT-9 and T-91 stock was received and machined into irradiation bars. These samples were pre-injected with 100 appm He at room temperature to simulate He production under irradiation. The first proton beam irradiations to 3 doses between 3–10 dpa at 450°C are scheduled to begin in July 2002. Hardness and micro-structural analysis will follow these irradiations.

Experiment Support

A University of Michigan student is working at LANSCE this quarter and next to assist in neutron spectrum measurements from a Pb-Bi target. Initial gamma spectra from the December 2001 irradiations were examined to identify measurement issues and rough spectral index computations were performed with MCNPX. The instability of the gamma background in the counting facility at LANSCE was identified as a concern.

4. SYSTEMS TECHNOLOGIES

Scope

The scope of Systems Technologies is to coordinate all technical elements to define requirements, perform system-level evaluations, develop preconceptual designs, and establishing technology development activities in a comprehensive R&D proof-of-principle (POP) effort. Overall system objectives, system performance requirements, and POP requirements are used to correlate R&D needs, data quality objectives, experimental facilities, resources, and materials. System-level modeling evaluates the performance of multi-strata options in establishing a technically feasible spent nuclear fuel management program, especially with regard to proliferation, economics, environment, safety, and institutional issues. Likewise, pre-conceptual designs serve as fundamental bases in defining critical R&D and focusing POP testing. Woven together, System and Technology Integration activities can provide a solid foundation for focused and coordinated AAA research and development.

Accelerator-Driven Test Facility (ADTF)

The preconceptual and conceptual design phases of the Accelerator-Driven Test Facility (ADTF) includes the Target and Materials Test (TMT) Station, the Subcritical Multiplier (SCM), the accelerator, and the balance of facility segments. The work performed in connection with the ADTF design must be documented, including the reference preconceptual designs of the TMT and the Na-cooled SCM-100, with a Pb-Bi reference target, and the studies of alternative engineering design solutions considered. The scope also includes collaboration with CEA. The following specifics are included:

- Completion of the ADTF preconceptual design documentation;
- Development of an ADS reference design—US will work on liquid-metal-cooled designs (Na, LBE) and CEA will work on a gas-cooled design;
- Proof-of-performance coupling tests—a plan for experimental POP coupling between an accelerator and a multiplier will be developed; and
- POP for accelerator reliability and accelerator development.

Integration activities include:

- Development of functional and performance requirements for ADTF;
- Definition of design interfaces between major facility segments;
- Coordination of internal and external design reviews;
- Technical risk assessment; and
- Cost estimating.

ADS Reference Design

The purpose of this task at ANL is to develop a preconceptual design for a Na-cooled, accelerator-driven system. LANL will lead the reference design for a Pb-Bi-cooled system. This work involves development of a preconceptual design for a large-scale (~800 MWth) ADS with liquid-Na cooling and a Pb-Bi eutectic target. The focus is on defining a set of top-level requirements for the ADS engineering design concept for the facility as a whole, including:

- Identifying the containment structure with ingress and egress routes for personnel, services, and radioactive and nonradioactive equipment;
- Routing and shielding of the accelerator beam;
- Configuring the subcritical multiplier, the vessel in which it is housed and its cover, and all other in- and ex-vessel ancillary components and systems; and
- Handling schemes for all of the above.

The ADS design will be used to update, as necessary, requirements developed for the ADTF.

Micro Accelerator-Driven Coupling Proof-of-Principle Experiments

Coupling Experiments – This task will investigate the use of an experimental facility such as the Transient Reactor Test (TREAT) facility, located at ANL-W, for the study of accelerator-driven-system control issues related to the coupling of a multiplier to an external source. The feasibility of using the TREAT reactor coupled with an accelerator-driven external source to be part of a POP for ADS will be assessed. The dynamic behavior of the experimental coupled system will provide useful information for simulation of operation of an actual ADS power system.

Fuels and Materials Experiments – The main deliverable for this year is to develop a preconceptual design, cost estimate and schedule for the implementation of an irradiation experiment (Fuel and Materials Test Station – FMTS) in the high power beam at LANSCE.

Advanced Cavity Development – The main effort is the procurement and testing of two $\beta=0.175$, 2-gap, 350-MHz superconducting spoke resonator cavities and the completion of the design of the power coupler for these cavities. Scope also includes the continuation of the DOE/CEA/CNRS technical collaboration on accelerators for waste transmutation.

Highlights

Accelerator-Driven Test Facility (ADTF)

- A report on the thermal-hydraulics analysis for an alternative tungsten target design for the ADTF was issued from FZK (Forschungszentrum in Karlsruhe).

ADS Reference Design

- A report was issued on the scale-up of the ADTF target assembly to a size suitable for use in the ADS reference design.
- A preliminary set of functional and design requirements for the ADS reference design was developed and distributed for review.

- Papers on thermal cycling in an ADS, ADS control, and ADTF targets (LBE and tungsten) were presented at the Third International Workshop on Utilization and Reliability of High Power Proton Accelerators held in Santa Fe, NM, in May.

Coupling Experiments

- A preliminary report, "TREAT – Accelerator Coupling Experiments (TREACS)," was prepared and delivered to DOE. The report includes the description of the proposed TREACS tests, their use in the AAA program, and a cost and schedule estimate.
- A preliminary TREACS engineering feasibility report was prepared. The document is currently being edited.

Advanced Cavity Development

- The fabrication of two $\beta=0.175$, 2-gap, 350-MHz superconducting spoke resonator cavities was completed by the vendor, E. Zanon, S.p.A. (Italy), one month ahead of schedule. The cavities were shipped the end of the quarter.
- Three meetings were held with CEA/Saclay and CNRS/Orsay personnel where a draft Memorandum of Understanding and two draft work packages were completed, and the membership of the Senior Executive Committee and Technical Steering Committee was established.
- The testing of the ANL $\beta=0.4$ Rare Isotope Accelerator (RIA) prototype spoke resonator cavity was completed.

Transmutation Technology Development Plan

- The Transmutation Technology Development Plan (TTDP) section on coupling experiments, including TREACS and TRADE, was completed and incorporated in the draft TTDP.
- A final draft of the Transmutation Technology Development Plan was issued for review.

Accelerator-Driven Test Facility (ADTF)

Representative from Forschungszentrum Karlsruhe (FZK, Germany), Dr. Xu Cheng, completed his stay at ANL at the end of May, working on different aspects of the AAA program. He completed a report on the thermal-hydraulics analysis for a solid tungsten target for an ADS: *Thermal-Hydraulic Design of a 5 MW Sodium-Cooled Tungsten Target for the Accelerator Driven Test Facility (ADTF)*. The models were sized for the ADTF (5 MW). The reference for the ADTF (and current ADS) is an LBE target, but consideration was also given to alternative target designs. Only the thermal-hydraulics of the tungsten target are studied and documented in the report (no structural analyses or potential material and fabricability issues were included).

ADS Reference Design

Functional Requirements

Discussions on whether or not control rods should be included in the ADS reference design have been reinitiated. Under some postulated scenarios for deployment of an

ADS, it may be desirable to operate at a k_{eff} that is very close to unity, in which case, control rods, in conjunction with an accelerator trip, would be necessary to ensure shutdown of the system. In a fertile-free multiplier, however, with a very small delayed neutron fraction (β) and little Doppler feedback, control rods that act fast enough may be difficult to design and qualify. Thus, addition of some fertile material to the fuel form may be necessary in this case, and this is a violation of the assumptions upon which the reference design activity is based.

The question of control rods needs to be considered in the broader context of the development of the functional requirements and design criteria. This activity was initiated in April, with a commitment to provide a preliminary set of functional and design requirements. A preliminary list of fourteen functional and design requirements was developed and provided to DOE and program participants for review. The list consists of only the highest-level requirements, in a very broad context, along with brief statements of justification for the preliminary choices, and is not prioritized or arranged hierarchically. They are presented here without narrative justifications:

- The transmutation efficiency of the reference design ADS should be maximized;
- License-ability requirements define safety, containment, seismic, emissions, etc., criteria. Safety characteristics of the ADS should be equivalent to, or better than, a similarly-sized LMR that could be designed and built contemporaneously;
- The fuel form for the ADS SCM should be as fertile-free as possible to maximize its efficiency as a back-end burner of residual actinides;
- The k_{eff} of the SCM of the ADS must be significantly different from 1.0 (*initial choice: $k_{\text{eff}} = 0.97$*);
- Instrument systems must be provided to measure k_{eff} at all times, to ensure subcriticality, both during operation and shutdown;
- The SCM power should be $\sim 800 \text{ MW}_{\text{th}}$;
- The accelerator energy should be between 600 MeV and 1 GeV to reduce cost (*initial choice: $E=600 \text{ MeV}$*);
- In addition to the shielding normally found as part of a reactor facility, shielding should be provided against radiation emanating from the accelerator beam tube (under both operational and accident conditions) and from the target;
- The thermo-hydraulics of the SCM should be optimized for whatever heat rejection cycle is coupled to it;
- Control of the gross power level of the ADS should be by adjustment of the accelerator beam current, with supplemental means as necessary;
- A useable lifetime of at least 40 years should be assumed, with identification of life-limiting components and cost of extension of life to a goal of 60 years;
- Provision should be made to allow development of maintenance operations that support the requirement for maximization of transmutation;
 - Refueling interval and fuel changeout fraction should be optimized considering core physics (i.e., initial k_{eff} and depletion swing) and transmutation maximization consistent with the complexity of refueling operations (*initial goal: refueling interval = 1 yr*);

- Target replacement should be consistent with the refueling interval;
- In-vessel spent-fuel storage (for cooldown) should be provided for the fraction removed during one refueling operation;
- The SCM of the ADS should be designed for the capability of continued operation, at least until end of the cycle, with fuel designed for a failure (by fission gas leakage only) probability of 10^{-6} / pin-yr; and
- The ADS should have equipment and facilities for handling target components and all SCM fuel, including processing and fabrication for recycle, but not necessarily for initial processing of spent LWR fuel and fabrication of first-pass SCM fuel.

The requirements list has identified the main parameters that need to be optimized in order to select the most desirable ADS configuration. The selection process for the optimum set of parameters has to be an integration of core physics modeling (core composition, k_{eff} , burnup swing, burnup compensation), safety analysis (multiplier response to specified transients) and engineering design (effects on accelerator requirements, design and placement of control devices, operational aspects such as fuel-cycle length, and cost impacts).

Studies of transient SCM response and physics estimates of the reactivity worth of six burnup compensators have provided information on the magnitude of the reactivity control that would be needed in different transients and the reactivity available using burnup compensator rods. These estimates will provide a frame of reference to initiate an iterative process leading to the establishment of a reference ADS that satisfies the functional requirements.

Sodium-Cooled Engineering Design

Work on the sodium-cooled ADS reference design continued. The arrangements of the equipment on top of the small rotating plug have been carefully studied. Placement of the equipment has implications on the control and burnup compensation method that can be used in the ADS, as well as on the cost of the facility (size of the rotating plugs is an important cost consideration).

In arranging the equipment layout, particular attention has been given to the intermediate heat exchanger (IHX), secondary sodium piping runs, and the target lead-bismuth eutectic (LBE) piping. The latter was changed from individual supply and return pipes to a single assembly with concentric tubes connecting to a coaxial flange at the target end and individual tubes at the LBE support system end.

The sizes of the equipment, particularly the target tube handling cask (~16 m long and 75-100 MT in weight) and its requirement for a laydown area, make the layout of the floor area difficult. A possible laydown area for the target assembly handling cask was identified (see Fig.71). Although routing of the secondary sodium piping runs is shown up the containment wall, consideration is being given to route them through the access tunnel used for personnel and equipment movement. This may require changing both the location of the laydown area, to avoid moving the cask over the piping, and the orientation of the SCM tank itself inside the containment building. It may also be necessary to change the locations of the IHXs in the SCM tank to group the piping runs more closely.

Lack of definition of the high-energy beam transport (HEBT) system, which connects the end of the horizontal accelerator to the vertical target tube and spreads the beam, is preventing further progress in the overall layout of the equipment in the containment building. There is no planned activity for the conceptual design of HEBT equipment, so the ADTF HEBT system has simply been scaled to the beam size and target tube length of the ADS SCM.

An alternative design solution to allow the reactor vessel cover to be raised for refueling only about 15 cm (instead of ~6 m) is being evaluated. This would substantially reduce the length of the cover lifting columns and the complexity of the lifting mechanism. Allocation of the space on the small rotating plug could be improved with this option.

A scheme was developed where six absorber assemblies for burnup compensation can be located in the SCM core. Because of space limitations imposed by the diameter of the small rotating plug of the primary tank cover, the locations of these assemblies are asymmetrical (see Fig. 72). Ideally, six assemblies would be located at the "corners" of the hex-shaped fuel assembly rings, whereas in the proposed arrangement, the ones whose drives are closest to the edge of the small rotating plug are shifted away from that edge, and the next ones are shifted as well, to make the distribution as uniform as possible. Calculations have shown that six absorber assemblies (B_4C with fuel followers) in the corners of the sixth row would provide a Δk of ~0.1, which is more than enough to compensate for the burnup swing (in fact, less may be necessary to avoid the possibility of criticality, which is easily accomplished by eliminating the fuel follower and/or reducing the B_4C loading). The asymmetric configuration shown is not expected to differ markedly from the symmetric one, although it will be much more difficult to calculate.

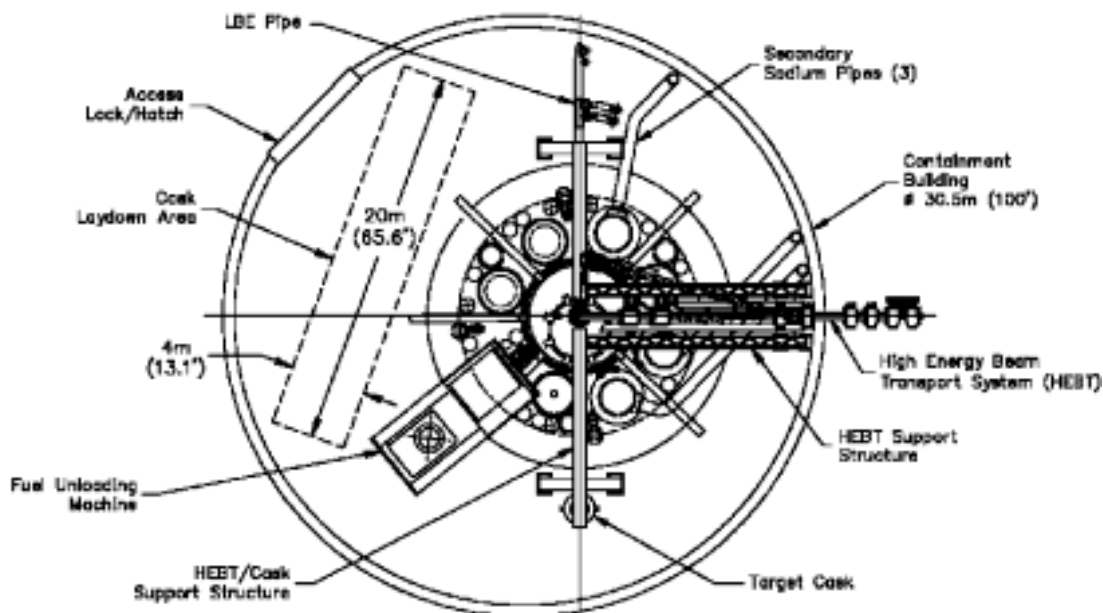


Fig. 71. Layout of the ADS containment-building floor.

Target Assembly

The baseline target for the ADS reference design has been completed on the basis of the reference target developed for the ADTF. The ADTF target is a liquid LBE target that is cooled by circulating the LBE to a heat exchanger outside the SCM primary tank. The ADS reference target has been developed by scaling up the ADTF target.

The detailed design and analysis completed for the ADTF LBE target showed that it would be sufficient to drive a 100-MW_{th} SCM of the ADTF with a proton beam energy of 600 MeV and current of 8 mA, and that the HT-9 alloy window would last for more than a year with a beam current density of 40 $\mu\text{A}/\text{cm}^2$. Sizing of the flow channels was dictated by a maximum LBE lineal velocity of ~ 2 m/sec for corrosion/erosion limitation.

Scale-up of this target assembly was accomplished using the flow velocity and beam-current constraints mentioned above and assuming that a total current of ~ 28 mA of 600-MeV protons would be required for the much larger SCM (with $k_{\text{eff}}=0.97$) of the reference-design ADS. The target assembly (the target itself and the housing for the accelerator beam vacuum tube and the various LBE flow tubes) has an overall length of 16.4 m and an outside diameter 60 cm where it passes through the core. A comparison of the main features of the current ADS target concept with the earlier ADTF target is summarized in Table 20.

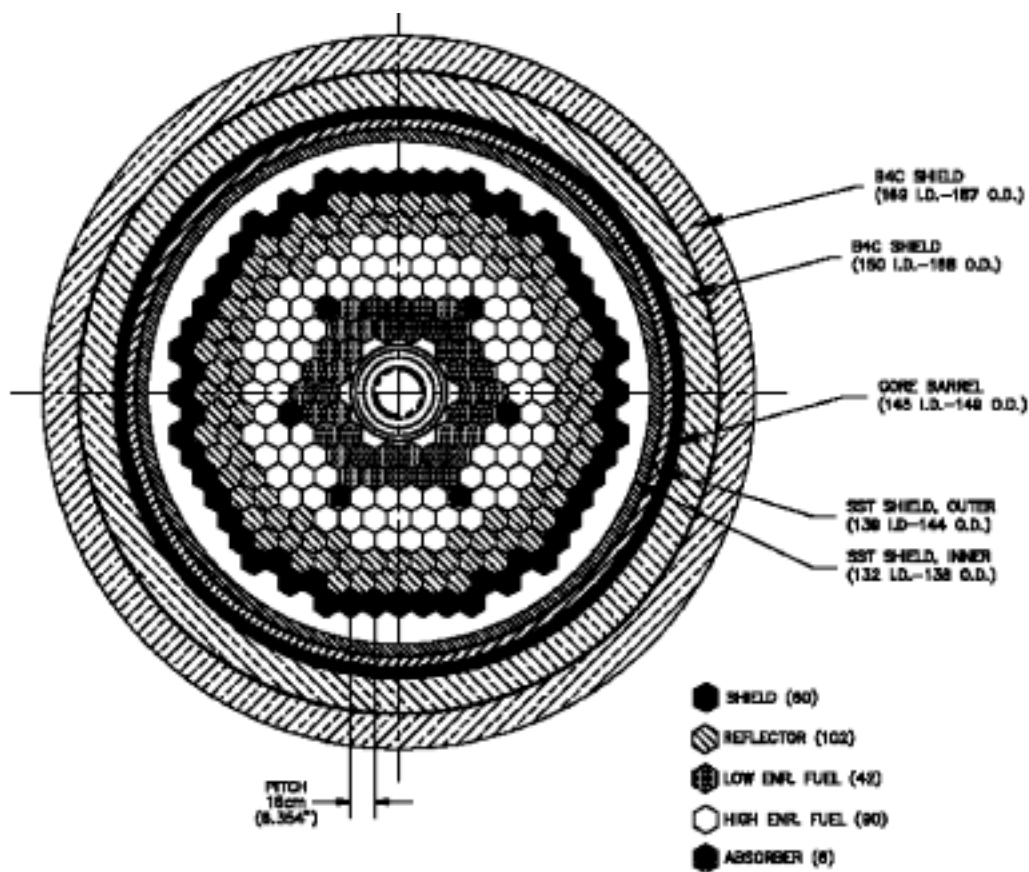


Fig. 72. Layout of the SCM core of the ADS.

Table 20. A Comparison of ADTF and Reference ADS Target Features

| Feature | ADTF Target | ADS Target |
|--|-------------|------------|
| SCM Power (MW_{th}) | 100 | 840 |
| SCM fuel zone diameter ¹ (cm) | 80.5 | 208.2 |
| SCM fuel zone height (cm) | 34.3 | 107 |
| Proton beam energy (MeV) | 600 | 600 |
| Proton beam current (mA) | 8.3 | 28 |
| Proton beam diameter (cm) | 16.3 | 30 |
| Window beam current density ($\mu A/cm^2$) | 40 | 40 |
| Target thermal power ² (MW) | 5 | 17 |
| LBE flow (kg/sec) | 425 | 1450 |
| LBE ΔT (K) | 80 | 80 |
| Active target diameter ³ (cm) | 16.3 | 30 |
| Active target length ⁴ (cm) | 41 | 41 |
| Buffer thickness ⁵ (cm) | 10.7 | 21.9 |
| Guard tube outer diameter (cm) | 34 | 60 |
| Overall target assembly length (m) | 10 | 16.4 |

¹ Diameter of circle having same area as fuel zone

² Assumes all beam power goes into heat, neglecting energy of neutrons

³ Includes flow divider tube

⁴ From hemispherical tip of beam tube to bottom of outer LBE tube

⁵ Includes all space from outside of flow divider tube to average radius of interface assembly

The report on the scale-up of the ADTF target assembly to a size suitable for use in the reference design ADS was issued as ANL-AAA-014, "A Lead-Bismuth Eutectic Target Concept for the Subcritical Multiplier of the Reference-Design Accelerator-Driven System."

Alternative Target Designs

Preliminary studies have shown that a simple scale-up of the ADTF target concept to accommodate the higher beam power of the full-scale ADS would present significant engineering challenges in the design and construction of the system. Therefore, alternate target concepts are being developed for the full-scale ADS.

Helical Tube LBE Target

One alternate concept under consideration would use a circulating loop of liquid LBE as the target material, but rely upon the sodium coolant of the SCM for heat removal. In this concept, the liquid LBE is pumped at low velocity (~ 0.5 m/s) through a single HT-9 steel tube that is bent into a number of concentric helical screws. The turns of each screw are arranged to insure sufficient stopping distance for the proton beam at all radial positions and to insure that the neutron source is sufficiently spread over the length of the fueled region of the SCM. Heat removal is accomplished through convective heat transfer to sodium coolant passing over the helical coils.

A preliminary thermal analysis was completed to evaluate the feasibility of this target concept. Wall and fluid temperatures were evaluated for a parametric set of cases that consider variations in the inner diameter of the tube, the thickness of the tube wall, and the SCM sodium coolant inlet temperature. For all cases, the coefficient of heat transfer from the tube wall to the sodium coolant is approximated using appropriate correlations for turbulent heat transfer from a staggered tube bank, and the coefficient of heat transfer from the liquid LBE target material to the tube wall is

estimated using appropriate correlations for laminar convection within a pipe. The minimum tube length that will provide sufficient heat transfer area to maintain inner wall surface temperatures below 600°C has also been determined. Based upon the trends shown in the parametric analyses, a helical target with a maximum tube diameter, minimum wall thickness, and minimum inlet coolant temperature can be expected to provide optimum thermal performance.

Packed Bed of Spheres – W or LBE – Target

A second target concept is under consideration in which the target consists of a packed bed of spheres of stainless-steel-clad solid tungsten or hollow HT-9 steel spheres partially filled with liquid lead-bismuth eutectic that are arranged in a hexagonal array and cooled by an external flow of liquid sodium. The packed bed must be designed to ensure that there is sufficient target material between the beam window and the end of the target to effectively stop the proton beam. Furthermore, the length of the spallation zone within the target where the source neutrons will be produced must be optimized to insure that it is no longer in the axial direction than the length of the fueled region in the surrounding blanket. As a result of the selection of a hexagonal array, the pattern of the packed layer of spheres is repeated in every third layer. Therefore, in order to determine the minimum target length to effectively stop the proton beam, the minimum total material thickness in the axial direction of three layers of the spheres has been determined with a geometrical model solved with the Mathematica software.

For a 3-layer-thick packed bed of spheres that are 4 cm in diameter in a hexagonal lattice, the minimum thickness in the axial direction is ~2.7 cm or 1.36 times the radius of a single sphere. For a 600-MeV proton beam, the required stopping distance is ~30 cm in lead-bismuth and 15 cm in tungsten. The thickness of a 3-layer hexagonal lattice of 4-cm spheres is ~8.5 cm. Thus the minimum target length for a packed bed of 4-cm spheres would be 46.7 cm for a tungsten target or 93.4 cm for an LBE target. Note that the minimum axial material thickness is a function of the sphere's diameter.

At least three layers of spheres are needed to form a hexagonal array where there are no completely open gaps. The minimum material thickness as seen by the proton beam for such a 3-layer array is considerably less than the diameter of the spheres. The minimum material thickness was evaluated for spheres of various radii and a function was fit to the numerical data using a linear regression.

From the minimum thickness of a 3-layer set, the minimum height of the target can be determined. Two design options are considered for each potential target material. First, it is assumed that the entire target is composed of a single close-packed array of spheres of uniform size. Second, it is assumed that each 3-layer set is separated from the adjacent sets by a divider plate. The second arrangement will allow optimization of the target material distribution to provide an optimum neutron source distribution. For an LBE target, the target height is approximately 95 cm regardless of ball size for the cases *without* the divider plates and ~105 cm regardless of ball size for the cases *with* the divider plates. It should be noted that spheres with radius greater than 5 cm are too large to allow a suitable array to be constructed within the space available for the target in the ADS, but were included in the evaluation to improve the accuracy of the functional representation of the minimum thickness of a 3-layer set.

The pressure drop in the ADS primary coolant as it passes through the core is approximately 60 psi, and the pressure drop through the target should not exceed this limit. The packed bed correlation of Ergun⁷ is employed to evaluate the pressure drop to the target. Most cases considered fall within the range of applicability for this correlation, although the extreme cases fall outside this range. Additional correlations are currently under evaluation to determine their applicability. According to preliminary evaluations, the use of spheres with radii ≥ 2 cm will provide an acceptable pressure drop.

For the target systems considered, the surface, cladding-target material interface, and center-point temperatures were evaluated as a function of ball radius. It was assumed that the uniform cladding thickness of 1 mm is employed regardless of ball size and that the total proton beam power of 17 MW is distributed uniformly throughout the target. Since it is anticipated that temperatures in the cladding that exceed 600°C will induce thermal stresses that exceed structural limits, the temperature at the surface and the interface must be less than 600°C. In order to satisfy these limits, the radius of the spheres must be ≤ 2 cm. Therefore, the optimum radius of the spherical target pebbles is ~ 2 cm for this application. Further studies indicate that changes in cladding thickness result in large changes in structural temperatures only for balls with large radii. Further studies for reducing the target height by rotating each successive 3-layer set have been initiated.

Multiplier Primary System Thermo-Hydraulics

A preliminary SAS4A input deck for the fast-reactor design will be modified for use in ADS modeling to take advantage of the similarity of an advanced ANL fast-reactor design and the ADS facility in analyzing system thermo-hydraulic performance. Model changes needed to accurately represent the ADS reference design are being considered.

Preliminary Results for SCM Target/Blanket

The preliminary results obtained for material damage and gas production due to high-energy protons and neutrons ($E > 20$ MeV) in the window and structural components of an ADS reference design target are summarized below. The nominal proton energy was assumed to be 600 MeV and the target material LBE. Sensitivity to proton energy was investigated for one case.

The proton beam profile was assumed to be uniformly distributed over a 15-cm radius circle with system dimensions consistent with the ADS reference design. Target dimensions were scaled from the ADTF target based on an assumed beam power of 17 MW and a maximum current density on the window of $40 \mu\text{A}/\text{cm}^2$. Beam entry was from the top, and the region downstream of the target module filled with a sodium or LBE-cooled iron shield. The two SCM blanket assemblies were represented in r - z geometry with fuel compositions varying both radially and axially. The compositions with the highest fissile content were placed furthest from the target. In one case, the blanket was cooled by LBE and in the other case the coolant was sodium. The fuel consisted of a TRU-Zr dispersion clad in stainless steel.

Results were determined for damage and gas production for systems using both coolant types. The results were normalized to 1 MW of proton beam power,

⁷ *Chem. Eng. Progress*, **48**, 93, 1952

operating for one year with 100% availability. Thus, once the desired power level is determined, the values can be scaled accordingly. Damage results (dpa/yr-MW) for both protons and neutrons ($E > 20$ MeV) in the window (inside beam and outside beam), and in the wall separating the target from the blanket show that the major contribution to damage occurs in the window inside the beam boundary and is due primarily to neutrons. The contribution from protons is approximately half that of the neutron damage. Both H and He production in the window are dominated by proton reactions, while in the wall separating the target from the blanket, the production is dominated by neutron reactions. The latter result is due to the very low flux of protons in this location. The type of coolant in the SCM blanket does not have a large effect on the results in this energy range.

Results determined for dpa/yr-MW at 1 GeV compared to the results obtained at 600 MeV show that the damage due to protons decreases with increasing energy. This is primarily because the proton flux decreases since the power is being held constant. The neutron contribution remains largely unchanged because the neutron production per proton essentially increases proportionally to the proton energy. The combined dpa rate per unit of time at a constant power decreases by ~13% when increasing the proton energy from 600 MeV to 1 GeV. A similar result is obtained for the production of H and He. At the higher proton energy, the production is decreased primarily because the proton flux is decreased. The decrease is inversely proportional to the proton energy. The production of gas from neutrons remains essentially constant, since the neutron production increases at the higher proton energy (increase proportional to the proton energy) despite the lower proton flux.

Neutron fluxes have been determined throughout the LBE-cooled SCM blanket. Flux magnitudes of $\sim 1.0 \times 10^{14}$ n/cm²-s were determined for neutrons with energies above 0.1 MeV. Finally, an estimate was made of the coolant worth in the case with the LBE-cooled SCM blanket. This estimate was made by voiding all the coolant from the volumes containing fissile material. The two values of the multiplication factor are:

$$\begin{aligned}\text{Multiplication factor with coolant} &= 0.9675 \\ \text{Multiplication factor voided} &= 0.9535\end{aligned}$$

It is seen that the value of the multiplication factor decreases, indicating an overall negative void coefficient for this arrangement.

Micro Accelerator-Driven System (ADS) Proof-of-Principle (POP)

Coupling Experiments

Accelerator-TREAT Coupling Experiments

A preliminary report on the planned experiments with the coupling of an electron accelerator to the TREAT reactor at ANL-W was prepared and distributed to DOE in May. The experiments are referred to as the TREAT Experiments for Accelerator-driven Systems (TREACS). The report summarizes the role of TREACS in the development of control strategies for ADS systems. TREACS would provide the first set of tests of a coupled accelerator and multiplier system at power, and its results would also support the licensing of a higher power facility based on a TRIGA reactor in Italy (the TRADE program). The TREACS experimental setup would couple an electron accelerator in existence at the Idaho Accelerator Center (Idaho State University) to TREAT. A cost estimate for both the restart activities for the TREAT

facility as well as for the experimental program was included in the report. The proposed schedule for TREACS has been based on its use in support of the TRADE facility, which is expected to startup in 2007.

The studies performed to date regarding the physics and the engineering design indicate the feasibility of performing the TREACS experiments. The design and applicability of the experiments with respect to the physics of an accelerator/multiplier coupling has been established and documented under the WBS for Transmutation Science. With regards to the engineering of the experiments, the major items studied have been the general layout of the assembly, the target design, a target mounting and cooling assembly, and a preliminary cost estimate. The engineering assessment was documented in a preliminary engineering feasibility report.⁸ The report is currently being edited and will be ready for distribution in July. The feasibility assessment will continue, primarily to determine the power range for operations to ensure thermal feedbacks, and a final feasibility report will be issued.

Engineering Design

A target concept for the TREAT accelerator test has been completed. The target consists of 31 EBR-II blanket elements inside a cylindrical primary containment vessel that extends to the outside of the TREAT reactor to a heat exchanger. Heat removal from the target is accomplished by a passive cooling scheme that uses nucleate boiling of water to remove heat from the surfaces of the elements. The entire assembly is contained inside a secondary containment tube to prevent cooling water from leaking into the reactor should a failure of the primary containment occur. The entire target assembly as presently configured occupies the space of one TREAT fuel assembly inside the reactor.

For development of this concept to proceed, several issues must be resolved: (1) use of existing Na-bonded blanket elements would be advantageous from both the fabrication and heat-transfer standpoints, but the sodium contained within the cladding could eliminate water as the cooling fluid, whereas unbonded elements might not be usable because of their poor thermal characteristics; (2) considerable heat-transfer analysis is necessary to provide further detailed design guidance; and (3) vessel thicknesses were arbitrarily chosen for scoping analysis, whereas safety (i.e., containment under various internal pressure scenarios) and neutronics issues will need to be addressed in order to arrive at final values.

Preliminary evaluations of flow stability and estimated critical heat flux (CHF) have been made for the "water boiler" target-cooling concept introduced in an earlier report. Once the target heat-generation rate is determined, the CHF limit sets a lower bound for the heat flux as a target vehicle design requirement. Important locations include both the target surfaces themselves and any nearby constricted flow paths. Heat flow estimates are shown in Fig. 73.

The TREAT reactor and its instrumentation have operated with stability down to low power levels (~50 W). However, if the ADS experiment power is too low, natural cooling (convection, radiation) will prevent temperature feedback effects, required by the ADS program, from happening. At the high-power end, it is known that operating cooling fans allow long term operation at TREAT powers up to ~100 kW and allows fuel temperature (and feedback) to be controlled or (at least) limited. However, a

⁸ Engineering Feasibility of Proof-of-Principle Testing of Accelerator-Driven Subcritical Reactor Operation Using TREAT

minimum TREAT power that will result in enough temperature feedback to meet experiment objectives is not known.

To estimate a low power limit for ADS operation, “global” thermal modeling of TREAT is needed to assess mechanisms of passive cooling and arrive at a “heat transfer coefficient” relating TREAT fuel temperature rise to passive heat loss. Moreover, a TREAT thermal model, that also includes the operation of the cooling fans, will allow estimation of temperature feedback effects at all power levels.

However, characterizing and modeling the thermal behavior of the TREAT reactor is a major undertaking. Therefore, a review of past experimentation and modeling has been performed. A significant documented effort toward this end was made in the 1958-1960 timeframe when the reactor was first placed into service. Experimentation in TREAT included both high power pulse transients and low power steady-state operations. A review of past experiments and analyses has been conducted with emphasis on significance to TREAT/ADS applications. Some results of current interest to TREAT/ADS experiment capabilities and planning are as follows:

1. Heat transport within the TREAT core is dominated by the axial flow of cooling air. Without cooling air flow, measured radial and axial temperature profiles, as determined by fission energy deposition, remained virtually unchanged for about 1 hour after a high power pulse. By contrast, measured temperature profiles responded within minutes to the introduction of nominal cooling airflow.
2. At steady state with nominal airflow, the “sensitivity” of reactivity feedback (Δk) to the TREAT power level is $\sim 0.03\%$ per kW TREAT.

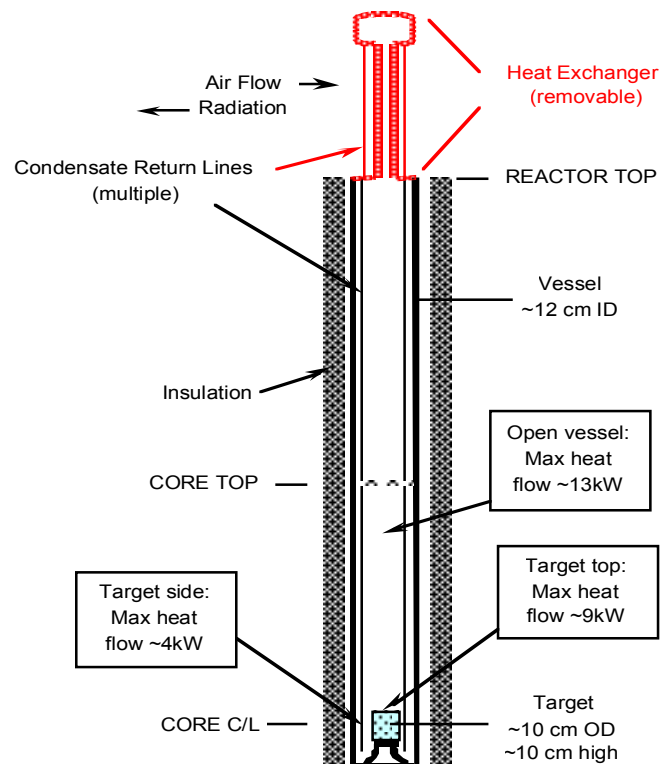


Fig. 73. The “Boiler” TREAT/ADS Concept. For an assumed geometry, CHF calculated maximum heat flows at different locations are indicated.

3. In low-power operation, heat balance measurements suggested that heat loss mechanisms other than cooling air may be present and account for approximately 3 kW.
4. Transient thermal models of individual, representative fuel assemblies and their air cooling should be sufficient for up-to-date thermal analyses of ADS simulations in TREAT.
5. For a simulation of ADS performance with a given feedback range and subcritical depth, the above-measured sensitivity of reactivity feedback to steady-state TREAT power suggests optimal operating TREAT power levels.

Transmutation Technology Development Plan

DOE requested the preparation of a Transmutation Technology Development Plan (TTDP) by Sept. 1, 2002 to address the facilities and associated research needed to demonstrate Proof-of-Principle for transmutation technologies. These activities will support decisions on the preferred technologies and path forward, and on the decision to proceed with the Proof-of-Performance phase. The TTDP will identify what experiments need to be performed to support critical programmatic decisions and what facilities are available for performing such experiments. A top-level strategy that will help guide the overall research and development program will be documented in a separate strategy document.

A meeting to discuss progress was held in conjunction with the Accelerator Workshop held in Santa Fe during May. The basic contents of the document were established; it will contain sections covering all basic technology areas of the AAA program (fuels, separations, transmutation physics, coupling, accelerators). Topics discussed included the downselection process and the need for a top-level strategy document. A draft of the Transmutation Science section of the TTDP had been provided in advance of the meeting and was used to discuss content and format for the plan.

Key questions regarding waste transmutation schemes and program schedules that must be addressed by the strategy document were identified in a videoconference held in May. There are three major groups of issues, which are: implementation strategy, R&D, and reference design. Three subgroups were established to provide input in these three areas.

The TTDP working group met in Los Alamos in June to finalize the format and content of the plan. The program plans from the technical leads were gathered and incorporated into the document. A schedule of major milestones was developed, as was budget numbers from individual plans. The draft of the TTDP was nearing completion with plans to submit it to the technical leads and management for review in early 4QFY02.

Fuels and Materials Experiments

The LANSCE Fuels and Materials Testing Station (FMTS) provides the capability for testing, under prototypic ADS irradiation and coolant conditions, fuels and materials proposed for consideration in the AAA program. This testing station will be located within the LANSCE Area A target facility. The preconceptual design team has been able to advance the maturity of several aspects of the station's design including physics performance, thermal-hydraulic performance, mechanical design of the vessel, target stalk, and surrounding shielding, and cost and schedule estimates.

The team is on schedule to produce a preconceptual design, cost estimate, and schedule to implement this FMTS irradiation station at LANSCE.

The physics performance of several spallation target configurations has been investigated. The current geometry allows for a central fuel region nested in a U-shaped target. Additionally, there are two irradiation locations located adjacent to the outside faces of the U-shaped target. Several target/coolant selections have been investigated for this configuration including LBE-cooled uranium plates, LBE alone, and water-cooled tungsten. The LBE-cooled uranium plates provide the highest total and peak neutron fluxes for the central fuel regions of 7.6×10^{14} n/cm²/s and 1.0×10^{15} n/cm²/s respectively (see Fig. 74). Additionally, proton irradiation locations are provided for ahead of the target structure for direct in-beam materials irradiations.

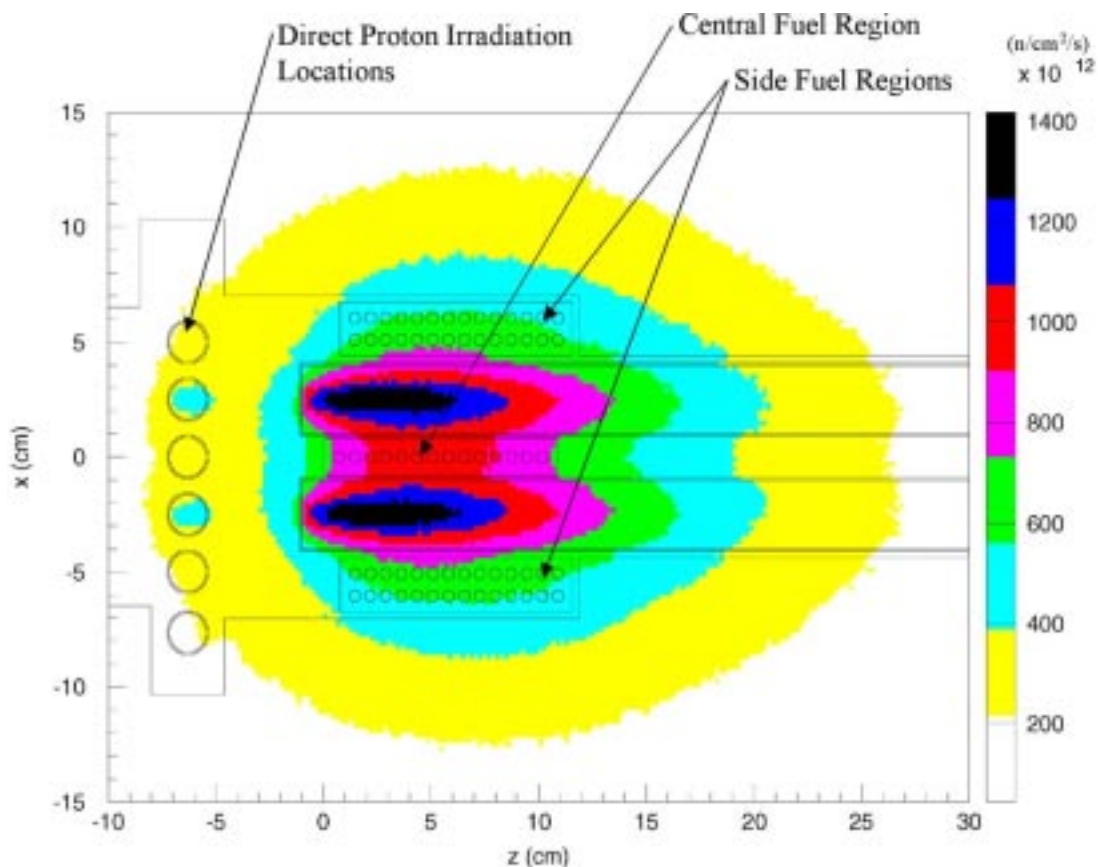


Fig. 74. Target geometry and peak neutron flux map.

The mechanical design of the irradiation station calls for a vacuum vessel into which a target stalk would be lowered. The vacuum vessel and stalk heights and weights have been sized to utilize the facility's existing overhead crane and existing hotcells. A preconceptual design print of the vacuum vessel was sent to a number of manufacturers to receive feedback on size and configuration, and to estimate cost and schedule for fabrication. A considerable amount of work has gone into determining the necessary target stalk size required for a LBE system. Layouts of the stalk have been made using components sized from the ISTC target assuming dual LBE coolant loops embedded within the stalk for separate target and fuel cooling.

Shielding layouts have also been completed showing the position of the current Area-A, target A-1 fixed shielding. These layouts allow for the sizing and positioning of the future vacuum vessel within that existing shielding structure. Additionally, should it be determined that the current shielding configuration is not satisfactory, the shield layouts allow for accurately estimating the number of lifts required to remove the shielding stack.

An integrated 3-year schedule has been developed and maintained which includes preliminary and final design stages, procurement, regulatory compliance activities, cleanout of current Area-A equipment and shielding, and construction of the irradiation station.

Advanced Cavity Development

The fabrication of two $\beta=0.175$, 2-gap, 350-MHz superconducting spoke-resonator cavities was completed one month ahead of schedule. A photograph of the cavity taken during the final inspection at the vendor's place of business during June is shown in Fig. 75.

Collaboration with ANL continued. We completed testing the ANL $\beta=0.4$, 2-gap 344-MHz RIA prototype spoke resonator cavity in April. These tests verified that Q-disease will not be a problem for the 350-MHz spoke cavities. This result was presented at the European Particle Accelerator Conference in June.



Fig. 75. AAA $\beta=0.175$ spoke cavity at final inspection (June 11, 2002)

5. PROJECT INTEGRATION

5.1 Systems Studies

Scope

Transmutation System Selection Studies

The FY02 AAA Systems Studies is focused on model development and subsequent analyses to support selection between the multi-tier transmutation system approaches. Nuclear Fuel Cycle (NFC) modeling emphasis has shifted from the equilibrium models to time-dependent simulation and optimization models, both of which require substantial development. Based on the results of the recently completed multiple-strata task force report and feedback from the Nuclear Energy Research Advisory Committee (NERAC) ATW Subcommittee meeting, two primary systems studies needed for this assessment are: (1) the evaluation of options to achieve deeper burnup in the Tier-1 thermal system, and (2) the refinement of systems evaluation techniques (e.g., include cost comparisons and more robust fuel cycle consequence analysis using the aforementioned time-dependent models). To this end, proliferation-resistant and conventional ALWR fuel cycles are being evaluated to clarify and assess the practical limits for Tier-1 partial destruction of the transuranics (TRU). As demonstrated in the FY01 study, partial burning of the TRU in a first-tier thermal-spectrum system can impact substantially the performance of the second-tier transmuter; therefore, the impact on Tier-2 fast-spectrum system performance for economic, waste-mitigation, and proliferation metrics must be self-consistently considered. If the TRU content in repository-directed materials can be reduced sufficiently, the repository licensing dose rates of the long-lived fission products (LLFPs) may dominate. Thus, the potential for LLFP transmutation is also being evaluated. In brief, Systems Studies scope includes:

- assess practical limits for Tier-1 partial destruction of TRU;
- consider the impact on Tier-2 fast-spectrum system performance;
- evaluate the potential for LLFP transmutation.

This scope is being fulfilled in the context of detailed time-dependent NFC simulation and optimization models using an array of economic, waste-mitigation, and proliferation metrics.

Report To Congress

The Department of Energy was directed to prepare a report for Congress by May 1, 2002 identifying the benefit of alternative nuclear fuel cycles employing transmutation and addressing a specific list of questions. These questions included (1) comparison of processing techniques, (2) comparison of transmutation approaches, (3) resulting waste streams, (4) life-cycle costs, (5) proliferation resistance, and (6) strategy for facility siting. Technical support was provided by the Systems Analysis team in support and fulfillment of these six charges. This support was underpinned using an equilibrium NFC parametric model that provided scenario-dependent economic, waste-mitigation, and proliferation metrics with which a range of multi-tiered NFC approaches were compared and assessed (within the limitations of the aggregated, equilibrium NFC model—e.g., the question looms of whether such equilibria can in

fact be achieved, and on what time scale, and at what cost in terms of dollars and added waste generation.).

Highlights

The majority effort in the Systems Analysis task this third quarter of FY02 has been directed at the development of a detailed time-dependent NFC simulation model (NFCSim) and a somewhat less-detailed optimization model (FCOPT). Both computer models are operative (NFCSim is JAVA-based, FCOPT is GAMS-based); both models, however, require additional development effort (NFCSim requires further process expansion, as well as integration of both neutronics and costing methods; FCOPT requires parametric testing under a range of constraint limits and additional controlling formulery). Significant progress in the development of both, however, has been made this third quarter. In addition, the NFCSim is targeted to reach a level of accomplishment and detail to permit benchmarking with a comparable simulation modeling effort at CEA/Cadarache (COSI model). Last, to aid in the direction taken by the NFCSim model, a commercial simulation package, *EXTEND*TM, has been developed and operated to simulate a simplified mock-up of a three-tiered transmuting NFC. In summary, highlights are as follows:

- The *NFCSim* simulation model is successfully simulating past history of nuclear power plant deployment and SNF generation in the US, and a workable framework is well established for integration of a range of Tier-1 and Tier-2 technologies and both the economic and neutronic (real-time) support required to meet the overall scope of AAA.
- The *FCOPT* optimization code is successfully optimizing a broad subset of NFC technologies on the basis of cost and proliferation risk, but more parametric systems studies and tuning of key constraints is required to better understand and align the projections so far emerging from this complex optimization model.
- The *EXTEND*TM simplified simulation is up and running and will be used to guide the development and modus operandi of the detailed NFCSim simulation model.

Approach and Direction

The aim of systems studies in the AAA Program is to provide quantitative, scenario-based guidance to policy and decision makers in the selection of advanced nuclear fuel cycles (ANFCs) that maximize *economic* (mainly energy costs, including fuel resource utilization), *ecological* (mainly short-and long-term waste and repository environmental and dose impacts), and *societal* (primarily proliferation risk) benefits of nuclear energy. Together, these three attributes characterize the *sustainability* of a given ANFC approach, and in this context AAA systems studies aim to begin the quantification of nuclear-energy sustainability.

Early studies (Van Tuyle, 2001) focused primarily on scenario-based analyses of a range of multi-tier transmutation ANFC strategies and the mass-balances related thereto. In parallel to and somewhat precedent to this AAA-based study was a similar investigation conducted by the OECD (OECD, 2002), with economic analyses being added for the estimation of system-wide electric-generation costs (COE). The addition of a “top-level” proliferation-risk metric (along with COE estimates) to the neutronics-driven material balances that define a given scenario, allowed each of the above-listed sustainability metrics to be quantitatively evaluated for a range of ANFC

scenarios (Brogli, 2002; Krakowski, 2002). The latter study (Krakowski, 2002) provided a technical basis for the Department of Energy Report to Congress (2002) on the economic, proliferation, and waste-mitigation potential of a range of selected, multi-tiered ANFCs. All of the above-listed studies and assessments were based on the assumption of steady-state, equilibrium (*per-TWeh*) analyses. The focus of AAA systems studies since the end of the Second Quarter FY02 and into the Third Quarter FY02 has been the development of time-dependent ANFC scenario analyses to address obvious short-comings of these early equilibrium analyses (e.g., important impacts of scheduling and lag-time constraints, transportation issues, time-value of capital and operating expenditure, waste inventory build up incurred during realistically constrained technology development and deployment scenarios, *etc.*).

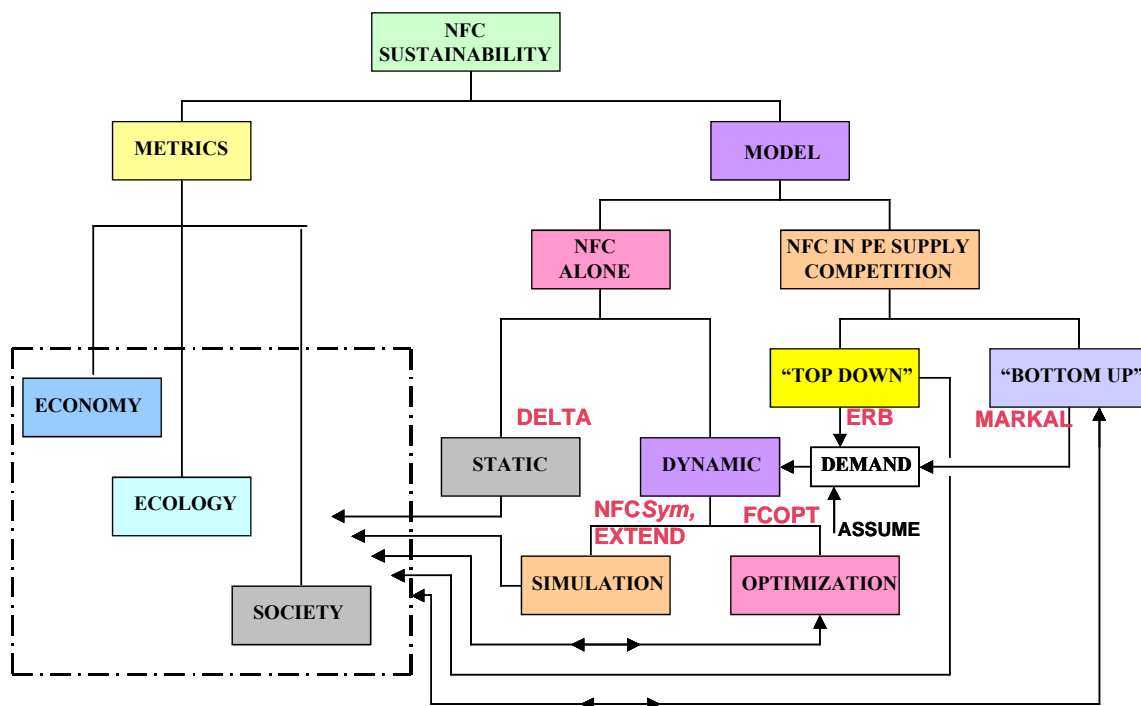


Fig. 76. Advance Nuclear Fuel Cycle (ANFC) modeling relationships, scope, and options, as applied the time-dependent scenario analyses.

The ANFC-specific/focused DELTA model was used to generate equilibrium sustainability metrics (Krakowski, 2002) in support of the Department of Energy Report to Congress (2002), as noted above. Systems-studies efforts for this and the previous FY02 Quarter have focused on the development of dynamic models that divide into either *simulation* or *optimization* models. Two approaches are being pursued for the former (NFCSim and an EXTEND™-based simulation), with the FCOPT optimization model being developed ultimately to guide use of both NFCSim

and EXTEND™ simulation models. All three dynamic models (NFCSim, EXTEND™ and FCOPT) are under development (including the buildup of the databases needed for their operation), but preliminary results have been generated from each. Ultimately, a reduced set of ANFC scenarios that have been distilled from the earlier equilibrium/static analyses (Krakowski, 2002) will be subjected to dynamic analyses. Figure 77 illustrates candidate scenarios evolved from the equilibrium analyses that are slated to be examined using the time-dependent models.

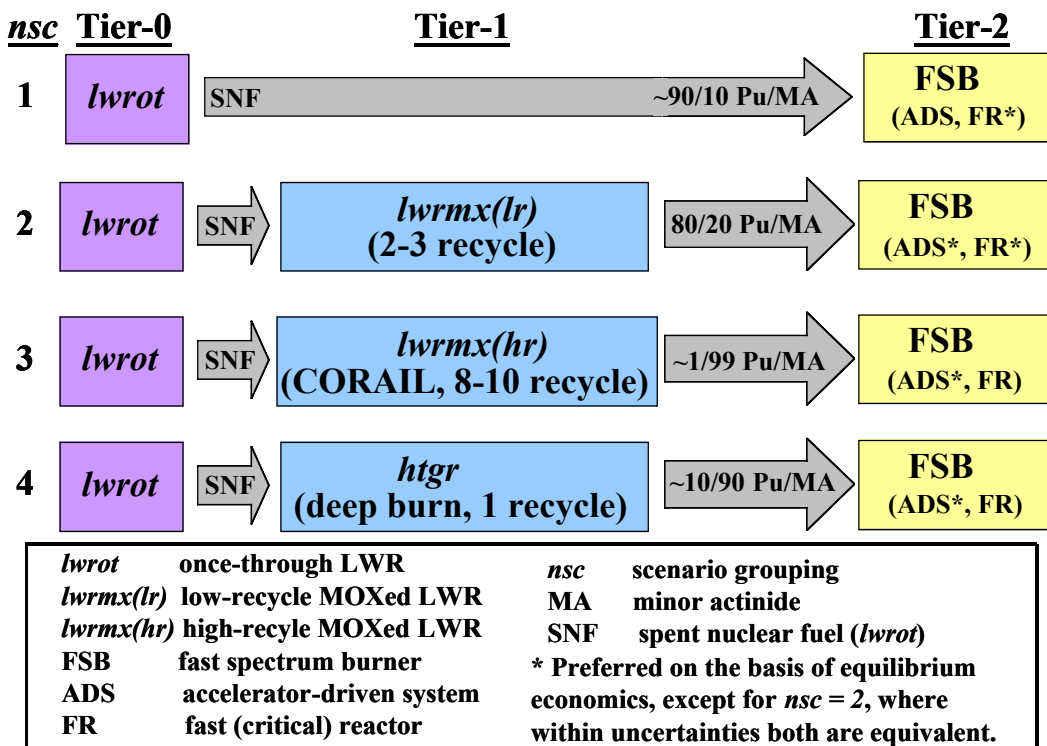


Fig. 77. Top-level scenarios evolved from earlier equilibrium analyses (Krakowski, 2002) being examined using dynamic simulation models (Fig. 76).

Sample (Interim) Results from NFCSim Simulation Model

Because of the lead dynamic-modeling role played by the NFCSim simulation model, interim results from this model are reported herein. Both the EXTEND™ (simulation) and the FCOPT (optimization) models support the development and operation of NFCSim. The NFCSim model is being developed to follow the life history of a Light Water Reactor (LWR) fuel charge from cradle (*i.e.*, mine) to grave (*i.e.*, repository) to accurately access the aforementioned *economic*, *ecological*, and *societal* benefits of nuclear energy. The starting point of an NFCSim simulation is the present-day nuclear industry legacy of 104 operating reactors and the spent nuclear fuel (SNF) they have generated from startup to the beginning of the simulation. At its present stage of development, NFCSim simulates these legacy LWRs, their associated cooling storage ponds, repositories, and the transportation of SNF between cooling storage and a repository. The results of an NFCSim simulation of the phase out of nuclear power in the US are shown in Fig. 78.

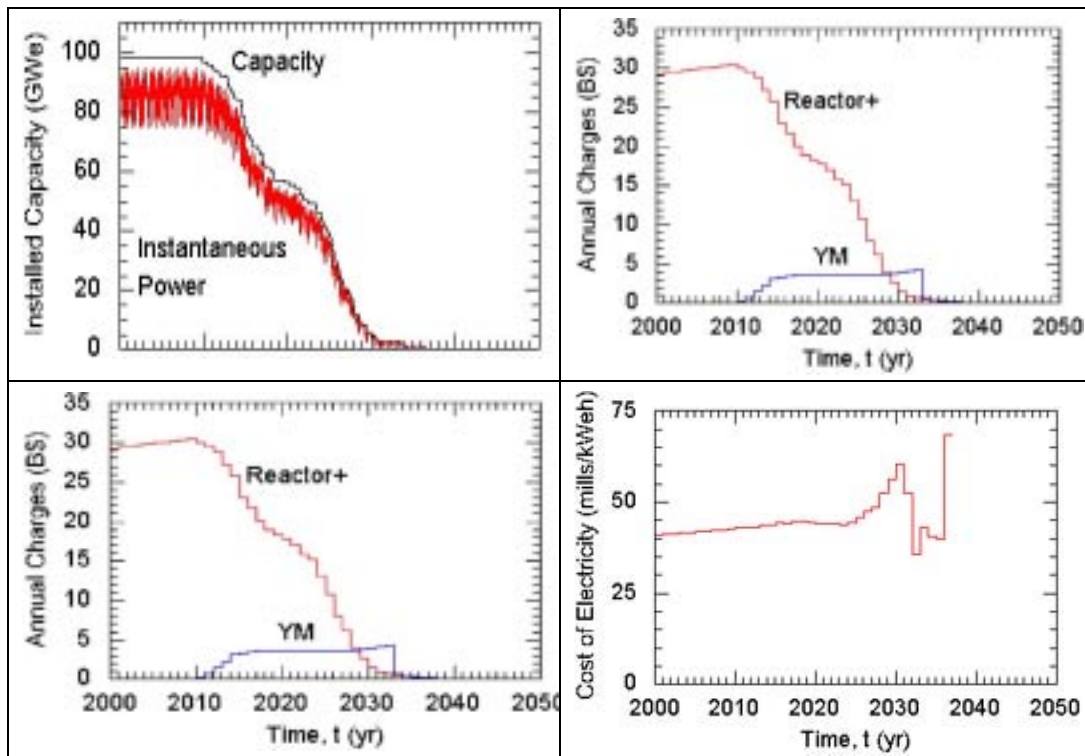


Fig. 78. Sample results generated with the current version of NFCSIM for a scenario in which nuclear power is phased out in the US.

For the simulation shown in Fig. 78, all reactors are shutdown after 40 years of operation. A repository (e.g., Yucca Mountain) is assumed to open in 2010. Transportation of SNF to the repository is assumed to ramp up over the course of four years from 0 to 200 shipments per year (for a total of 300 shipments during the ramp period) and remain at 200 shipments per year until all waste is disposed. The first repository is assumed to stop receiving shipments after 24 years and a total of 4300 shipments. A shipment is assumed to be a single discharge from a reactor (~1/3 of a core) that is determined from an assumed burnup of 40 MWt d/kg and burn fraction of 5%. For these conditions NFCSim calculates a capacity of 77,000 MT for the first repository, consistent with projections for Yucca Mountain. Furthermore, this simulation indicates the need for a second repository with a capacity of ~10,000 MT just for civilian SNF.

Applying the costing model used in the steady-state DELTA model has revealed several issues that must be addressed. One such issue is that the reactor plus cooling storage annual costs should be constant during the period between 2000 and 2010 when the capacity is constant, and there are no charges incurred that are associated with a repository other than a fixed 1 mill/kWe h. The NFCSim simulation shown in Fig. 78 reveals that the cooling storage costs rise linearly as the cooling storage capacity is filled. A more accurate costing model should charge a leveled cost based only on capacity.

Another costing issue is the persistence of liabilities after revenue streams have stopped. An example of persistence is an assumption that SNF should remain in cooling storage for a minimum of seven years. Applying the steady-state costing model, costs for cooling storage and for transportation of SNF to a repository are then

incurred after a reactor has shutdown. A more accurate time-dependent costing model would require increasing the D&D escrow account or establishing a separate escrow account over a reactor's lifetime to pay for these post-shutdown charges. As we delve further into the realm of time-dependent simulations, many other such issues will arise and must be addressed.

Neutronics Support

Both the time-dependent simulations and optimizations require neutronics calculations. Although inclusion of a simple neutronic calculational capability into NFCSim is planned, parametric results from detailed neutronic calculations are also needed. An example of such a calculation is described below.

Basic irradiation calculations were performed for the multi-recycle of Pu from SNF in an LWR (see Fig. 79). For these calculations, a MIX design was assumed (100% core of MOX fuel with enriched uranium support) in an infinitely reflected PWR assembly.

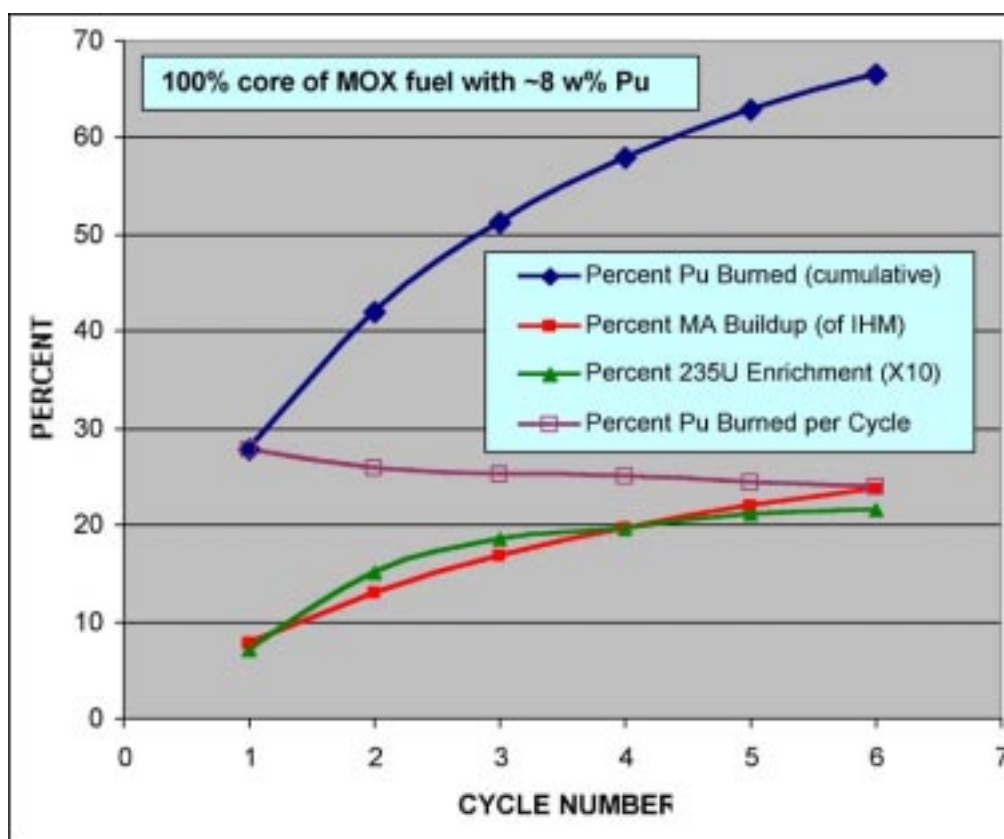


Fig. 79. Percent burnup of Pu and buildup of Minor Actinides (MA) as a function of the number of MOX Recycles in an LWR.

However, the neutronic safety of this design was not established. To explore the safety aspects of a full core of MOX fuel, a detailed 1/8-core model of a PWR was developed. Then safety calculations using MOX fuel were performed, and a design was developed to meet safety criteria. This design includes extra water holes instead of fuel rods (12 per 15x15 assembly) and slightly enriched boron (25% B-10) in the

water. This will be the basis of the detailed multi-recycle calculations next quarter. Such multi-recycle calculations will be performed for three different cases: recycle of plutonium only, recycle of plutonium plus minor actinides, and recycle of plutonium fabricated along with strontium and cesium. This last case is proposed as a way to increase the proliferation resistance of the MOX fuel by increasing the heat-load and activity of the material. ^{90}Sr and ^{137}Cs comprise ~36% of the activity of SNF (Pu is ~26%) after 10 years. By including them with the Pu and doubling their presence, MOX fuel could have about the same activity as SNF, which would mitigate proliferation risk. The enriched uranium support means that the plutonium content of the MOX fuel will remain the same for each recycle; the uranium will just become more enriched as the number of recycles increases. Each recycle is comprised of plutonium from initial SNF as well as plutonium burned in the previous recycles (the “fresh” SNF comprises “make-up feed” to replace the plutonium burned during the last recycle, so that the initial plutonium inventory is the same for each recycle).

5.2 University Programs

Scope

University Programs consists of four major aspects: the University of Nevada-Las Vegas (UNLV) Transmutation Research Program (UNLV TRP), AAA Program at the Idaho Accelerator Center (IAC) of Idaho State University (ISU), University Fellowships Program (UFP), and AAA Directed University Research within the Transmutation Sciences technical area. In addition, the scope of this effort involves coordination between other AAA activities and academia. The Scope, Highlights, and Technical Progress for AAA-Directed LANL-supported university research were reported earlier under Transmutation Sciences.

UNLV AAA University Participation Program

The University of Nevada supports the AAA Program through “research and development of technologies for economic and environmentally sound refinement of spent nuclear fuel...”⁹ The UNLV Program has four components: student-based research, infrastructure, international collaborations, and support.

Idaho Accelerator Center

The IAC at Idaho State University (ISU) will develop a long-term plan and a research program to conduct a variety of investigations that depend on high-energy electron accelerators.

University Fellowships Program

The University Research Alliance (URA, formerly ANRC—the Amarillo National Research Center) acts as the executive agency for the AAA Program to select, award, and administer fellowships for ten graduate students who were selected in FY01 and ten more selected in FY02.

⁹ ref. H.R. 5483, P.L. 106-377

AAA-Directed University Research

Other universities currently support R&D and technology development. LANL has ongoing support contracts with the University of Michigan, the University of California-Berkeley, and the University of Texas-Austin. North Carolina State University and the University of Illinois at Urbana Champaign are being added to support LANL's research responsibilities. ANL is in the process of contracting with U of Michigan and MIT.

Highlights

UNLV Transmutation Research Program

- The ISTC Target arrived at UNLV in May and was carefully unloaded. Two accelerometers indicated that an overlimit acceleration had occurred sometime during shipment, so it will remain as received in the Engineering Complex staging area until insurance issues are resolved.
- The UNLV AAA University Participation Program (UPP) now supports a total of 25 graduate students with assistantships as two new tasks were added: one on oxygen sensing systems and one on positron annihilation spectroscopy techniques in materials evaluation (collaboration with ISU-IAC).
- Remodeling of the Materials Performance Laboratory (MPL) at the UNLV Thomas Beam Engineering Complex was completed with plumbing, electrical, furniture and most equipment installed. Experiments have begun.
- The UNLV AAA Program purchased a state-of-the-art Transmission Electron Microscope (TEM) for half of its book price in mid-June. The TEM includes a field emission gun with 300 kV acceleration voltage, ultra-high resolution with 0.20 nm point resolution and 0.10 line resolution, complete digital control under Windows NT operating system, and an integration microscope with detector systems including STEM, TV cameras, EDX, and EELS.

Idaho State University

- ISU began calculations on accelerator target concepts for neutron production for the proposed TREAT/accelerator coupling experiments. They also began preliminary neutron production measurements with a 22-MeV linac for benchmark calculations and heat removal studies.
- Calculations on a neutron-producing target continued, including calculations associated with total neutron yield measurements that began in June. The IAC "20" linac beam line was modified for neutron yield measurements, and is currently being used for benchmarking calculations completed for the linac-driven neutron source. This work is aided by the efforts of an AAA UNLV student working at IAC.
- Accelerator and measuring apparatus for positron stress measurements (for a collaboration with UNLV) is operational in a new laboratory space in the Physics Department Particle Beam Laboratory. Preliminary positron stress data has been taken on AAA project samples provided by UNLV.
- All of the Boeing accelerator components (SLIA pulse accelerator--former SDI electron accelerator from Titan Systems) are now in storage in Pocatello.

Immediate use will be made of a quantity of this equipment to upgrade the performance of the Fast Pulse Linac, and some will serve as the foundation for the neutron source linac for the proposed TREAT experiment.

- ISU hired an AAA Project financial manager (half-time), 15 summer students, and 2 engineers (partially supported by AAA).

University Research Alliance

- URA finalized selection of AAA Fellowships for 2002 and notified recipients. Through this new group of fellows, the AAA Project engaged seven new universities: Purdue, Georgia Tech, University of Florida, University of Illinois at Chicago, North Carolina State, University of New Mexico, and University of Tennessee Knoxville.
- AAA Fellow Leigh Outten completed her MSNE from MIT. The title of her thesis is "Development of a Master Logic Diagram and Event Trees for an Accelerator Driven System." Also, Fellow Coy Bryant received his MS degree from the University of Texas in May.
- The URA organized several meetings in Washington DC between the new class of AAA fellows and DOE headquarters. Fellows received a good overview of all aspects of the AAA program and received some detailed information about the technical areas of interest to the program.
- In conjunction with the DOE headquarters meetings, the Fellows visited ANL-East where they were able to learn more about the ANL programs and were able to see the facilities and some of the experiments that are being conducted at ANL.

Technical Progress

Technical progress of ongoing investigations by direct university research projects is reported under appropriate technical areas (e.g., Transmutation Science). Some technical progress made under the UNLV program has been reported separately (viz., quarterly progress reports by primary investigators). The Idaho State University report is included below.

Idaho State University

We acquired the Titan and Boeing accelerators, and they are in storage in Pocatello. These accelerators are former SDI test beds, donated to the IAC. The Titan accelerator is a 10-MeV 15-ka pulsed power electron accelerator and the Boeing machine is a CW 120-MeV electron linac. Some parts of the latter are being used to upgrade the IAC FPL and other operational accelerators. Total value of this material is \$50-\$100M.

A group headed by one of ISU's post docs has begun calculations and benchmark measurements on neutron producing targets for subcritical accelerator coupling experiments. This work utilizes various standard codes such as MCNP and the experiments are being done on our "20" linac. Measurement results will be completed next quarter. A visiting UNLV student is part of this group.

We have begun positron stress measurements as applied to AAA materials, in collaboration with UNLV.

Accelerator-Produced Neutrons for Reactor/Accelerator Coupling Experiments

The neutron-producing target being studied is a lead cylinder with dimensions of 2x4 inches. Neutron yield and neutron spectra calculations, as a function of incident electron energy, use various codes including MCNP. Sample results can be seen in Fig. 80. Variation of neutron yield with energy and beam power is shown in Fig. 81. Experimental neutron yield measurements are done with off-line measurements of the gamma-ray activity of ^{203}Pb produced by (n,gamma) reactions in lead foils distributed in the target.

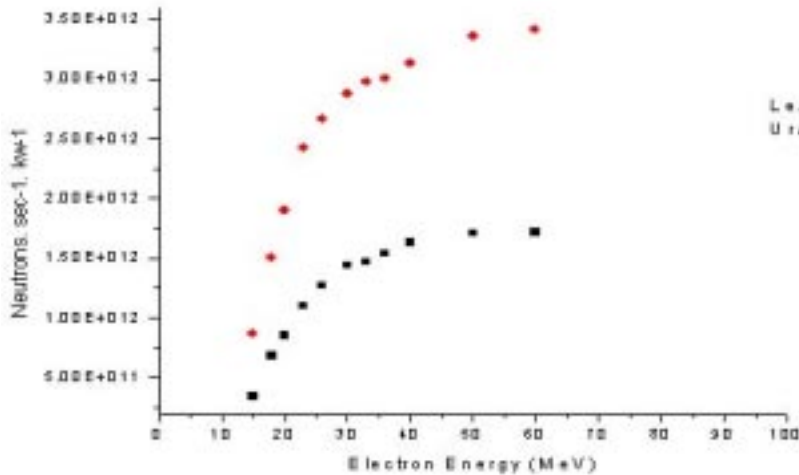


Fig. 80. Calculated yield of neutrons versus of electron beam energy for a 2x4-inch cylinder of indicated material.

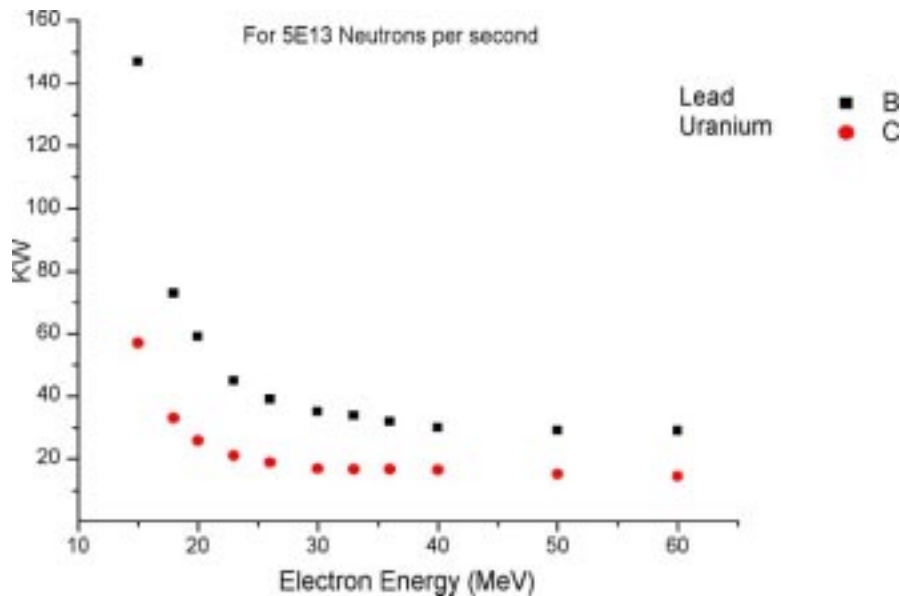


Fig. 81. Electron beam power vs. energy required to produce 1×10^{13} neutrons/second.

Stress Measurements

A new method has been developed to perform γ -ray induced positron annihilation spectroscopy (PAS). The new technique uses an MeV γ -ray instead of a positron beam to bombard the material. MeV γ -rays penetrate deeply inside the material and create positrons via pair production. The subsequent annihilation of positrons produces 511-keV photons whose spectrum reflects the electron momentum in the material. This method allows stress and defect analysis by measuring the resulting Doppler broadening with a high-resolution gamma detector. This scheme works because defects in a material lead to a large contribution of annihilation photons from low momentum electrons; thus, a relatively narrow peak is produced, the measure of which is proportional to the stress in the material. Measurements are being carried out on standard coupons as shown in Fig. 82. Because of the high penetration of γ -rays, this method has the advantage of being able to assess bulk properties to predict failure, etc. Defects can be investigated in very thick samples, up to tens of gm/cm^2 , (not available with other techniques). The method is simple, low cost and potentially portable.

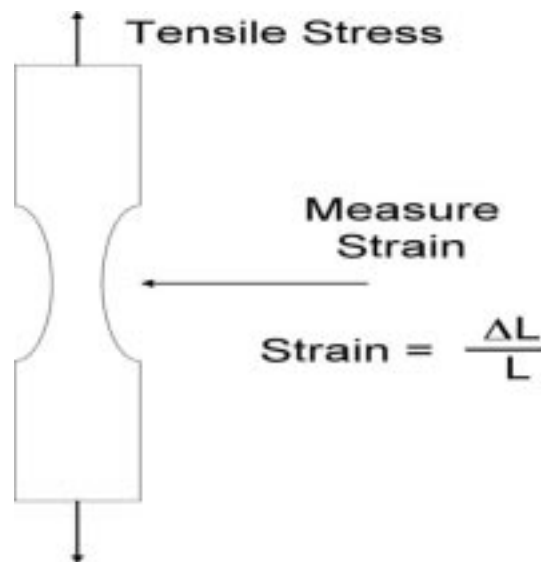


Fig. 82. Test coupons for positron measurements. Different tensile loads are applied.

References

- [1] J. Bugl and A. Bauer, Battelle (USA) Report BMI-1692 (1964)
- [2] R. Benz and W. B. Hutchinson, "U + N₂ Reaction Layer Growths," J. Nucl. Mater. 36 (1970) 135-146.
- [3] R. B. Matthews, K. M. Chidester, C. W. Hoth, R. E. Mason, and R. L. Petty, J. Nucl. Mat. 151 (1988) 334-344.
- [4] M. Born and J.E. Mayer; *Z. Physik* **75** 1-18 (1932).
- [5] N. Mott and M. Littleton; *Trans Faraday Soc.* **34** 485-499 (1938).
- [6] C.R.A. Catlow and W.C. Macrodt (eds.); Computer Simulation of Solids, Springer-Verlag, Berlin, Germany (1982).
- [7] J.D. Gale; Technical Report, The Royal Institution of Great Britain (1994).
- [8] R.D. Shannon, *Acta Cryst. Sec. A* **32** 751-767 (1976).
- [9] J.H. Harding and A.H. Harker; AERE-R10425, Technical Report, Harwell Laboratory (1982).
- [10] Akimoto, Y. (1967) *Journal of Inorganic and Nuclear Chemistry* **29** 2650-2652
- [11] D.A. Damien, R.G. Haire and C.R. Peterson, CONF 780823-8, 1973.
- [12] P. Ettmayer, J. Waldhart and A. Vendl; *Monatshefte fuer Chemie* **110** 1109-1112 (1979).
- [13] A.N. Christensen, *Acta Chemica Scandinavica Series A:* **29** 563-568(1975).
- [14] K.E. Sickafus, L. Minervini, R.W. Grimes, J.A. Valdez, M. Ishimaru, F. Li, K.J. McClellan and T. Hartman, *Science* **289** 748-751 (2000).
- [15] W. Lengauer, *Journal of Alloys and Compounds* **168** 293-307 (1992).
- [16] M.C. Payne et al., *Rev. Mod. Phys.* **64** 1045 (1992).
- [17] N. Schoenberg; *Acta Chemica Scaninavica* **8** 213-220 (1954).